Synthesis of Sol-gel Based Titanium dioxide Photocatalyst: Investigations on their Modification, Interaction with Metal ions, and Antimicrobial Activity

THESIS

Submitted in partial fulfillment

of the requirements for the degree of

DOCTOR OF PHILOSOPHY

by

DESAI VILAS SHIVAJI

Under the Supervision of

Dr. Meenal Kowshik

BIRLA INSTITUTE OF TECHNOLOGY AND SCIENCE

PILANI (RAJASTHAN) INDIA

2013

BIRLA INSTITUTE OF TECHNOLOGY AND SCIENCE

PILANI (RAJASTHAN)

CERTIFICATE

This is to certify that the thesis entitled **"Synthesis of Sol-gel Based Titanium dioxide Photocatalyst: Investigations on their Modification, Interaction with Metal ions, and Antimicrobial Activity"** and submitted by **Desai Vilas Shivaji**, ID No. 2007PHXF446G for award of Ph.D. Degree of the Institute, embodies original work done by him under my supervision.

Signature in full of the Supervisor: _____

Name in capital block letters: Dr. MEENAL KOWSHIK
Designation: Associate Professor
Department of Biological Sciences

Signature in full of the Co-supervisor: _____

Name in capital block letters: Dr. HALAN PRAKASH
Designation: Assistant Professor
Department of Chemistry

Date:

Acknowledgements

First of all, I would like to express my sincere gratitude towards my research advisor and mentor, Dr. Meenal Kowshik, for her persistence and thoughtful guidance for me to stand as an independent researcher. I am deeply indebted to her, for her constant encouragement throughout my Ph.D studies, her faith in the abilities of the students, patience and invaluable suggestions.

I am indebted to my co-advisor, Dr. Halan Prakash for his patience, insightful discussions and invaluable advices during my Ph. D work. I am also grateful to him and Dr. Saby John for their service as my doctoral committee members.

My special thanks to Prof. B. N. Jain, Vice-Chancellor, BITS Pilani, Prof. K. E. Raman, Director, BITS, Pilani - K K Birla Goa Campus, Prof. **R. N. Saha**, Deputy Director (Research & Education Development), Prof. Sanjay Kumar Verma, Dean, Academic Research (Ph. D. Programme) Division BITS, Pilani, Prof. A. K. Das, Dean, Research and Consultancy Division BITS, Pilani, Dr. S. D. Manjare, Faculty In-charge, Research and Consultancy Division, BITS, Pilani - K K Birla Goa Campus, for providing the necessary facilities and environment to conduct my research work at this beautiful campus.

I would like to thank Dr. N. N. Ghosh (Assistant Professor, Department of Chemistry) for his kind help and support. I thank Dr. Sutapa Roy Ramanan, for her kind help and advice during my Ph. D studies.

I wish to thank Prof. Pao Chi Chen, Dr. Rosilda Selvin and Dr. Ruey-Chang Hsiao, at the Dept. of Chemical and Materials Engineering, Lunghwa University of Science and

Technology, Taiwan, for their helpful discussions and for providing me a friendly environment to work and study during my stay in Taiwan.

I would like to express my sincere gratitude to Dr. Utpal Roy (Head of the department of Biological Sciences), and all the staff members of the Department of Biological Sciences for their kind support and co-operation in different areas of research.

I gratefully acknowledge the financial support from the Department of Science and Technology (DST) Delhi, for my Ph.D work.

Special thanks are due to all my fellow research scholars Dr. Bhanudas Naik, Dr. Celisa Santimano, Mrs. Vidhya Kamat, Mr. Gokulkrishnan for the helpful discussions, constant encouragement and support.

I am indebted to my friends Nita Chandrasekhar, Kshipra, Pallavee, Yogesh, Ketaki, Bhakti, Meghnath, Mansoor for their constant support and encouragement when it was most needed.

I also wish to thank Mrs. Kamana Upadhyay and Mr. Mahadeo Shetkar for their help and co-operation throughout my research work.

Finally, I wish to express my profound regards and deep gratitude to my parents, family members and all my well wishers for their unstoppable support and encouragement.

Vilas Desai

Abstract

The impact of nanotechnology has become increasingly evident in different areas of science and technology, including the field of environmental remediation and disinfection. A number of environmentally beneficial technologies such as heterogeneous photocatalysis (HP) and Solar Disinfection (SODIS) using nanosized TiO_2 as photocatalysts have been developed and applied extensively for air purification, water treatment and environmental remediation. TiO_2 is a promising photocatalyst in terms of catalytic performance and stability in aqueous media and has gained considerable attention due to its chemical stability, insolubility in water, non-toxicity, low cost, and other advantageous properties.

In this research work we have synthesized mesoporous TiO_2 nanoparticles by a simple sol-gel method using titanium tetrachloride as a precursor. The characterization of TiO_2 nanoparticles by XRD, TEM, TG-DTA, and N_2 adsorption-desorption analysis indicate formation of pure anatase phase, polycrystalline TiO_2 showing good physicochemical properties with a particle size of ~13 nm and surface area of 72.80 m^2/g. The synthesized TiO_2 nanoparticles exhibited good photocatalytic activity under both UV light and sunlight for the degradation of toxic dyes Malachite green and Methylene blue. The TiO_2 also showed promising bactericidal activity against pure bacterial cultures of *E. coli*, *P. aeruginosa*, *S. aureus* and *K. pneumoniae* as well as microorganisms from the discharge water from a sewage treatment plant which had a high microbial load.

Although TiO_2 is considered an ideal photocatalyst because of its photocatalytic properties, it has a wide band gap of 3.2 eV that limits its photocatalytic activity to the ultraviolet (UV) region of the light spectrum, which is ~4 % of the total solar energy available, far too small for practical applications. Hence, to lower the band gap of TiO_2 and to improve its absorption in the visible light region the TiO_2 was doped with transition metals, non-metal anions, and surface modified with organic acids, amino acids, phosphate etc. Among the metal doped TiO_2, silver doped TiO_2 showed good antibacterial activity under visible light irradiation, whereas, in case of modified TiO_2 antibacterial activity was in the order of FA-TiO_2 > Fu-TiO_2 > MA-TiO_2 > S-TiO_2 > SA-TiO_2 under visible light conditions.

Surface functionalization of metal oxide nanoparticles add to their versatility since hybridization with functional molecules provides biocompatibility, catalytic abilities, and controlled surface properties. Since, both silver doped TiO_2 and organic acid modified TiO_2 showed promising bactericidal activity, further studies were performed to synthesize silver-titania nanocomposites functionalized with organic acids, and their bactericidal activity against various microorganisms was evaluated. The antimicrobial activity in terms of MIC and MBC of FA-AgCl/TiO_2 and Fu-AgCl/TiO_2 was found to be better than the unfunctionalized AgCl/TiO_2. However, in case of MA-AgCl/TiO_2 and SA-AgCl/TiO_2 the MIC and MBC was higher than the unfunctionalized AgCl/TiO_2. Similarly, no enhancement in antimicrobial activity was observed for Arg-AgCl/TiO_2 and Cys-AgCl/TiO_2 after functionalization. The enhanced antimicrobial activity of FA-AgCl/TiO_2 and Fu-AgCl/TiO_2 was attributed to the increased uptake of functionalized

AgCl/TiO_2 and increase in the ROS species resulting in oxidative damage of the microbial cells.

Another strategy to improve the photocatalytic acitivity of TiO_2 is to combine it with transition metals such as Nickel (II). Nickel (II) in presence of TiO_2 can undergo photochemical oxidation to form Nickel (III) species or can behave as an electron trap and get reduced to Ni (I) species. Ni (I) is known to activate molecular oxygen, and produce reactive oxygen species, while Ni (III) species are highly oxidizing species, capable of causing in-vitro DNA damage. The highly reactive radicals generated during TiO_2 photocatalysis could also react with the Nickel (II) to produce reactive species. Hence, to investigate the effect of addition of catalytic amount of Nickel (II) azamacrocyclic complex to TiO_2 for the photoinduced inactivation of the microorganisms, studies were carried out. The antimicrobial study of TiO_2 in presence of complex 1 show that 20 μM Ni (II) + 5 μg/ml TiO_2 is effective for complete inactivation of Gram positive, Gram negative as well as fungal cultures. Thiobarbituric acid assay (TBA) showed that the complex 1 in presence of oxidant induces significant lipid peroxidation which was further confirmed by the SEM results. This effective microbial inactivation is mainly attributed to its ability to cause damage to the cell membrane than the complex 1 alone in the divalent state.

TABLE OF CONTENTS

COVER PAGE i
ACKNOWLEDGEMENTS iii
ABSTRACT v
TABLE OF CONTENTS viii
LIST OF TABLES xii
LIST OF FIGURES xiii
LIST OF ABBREVIATIONS AND SYMBOLS xx

CHAPTER 1: Introduction and Review of Literature

1.1 Introduction to Nano 1
1.2 Basic principles of Heterogeneous photocatalysis 6
1.3 Titanium dioxide (TiO_2) as a photocatalyst 8
1.4 Chemical structure of TiO_2 10
1.5 Synthesis of nanoparticles 13
1.5.1 Gas phase methods 14
1.5.1.1 Chemical vapor deposition (CVD) 14
1.5.1.2 Physical vapor deposition (PVD) 14
1.5.2 Solution routes 15
1.5.2.1 Microemulsion method 15
1.5.2.2 Hydrothermal Method 16
1.5.2.3 Solvothermal method 17
1.5.2.4 Sol-gel method 17
1.6 Mechanism of heterogeneous photocatalysis 19
1.7 Enhancement of photocatalytic activity 24
1.7.1 Metal ion dopants 25
1.7.2 Transition metal ion doping 26
1.7.3 Coupled/composite semiconductors 27
1.7.4 Surface modification/surface functionalization 29
1.8 Applications of photocatalysis 30
1.9 Bactericidal effects of Photocatalysis 32
1.9.1 Mechanisms of action of TiO_2 photocatalysis on bacteria 33
1.10 Definition of the problem 38
1.11 Outlay of the thesis 40

CHAPTER 2: Synthesis, characterization of TiO_2 nanoparticles and study of its photocatalytic activity on microorganisms and dyes

2.1 Introduction 42
2.2 Materials and methods 44
2.2.1 Preparation of TiO_2 nanoparticles 44
2.2.2 Characterization of TiO_2 nanoparticles 45
2.2.3 Bacterial strains and cultures 46
2.2.4 Preparation of TiO_2 suspension for photocatalytic experiments 47
2.2.5 Photocatalytic reaction and Cell viability assay 47
2.2.6 Chemical Oxygen Demand (COD) analysis 48
2.2.7 Photocatalytic degradation of dyes 49
2.3 Results and Discussion 50

CHAPTER 3: Doping/surface modification of TiO_2 nanoparticles for improved photocatalytic activity under visible light irradiation

3.1 Introduction 68
3.2 Materials and methods 70
3.2.1 Doping with non metal anions 71
3.2.1.1 Nitrogen doped TiO_2 71
3.2.1.2 Synthesis of metal and non metal ions (C, N, S, and Fe)-doped TiO_2 71
3.2.1.3 Synthesis of metal ion doped TiO_2 (Ag-TiO_2) 72
3.2.2 Synthesis of Phosphate modified TiO_2 (P-TiO_2) 73
3.2.3 Modification of TiO_2 with organic acids (Salicylic acid, Folic acid, Fumaric acid, Succinic acid and Malic acid) 73
3.2.3.1 Salicylic acid modified TiO_2 (S-TiO_2) 73
3.2.3.2 Folic acid, Fumaric acid, Succinic acid and Malic acid modified TiO_2 73
3.2.4 Synthesis and modification of TiO_2 with amino acids 74
3.2.4.1 Arginine modified TiO_2 (Arg-TiO_2) 74
3.2.4.2 Cysteine modified TiO_2 (Cys-TiO_2) 74
3.3 FTIR analysis 75
3.4 Bacterial cultures 75
3.5 Preparation of TiO_2 suspension 75
3.6 Photocatalytic reaction and Cell viability assay 75
3.7 Results and discussion 76

CHAPTER 4: Functionalization of $AgCl/TiO_2$ nanocomposites and evaluation of its antimicrobial activity

4.1 Introduction 95
4.2 Materials and Methods 99
4.2.1 Synthesis of functionalized nanocomposites 99
4.2.2 Microbial cultures 100
4.2.3 Antimicrobial activity evaluation 101
4.2.3.1 Determination of MIC and MBC 101
4.2.3.2 Study by microbial inactivation kinetics 102
4.2.4 Characterization studies of FA-$AgCl/TiO_2$ and Fu-$AgCl/TiO_2$ 102
4.2.4.1 Particle size analysis 103
4.2.4.2 FTIR analysis 103
4.2.4.3 EDAX analysis 103
4.2.5 Hemolytic assay 103
4.2.6 Scanning Electron Microscopy SEM) 104
4.2.7 Detection of intracellular reactive oxygen species (ROS) 105
4.2.8 Study of microbial inactivation kinetics in presence of antioxidants 105
4.3 Results and Discussion 106
4.3.1 Synthesis & characterization of functionalized $AgCl/TiO_2$ 106
4.3.2 Studies on microbial inactivation kinetics 110
4.3.3 Characterization studies 115
4.3.4 Hemolytic assay results 125
4.3.5 Scanning Electron Microscopy (SEM) 125
4.3.6 Mechanistic studies of antibacterial activity of FA-$AgCl/TiO_2$ 127
4.3.6.1 Detection of intracellular reactive oxygen species (ROS) 127
4.3.6.2 Study of microbial inactivation kinetics in presence of antioxidants 128

CHAPTER 5: Antimicrobial effects of titanium dioxide nanoparticles and ammonium persulphate in presence of 1, 8-dimethyl-1, 3, 6, 8, 10, 13 - hexaazacyclotetradecane) nickel (II) perchlorate

5.1 Introduction 132
5.2 Materials and methods 136

5.2.1 Bacterial strains and cultures 136
5.2.2 Photocatalytic reaction and Cell viability assay 137
5.2.3 UV- visible spectral measurements & kinetic studies of complex 1 138
5.2.4 ESR spectral measurements 138
5.2.5 Antimicrobial assay of complex 1 in presence and absence of oxidant 138
5.2.6 Determination of lipid peroxidation 139
5.2.7 Sample preparation for Scanning Electron Microscopy (SEM) 140
5.3 Results and discussion 140
5.3.1 UV-visible spectra and kinetic studies of the complex 1 147
5.3.2 Antimicrobial assay of complex 1 in presence and absence of oxidant 154
5.3.2.1 Effect of APS alone, and APS in presence of complex 1 on Microorganisms 154
5.3.2.2 Effect of stable trivalent nickel species on *E. coli* cell viability 158

Summary of results and conclusions 163

Future scope of work 168

References 169

List of publications **Appendix I**

Conferences and workshops **Appendix I**

A Brief Biography of the Candidate **Appendix II**

A Brief Biography of the Supervisor **Appendix III**

List of tables

Table. 1.1. Crystal structure data of major TiO_2 polymorphs.

Table. 2.1. The COD values obtained for the sewage water (SW) sample treated with TiO_2 nanoparticles in Sunlight.

Table. 4.1. The MIC and MBC values determined by the resazurin assay.

Table. 4.2. The MIC and MBC values obtained for FA-AgCl/TiO_2 and AgCl/TiO_2 against the test microorganisms by resazurin assay.

Table. 5.1. Antibacterial effects of TiO_2 at varying concentrations under UV light (352 nm) exposure.

Table. 5.2. Antibacterial effects of Ni (II) azamacrocyclic complex solution at varying concentrations.

Table. 5.3. Antibacterial effects of TiO_2 (5 µg/ml) at varying concentrations of Ni (II) azamacrocyclic complex solution under UV light irradiation.

Table. 5.4. First order rate constants (K_{obs}) for the reaction between complex 1 and oxidant.

Table. 5.5. Effective concentrations of APS alone and APS in presence of complex 1 for inactivation of microorganisms in NB/SDB media and SGW.

Table. 5.6. Effective concentrations of APS in presence of complex 1 for inactivation of microorganisms in NB/SDB media and SGW.

List of figures

CHAPTER 1

Fig. 1.1. Examples of natural and synthetic nanometer-sized materials.

Fig. 1.2. General scheme for a photocatalytic reaction.

Fig. 1.3. Photoinduced processes of photoirradiated TiO_2.

Fig. 1.4. Band positions (top of valence band and bottom of conduction band) of several semiconductors together with some selected redox potentials.

Fig. 1.5. Bulk structures of rutile and anatase TiO_2. In both structures, slightly distorted octahedral are the basic building units. The bond lengths and the angles of the octahedrally coordinated Ti atoms are indicated and the stacking of the octahedral in both structures is shown on the right side.

Fig. 1.6. Charge trapping reactions in UV/TiO_2 process.

Fig. 1.7. Major processes and their characteristic times for TiO_2-sensitized photooxidative mineralization of organic compounds by dissolved oxygen in aqueous solutions.

Fig. 1.8. Schematic of an irradiated TiO_2 semiconductor particle with possible photo-chemical and photo-physical processes.

Fig. 1.9. Major areas of applications of TiO_2 photocatalysis.

Fig. 1.10. (a-c) Schematic illustration of the process of *E. coli* photokilling on TiO_2 film. In lower row, the part of cell envelope is magnified.

Fig. 1.11. Possible mechanisms by which nanoparticles interact with biological tissue (Nel et al. 2006).

Fig. 1.12. TEM image showing the attachment of NPs to bacterial surfaces (a). Schematic illustration of NPs approaching to the bacterial cell surface and causing damage to cell envelope (b). Enlarged PE chemical structure, showing the potential damage caused by the NP surface as revealed by FTIR (c).

CHAPTER 2

Fig. 2.1. The gel obtained after the dialysis of the sol during the sol-gel synthesis of TiO_2.

Fig. 2.2. XRD pattern of TiO_2 nanoparticles synthesized by sol-gel method using titanium tetrachloride as the precursor.

Fig. 2.3. The TGA-DTA analysis plot of TiO_2 nanoparticles.

Fig. 2.4. TEM micrographs of TiO_2 nanoparticles.

Fig. 2.5. The N_2 adsorption-desorption isotherm of TiO_2 nanoparticles: (A) Hysteresis loops and (B) BJH pore size distribution.

Fig. 2.6. Antibacterial activity of TiO_2 nanoparticles against Gram positive and Gram negative bacteria irradiated with sunlight: A] *S. aureus*, B] *E. coli*, C] *K. pneumoniae*, D] *P. aeruginosa*.

Fig. 2.7. Antimicrobial activity of TiO_2 nanoparticles against microorganisms from treated sewage water sample exposed to: A] UV light, B] Sunlight.

Fig. 2.8. Photocatalytic degradation of methylene blue (0.1 mM) by aqueous TiO_2 nanoparticle dispersion as a function of irradiation time under: A] Sunlight, B] UV. light.

Fig. 2.9. Photocatalytic degradation of malachite green (0.1 mM) by aqueous TiO_2 nanoparticle dispersion as a function of 80 minutes of irradiation time under: A] Sunlight, B] UV light.

CHAPTER 3

Fig. 3.1. Antibacterial activity of N-TiO_2 at 50 µg/ml under visible light PBS.

Fig. 3.2. Antibacterial activity of Fe(C/N/S-TiO_2) at 50 µg/ml under visible light in PBS.

Fig. 3.3. Antibacterial activity of $AgTiO_2$ at 50 µg/ml under visible light in PBS.

Fig. 3.4. FTIR spectra of P-TiO_2.

Fig. 3.5. Antibacterial activity of P-TiO_2 at 50 µg/ml under visible light in PBS.

Fig. 3.6. FTIR spectra of FA-TiO_2, Fu-TiO_2, MA-TiO_2, SA-TiO_2 and S-TiO_2.

Fig. 3.7. Antibacterial activity of S-TiO_2 at 50 µg/ml under visible light in PBS.

Fig. 3.8. Antibacterial activity of FA/Fu/SA/MA-TiO_2 at 50 µg/ml under visible light in PBS.

Fig. 3.9. FTIR spectra of Arg-TiO_2 and Cys-TiO_2.

Fig. 3.10. Antibacterial activity of Arg-TiO_2 and Cys-TiO_2 at 50 µg/ml under visible light in PBS.

CHAPTER 4

Fig. 4.1. Photographs showing the comparison between antimicrobial activity of (A) FA-AgCl/TiO_2 and (B) AgCl/TiO_2 for the various test organisms (from top to

bottom) *E. coli*, *P. aeruginosa*, *M. luteus*, *S. aureus** and *C. albicans* at a concentration of 50 μg/ml. For *S. aureus** the concentration used was 100* μg/ml (C) shows the growth of test organisms in the absence of the nanocomposite.

Fig. 4.2. Antimicrobial activity of (A) Fu-AgCl/TiO_2 and (B) AgCl/TiO_2 for the test organisms, *E. coli* (top) and *M .luteus* (bottom) at a concentration of 100 μg/ml. (C) shows matt growth of cells in the absence of nanocomposite.

Fig. 4.3. X-ray diffractogram of A] FA-AgCl/TiO_2 and B] Fu-AgCl/TiO_2 nanoparticles showing peaks for the anatase phase of TiO_2 and cubic AgCl.

Fig. 4.4A. The N_2 adsorption-desorption isotherm plot for FA-AgCl/TiO_2.

Fig. 4.4B. Plot showing the average pore size distribution in FA-AgCl/TiO_2 nanocomposite.

Fig. 4.5. The N_2 adsorption-desorption isotherm of Fu-AgCl/TiO_2: (A) Hysteresis loops and (B) BJH pore size distribution.

Fig. 4.6. The TEM micrographs showing the nanocrystallite size of FA-AgCl/TiO_2 nanocomposite.

Fig. 4.7. The TEM micrographs showing the nanocrystallite size of Fu-AgCl/TiO_2 nanocomposite.

Fig. 4.8. Particle size analysis of FA-AgCl/TiO_2 nanocomposite by A] Intensity size distribution, B] Number distribution in DLS.

Fig. 4.9. The particle size analysis of Fu-AgCl/TiO_2 nanocomposite by A] Intensity size distribution B] Number distribution in DLS.

Fig. 4.10. The FTIR spectra of (A) FA-AgCl/TiO_2 and (B) AgCl/TiO_2 nanocomposite.

Fig. 4.11. The FTIR spectra of Fu-AgCl/TiO_2 nanocomposite.

Fig. 4.12. EDAX spectrum of AgCl/TiO_2 nanoparticles.

Fig. 4.13. SEM micrographs showing the intact *E. coli* cells unexposed to FA-AgCl/TiO_2 or Fu-AgCl/TiO_2 (a), *E. coli* cells exposed to 50 μg/ml of FA-AgCl/TiO_2 (b) and Fu-AgCl/TiO_2 (c) for 2 h. The micrographs clearly show the electron translucent regions (indicated by arrows) in the cells exposed to FA-AgCl/TiO_2 & Fu-AgCl/TiO_2.

Fig. 4.14. Effect of antioxidants, (A) Glutathione and (B) NAC on the antimicrobial activity of FA-AgCl/TiO_2 against *E. coli* at a concentration of 400 μg/ml in MHB. In presence of antioxidant (▨) and in the absence of antioxidant (■).

CHAPTER 5

Chart 5.1: Chemical structure of (a) complex 1, (1, 8-dimethyl-1, 3, 6, 8, 10, 13 hexaazacyclotetradecane) nickel (II) perchlorate) and (b) Ammonium persulphate.

Fig. 5.1. Figure showing the antibacterial effects of 20 μM Ni(II) complex solution + 5 μg/ml TiO_2 and 5 μg/ml TiO_2 alone, on Gram negative bacterial cultures *E. coli* (Left) and *K. pneumoniae* (Right).

Fig. 5.2. Figure showing the antibacterial effects of 20 μM Ni(II) complex solution + 5 μg/ml TiO_2 and 5 μg/ml TiO_2 alone, on Gram positive bacterial cultures *S. aureus* (Left) and *E. faecalis* (Right).

Fig. 5.3. Figure showing the antifungal effects of 20 µM Ni(II) complex solution + 5 µg/ml TiO_2 and 5 µg/ml TiO_2 alone, on *C. albicans*.

Fig. 5.4. Absorption spectrum of the complex 1 in water and the spectral changes changes on addition of oxidant ammonium persulphate in water. [Complex 1] = 250 µm and [Oxidant] = 1250 µM. The inset shows the d-d absorption band of complex 1 in water. [Complex 1] = 5.7 mM.

Fig. 5.5. Absorption changes with time at 300 nm for the solutions having 1:1, 1:2, 1:5 and 1:10 ratios of complex 1 and oxidant, respectively in water . [Complex 1] = 250 µm.

Fig. 5.6. Absorption spectral changes during the oxidation of complex 1 by ammonium persulphate in 1X NB medium. Formation of the trivalent nickel species with absorption maximum ~ 290 nm with time on addition of the oxidant to the complex 1. [Complex 1] = 250 µm and [oxidant] = 1250 µM. (inset) Change in the absorption at 300 nm Vs time and the first order fit for the absorption change.

Fig. 5.7. Absorption changes with time at 300 nm for the solutions with 1:1, 1:2, 1:5 and 1:10 ratios of complex 1 and oxidant, in 1X NB . [Complex 1] = 250 µm.

Fig. 5.8. Electron spin resonance spectrum observed after the addition of ammonium persulphate to complex 1 in NB medium. Temperature = 90 K. [Complex 1] = 265 µm [oxidant] = 2 mM.

Fig. 5.9. Picture showing the formation of pink coloured adduct (TBA-MDA) as a result of MDA reacting with thiobarbituric acid (TBA) in case of cells exposed to complex 1 and oxidant. [Complex 1] = 2.5 mM [oxidant] = 2 mM cell concentration of 10^8 cfu/ml were used in the assay. The pink coloured adduct is observed only in

case of complex 1 + oxidant, whereas no pink color formation was seen in the other three controls.

Fig. 5.10. Absorption spectra of the MDA-TBA adduct. The absorption band of adduct was clearly observed for the cells treated with complex 1 (2.5 mM) + oxidant (2 mM). The absorption of the adduct was not significant for the controls, i.e cells treated with 2.5 mM (complex 1); cells treated with 2 mM (oxidant); cells without complex 1 and oxidant (only *E.coli*). [Cell]= 10^8 cfu/ml.

Fig. 5.11. Scanning electron micrographs showing the effect of complex 1 + ammonium persulphate on *E. coli* cells after 30 minutes of incubation. A) *E. coli* cells after treatment with 312 μM complex 1 and 2 mM ammonium persulphate B) *E. coli* cells alone not treated with complex 1 or ammonium persulphate.

List of abbreviations and symbols

·OH – Hydroxyl radical

·OOH – Peroxyl Radical

$AgCl/TiO_2$ – Silver chloride TiO_2

APS – Ammonium perdisulphate

Arg-$AgCl/TiO_2$ – Arginine functionalized Silver chloride TiO_2

Arg-TiO_2 – Arginine modified TiO_2

BET – Brunauer-Emmett-Teller

BJH – Barrett, Joyner and Halenda

CB – Conduction band

Cfu/ml – Colony Forming Units per ml

COD – Chemical Oxygen Demand

-COOH – Carboxyl

Cys-$AgCl/TiO_2$ – Cysteine functionalized Silver chloride TiO_2

Cys-TiO_2 – Cysteine modified TiO_2

DCFH-DA – Dichlorofluorescein diacetate

DLS – Dynamic Light Scattering

EDAX – Energy-dispersive X-ray spectroscopy

Eg – Band gap energy

ESR – Electron Spin Resonance

FA-$AgCl/TiO_2$ – Folic acid functionalized Silver chloride TiO_2

FA-TiO_2 – Folic Acid modified TiO_2

Fe (C/N/S-TiO_2) – Iron (Carbon/Nitrogen/Sulphur) doped TiO_2

FTIR – Fourier Transform Infrared Spectroscopy

Fu-AgCl/TiO_2 – Fumaric acid functionalized Silver chloride TiO_2

Fu-TiO_2 – Fumaric Acid modified TiO_2

GSH – Glutathione

h^+ – Positive hole

hv – Light energy

LMCT – Ligand to Metal Charge Transfer

MA-AgCl/TiO_2 – Malic acid functionalized Silver chloride TiO_2

MA-TiO_2 – Malic acid modified TiO_2

MBC – Minimum Bactericidal Concentration

MDA – Malondialdehyde

MFC – Minimum Fungicidal Concentration

MIC – Minimum Inhibitory Concentration

MTCC – Microbial Type Culture Collection

NAC – N-acetyl cysteine

NCIM – National Centre for Industrial Microorganisms

-NH_2 – Amine

N-TiO_2 – Nitrogen doped TiO_2

$O_2^{\cdot -}$ – Superoxide anion

OH^- – Hydroxyl group

PBS – Phosphate Buffer Saline

P-TiO_2 – Phosphate modified TiO_2

ROS – Reactive Oxygen Species

SA-AgCl/TiO_2 – Succinic acid functionalized Silver chloride TiO_2

SA-TiO_2 – Succinic Acid modified TiO_2

SEM – Scanning Electron Microscopy

S-TiO_2 – Salicylic acid modified TiO_2

TBARS – Thiobarbituric Acid Reactive Substances Assay

TEM – Transmission Electron Microscopy

TGA – Thermogravimetric Analysis

TG-DTA – Thermogravimetric Differential Thermal Analysis

VB – Valence band

XRD – X-Ray Diffraction Analysis

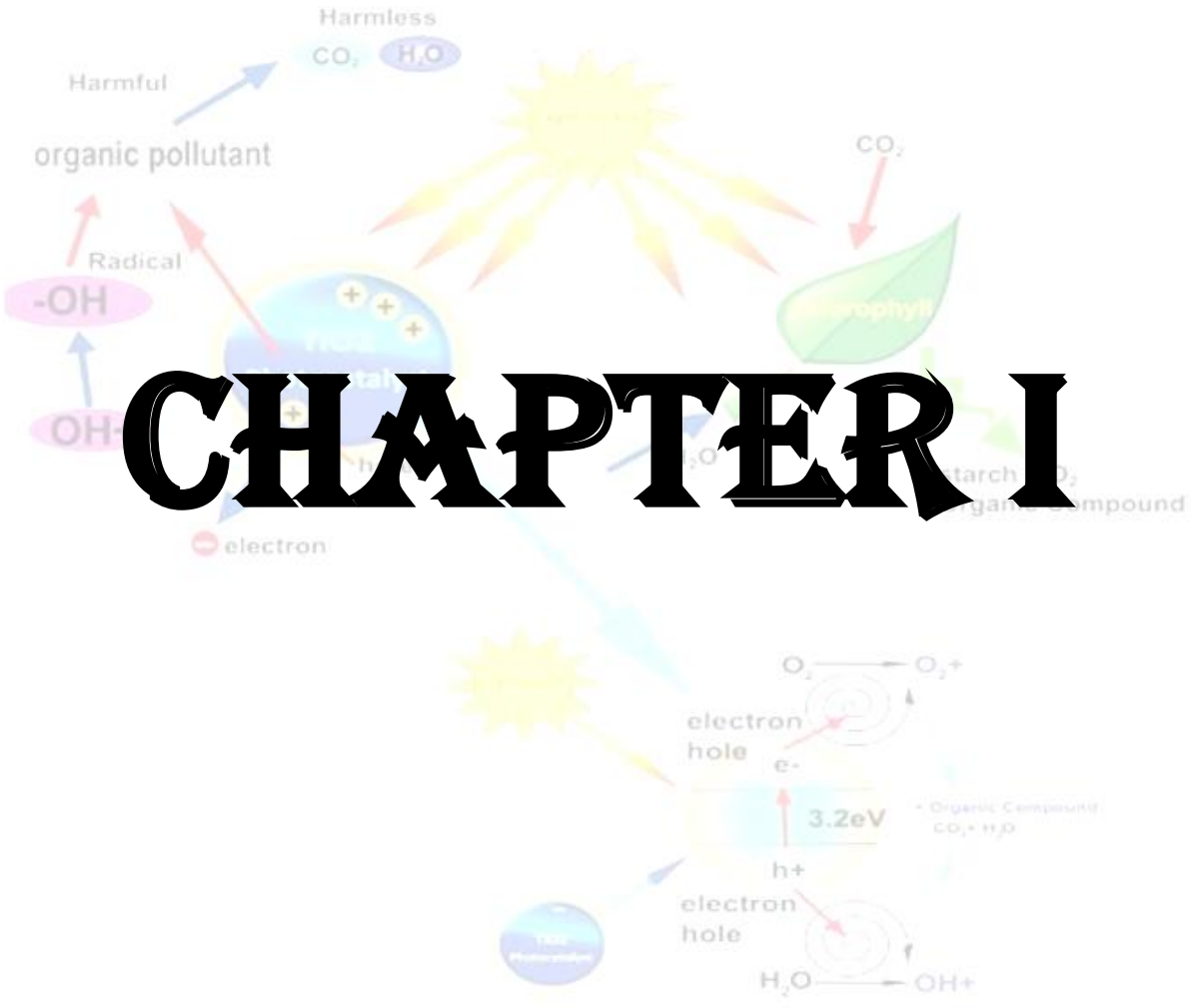
Harmless
CO_2
H_2O
Harmful
organic pollutant
Radical
-OH
OH-
electron
CO_2
O_2
O_2+
electron
hole
e-
3.2eV
h+
electron
hole
H_2O
OH+

CHAPTER I

Chapter 1

Introduction and Review of Literature

1.1 Introduction to Nano

Nanotechnology is an emerging interdisciplinary technology seeking to explore the unique technological advances of manipulating the structure of materials at a scale of individual atoms, molecules and their organised aggregates. The prefix *nano* in the word nanotechnology refers to a reduction of size, time, or volume/weight by 10^{-9} (Nanoscale). One nanometer (*nm*) is "one billionth of a meter" or is equivalent to ten angstroms (Kohler and Fritzsche, 2004; Hosokawa et al. 2007). To put things in perspective, Figure 1.1 shows various size ranges for different nanoscale objects starting with such small entities like ions, atoms and molecules. Size ranges of a few nanotechnology related objects (like nanotube, single-electron transistor and quantum dot diameters) are also shown (www.nano.gov).

The roots of the concept of nanotechnology may be traced back to 1959, when Richard Feynman, an American physicist, delivered a talk entitled "*There is plenty of room at the bottom*" at an American Physical Society meeting at California Institute of Technology. Though he did not explicitly mention "Nanotechnology", he suggested the eventual possibility of manipulating atoms and molecules precisely in a desired fashion to create molecular-machines. Inspired by Richard Feynman's talk, Eric Drexler in 1979, decided to put these ideas into motion and further the vision by manufacturing materials at molecular level. In 1981, Drexler published his first article titled "Molecular engineering: An approach to the development of general capabilities for molecular manipulation," that expanded the idea of molecular manufacturing. Subsequently as the concept of nanotechnology continued to evolve he published his

now infamous book "Engines of Creation: The Coming Era of Nanotechnology" in which he used the word nanotechnology to describe engineering on the billionth of a meter scale.

According to the National Nanotechnology Initiative (NNI), "Nanotechnology is the understanding and control of matter at dimensions of approximately 1 to 100 nm, where properties of matter differ fundamentally from those of individual atoms, molecules or bulk materials and involves manipulating matter at this scale, to understand and create materials to exploit this phenomenon for novel applications (Lewis et al. 2003). By manipulating the structural arrangements and bonding of atoms, novel materials can be designed with a vast range of physical, chemical and biological properties.

These nanomaterials are envisaged to have a substantial impact on diverse range of areas such as agriculture, communication, energy generation/transmission, environmental monitoring, food manufacturing/processing, health care and medicine. In general, nanotechnology is acknowledged to represent a new frontier in science and technology of the 21st century.

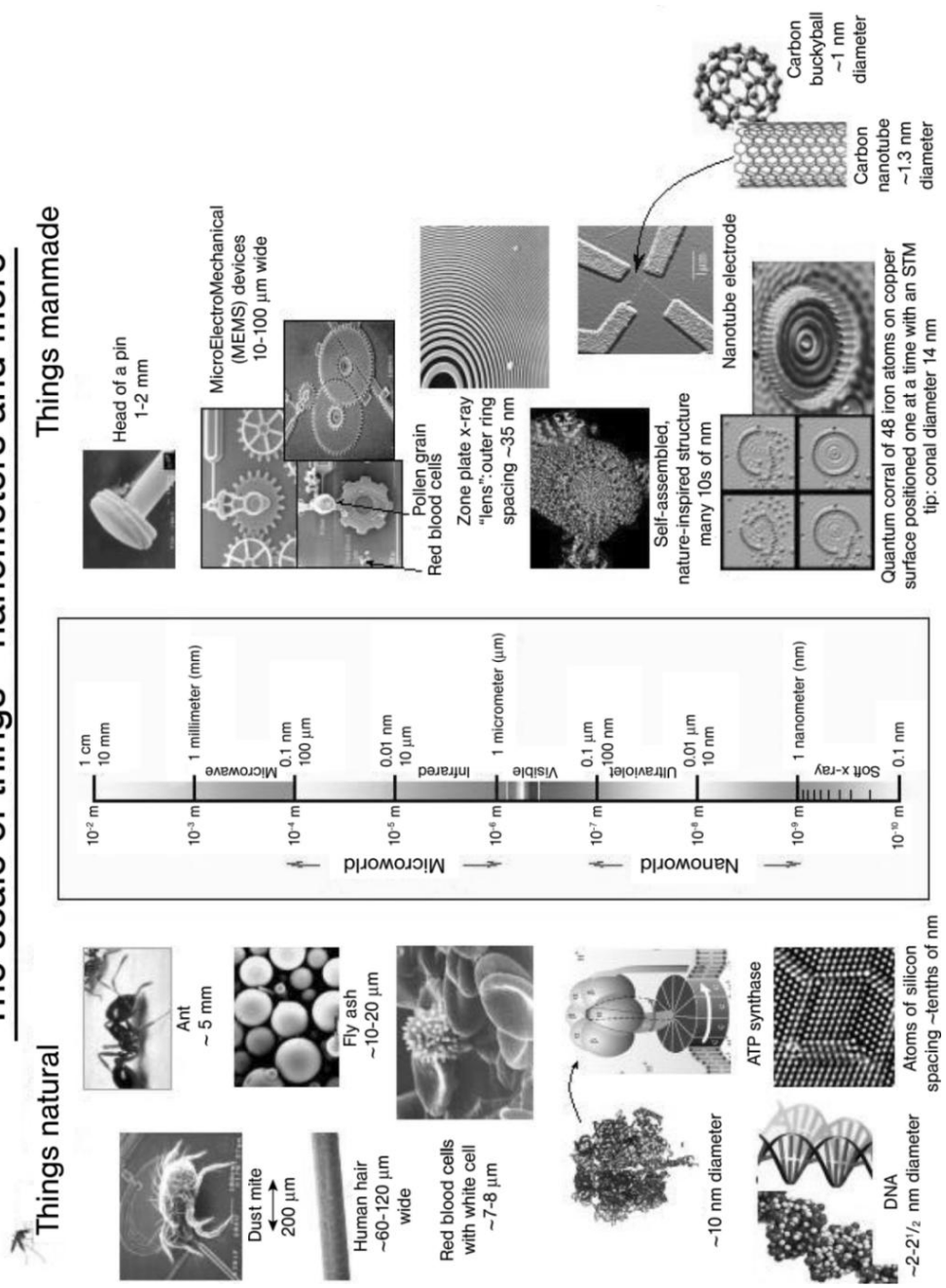

Fig. 1.1. Examples of natural and synthetic nanometer-sized materials.

There are several reasons why nanoscale technology has become so important (Kohler and Fritzsche, 2004; Cao G. 2004; Hosokawa et al. 2007):

(i) The nanomaterials at the nanoscale exhibit rather unique properties (Quantum effects) as compared to their bulk counterparts. Hence, by the nanoscale design of materials it is possible to vary the properties, such as strength, color, conductivity, thermal behavior, magnetization, and toxicity without changing their chemical composition.

(ii) A key feature of the nanomaterials is their size, and nanoscale operates at the same scale as our biological molecules and pathways. This means nanoscale materials can easily enter most cells without triggering any immune response. Hence, nanoscale materials can be designed to interact with biological entities in a more direct, efficient and precise manner and help understand the biological processes and pathways in much detail. Such nanomaterials can also be powerful tools for detection, diagnosis and treatment of diseases at the molecular level. This certainly can be a powerful combination of biology with materials science.

(iii) In miniaturization of solid particles the specific surface area increases generally in inverse proportion to the particle size. Hence, nanoparticles have very high surface to volume ratio, which makes them ideal for use in composite materials, reacting systems, drug delivery etc.

(iv) Macroscopic devices constructed using nanomaterials can have much higher density, conductivity as compared to those made up of microstructures. Such devices can be used in high-power rechargeable battery systems, thermoelectric materials, high-efficiency/low-cost sensors and electronics, thin-film smart solar panels for

efficient conversion of sunlight to electricity, and additives for enhanced catalysis, by controlling interactions and behavior at the nanoscale.

The two important areas that nanotechnology is likely to have a major impact are environmental remediation/disinfection and medical technology. The emergence of new crop of alternative disinfection technologies (AOTs) such as heterogeneous photocatalysis (HP) and SODIS (SOlar DISinfection) has been a very significant step in the direction of the concept of "green technologies" (Masakazu A. 2000; Diebold U. 2003). Over the last couple of decades the scientific and engineering interest in the application of semiconductor photocatalysis has increased exponentially. Semiconductor photocatalysis with major emphasis on TiO_2 as a durable photocatalyst has been applied to a variety of problems of environmental interest such as air purification, wastewater treatment (Peral et al. 1997; Hur and Koh, 2002), photodegradation of toxic organic compounds, disinfection (Huang et. al., 1999; Maness et. al, 1999; Vohra et. al, 2005), photosplitting of water to produce hydrogen gas (Fujishima and Honda, 1972; Fujishima et al. 2000; Hashimoto et al. 2005), nitrogen photofixation (Carp et al. 2004), cleanup of oil spills (Carp et al. 2004) etc (Fig. 1.3). A number of technologies have been proposed and applied over the years for the removal of toxic organic pollutants from wastewaters (Herrmann JM, 2005; Serpone et al. 2005; Teoh et al. 2012) but most of these methods have a problem of secondary disposal. On the other hand, for photocatalytic processes there is no further requirement of secondary disposal, and expensive oxidizing chemicals, as ambient oxygen is the oxidant (Beydoun et al. 1999; Matthews et al, 1993). In addition, the photocatalysts are also self-regenerated and can be reused or recycled.

1.2 Basic Principles of Heterogeneous Photocatalysis

In a heterogeneous photocatalytic system, the semiconductor particles (photocatalyst) are in close contact with the fluid (liquid or gaseous) reaction medium. On exposure of photocatalyst to light, excited states are generated which initiate a cascade of redox reactions and molecular transformations (Beydoun et al. 1999; Fujishima et al. 2000; Thompson and Yates. 2006). In fig. 1.2, simplified reaction scheme of photocatalysis is shown. The electronic structure of semiconductors (metal oxides such as ZnO, TiO_2, Fe_2O_3) is characterized by a filled valence band (VB) and an empty conduction band (CB), and they can act as sensitizers for light-induced redox reactions. The difference in the energy between the lowest energy level of the CB and the highest energy level of the VB is called band gap energy (Eg), which is defined as the minimum energy of light required to make the material electrically conductive (Fox and Dulay. 1995; Thompson and Yates. 2006; Teoh et al. 2012).

The irradiation of a semiconductor with a photon of energy hν, that exceeds its band gap energy results in the excitation of an electron from the valence band (VB) to the conduction band (CB), leaving a positive hole behind. In electrically conducting materials like metals, the produced charge-carriers are immediately recombined. However, in semiconductors a part of these photoexcited electron-hole pairs (EHPs) diffuse to the surface (electron-hole pairs are trapped at the surface) and participate in the chemical reaction with the adsorbed donor (D) or acceptor (A) molecules. The positive holes can oxidize donor molecules (1) whereas, the conduction band electrons can reduce appropriate electron acceptor molecules (2). However, in the absence of any electron and hole scavengers, the stored energy is dissipated by recombination.

$$D + h^+ \rightarrow D^{\bullet+} \qquad (1)$$

$$A + e^- \rightarrow A^{\bullet-} \qquad (2)$$

In semiconducting metal oxides the holes (h^+) can react in a one-electron oxidation step with water (3) to produce highly reactive hydroxyl radical ($^{\cdot}OH$). In presence of water, the photogenerated electrons reduce the water molecules to produce H_2, while the positive holes oxidize them to produce O_2, leading to overall water splitting. The resultant holes as well as the hydroxyl radicals are highly reactive oxidants and can oxidize a number of organic contaminants.

$$H_2O + h^+ \rightarrow {}^{\cdot}OH + H^+ \qquad (3)$$

Further, the oxygen in the air acts as an electron acceptor (4) and catalyses the formation of super-oxide ion $O_2^{\cdot-}$.

$$O_2 + e^- \rightarrow O_2^{\cdot-} \qquad (4)$$

Super-oxide ions are also highly reactive species that can oxidize organic materials. Hence, in the EHPs, the excited electrons with high redox activities react with water and oxygen to generate reactive oxygen species (ROS), such as super oxide anions (O_2^-) and hydroxyl radicals ($^{\cdot}OH$). The process of photocatalysis is highly versatile and different possibilities of $^{\cdot}OH$ radical production could be adapted for specific treatment requirements (Galvez et. al. 2007; Fujishima et al. 2000).

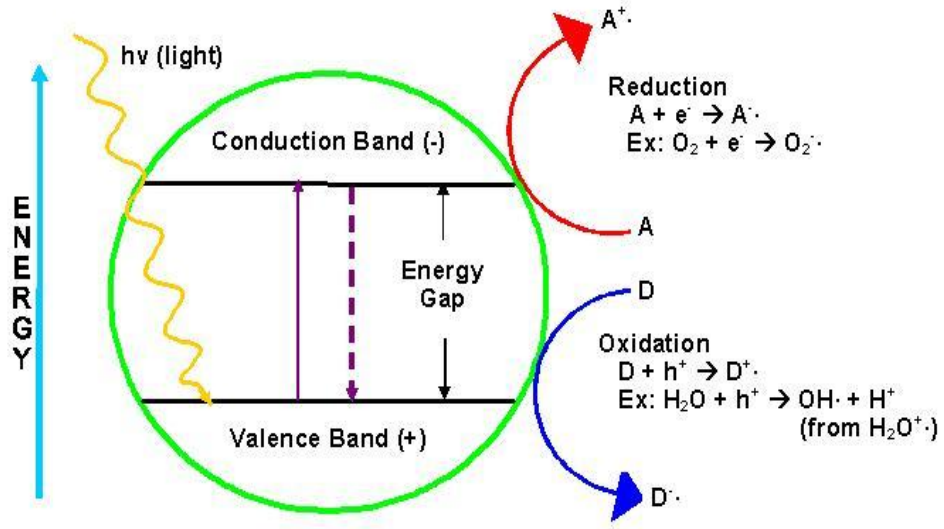

Fig. 1.2. General scheme of a photocatalytic reaction

1.3 Titanium dioxide (TiO_2) as a photocatalyst

Semiconductor photocatalysis, with a primary focus on TiO_2, has been applied to a number of problems of environmental interest such as water and air purification (Chen and Mao, 2007; Teoh et al. 2012; Kamat and Meisel, 2003). The oxygen vacancies in TiO_2, makes it a n-type semiconductor, transition metal oxide (Carp et al. 2004; Diebold U. 2003). Its industrial production started in the beginning of the 20th century, to replace the toxic lead oxides as pigments for white paint and its usage has exponentially increased in the last few years in fields like textiles, food (as a food colorant and food additives), leather and pharmaceuticals (tablet coatings, toothpaste, in sunscreen cream and other cosmetic products). Several semiconductors such as WO_3, $SrTiO_3$, ZnO and ZnS, have been studied for catalysing a broad range of chemical reactions. However, TiO_2 seems the most promising for photocatalytic destruction of organic pollutants in terms of catalytic performance and stability in

aqueous media (Kamat and Meisel, 2003; Diebold U. 2003). The anatase phase of TiO_2 has the highest photocatalytic activity (Bahnemann et al., 1993) and has received a great deal of attention due to its chemical stability, insolubility in water, non-toxicity, low cost, and other advantageous properties.

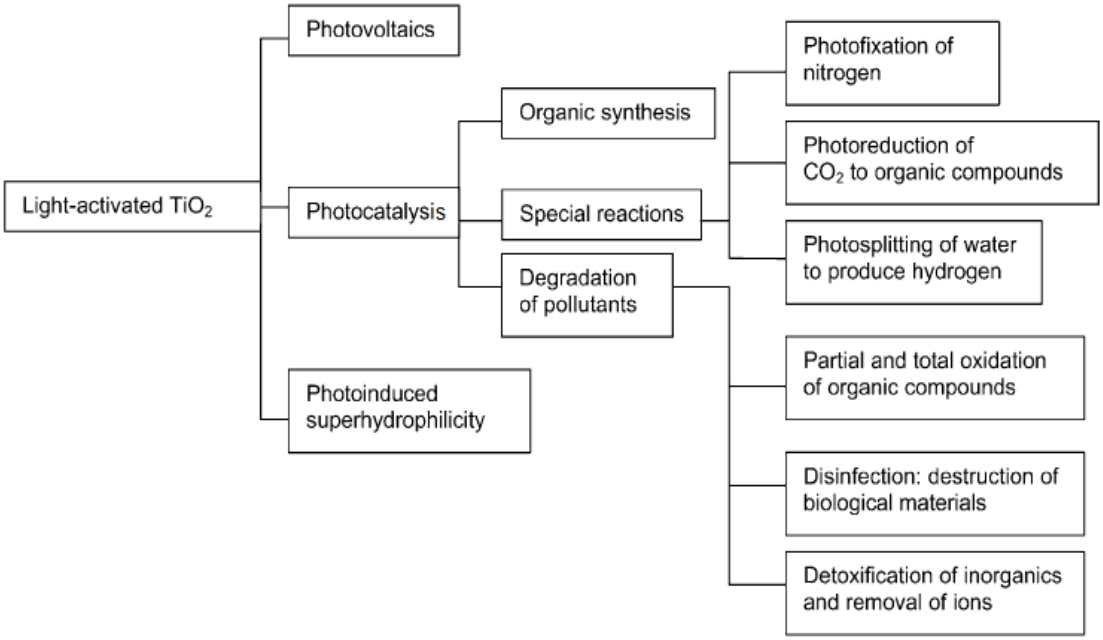

Fig. 1.3. Photoinduced processes of photoirradiated TiO_2 (Carp et al. 2004)

A photocatalyst has the capability to adsorb two reactants simultaneously, which may be reduced and oxidized by photoactivation. Also, the band energy positions of the photocatalyst and the redox potential of the adsorbates play a vital role in the ability of a photocatalyst to catalyze photoinduced electron transfer (Fig. 1.4). The energy level at the bottom of the conduction band determines the reduction potential of photoelectrons and at the top of valence band determines the oxidizing ability of the photoholes.

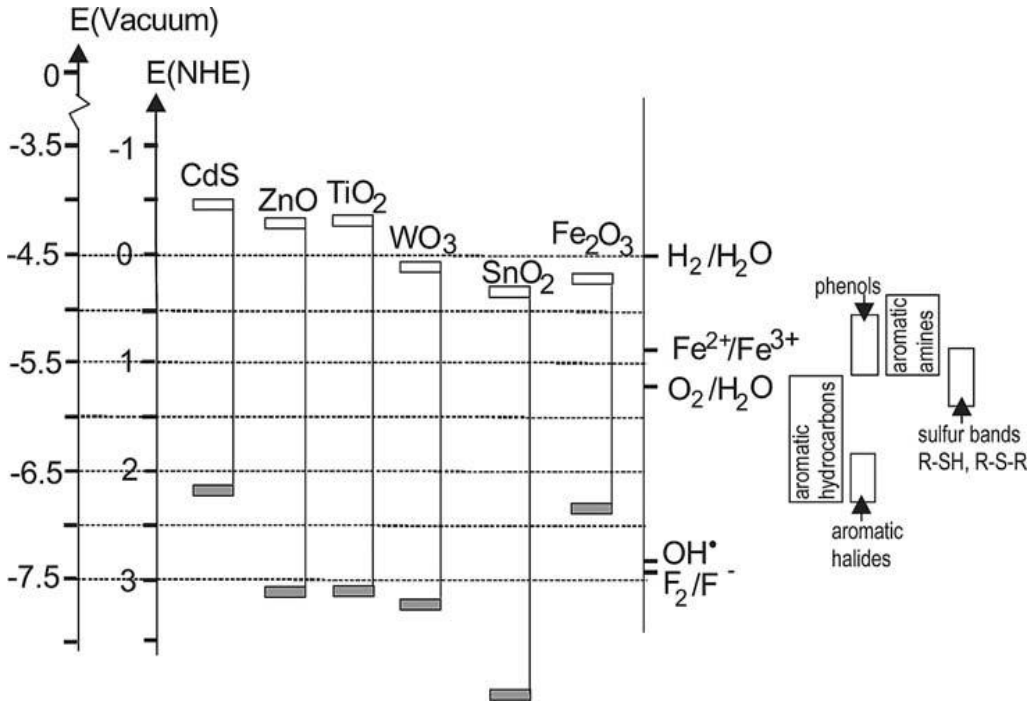

Fig. 1.4. Band positions (top of valence band and bottom of conduction band) of several semiconductors together with some selected redox potentials (Carp et al. 2004).

Unlike metals, semiconductors do not have a range of interband states that facilitate the recombination of electron-hole pairs, and assure a sufficiently long lifetime for e^--h^+ pair to diffuse to the catalyst's surface and initiate a redox reaction (Carp et al. 2004). The anatase and rutile TiO_2 have different densities and electronic band structures (for bulk materials: anatase 3.20 eV and rutile 3.02 eV) leading to different band gaps and absorption thresholds of 384 and 410 nm, respectively.

1.4 Chemical structure of TiO_2

TiO_2 has four commonly known crystalline forms viz: anatase (tetragonal), brookite (orthorhombic), rutile (tetragonal), and TiO_2 (B) (monoclinic) (Carp et al. 2004; Diebold U. 2003). Besides these crystalline forms, two more forms have been synthesized from the rutile phase, TiO_2 (II) with a PbO_2 structure and TiO_2 (H) with a

hollandite structure. The structures of rutile, anatase and brookite can be discussed in terms of (TiO_2^{6-}) octahedrals (Table 1.1) (Ohno et al. 2001; Carp et al. 2004; Diebold U. 2003). The three crystal structures differ by the distortion of each octahedral and the assembly patterns of the octahedral chains. The TiO_6 octahedron is slightly distorted and both rutile and anatase have tetragonal crystal lattice but the number of common edges in TiO_6 octahedra is two for rutile and four for anatase (Carp et al. 2004; Diebold U. 2003).

Rutile: Rutile TiO_2 has a tetragonal structure with 6 atoms per unit cell (Fig. 1.5). The rutile phase is thermostable at most temperatures and pressures up to 60 kbar, and is the thermodynamically favorable phase. Zhang et al. found that anatase and brookite structures transformed to the rutile phase after reaching a certain particle size, with the rutile phase becoming more stable than anatase for particle sizes greater than 14 nm. The activity of rutile phase as a photocatalyst is generally very poor (Gupta and Thripathi, 2011; Carp et al. 2004; Diebold U. 2003; Mo and Ching, 1995).

Anatase: Anatase TiO_2 also has a tetragonal structure but the distortion of the TiO_6 octahedron is slightly larger for the anatase phase (Fig. 1.5). Anatase phase is thermodynamically stable at 800 °C, but above that it transforms to rutile phase and the reverse transition on cooling does not occur due to high activation energy required. The higher photoreactivity of anatase is attributed to a slightly higher Fermi level, lower capacity to absorb oxygen and higher degree of hydroxylation in the anatase phase. Anatase also has a higher adsorptive affinity for organic compounds and exhibits lower rates of recombination due to its higher rate of hole trapping (Gupta and Thripathi, 2011; Carp et al. 2004; Diebold U. 2003).

Brookite: Brookite TiO_2 belongs to the orthorhombic crystal system with its unit cell composed of 8 units of TiO_2, formed by edge-sharing TiO_6 octahedra. Its crystals are dark brown to greenish black opaque. It has a larger cell volume with 8 TiO_2 per unit cell, but less density compared to the other two polymorphs (Gupta and Thripathi, 2011).

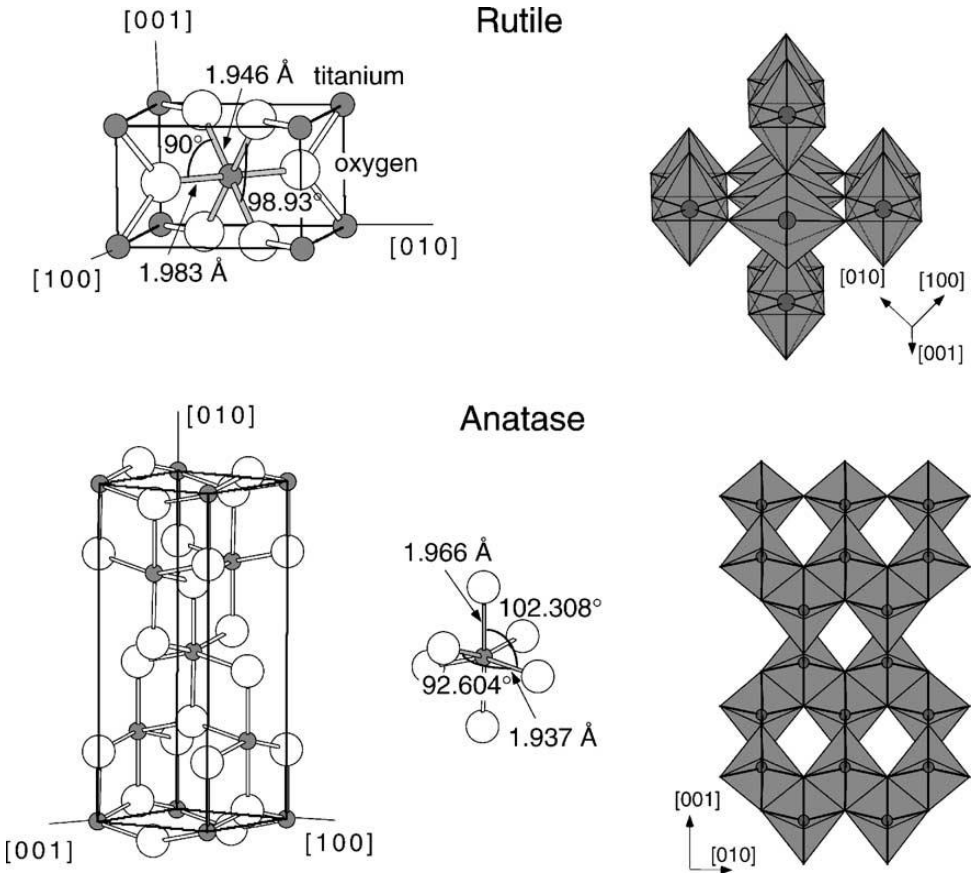

Fig. 1.5. Bulk structures of rutile and anatase TiO_2. In both structures, slightly distorted octahedral are the basic building units. The bond lengths and the angles of the octahedrally coordinated Ti atoms are indicated and the stacking of the octahedral in both structures is shown on the right side (Diebold U. 2003).

Table. 1.1. Crystal structure data of major TiO_2 polymorphs (Carp et al. 2004; Diebold U. 2003).

Crystal structure	System	Space group	Lattice constants (nm)			
			a	*b*	*c*	*c*/*a*
Rutile	Tetragonal	D_{4h}^{14}-$P4_2/mmm$	0.4584	–	0.2953	0.644
Anatase	Tetragonal	D_{4h}^{19}-$I4_1/amd$	0.3733	–	0.937	2.51
Brookite	Rhombohedral	D_{2h}^{15}-Pbca	0.5436	0.9166	–	0.944
Density (kg/m^3)						
Rutile	4240					
Anatase	3830					
Brookite	4170					
Dielectric properties	Frequency (Hz)	Temperature (K)	Dielectric constant			
Rutile, perpendicular to optical *c*-axis	10^8	290–295	86			
Rutile, parallel to optical *c*-axis	–	290–295	170			
Rutile, perpendicular to optical *c*-axis	10^4	298	160			
Rutile, along *c*-axis	10^7	303	100			
Anatase, average	10^4	298	55			
Band gap (eV)						
Rutile	3.05					
Anatase	3.26					
Refractive index	n_g	n_p				
Rutile	2.9467	2.6506				
Anatase	2.5688	2.6584				
Brookite	2.809	2.677				

1.5 Synthesis of nanoparticles

TiO_2 can be synthesized as powder, crystals, or thin films of varying size range. Various synthesis methods produce TiO_2 particles with different crystallinity, porosity and surface properties, all of which play an important role in the overall photocatalytic activity of TiO_2. Both powders and films can be built up from crystallites ranging from a few nanometers to several micrometers. It should be noted that nanosized crystallites tend to agglomerate which decreases their overall activity and hence an ideal method should be the one which allows control over the size,

morphology and crystallinity of the nanoparticles, is economical and environment friendly (Carp et al. 2004). Some of the gas phase methods commonly used for the synthesis of nanoparticles such as, chemical vapor deposition (CVD) and physical vapor deposition (PVD) are discussed below.

1.5.1 Gas phase methods

1.5.1.1 Chemical vapor deposition (CVD)

Vapor deposition is a technique where the materials in their vapor state are condensed to form a solid-state material (Kohler and Fritzsche, 2004; Hosokawa et al. 2007). This is a versatile technique used to coat large surface areas and produce optoelectronic thin films, semiconductor thin films and to infiltrate fabric to form composite materials. The vapor deposition process is usually carried out in a vacuum chamber, where the gases are heated up that drives the deposition reaction. The phase and morphology of the nanoparticles such as TiO_2 can be controlled by regulating the reaction conditions (Carp et al. 2004). The stoichiometry for CVD can be easily controlled by monitoring the flow rates of the precursors, and this method generally gives high purity thin films. However, some CVD processes require high deposition temperatures, which are sometimes detrimental to the substrate itself. The precursors required for the CVD processes are often toxic and so are the byproducts produced during the process.

1.5.1.2 Physical vapor deposition (PVD)

In PVD the thin films are formed from the gas phase where materials are first evaporated and then condensed. The evaporated atoms travel at a very high velocity in straight-line trajectories and can be applied for metal and metal compounds. Therefore, the substances used in this method should be stable in the gas phase. Some

of the PVD methods include thermal deposition, ion implantation, sputtering, ion plating etc (Kohler and Fritzsche, 2004; Hosokawa et al. 2007; Carp et al. 2004). It is preferable that the evaporation take place under reduced pressure as it reduces the rate of collision of gas molecules and protects the deposited films. The PVD technique enables the deposition of materials with improved properties compared to the substrate material and almost any inorganic material and some organic materials can be used. Also the process of PVD is quite environment friendly as compared to processes such as electroplating. However, since the deposition takes place in typically straight lines the substrate may not be completely covered as this leads to shadowing effects. Some of the PVD processes require high vacuums and temperatures and the deposition rates in PVD are generally slower. Also, varying the evaporation rates makes the stoichiometry hard to control (Rodriguez and Fernancez-Garcia, 2007).

1.5.2 Solution routes

Liquid-phase processing is a convenient and widely used method for the synthesis of nanoparticles for applications in thin films. This method allows control over the stoichiometry, producing homogeneous materials, and for preparation of composite materials. The most commonly used solution routes in the synthesis of TiO_2 are microemulsion, hydrothermal, solvothermal and sol-gel methods (Cao G. 2004; Chen and Mao, 2007).

1.5.2.1 Microemulsion method

Water-in-oil microemulsion (Micelle) has been successfully applied for the synthesis of nanoparticles. Microemulsions are thermodynamically stable, optically isotopic solutions of two immiscible liquids stabilized by an interfacial layer of surfactant.

Generally, in micelles the polar (hydrophilic) head orient towards the surrounding and the long-chained aliphatic (hydrophobic) tail orient towards inside of the micelle. The surfactant molecules optimize their interactions at the two-liquid interface, thereby reducing the interfacial tension. There have not been many reports on the controlled synthesis of titania using this method. In particular, hydrolysis of titanium alkoxides in microemulsions using sol-gel methods has caused uncontrolled agglomeration and flocculation except at very low concentrations (Carp et al. 2004; Chen and Mao, 2007). The TiO_2 nanoparticles prepared with the microemulsion methods normally have amorphous structure, and usually require calcination to induce high crystallinity. The crystallinity can be improved by annealing the nanoparticles in presence of micelles at temperatures lower than those required for traditional calcination for solid state materials.

1.5.2.2 Hydrothermal Method

The hydrothermal synthesis method is widely used for the synthesis of small particles in a closed system, normally carried out in steel pressure vessels called autoclaves with or without Teflon liners under controlled conditions of temperature and/or pressure in aqueous solutions. The major parameters that determine the kinetics of the process and the properties of the end product are the initial pH of the medium, the duration of the temperature-pressure conditions in the system and the concentration of the precursor and other solvents inside the system. The temperature for hydrothermal syntheses varies from 150-200 ℃, and along with the volume of the solution in the autoclave determines the pressure produced inside the vessel (Carp et al. 2004; Rodriguez and Fernancez-Garcia, 2007; Chen and Mao, 2007). The particle sizes can be controlled by adjusting the concentration of titanium precursor and the solvents. Hydrothermal method is also used for the synthesis of TiO_2 nanostructures with

controlled crystallinity and morphology (such as nanorods, nanowires and nanotubes) by varying the hydrothermal conditions inside the closed vessel and also by varying the concentration of the solvent system. However, the disadvantages of the system are the high cost of the equipment, maintaining the closed reaction system for prolonged time at high temperature-pressure conditions and inability to monitor the crystals in the process of their growth (Rodriguez and Fernancez-Garcia, 2007).

1.5.2.3 Solvothermal method

Solvothermal synthesis method is similar to the hydrothermal method of nanoparticle synthesis but in solvothermal method, solvents used are non-aqueous. Hence, in solvothermal method temperature can be elevated much higher than hydrothermal method, a number of solvents with high boiling points can be used. The solvothermal synthesis method is better for synthesis of nanoparticle with narrow size distribution, controlled particle morphology, and crystallinity by regulating the precursor/surfactant/solvent weight ratio, reaction temperature, pressure, additives, and the ageing time. Solvents with different physicochemical properties also influence the reactivity and solubility of the reactants which can further affect the morphology and crystallization behavior of the nanostructures. However, the disadvantages of this method are the need for expensive solvents, long processing times, and the presence of carbon as an impurity (Rodriguez and Fernancez-Garcia, 2007).

1.5.2.4 Sol-gel method

In sol-gel methods, two syntheses routes are known: the non-alkoxide and the alkoxide route and oxides with different physicochemical properties may be obtained depending on the synthetic approach used. The non-alkoxide route uses inorganic salts (such as nitrates, chlorides, acetates, carbonates, acetylacetonates etc.), while the

alkoxide route (the most employed) uses metal alkoxides as starting material. In a typical sol-gel process, a colloidal suspension (sol) is formed from the hydrolysis and polymerization reactions of the precursors, which are usually inorganic metal salts or metal organic compounds such as metal alkoxides (Sreethawong et al. 2005; Su et al. 2004). After complete polymerization and removal of solvent the liquid sol forms a solid gel phase. The sol-gel method is advantageous over the other methods in terms of the purity, homogeneity and flexibility in introducing dopants in large concentrations, stoichiometry control, ease of processing, control over the composition, and the ability to coat large and complex areas. TiO_2 nanomaterials have been synthesized with the sol-gel method from hydrolysis of a titanium precursor, which proceeds by an acid-catalyzed hydrolysis step of titanium (IV) alkoxide followed by condensation. The development of Ti-O-Ti chains is favored with low water content, low rates of hydrolysis, and excess titanium alkoxide in the reaction mixture. The growth kinetics study of TiO_2 nanoparticles in aqueous solution indicates that, the rate constant for coarsening increases with temperature because of the temperature dependence of viscosity of the solution and the equilibrium solubility of TiO_2. These reactions are then subjected to heat treatment (450-600 ℃) to remove the organic part and crystallize either anatase or rutile TiO_2. The calcination at high temperatures causes a decrease in surface area (due to sintering and crystal growth), coupled with loss of surface hydroxyl groups and even induces phase transformation. A prolonged heating time for the gel at ≤ 100 ℃ can avoid the agglomeration of the TiO_2 nanoparticles during crystallization process (You et al. 2005). The advantages of sol-gel synthesis include its simplicity, ability to form nanoparticles with high surface area and crystallinity make it an ideal method for nanoparticle synthesis. This method has been used for the synthesis of TiO_2 nanoparticles in this thesis.

1.6 Mechanism of heterogeneous photocatalysis

According to IUPAC (International Union of Pure and Applied Chemistry) chemical terminology, photocatalysis is defined as a "catalytic reaction involving light absorption by a catalyst or by a substrate." The mass transfer in a UV/TiO_2 photocatalytic process depends on the reactant/product concentration as well as photocatalyst dosage and particle size (Tanaka et. al. 1991; Tahiri et. al. 1996; Riegel and Bolton, 1995). The photocatalytic reaction occurs upon absorption of a photon by TiO_2 producing electron-hole pairs (e^--h^+) that diffuse to the surface of the TiO_2 photocatalyst. The charged electrons reduce O_2 to form superoxide ($O_2^{\cdot}$), whereas, the holes oxidize water to form hydroxyl radicals ($OH^{\cdot}$). Thus, the reductive and oxidative abilities of electron-hole pairs leads to the production of strong oxidizing agents that can oxidize organic compounds and mineralize them completely (Fox and Dulay, 1993; Hoffmann et al. 1995; Herrmann JM. 2005) (Scheme 1.1):

1.6.1 Charge-carrier generation

Upon irradiation of TiO_2 with light energy greater than its bandgap energy, electrons are transferred from the valence band to the conduction band, leaving a positive hole behind to form paired e^--h^+.

$$TiO_2 + h\nu \rightarrow TiO_2 (h^+_{vb} + e^-_{cb}) \quad (5)$$

Consequently, the TiO_2 particle can either act as an electron donor or acceptor for molecules in the surrounding medium. Also, the redox capability of a photoexcited semiconductor particle in aqueous solution can be estimated from the band-edge positions of valence and conduction bands. The electrons possess the reducing power of the conduction band energy while the holes have the oxidizing power of the

valence band. As a result, photo-excitation of the semiconductor can lead to chemical (redox) reactions.

1.6.2 Charge-carrier trapping

The e^{-}-h^{+} pairs are trapped by electron and hole scavengers and prevented from recombination. In the presence of adsorbates in equilibrium with a gaseous, liquid or aqueous phase, electrons are attracted by electron acceptors, whereas the photoinduced holes react with electron donors. Reactions involving the electrons and holes should proceed simultaneously to suppress the recombination of electrons and holes. Therefore the effective removal of electrons is essential for efficient photocatalytic oxidation.

1. Hole trapping

On diffusing to the TiO_2 particle surface, the positively charged trapped holes can directly oxidize adsorbate pollutants or react with surface hydroxyl groups (OH^{-}) or adsorbed water molecules to form hydroxyl radicals ($^{\cdot}OH$) (Hoffmann et al. 1995; Fujishima et al. 2008).

$$h^{+} + H_2O \rightarrow {}^{\cdot}OH + H^{+} \quad (6)$$

$$h^{+} + OH^{-} \rightarrow {}^{\cdot}OH \quad (7)$$

2. Electron trapping

Molecular oxygen prevents e^{-}-h^{+} pair recombination through the reduction of oxygen with e^{-}, and reactive superoxide radical anions ($O_2^{\cdot -}$). The final product of the reduction may be oxidizing species such as H_2O_2, $HO_2^{\cdot}$ and $^{\cdot}OH$ radicals which would be generated through subsequent reactions (Hashimoto et al. 2005; Henderson, 2011).

$$O_2 + e^-_{cb} \rightarrow O_2^{\cdot -} \quad (8)$$

$$O_2^{\cdot -} + H^+ \rightarrow HO_2^{\cdot} \quad (9)$$

$$2HO_2^{\cdot} \rightarrow H_2O_2 + O_2 \quad (10)$$

$$O_2^{\cdot -} + HO_2^{\cdot} \rightarrow HO_2^- + O_2 \quad (11)$$

$$HO_2^- + H^+ \rightarrow H_2O_2 \quad (12)$$

$$H_2O_2 + e^- \rightarrow {}^{\cdot}OH + OH^- \quad (13)$$

Hydroxyl radicals are known to be strong, oxidizing agents and can react with organic compounds adsorbed onto the semiconductor surface and cause complete degradation to carbon dioxide and water. For a comparison, the oxidation potential of hydroxyl radical ($^{\cdot}OH$) is 2.8 V relative to the normal hydrogen electrode (NHE). Other substances which are commonly used for water disinfection such as ozone, H_2O_2, HOCl and chlorine have an oxidation potential of 2.07 V, 1.78 V, 1.49 V and 1.36 V, respectively (Carp et al. 2004).

1.6.3 Charge-carrier recombination

The various processes occurring during photocatalysis have been determined to have characteristic time as indicated in Figure 1.7. The e^--h^+ pairs generation upon absorption of a photon is extremely fast (fs) and the trapping of electrons and holes takes nanoseconds (ps-10 ns). Recombination has a characteristic time of 10 to l00 ns and the interfacial transfer of holes is slow (~100 ns).

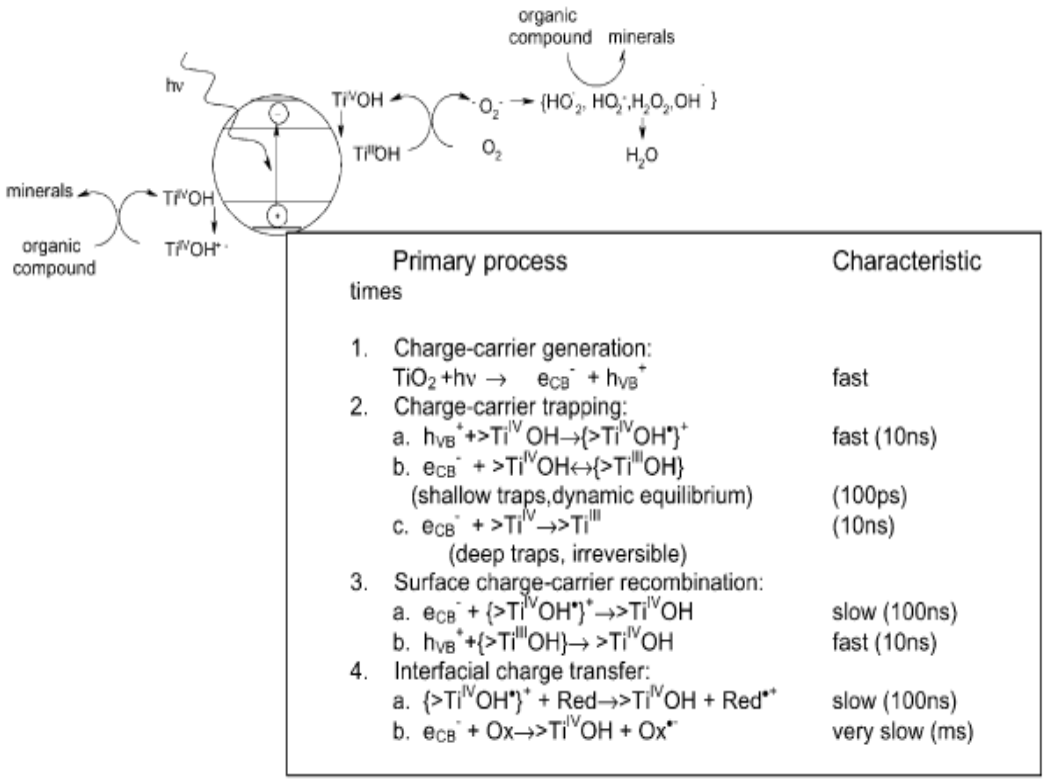

Fig. 1.7. Major processes and their characteristic times for TiO_2-sensitized photooxidative mineralization of organic compounds by dissolved oxygen in aqueous solutions (Carp et al. 2004).

Photocatalytic efficiency is often controlled by the suppression of e^--h^+ pair recombination, carrier trapping and interfacial charge transfer (Hoffmann et al. 1995; Fujishima et al. 2000). The e^--h^+ pairs recombination can occur in the volume of the semiconductor particle surface with release of heat.

$$e^- + h^+ \rightarrow TiO_2 + \text{heat} \qquad (14)$$

EQUATION	ELECTRONIC STEPS
$TiO_2 + h\nu \rightarrow e^-_{CB} + h^+_{VB}$ $M^{n+} + h\nu \rightarrow M^{(n+1)+} + e^-_{CB}$ $M^{n+} + h\nu \rightarrow M^{(n-1)+} + h^+_{VB}$	**charge generation**
$Ti^{4+} + e^-_{CB} \rightarrow Ti^{3+}$ $M^{n+} + e^-_{CB} \rightarrow M^{(n-1)+}$ $M^{n+} + h^+_{VB} \rightarrow M^{(n+1)+}$ $OH^- + h^+_{VB} \rightarrow OH^\bullet$	**charge trapping**
$M^{(n-1)+} + Ti^{4+} \rightarrow M^{n+} + Ti^{3+}$ $M^{(n+1)+} + OH^- \rightarrow M^{n+} + OH^\bullet$	**charge release**
$e^-_{CB} + h^+_{VB} \rightarrow h\nu$ $Ti^{3+} + OH^\bullet \rightarrow Ti^{4+} + OH^-$ $M^{(n-1)+} + h^+_{VB} \rightarrow M^{n+}$ $M^{(n+1)+} + Ti^{3+} \rightarrow M^{n+} + Ti^{4+}$ $M^{(n-1)+} + OH^\bullet \rightarrow M^{n+} + OH^-$ $M^{(n+1)+} + e^-_{CB} \rightarrow M^{n+}$	**recombination**
$e^-_{CB}(or\ Ti^{3+}, M^{(n-1)+}) + O \rightarrow O^-$ $h^+_{VB}(or\ OH^\bullet, M^{(n+1)+}) + R \rightarrow R^+$	**interfacial charge transfer**

Scheme. 1.1. The step-wise mechanism of semiconductor photocatalysis (Rodriguez and Fernandez-Garcia., 2007).

The competition between charge-carrier recombination and charge-carrier trapping followed by the competition between recombination of trapped carriers and interfacial charge transfer determine the overall quantum efficiency for interfacial charge transfer (Hoffmann et al. 1995). Also, the band positions or flat band potentials of the semiconductor material are important. These indicate the thermodynamic limitations for the photoreactions that can take place (Hagfeldtt et al. 1995). Environmental

decontamination by semiconductor photocatalysis is more convenient than conventional chemical oxidation methods as semiconductors are inexpensive, nontoxic, and reusable without substantial loss of photocatalytic activity.

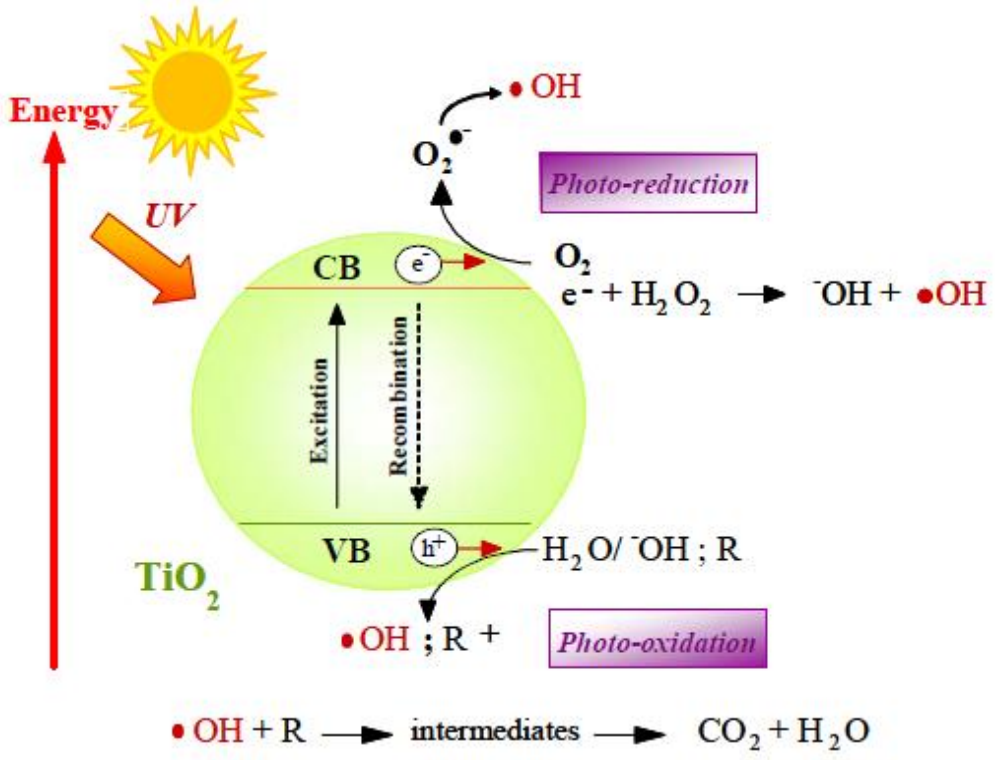

Fig. 1.8. Schematic of an irradiated TiO_2 semiconductor particle with possible photo-chemical and photo-physical processes.

1.7 Enhancement of photocatalytic activity

Although, TiO_2-driven photocatalytic degradation of chemical pollutants and microorganisms has been widely applied for decontamination and environmental purification, many disadvantages have emerged to limit its usage. TiO_2-driven photocatalysis requires high energy to induce a photocatalytic response (photoresponse), as the band gap of TiO_2 is 3.2 eV, and the anatase crystal can only absorb photons of wavelengths shorter than 388 nm (Gupta and Tripathi, 2011; Diebold U, 2003). So, practically TiO_2 nanoparticles can only absorb approximately 4

– 5 % of solar light energy, which makes the commercial applications of TiO_2 nanoparticles difficult with natural light sources. The second problem of TiO_2 nanoparticles is their lower photocatalytic efficiency due to electron- hole pair recombination (Diebold U, 2003; Carp et al. 2004). The major strategies utilized to overcome such drawbacks include, doping with metal and nonmetal ions, coating with photosensitizing dyes, compositing with polymers, conjugation to suitable molecules, and surface modification/functionalization. Although each of the method has different mechanisms to increase photoresponse or photocatalytic efficiency, most are found to enhance the overall photocatalytic properties of TiO_2 (Gupta and Tripathi, 2011; Diebold U, 2003; Carp et al. 2004).

1.7.1 Metal ion dopants

Incorporating metal ion dopants into the TiO_2 crystal structure influences the dynamics of electron-hole recombination and interfacial charge transfer. A large enhancement of photoactivity through doping is observed in nanoparticles sized 1-2 nm and having a high surface area (100-500 m^2/g) (Choi et al. 1994; Hamal and Klabunde, 2007). The dopant ions incorporated in the lattice (substitutional) or interstitial sites can function as both hole and electron traps and can significantly influence photoreactivity, charge carrier recombination rates and mediate interfacial charge transfer (Dvoranova et al. 2002; Choi et al. 1994). Metal dopants such as lanthanum are found to inhibit phase transformation of TiO_2, improve its thermal stability, reduce the crystallite size and increase Ti^{3+} content on the surface (Li et al. 2009). In such doped TiO_2 the Fermi levels of the metal and semiconductor align resulting in a flow of electrons from the catalyst to the metal. This process leads to an increase in hydroxyl groups and hence improves the photocatalytic efficiency. In case of TiO_2 doped with metals such as V, Mn or Fe a shift to visible light absorption

spectra is also observed with an increase in the dopant concentration, which is attributed to the charge transfer transition between the d electrons of the dopant and the CB (or VB) of TiO_2 (Gupta and Tripathi, 2011; Diebold U, 2003).

1.7.2 Transition metal ion doping

The inherent small size of TiO_2 nanoparticles increases the generation of electrons and holes which enhances the photocatalytic activity of TiO_2. However, the recombination of electron and hole pairs needs to be prevented during their movement from the interior to the surface to improve the photocatalytic activity of TiO_2. Transition metal ions trap these electron hole pairs and enhance their lifetime, consequently enhancing the efficiency of the photocatalyst. The number and lifetime of these charged carriers is size and dopant dependent and different dopants have diverse effects on the trapping of these charged carriers during interface transfer because of their different positions in the host lattice structure, and hence the photocatalytic efficiency varies (Nishikawa et al. 2001; Liu et al. 2007; Hu et al. 2006). Doping TiO_2 with transition metal ions improves the trapping-to-recombination ratio, however, doping can also lead to increased rate of recombination between electrons and holes. Since, photoinduced reactions can occur only if the charged carriers are transferred to the surface of the photocatalyst, the metal ions should be doped at the surface for efficient charge transfer.

An elaborate study on the effects of transition metal ion doping of quantum-sized TiO_2 nanoparticles with Fe^{3+}, Mo^{5+}, Ru^{3+}, Os^{3+}, Re^{5+}, V^{4+}, and Rh^{3+} has reported that although there is a strong positive relationship between photoreactivity and dopant concentration, it also has a complex dependence on parameters such as dopant energy state, the d-electron configuration, the distribution of dopants in the lattice, and the

light intensity (Choi et al. 1994; Zaleska A, 2008; Wu et al. 2004). Karvinen et al. theoretically investigated the role of such transition metal dopants (Ti^{3+}, V^{3+}, Cr^{3+}, Mn^{3+}, and Fe^{3+}) in both anatase and rutile TiO_2 and reported a significant band gap narrowing for anatase TiO_2 but no effect on the rutile phase. In another study, the TiO_2 doped with transition metal ions such as V, Cr, Mn, Fe and Ni showed a large shift in absorption spectra towards the visible light spectrum and the efficiency of this spectral shift was observed to be in the order of V > Cr > Mn > Fe > Ni. The photoexcitation of V, Cr, Mn and Fe doped TiO_2 occurred through the t_{2g} level of the metal ion dopant whereas, in case of Mn and Fe doped TiO_2 the absorption in visible light spectrum was attributed to the transitions from impurity band tail of the conduction band (Hu et al. 2006). However, transition metal ion dopants have shown both positive and negative effects on the photocatalytic activity of TiO_2. In case of dopants that serve as acceptor centers (Al^{3+}, Cr^{3+}, Ga^{3+}) or donor centers (Nb^{5+}, Ta^{5+}), when the concentration of conduction electrons is increased they favour the electron-hole recombination which decreases the photocatalytic efficiency. The concentration of dopants is also an important factor as at high dopant concentration the metal ions may serve as a recombination center for electrons and holes, thus lowering the overall efficiency of the photocatalyst. Hence, there is an optimum dopant concentration where the width of the space-charge region and the depth of light penetration are almost similar, and hence the photocatalytic efficiency of the doped TiO_2 is optimum (Gupta and Tripathi, 2011; Carp et al. 2004).

1.7.3 Coupled/composite semiconductors

It is possible to couple two semiconductors that have different energy levels for both their conduction and valence bands as such a configuration would enable efficient charge separation, increase the lifetime of charged carriers and facilitate interfacial

charge transfer to the surface. Here, the properties of the semiconductor particles such as size, surface structure play an important role in the interparticle transfer. Several coupled semiconductors have been reported such as TiO_2-CdS, Bi_2S_3-TiO_2, TiO_2-WO_3, TiO_2-SnO_2 among which the TiO_2-CdS coupled semiconductor has received considerable attention (Gupta and Tripathi, 2011; Carp et al. 2004). A proper positioning of the individual semiconductors and optimal thickness of the covering semiconductor are important factors for the efficient charge separation. In coupled semiconductors there are two possibilities, one where only one semiconductor is activated on illumination or both semiconductors are activated (Bessekhouad et al. 2004; Vinodgopal et al. 1996).

In case of TiO_2-CdS coupled semiconductor, the light energy required for CdS to be activated is lower than that for TiO_2 and hence CdS will get activated. So, the photogenerated electron will be injected from the CdS to TiO_2 while the positive hole will remain in CdS. The transfer of electron from CdS to TiO_2 increases the charge separation and hence the overall efficiency of the process of photocatalysis. After the separation of the charge carriers they are free to undergo electron transfer with adsorbates at the surface. However, from an application point of view, the usage of CdS alone or in a semiconductor couple is found to release considerable amount of toxic cadmium in the aqueous media which makes it environmentally undesirable (Kumar and Jain, 2001; Rajeshwar et al. 2001).

However newer composites of TiO_2 with CdSe, WO_3, ZnO etc are being widely studied for development of visible light responsive photocatalytic systems (Kumar and Jain, 2001; Bessekhouad et al. 2004).

1.7.4 Surface modification/surface functionalization:

TiO_2 is a catalyst of choice for a variety of applications as it is inexpensive, non toxic, and has redox properties favourable for both oxidation and reduction reaction processes. The surface properties of nanoparticles can be modified for specific needs and applications. In a functionalized nanostructure, the core provides the typical function while the shell interfaces with the host matrix. Surface functionalization/modification can be used to increase or decrease the surface hydrophilicity of the material and to minimize agglomeration to achieve uniform, stable dispersion of the material. Surface modification of metal oxide nanoparticles such as TiO_2 adds to the usefulness of the nanoparticles on top of their intrinsic characteristics, since hybridization of functional molecules on the nanoparticle surface provides target-specific recognition, catalytic abilities, and controlled surface properties (Schliephake and Scharnweber, 2008).

For biological applications assemblies of metal oxide nanoparticles and biomolecules such as antibodies, enzymes, and streptavidin via surface modification of the nanoparticles have drawn a growing interest in the areas of bioanalysis and fabrication of bioelectronic devices (Daoud et al. 2005). Surface functionalization also improves the biocompatibility of nanomaterials, alter their surface properties and can function as barriers against moisture and oxygen (Vimala et al. 2011; Lu et al. 2008). Depending upon the choice of the functionalizing agent, highly stable molecules can be obtained and these physico-chemical modifications influence the interaction of cells with the nanomaterials thereby improving cell adhesion and increasing uptake. Surface modification can also help to tailor particle solubility/dispersion and stability (Choi et al. 2003), enhance cell uptake (Win and Feng, 2005), and provide chemical

reactivity on the particle surface for further conjugation of bioactive ligands (Nobs et al. 2003).

1.8 Applications of photocatalysis

1.8.1 Self cleansing materials

TiO_2 coated tiles are considered to be very effective against organic and inorganic pollutants as well as against microorganisms. The application of such tiles in hospitals, schools, residential areas and other public and commercial facilities can drastically improve the hygienic conditions, reduce the spread of infectious diseases and improve the overall hygiene of the personnel. Furthermore, these TiO_2 coated tiles show super hydrophilic behavior, where water forms a uniform sheet over the surface of the tile at a contact angle of 7 (exterior) and 25 (interior) degrees. Grease, dirt and other staining materials can easily be swept away with a stream of water. Super hydrophilicity, combined with the strong photocatalytic oxidizing properties makes this tile self cleaning in exterior applications (Cho et. al. 2005; Parkin and Palgrave, 2005; Mills et al. 2005).

1.8.2 Air cleaning/purification

Volatile organic compounds (VOCs) are major air pollutants emitted into the atmosphere by human activities in urban and industrial areas that degrade the quality of air. Photocatalytic oxidation (PCO) has been applied for removing and decomposing pollutants in indoor air. The used photocatalytic reactors trap and chemically oxidize organic compounds, converting them primarily to CO_2 and water. These reactors operate at room temperature and with negligible pressure. Therefore, they may be readily integrated into new and existing heating, ventilation and air conditioning systems due to their modular design and operation at room temperature

with no pressure drop. These reactors can be scaled to suit a variety of indoor air quality applications and offer usage of solar light (Peral et al. 1997; Schwitzgebel et al. 1995; Sopyan et al. 1999).

1.8.3 Water treatment

In the field of waste water detoxification several concepts have been proposed. The process of heterogeneous photocatalysis using TiO_2 has several advantages as it is non toxic, inexpensive and causes complete mineralization of organic pollutants like aliphatics, aromatics, dyes, surfactants, pesticides, herbicides etc to CO_2, H_2O and mineral acids (Fujishima et al. 2008; Dunlop et al. 2002; Huang et al. 1996). In previous studies, systems have been considered in which the fine TiO_2 photocatalyst powder was dispersed in liquid suspension. However these systems were difficult to handle as after the photocatalytic degradation process, the powder remained suspended in water. The use of filters or other methods to remove TiO_2 has proved to be inefficient and expensive. Subsequently, photocatalytic reactors were designed where the titanium dioxide is fixed on a glass, ceramic or metal surface. Presently there is a great interest in development and improvement of thin-film-fixed-bed reactors (Rincon and Pulgarin, 2005; Teoh et al. 2012).

1.8.4 Antifogging effects

Nanoparticles of composite TiO_2 in an aqueous solution are coated onto the surface of materials, such as glass, mirror, plastic, metal plate, tile, automobile body, decorative resin sheet etc. The coated material surfaces under illumination exhibit hydrophilicity and photocatalytic activity without causing any changes in the original characteristics of the surface (Parkin and Palgrave, 2005). These new functions of the coated material imparts them new features of antifogging, anti-soiling and self-cleaning and

therefore, adhesive dust, stains on the surface could be removed easily by washing the surface of the material (Wang et al. 1997). The thickness of the coated film is generally less than 50 nm and hence the application of the coating is economical and practical.

1.8.5 Outdoor applications

As a result of air pollution, most of the building walls and other structures spoil from the exhaust gases, and VOCs which at times contain oily components. By coating the original building materials with a super hydrophilic photocatalyst, the dirt of the walls can easily be washed away by rain, keeping the external walls of the building clean for long times (Benedix et al. 2000; Chen and Mao, 2007).

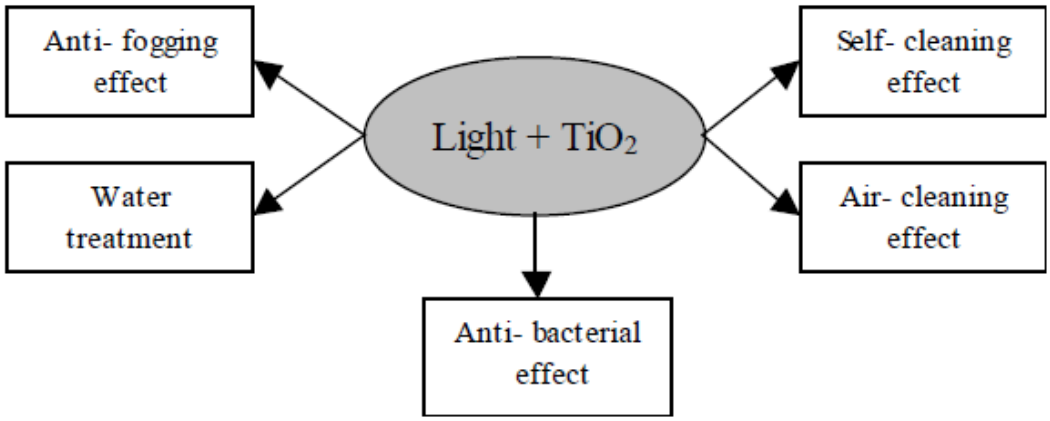

Fig. 1.9. Major areas of applications of TiO_2 photocatalysis (Benedix et al. 2000).

1.9 Bactericidal effects of Photocatalysis

The antibacterial and decontamination applications of TiO_2 nanoparticles have undergone extensive investigation since 1985, when Matsunaga et al. first demonstrated the microbicidal effect of TiO_2. The findings of Matsunaga et al. created a new avenue for sterilization techniques and resulted in attempts to use this novel photocatalytic technology for disinfecting drinking water and removing bioaerosols

from indoor air environments. Since then, research work on TiO_2 photocatalytic killing has been conducted intensively on a wide spectrum of microorganisms (Huang et. al. 1999; Maness et. al. 1999; Tongpool et. al. 2007; Cho et. al. 2005; Gerrity et. al. 2008; Lee, et. al. 1997; Mitoraj et. al. 2007) and cancer cells (Zhang and Sun, 2004). Reactive oxygen species generated on irradiated TiO_2 surfaces, have been shown to operate in concert to attack polyunsaturated phospholipids in bacteria (Wong et. al. 2006) and to catalyze site-specific DNA damage by generating H_2O_2 (Hirakawa et. al. 2004) which might therefore result in subsequent cell death. TiO_2-mediated photooxidations have emerged as a promising technology for the elimination of microorganisms in many applications, e.g., self-cleaning and self-sterilizing materials (Cho et. al. 2005; Parkin and Palgrave, 2005; Mills et al. 2005).

Although the applications of TiO_2 photocatalyst as a microbiocide has been receiving increasing attention worldwide, the initial response of living organisms to TiO_2 photocatalytic reaction, the cell-nanoparticle interaction and the mechanisms leading to cell death have not yet been fully understood. Hence, a basic understanding of the killing mechanisms would provide valuable information for the optimal use of the TiO_2 photocatalyst and the rational design of TiO_2 photocatalytic reactors (Rincon and Pulgarin, 2004; Maness et al. 1999; Bahnemann et al. 1991).

1.9.1 Mechanisms of action of TiO_2 photocatalysis on bacteria

Although, several papers have reported the microbicidal/antimicrobial effects of TiO_2 photocatalysts over a wide range of microorganisms, only a few publications have attempted to investigate the different modes of action TiO_2 exerted on microbial cells that lead to cell death (Fig. 1.11). A fundamental understanding of the underlying principles of the cell killing mechanism is critical in developing feasible disinfection

and medical treatment systems. Several reports have proposed different mechanisms for the inactivation/killing of these microorganisms.

In the initial study by Matsunaga et al. (1985), a decrease in intracellular coenzyme A (CoA) in the TiO_2-treated cells was detected for various microorganisms. Hence, it was proposed that the direct contact between TiO_2 and target cells causes oxidation of CoA that inhibits cell respiration leading to cell death. A few TiO_2 photocatalytic killing studies have revealed the susceptibility of microorganisms to TiO_2 photocatalysis to be in the order: virus > bacterial cells > bacterial spores. This difference in response of microorganisms to TiO_2 photocatalyst was attributed to the structural differences, particularly the complexity and thickness of the cell envelope.

The role of cell wall and cytoplasmic membrane in cell death was not considered until Saito et al. (1992) reported the disruption of cell envelope after TiO_2 treatment, by TEM studies. They also demonstrated the 'rapid' leakage of potassium ions and 'slow' leakage of RNA and proteins induced by TiO_2 photocatalytic reaction and proposed that, bacterial death was caused by an extensive disorder in cell permeability and decomposition of the cell wall. Sakai et al. showed a significant increase in intracellular calcium ions in cancerous cells induced by UV/TiO_2 treatment. Thus, confirming that the cell envelope may be a primary target for TiO_2 photocatlytic damage for both prokaryotic and eukaryotic cells. The intracellular macromolecules, such as nucleic acids, may be a potential target once the cell envelope is degraded (Sakai et al. 1994).

Some investigators also reported that there was no significant difference between the time required for killing of Gram positive or Gram negative bacteria, even though the former has a thicker cell wall. Nevertheless, the proposed modes did not describe the

progressive damages to various components of the cell envelope and their role in overall cell killing.

Kikuchi and co-workers (1997) studied the role of different ROS in bactericidal effects using catalase enzyme (that neutralises H_2O_2) and showed that it significantly quenched the cell inactivation, and proposed that it is hydrogen peroxide and not hydroxyl radicals that were responsible for the bactericidal effects. Further, Maness and co-workers (1999) studied the effects of photooxidation on *E. coli* cytoplasmic membranes by TBARS assay and detected malondialdehyde (MDA), a byproduct of lipid peroxidation, the production of which correlated with the decrease in cell viability. The authors thus concluded that lipid peroxidation of membranes led to failure of electron-transport during respiration and subsequent cell death.

In a study by Sunada and co-workers, they measured the rate of inactivation of intact *E. coli* cells and spheroplasts (viable cells no cell walls). In case of the intact cells two step "photo killing" reactions: an initial slower rate, followed by a faster reaction were observed. On the other hand, the spheroplasts exhibited only a single step higher rate reaction, implying that the cell wall of the *E. coli* cells protects the cytoplasmic membrane and other cytoplasmic contents. Further, AFM measurements of the intact *E. coli* cells showed the decomposition of outer cell wall membrane first and with continued irradiation, the cells were completely decomposed. Figure 1.10 shows a schematic illustration of the process of *E. coli* "photo-killing" on a TiO_2 film proposed by the authors (Sunada et al. 1998).

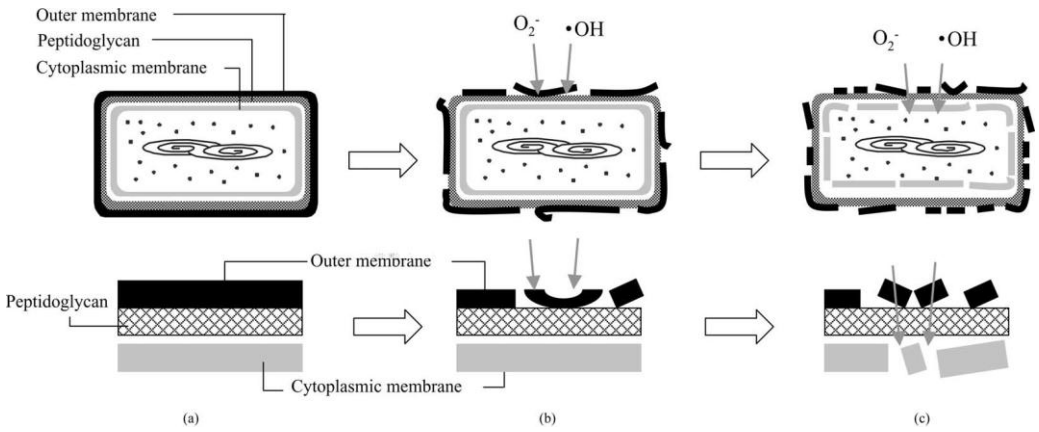

Fig. 1.10. (a-c) Schematic illustration of the process of *E. coli* photokilling on TiO_2 film. In lower row, the part of cell envelope is magnified.

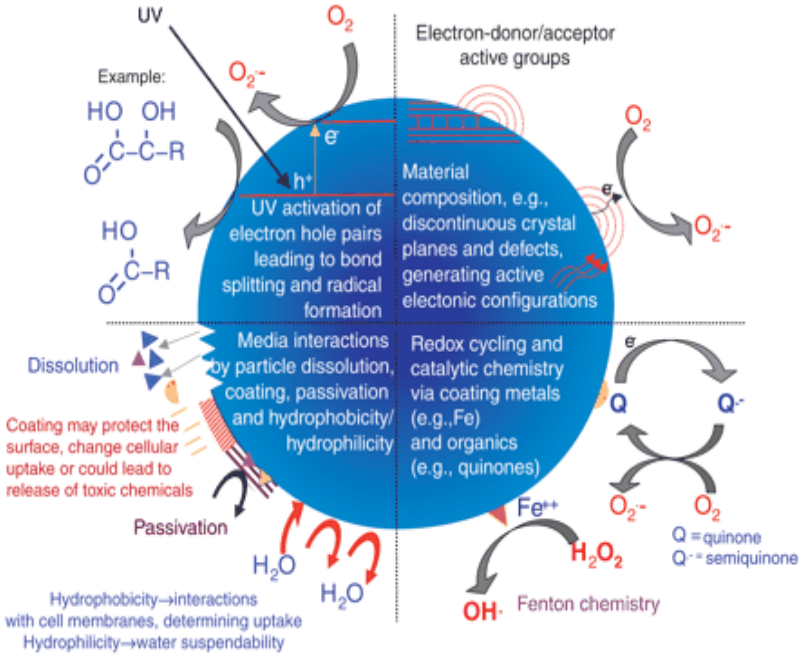

Fig. 1.11. Possible mechanisms by which nanoparticles interact with biological tissue (Nel et al. 2006).

In summary, there are still conflicting reports in the literature as to which reactive oxygen species are directly involved in the photo killing process. As per a few reports, hydrogen peroxide may be more involved, perhaps due to the generation of hydroxyl radicals by the Fenton reaction. This is quite likely as biological systems normally contain Fe^{++}, and cells generally have low redox reducing equivalents in abundance.

Moreover, hydrogen peroxide and superoxide in presence of ferric ions can participate in the Haber-Weiss reaction to yield more hydroxyl radicals. However, further studies are needed to clarify which species contributes to the photocatalytic activity as that can help devise a suitable photocatalytic system with good photocatalytic efficiency. Irrespective of the oxidative species involved, there is substantial evidence that cell membrane damage is a direct result of oxidative cell damage (Fig. 1.12). The cell membrane consists of unsaturated phospholipids and is a potential target leading to lipid peroxidation. The detrimental impact of lipid peroxidation to all forms of life has been well documented in the literature (Maness et al. 1999; Soekmen et al. 2001). Once the cell membrane barrier is compromised or upon entry into the cell via phagocytosis, TiO_2 particles can exert its oxidative actions directly on all the essential macromolecules in the cytoplasm.

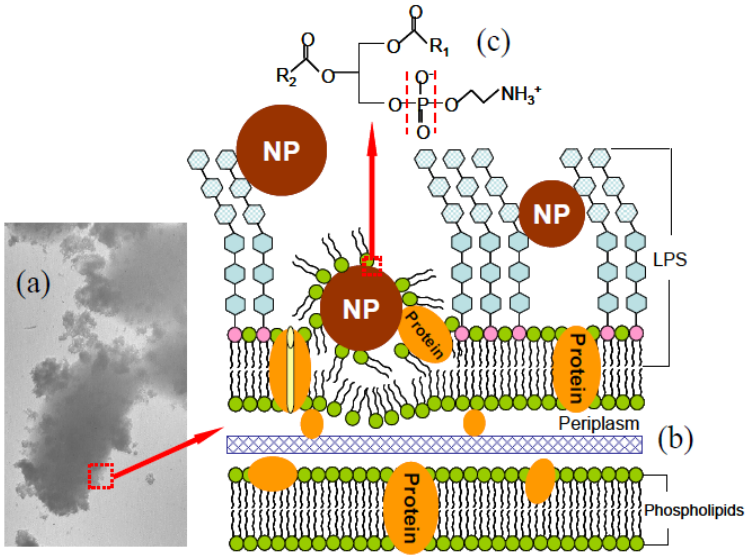

Fig. 1.12. TEM image showing the attachment of NPs to bacterial surfaces (a). Schematic illustration of NPs approaching to the bacterial cell surface and causing damage to cell envelope (b). Enlarged PE chemical structure, showing the potential damage caused by the NP surface as revealed by FTIR (c).

1.10 Definition of the problem

The need for highly efficient, novel methods for the remediation of toxic chemical and biological compounds has led to an imperative interest in the process of TiO_2 photocatalysis. One major driving force for pursuing research on the nanocrystalline TiO_2 is its extremely broad range of applications and the anticipation that further studies of the surface properties at fundamental level will improve the performance of TiO_2 nanomaterials and devices in different areas. Titanium dioxide is being extensively used as a photocatalyst in heterogeneous photocatalysis, in solar cells, as a white pigment in paints and cosmetics, in optoelectronics, in medicine for drug delivery and as a biocompatible implant material, in production of hydrogen and electric energy etc. Also, the studies of the novel properties of these materials at nanoscale and their applications are possible only when the materials are available with desired size, morphology, surface properties and chemical composition. Hence, the synthesis and processing of these nanomaterials is an important aspect of nanotechnology. TiO_2 has been the photocatalyst of choice in photocatalytic processes owing to its superior properties such as non-toxicity, inertness, and redox properties through both oxidative and reductive reactions. However, many drawbacks of TiO_2-driven photocatalytic degradation have emerged, that have limited the usage of TiO_2. As evident from the literature review of the optical properties, in particular the absorption, of TiO_2 is essential to its photon-driven applications. Typically, TiO_2 absorbs in the UV regime (because of its wide band gap of 3.2 eV), and hence requires high energy for triggering a photocatalytic response (photoresponse). Since only a small fraction of the sun's energy (4 %) is in this wavelength range, it makes the commercial applications of TiO_2 nanoparticles using natural light sources ineffective. The other major drawback of using TiO_2 nanoparticles in industrial

applications is its low photocatalytic efficiency, due to high rate of recombination of charge carriers within the material, before they are transferred to the surface. The other limitation of TiO_2 which needs to be addressed is its instability in aqueous medium leading to photocatalyst decomposition and agglomeration which again affects the efficiency. The performance of TiO_2 can be enhanced by shifting the onset of its absorption from the UV to the visible region. This will enable the effective utilization of the cheaper visible light sources or the greater quantity of the inexhaustible sunlight to carry out the process of photocatalysis. Further, in order to enhance the microbicidal activity of TiO_2, its surface can be modified or functionalized to enhance its uptake by microorganisms.

In this work an attempt has been made to address the problems associated with TiO_2 application and usage. Some of the specific objectives of this thesis are:

1. To synthesize nanosized TiO_2 and its physicochemical characterization.

2. To study nanosized TiO_2 as a photocatalyst in UV light and sunlight conditions against standard microbial cultures, microorganisms from environmental samples and dyes.

3. To improve the photocatalytic efficiency of TiO_2 in visible light region by:

(A) Doping/modifying with metal ions, non metal ions and organic acids.
(B) Synthesizing functionalized nanocomposites for improved activity.
(C) By using it in combination with transition metal ion complexes.

4. To study the antimicrobial activity of modified TiO_2 and study its mechanism of action.

1.11 Outlay of the thesis

The thesis has been divided into five different chapters and each chapter is followed by a summary:

In Chapter 1, a brief introduction to nanotechnology followed by a detailed description of the process of semiconductor photocatalysis and the role of TiO_2 as a photocatalyst is discussed. The chapter also discusses the various syntheses routes of TiO_2, various techniques employed to enhance the photocatalytic activity and the different applications of TiO_2 photocatalysis.

Chapter 2 discusses the synthesis and characterization of TiO_2 nanoparticles and the determination of its photocatalytic efficiency against different microbial cultures, microorganisms in sewage water and in photodegradation of toxic dyes by UV as well as sunlight irradiation.

Chapter 3 discusses the synthesis of TiO_2 doped with metal ions and non metals in order to shift its absorbance spectra towards the visible light region and to prevent electron hole recombination to increase its photocatalytic efficiency. The efficiency of doped TiO_2 is tested against *E. coli* as the model microorganism.

Chapter 4 describes the synthesis of silver-TiO_2 nanocomposites and its functionalization with organic acids, amino acids and other non-immunogenic molecules, characterization of its physicochemical properties, its antimicrobial effects and the mechanism of action of these functionalized nanocomposites on microorganisms.

Chapter 5 describes the study of a combined action of TiO_2 with Ni (II) hexaazamacrocyclic complex against various microorganisms in different media.

CHAPTER II

Chapter 2

Synthesis, characterization of TiO_2 nanoparticles and study of its photocatalytic activity on microorganisms and dyes

Abstract

Heterogeneous photocatalysis using titanium dioxide as photocatalysts is a very effective process for the photocatalytic degradation of organic compounds, due to its high photocatalytic activity and excellent stability. During the process of photocatalytic oxidation, organic compounds are completely mineralized to CO_2, H_2O and mineral compounds. The surface properties of TiO_2 play an important role in its photocatalytic processes. Upon UV light or visible light illumination, the TiO_2 photocatalysts generate reactive oxygen species (ROS) such as OH^-, O_2^- and H_2O_2. These extremely reactive ROS cause damage to living organisms by attacking different components of the cell wall and cell membrane such as polyunsaturated phospholipids, antitoxins and causing site-specific DNA damage.

In this study we report the synthesis of TiO_2 nanoparticles by a simple sol-gel method using titanium tetrachloride as a precursor. XRD analysis has revealed that these TiO_2 nanoparticles are in anatase phase and are polycrystalline. Using Debye-Scherrer formula the particle size was calculated to be ~13 nm. TEM imaging confirms this finding. BET surface area analysis has shown that the particles are mesoporous and the BET surface area is about 72.80 m^2/g. Thermogravimetric analysis has confirmed the purity of the nanoparticles.

These TiO_2 nanoparticles have been shown to exhibit photocatalytic activity in the UV as well as visible range. Studies on dye degradation using TiO_2 and dyes such as Malachite green, and methylene blue has shown that these dyes are degraded within

30/80 minutes on exposure to sunlight. The bactericidal activity of TiO_2 has been studied on pure cultures of *Escherichia coli, Pseudomonas aeruginosa*, *Staphylococcus aureus* and *Klebsiella pneumoniae* and discharge water from a sewage treatment plant which had a high microbial load. Cell viability and cell proliferation in presence and absence of TiO_2 is reported. The use of these relatively inexpensive photocatalyst based antimicrobial agents is quite promising and has potential applications in the development of alternative disinfectants for environmental and medical purposes.

2.1 Introduction

Heterogeneous photocatalysis using mesoporous Titanium dioxide as a photocatalyst is a widely studied area and has been applied in a variety of fields such as air purification, wastewater treatment (Bahnemann et. al. 1991; Rincon et. al. 2001; Hur and Koh, 2002; Augugliaro et. al. 2006), photodegradation of toxic organic compounds, as disinfectant etc. (Huang et. al. 1999; Maness et. al. 1999; Vohra et. al. 2005). Mesoporous TiO_2 has attracted much attention owing to its high surface-to-volume ratio, which is important for the process of photocatalysis, photosplitting of water etc. Anatase TiO_2 absorbs light in the UV region of the solar spectrum resulting in electron-hole pair (EHPs) generation. These excited electron and hole pairs are highly reactive and on reaction with water and oxygen form reactive oxygen species (ROS), such as super oxide anions (O_2^-) and hydroxyl radicals ($^{\cdot}OH$) (Kikuchi et. al. 1997; Cho et. al. 2004; Galvez et. al. 2007). Following the pioneering work of Matsunaga et al. which showed the microbiocidal effect of TiO_2 photocatalytic reactions (Matsunaga et. al. 1985; Matsunaga et. al. 1988), interest in the field of TiO_2 photocatalysis has grown exponentially (Cho et. al. 2005; Huang et. al. 1999; Anpo,

2000; Wong et. al. 2006). Now, TiO_2 photocatalytic killing is being applied extensively to a broad range of organisms viz, bacteria (Huang et. al. 1999; Maness et. al. 1999; Soekmen et. al. 2001), viruses (Cho et. al. 2005; Gerrity et. al. 2008; Lee, et. al. 1997), fungi (Mitoraj et. al. 2007), cancer cells (Zhang and Sun, 2004), algal toxins (Srinivasan and Somasundaram, 2003), etc. Photocatalysis using TiO_2 has also been used to disinfect selective food-borne pathogens such as *Salmonella spp*. and *Listeria monocytogenes*, and to destroy *Bacillus anthracis* and the spores of *Bacillus subtilis* (Kau et. al. 2009; Guin et al. 2007; Vohra et. al. 2005). The main objectives of all these studies ranged from identifying the factors involved in photocatalytic disinfection, optimizing the conditions for the process, and studying the mechanism as well as kinetics of photocatalytic disinfection on field applications (Cho et. al. 2005; Sunada et. al. 1998). The major challenge however has been to improve the photocatalytic efficiency of the process (Egerton et. al. 2005).

The use of TiO_2 in the photocatalytic oxidation of dyes and organic systems represents a promising remediation strategy for wastewater systems. Much attention has been directed at investigating the photocatalytic degradation of organic pollutants such as dyes mediated by TiO_2 particles in aqueous dispersions under UV light irradiation. However, the limitation of solar UV-light reaching the surface of the earth is relatively small (~3-5 % of the solar spectrum) and artificial UV light sources are quite expensive. Hence, efforts have been made to explore ways to effectively utilize cheaper visible light sources such as the inexhaustible sunlight for treating polluted ecosystems. The electron transfer processes between dyes and TiO_2 semiconductors have practical potential, and several studies on photodegradation of dyes such as Malachite green, Acid orange 7, Naphthol Blue Black, terbutylazine on rose bengal coated TiO_2 particles have been reported (Chen et al. 2006; Chen et al. 2007;

Saggioro et al. 2011; Chen et al. 2004; Vinodgopal and Wyncoop, 1996; Wu et al. 1999). The TiO_2 photocatalytic process is a conceptually feasible technology. However, since the UV region occupies only around 4 % of the entire solar spectrum and 45% of the energy belongs to visible light (Yao et. al. 2006), the potential applications of this promising technology are limited. Hence, the development of a visible-light responsive photocatalyst would greatly enhance the practical feasibility of this technology.

In this study we report the synthesis of sunlight responsive TiO_2 nanoparticles by a simple sol-gel method. The antibacterial activity of these TiO_2 nanoparticles was tested against four different pathogenic microorganisms viz. *Escherichia coli*, *Pseudomonas aeruginosa*, *Klebsiella pneumoniae* and *Staphylococcus aureus*, as well as the microorganisms in treated sewage water from a sewage treatment plant. Further, the TiO_2 nanoparticles were also tested for their photocatalytic activity in photodegradation of organic/toxic dyes. The results obtained from this study clearly indicate that the synthesized TiO_2 nanoparticles are effective antibacterial as well as photocatalytic agents.

2.2 Materials and methods

2.2.1 Preparation of TiO_2 nanoparticles

Titanium (IV) chloride (Merck, 99 %), was used as a precursor reagent for the synthesis of TiO_2 nanoparticles. The synthesis was carried out by adding $TiCl_4$ dropwise, to deionised water placed in an ice bath, within a fumehood to avoid the $TiCl_4$ fumes. The $TiCl_4$: water ratios used were 1:25, 1: 50 and 1:100. The $TiCl_4$-water mixture was stirred continuously for ~2 hrs on a magnetic stirrer to allow the formation of uniform, homogeneous sol. The resultant sol was dialysed for about 12

hrs, against deionised water with regular changing of water every 2 hrs. At the end of dialysis a translucent, solid gel was obtained (Fig. 2.1), that was dried overnight at 100 ^{o}C and the crystals obtained were ground thoroughly into a fine powder. The resultant white crystalline powder was then calcined at 500 ^{o}C and subsequently used for the study.

2.2.2 Characterisation of TiO_2 nanoparticles

2.2.2.1 X-ray diffraction (XRD) analysis

The powder XRD analysis of the TiO_2 nanoparticles was done on a Rigaku Miniflex, operated at a voltage of 30 kV and a current of 15 mA using a Cu-Kα radiation of wavelength 1.5408 Å and a 2θ range of 20 to 80°. The average crystallite size of the nanoparticles was calculated using the Debye Scherer's equation:

$$D = k \lambda / B \cos \theta$$

Where D is the crystallite diameter in Å, *k* the shape constant (0.9), λ is the X-ray (Cu Kα) wavelength in Å, θ the diffraction angle and B (in radian) is the half width measured for the XRD peak.

2.2.2.2 TG-DTA analysis

The thermogravimetric analysis of uncalcined TiO_2 was performed with TG-DTA analyzer (Shimadzu) in air atmosphere at a flow rate of 10 ml/min. The thermal properties of the sample were studied over a temperature range of 40 ^{o}C - 550 ^{o}C in an Aluminium pan.

2.2.2.3 Transmission electron microscope (TEM) analysis

The morphology and the particle size of the TiO_2 nanoparticles was analyzed using transmission electron microscope. For TEM analysis, the samples were dispersed in absolute ethanol by ultrasonication and a drop of the solution was placed on the 200 mesh carbon coated copper grid and examined using a Phillips CM 200 electron microscope with an EDAX detector type SUTW (Super ultrathin window) at a voltage of 200 kV and the resolution was 0.23 nm.

2.2.2.4 Surface area and porosity study

The surface area and porosity studies of the synthesized TiO_2 nanoparticles were carried out by N_2 adsorption-desorption isotherms using a Micromeritics Tristar 3000 surface area and porosity analyzer. The samples were prepared for analysis by drying them at 100 ℃ for 12 h with a constant flow of dry nitrogen gas.

2.2.3 Bacterial strains and cultures

The bacterial strains *Escherichia coli*, *Pseudomonas aeruginosa*, *Klebsiella pneumoniae* and *Staphylococcus aureus* were enriched in nutrient broth (NB) (Hi-media laboratories, India) at 37 ^{o}C for 18 h on a rotary shaker at 150 rpm. The enriched culture was reinoculated in NB, incubated at 37 ^{o}C until the exponential phase was reached, and then serially diluted in sterile normal saline and used for the study. Treated sewage water was procured from the local sewage treatment plant and was used after filtration to remove any suspended solids.

2.2.4 Preparation of TiO_2 suspension for photocatalytic experiments

The suspension of TiO_2 nanoparticles was prepared in sterile distilled water. The suspension was thoroughly mixed by sonication to avoid settling of the nanoparticles before being used for the photocatalytic experiment. The suspension was always prepared fresh, immediately prior to photocatalytic reaction and kept in the dark.

2.2.5 Photocatalytic reaction and Cell viability assay

All the solutions and reagents were prepared with deionized and distilled water, and analytical grade reagents were used throughout. All the glasswares and accessories used were washed with distilled water and then autoclaved at 121 ^{o}C for 15 minutes to ensure sterility.

The photocatalytic reaction was carried out in a 100 ml glass beaker containing the bacterial cell suspension to which uniformly mixed 0.1 M TiO_2 was added. The concentration of TiO_2 was optimized by carrying out photodegradation experiments at different concentrations (0.01, 0.05 and 0.1 M). The TiO_2-cell suspension was placed on a magnetic stir plate for continuous stirring to ensure proper nanoparticle-cell contact. The suspension was separately illuminated with UV light (352 nm), visible light (420 nm) and sun light. The loss of viability of bacterial cells was monitored by taking the viable count at regular time intervals of 10, 20, 30 and 40 minutes. A control without TiO_2 was maintained. Aliquots of the TiO_2-cell suspension were withdrawn, serially diluted with saline and spread plated in duplicates on nutrient agar plates. All the plates were incubated at 37 ^{o}C for 24 h. At the end of incubation, the cell viability was checked by recording the number of colonies as colony forming units per ml (cfu/ml).

In a tropical country like India ((8º 4' - 37º 6' N latitude), very high levels of global solar UV radiation is received. The latitude and longitude of the place of experiment (Vasco, Goa) was Latitude: 15^{o} 24' and Longitude: 73^{o} 50' with the day time temperature reaching upto ~33 ^{o}C during noon times. All the photodegradation studies under sunlight were carried out during bright sunny afternoons approximately between 11:30 am to 2:30 pm.

2.2.6 Chemical Oxygen Demand (COD) analysis

One of the most important parameters of water quality for the environmental regulatory agencies is the "oxygen demanding" substances in water. COD is the amount of oxygen consumed to chemically oxidize the organic contaminants in water completely to inorganic end products such as CO_2 and H_2O. Hence, the amount of oxygen consumed during the COD test can give an estimate of the organic pollutants present in water and is a principal water quality criterion for water treatment plants (Raposo et. al. 2008; Augugliaro et. al. 2006). COD analysis of the treated sewage water sample was carried out before and after photodegradation with 0.1 M TiO_2 suspension. The original treated sewage water (without photodegradation) and tap water were used as the positive and negative controls. Photodegradation was carried out for the treated sewage water with synthesized TiO_2 and commercial TiO_2 (Hombikat) under sunlight for 40 minutes. The sample was then filtered with a whatman paper to remove the suspended TiO_2, and the filtrate was used for the COD analysis. In brief, a known volume of the sample was refluxed with an excess of Potassium dichromate (oxidizing agent) in a sulphuric acid medium using silver sulphate as a catalyst. The unreacted potassium dichromate was then titrated with ferrous ammonium sulphate solution using 1, 10- phenantroline monohydrate as an

indicator. Potassium dichromate is a strong oxidizing agent under acidic conditions. Mercuric sulphate is added to the sample to eliminate the interference of halides while, silver sulphate acts as a catalyst (Raposo et. al. 2008; Augugliaro et. al. 2006).

The chemical oxygen demand of the liquid samples was calculated using the following equation:

$$COD\ (mg\ O_2\ L^{-1}) = \frac{(FAS_{B1}\text{-}FAS_{liquid\ sample}) \times N_{FAS} \times 8000}{V_{liquid\ sample}}$$

Where FAS_{B1}: volume of FAS used in the titration of the blank sample (ml)

$FAS_{solid\ sample}$: volume of FAS used in the titration of the liquid sample (ml)

N_{FAS}: Concentration of reducing agent (N)

$V_{liquid\ sample}$: Volume of liquid sample

2.2.7 Photocatalytic degradation of dyes

In the past decades, hundreds of dyes have been manufactured which are potentially dangerous for the environment. Titanium dioxide can help degrade these harmful dyes to less harmful substances in the environment. In this study Malachite green and Methylene blue were used for TiO_2 photodegradation analysis. The photodegradation of these dyes under UV light exposure was carried out at three different concentrations of TiO_2 i.e. 0.05 M, 0.1 M and 0.2 M.

For the dye photodegradation studies, 10 ml of 0.1 mM, Malachite green and Methylene blue dye solutions were mixed with 10 ml of 0.1 M TiO_2 suspension in a clean glass beaker. The TiO_2-dye mixture was continuously stirred on a magnetic stirrer, while being exposed to the light source. A control study under similar experimental conditions was carried out for Standard TiO_2 (Hombikat). One set of

beakers was exposed to UV light (352 nm) in a UV dosing chamber and another to sunlight for different intervals of time (10, 20, 40, 60 and 80 minutes for MB and MG). The treated dye suspension in each beaker was then centrifuged and the degradation kinetics was monitored by recording the UV-visible spectra of the supernatant after each time interval to check for photodegradation.

2.3 Results and Discussion

The TiO_2 nanoparticles were synthesized by the simple sol-gel method. The effective removal of chloride and other ions was achieved through dialysis (Desai and Kowshik, 2009). Among the various synthesis routes such as sol-gel, microemulsion, hydrothermal etc, sol-gel is an attractive method for obtaining nanoparticles with high surface area, porosity and monodispersity (Liu et al. 2008; Azizi et al. 2012). Moreover, the sol-gel synthesis method used in this study has short processing time, needs few chemical reagents, lab controlled annealing temperature and relatively short curing time. Similar studies for sol-gel synthesis of nanoparticles have been reportedly used because of the simplicity and controlled conditions of synthesis (Lee et al. 2005; Zhang and Chen, 2009; Jeon et al. 2003). High calcination temperature (> 700 °C) (Hamal and Klabunde, 2007; Lee et al. 2005), not only leads to phase transformation from anatase to rutile TiO_2, but also causes the pores to collapse due to thermal nucleation leading to formation of particle aggregates, thereby decreasing the surface area of the nanoparticles (Tian et al. 2009; Lee et al. 2005; Peng et al. 2005). On the whole, the simplicity and cost-efficiency of the procedure to generate a high yield of TiO_2 nanoparticles makes sol-gel an attractive synthesis method.

Optimization of the $TiCl_4$: water concentration was carried out at ratios of 1:25, 1:50 and 1:100. In solution phase synthesis such as the sol-gel method, processes such as coarsening or agglomeration of particles can compete with nucleation and growth,

thereby affecting the particle size distribution. It has been reported that the stability, size and morphology of the sol is influenced by the ratio of Ti precursor to water, and at lower ratios the particle size tends to decrease (Azizi et al. 2012; Oskam et al. 2003). During the synthesis process it was observed that at $TiCl_4$: water ratio of 1:25 and 1:50, the rate of sol formation was high but the sol formed was not homogeneous and had large aggregates. Moreover, the sol looked unstable during synthesis and was observed to precipitate during dialysis. However, at a ratio of $TiCl_4$: water (1:100), the sol formation was slow and uniform, and no precipitate formation was observed during dialysis. The specific surface area and pore volume of the nanoparticles increase with increase in the amount of water (Han et al. 2012). Hence the ratio of 1:100, was considered suitable for the synthesis of TiO_2 nanoparticles with high surface area, porosity and thus photocatalytic efficiency.

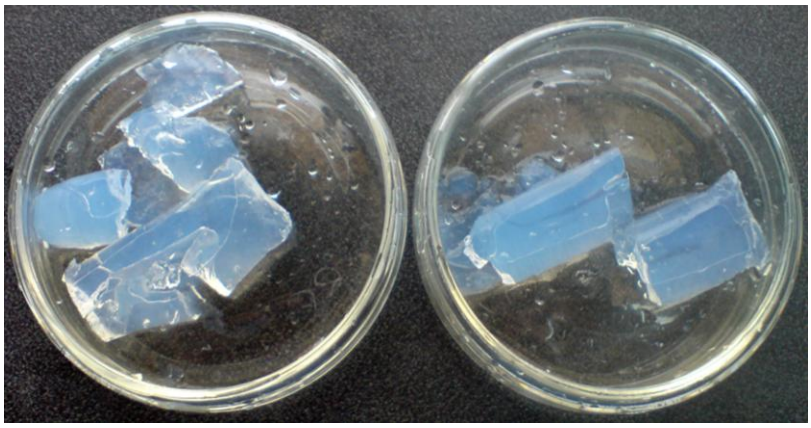

Fig. 2.1. The gel obtained after dialysis of the sol during the sol-gel synthesis of TiO_2.

To investigate the phase structure and size of the nanoparticles, XRD analysis was carried out. The XRD analysis results showed 2θ peaks at 25.08, 37.96, 48.02, and 54.8° that correspond to the anatase phase of TiO_2 as per ICDD powder diffraction data card no. 21-1272 (Fig. 2.2) (Peng et. al. 2005; Zhang et al. 2008). The average crystallite size calculated using the Debye-Scherrer equation from the broadening of

(1 0 1) XRD peak of anatase TiO_2 was ~13 nm. Even after calcination at 500 ^oC, the XRD pattern shows that the main crystal phase of the TiO_2 is anatase, possessing high crystallinity in the mesoporous walls, which is consistent with the TEM analysis data. Similar studies have been reported for the synthesis of mesoporous, anatase phase TiO_2 nanoparticles in the size range of ~7 – 20 nm, with anatase as the prominent phase indicating their thermal stability at high calcination temperature of ≥ 500 ^oC (Peng et al. 2005; Wahi et al. 2006; Zhang et al. 2008; Agarwala et al. 2010).

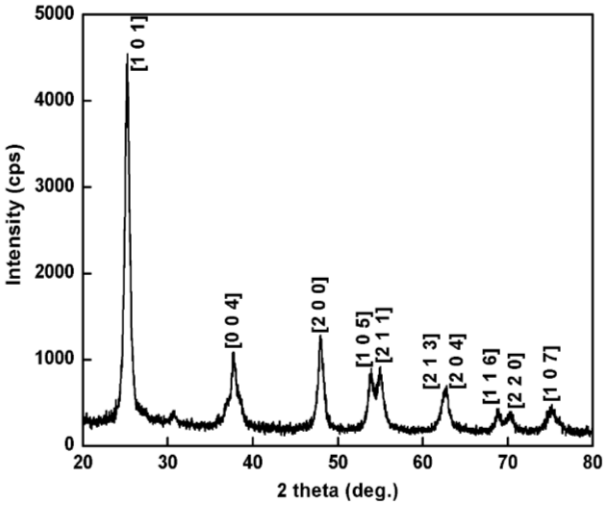

Fig. 2.2. XRD pattern of TiO_2 nanoparticles synthesized by sol-gel method using titanium tetrachloride as the precursor.

The thermogravimetric analysis (TGA) plot shows a weight loss of ~22.5 % when heated in the temperature range of 40 ^oC - 550 ^oC, which can be attributed to the dehydration and evaporation of water from the uncalcined sample (Hydroxide gel), to form a pure oxide (TiO_2) (Fig. 2.3).

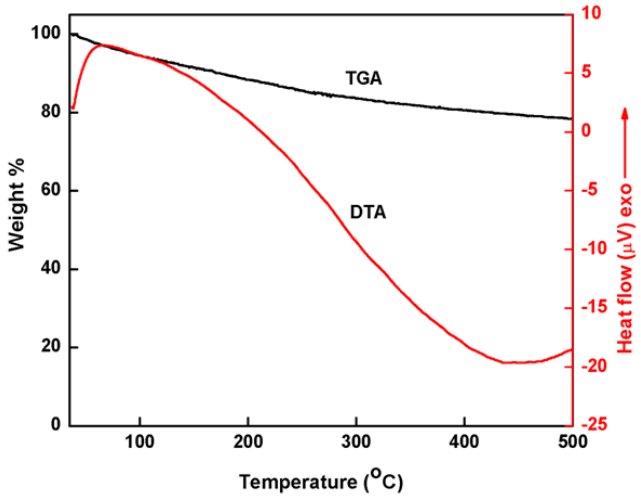

Fig. 2.3. The TGA-DTA analysis plot of TiO_2 nanoparticles.

Corresponding to this weight loss, a broad endothermic peak in the DTA (Differential Thermal Analysis) curve in the same temperature range (40 ^{o}C - 550 ^{o}C) is also observed. However, further heating above 500 ^{o}C did not show any further weight loss, confirming the total decomposition of the compound. In a similar study with uncalcined TiO_2 microspheres, a weight loss of ~35 % was reported at a temperature of upto 400 ^{o}C (Yang et al. 2008). This data is also supported by the XRD analysis graph of the TiO_2 sample calcined at 500 ^{o}C, which shows the formation of pure anatase TiO_2 without any impurities. Thus, the calcination temperature of 500 ^{o}C is optimal for achieving highly crystalline TiO_2 without compromising the stability of its porous framework. Similar studies have been reported showing the stability of anatase TiO_2 nanostructures at temperatures $\geq$ 500 ^{o}C (Agarwala et al. 2010; Peng et al. 2005).

The morphology and the particle size of the TiO_2 nanoparticles was analyzed using TEM, that showed a detailed microstructure of the sample. TEM images (Fig. 2.4) show the irregularly ordered, mesoporous structure of TiO_2 matrix with a mixed morphology. The morphologies of the pores and particles are not significantly

modified upon calcinations at 500 ^{o}C indicating that the collapse of mesoporous structure does not occur drastically upon calcinations (Peng et al. 2005; Agarwala et al. 2010). The size of the nanoparticles as determined by TEM analysis was found to be ~7-15 nm. Further, the mesoporous structure does not possess pores with long range ordering and are interconnected as shown by the hysteresis loop in the nitrogen adsorption-desorption studies, which is ideal for improving the surface properties.

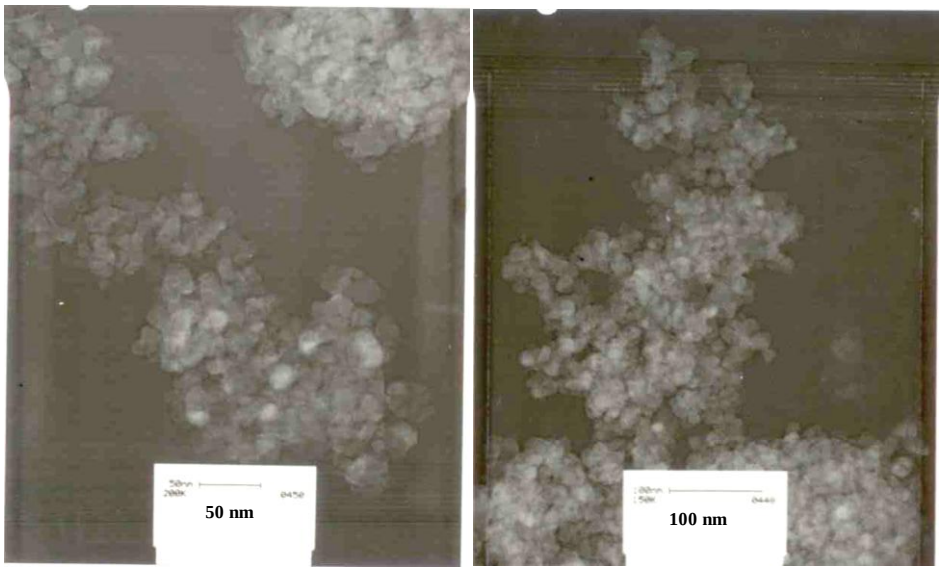

Fig. 2.4. TEM micrographs of TiO_2 nanoparticles.

The physicochemical sorption properties and pore parameters of the "as synthesized" TiO_2 nanoparticles were determined by nitrogen adsorption-desorption isotherm measurements. The adsorption-desorption isotherms of the sample showed type IV isotherm with H2 hysteresis loop (Fig. 2.5A), a characteristic of mesoporous materials (Sing et al. 1985). The pore volume by BJH (Barrett-Joyner-Halenda) desorption method was found to be 0.237 cm^3/g for the TiO_2 nanoparticles. The Brunauer-Emmett-Teller (BET) surface area of the TiO_2 was ~72.80 m^2/g, with an average pore size distribution of 9.0 nm (Fig. 2.5B). It has been reported that the BET surface area

of nanoparticles depends on the temperature and duration of calcinations as well as precursor concentration used (Hamal & Klabunde, 2007). Similar BET surface areas, ranging from 55 m^2/g to ~106 m^2/g have been reported for TiO_2 nanoparticles synthesized by solution route methods with annealing carried out at a temperature of 300-500 ^oC (Liu et al. 2004; Wahi et al. 2006).

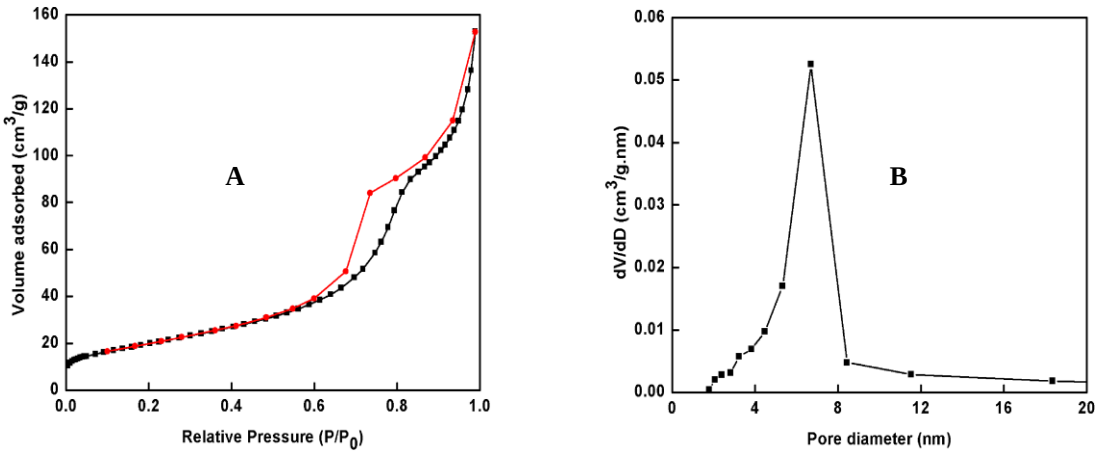

Fig. 2.5. The N_2 adsorption-desorption isotherm of TiO_2 nanoparticles: (A) Hysteresis loops and (B) BJH pore size distribution.

When the surface area of the nanoparticles is high, it provides more number of surface active groups that can effectively interact with the adsorbates thereby improving the efficiency of the photocatalytic reaction (Enterkin et al. 2011; Wahi et al. 2006). Hence, the nanoparticle size and surface area play an important role in the photocatalytic activity of nanoparticles (Peng et al. 2005; Liu et al. 2004). In addition, the smaller particles with different shapes have more active surface atoms with a large fraction of them on low-coordination and high-energy sites (corners, edges, steps, kinks etc.), which makes them more reactive than larger particles upon contact with the toxic compounds/bacterial cells (Asharani et al. 2010; Zhang and Chen, 2009). Since the particle size of the synthesized TiO_2 nanoparticles is ~13 nm, and posseses a

mixed morphology, these properties are expected to contribute to the photocatalytic activity of the TiO_2 nanoparticles.

TiO_2 photocatalysts on irradiation with light of suitable wavelength causes the formation of reactive oxygen species (ROS) which initiate a cascade of redox reactions which can mineralize a variety of organic compounds (Hirakawa et. al. 2004; Lee et. al. 1997). The antibacterial activity of TiO_2 nanoparticles (0.1 M TiO_2) was evaluated against bacterial cells in sunlight. Samples were withdrawn at regular time intervals and the number of surviving cells determined by the conventional viable count method. Figures 2.6 (A-D) show the kill curves for the four test organisms viz. *Escherichia coli*, *Pseudomonas aeruginosa*, *Klebsiella pneumoniae* and *Staphylococcus aureus.* From an initial count of ~10^5 cfu/ml a 2 log reduction (99 %) in viable count could be obtained after 20 minutes of exposure in the case of *Klebsiella pneumoniae* and *Pseudomonas aeruginosa,* whereas for *Staphylococcus aureus* a 1 log reduction (90 %) was obtained after exposure for the same interval of time. At the end of 40 minutes, a complete reduction (99.999 %) was obtained for *Klebsiella pneumoniae*, *Pseudomonas aeruginosa,* and *Staphylococcus aureus. Escherichia coli* exhibited minimal susceptibility to photocatalytic inactivation and a 3 log reduction could be obtained only after 40 minutes of exposure. Similar results for bactericidal activity were obtained with commercially available photocatalytic TiO_2 (Hombikat). The order of susceptibility of the organisms to inactivation by TiO_2 was *Staphylococcus aureus* > *Klebsiella pneumoniae* > *Pseudomonas aeruginosa* > *Escherichia coli*.

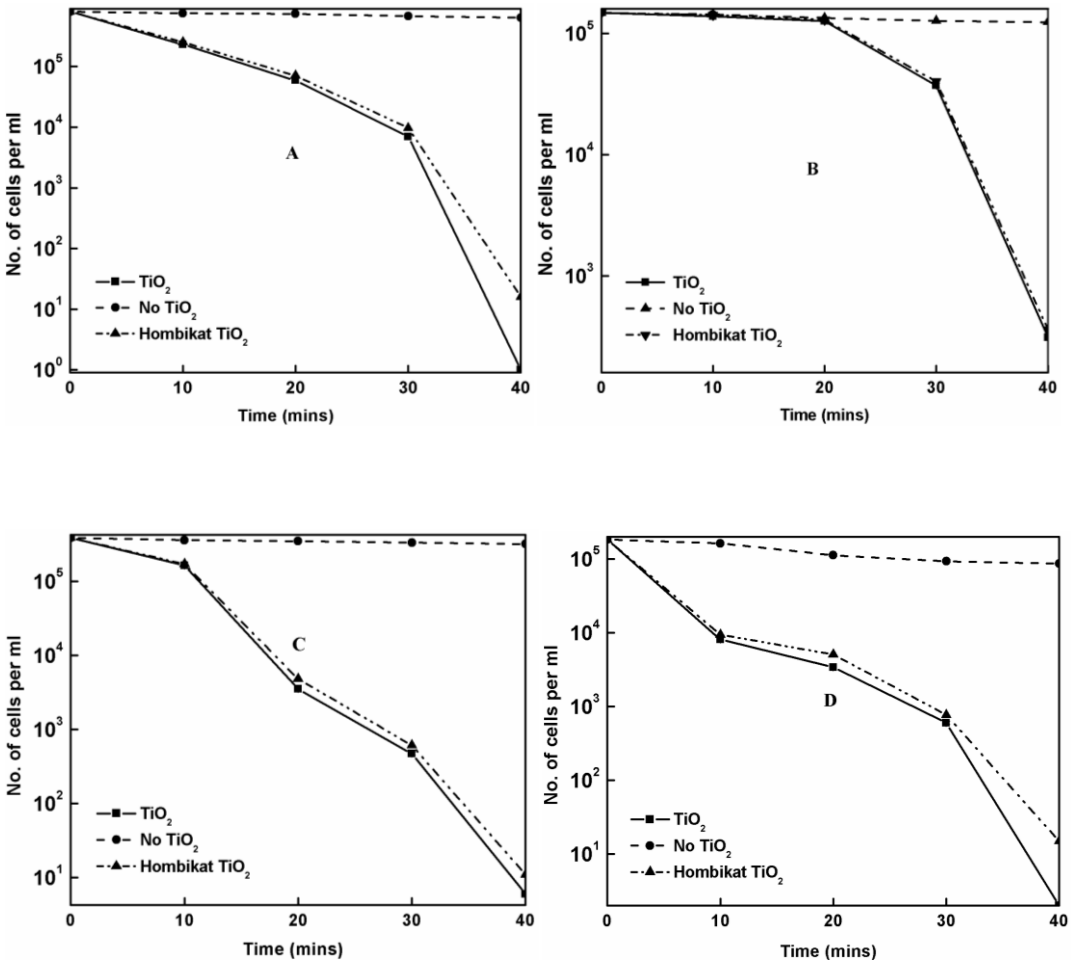

Fig. 2.6. Antibacterial activity of TiO_2 nanoparticles against gram positive and gram negative bacteria irradiated with sunlight: A] *S. aureus*, B] *E. coli*, C] *K. pneumoniae*, D] *P. aeruginosa*.

In all these experiments we observed that the efficiency of the process was reduced when the bacterial suspensions were not stirred continuously on a magnetic stirrer. To evaluate this we exposed the bacterial suspension + TiO_2 to sunlight and manually stirred the suspension once every 4 minutes. A 3 log reduction in viable count was obtained in the manually stirred beakers compared to the 5 log reduction that was observed in beakers stirred continuously using the magnetic stirrer after 40 minutes of exposure to sunlight. Thus, the bactericidal action of TiO_2 was dependent on the amount of dissolved molecular oxygen and proper cell-TiO_2 contact, both of which

are increased during stirring. It has been reported earlier that, since TiO_2 photoreacts with oxygen present in O_2 and H_2O, more dissolved oxygen produces more $^{\cdot}OH$ radicals by scavenging the conduction band electrons and reducing the rate of EHP recombination. Thus, the lack of sufficient oxygen reduces the rate of reaction (Cho et. al. 2004). In addition, free movement of the nanoparticles in suspension form facilitates the better contact with microbes and accelerates the translocation of nanoparticles through the bacterial cell membrane (Williams et. al. 2006).

A closer analysis of the survival curves of the microorganisms revealed that the bacterial inactivation had occurred in two distinct phases, the microorganisms were not much affected in the first 10 minutes. This could be because of the $^{\cdot}OH$ radical scavengers in water that react with $^{\cdot}OH$ radicals and reduce the efficiency of the photoinactivation process as has been observed during studies of TiO_2 photocatalysis on *E. coli* (Egerton et. al. 2005). Studies on the mechanism of bactericidal activity of TiO_2 suggest that oxidative damage first takes place on the cell wall when the TiO_2 makes contact with the cell. Such cells are still viable, however, as photocatalytic action progresses the cell permeability increases and TiO_2 particles have easier access to the cell cytoplasm. This causes photooxidation of intracellular components thereby accelerating cell death (Galvez et. al. 2007). This further explains the initial delay in the bactericidal activity of TiO_2 nanoparticles.

Studies on the killing of microorganisms by TiO_2 photocatalysis in sewage water sample exposed to UV for 40 minutes showed a 99 % (2 log reduction) reduction in the microbial load as did the sample exposed to sunlight for the same duration. In comparison to the results of bacterial cultures where complete reduction in the bacterial count was observed, the photocatalytic inactivation of microorganisms in sewage sample appeared less effective. This could be attributed to the ionic strength

of the medium i.e treated sewage water. Treated sewage water is a complex medium containing a variety of organic and inorganic compounds. During the photocatalytic reactions involving TiO_2, various ROS species such as super oxide anions (O_2^-) and hydroxyl radicals ($^{\cdot}OH$) are generated that are primarily responsible for the photocatalytic action of TiO_2. However, in complex media such as the sewage water, these reactive oxidising species could be easily scavenged by the components of the medium (Li et al. 2011; Ando et al. 2010). Moreover, the organic and inorganic content of the sewage water also slows down the rate of the photocatalytic reaction thereby decreasing its bactericidal efficiency. Thus, these results indicate that the inactivation of microorganisms during photocatalytic reactions depends on the complexity of the media, and in complex medium such as sewage water, the photocatalytic reaction is not as effective as it in less complex media.

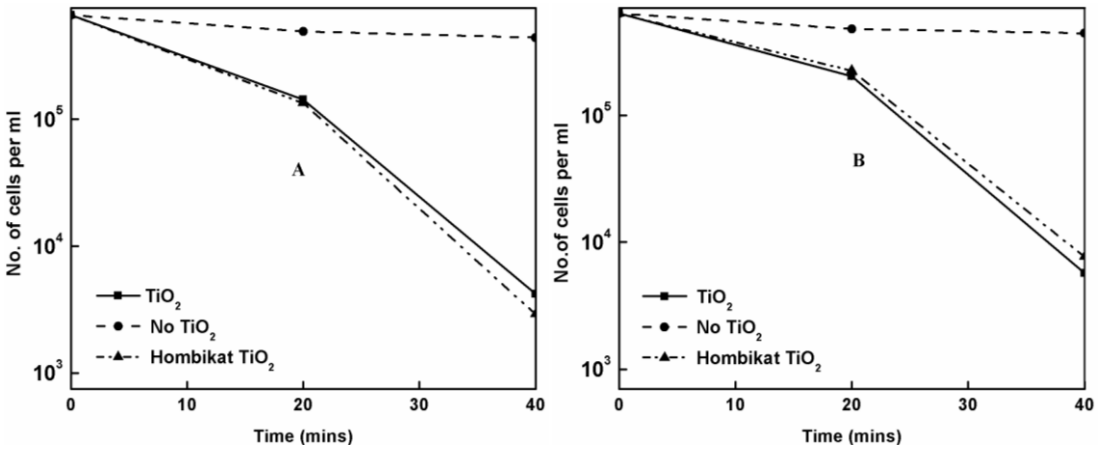

Fig. 2.7. Antimicrobial activity of TiO_2 nanoparticles against microorganisms from treated sewage water sample exposed to: A] UV light, B] Sunlight.

It has also been reported that under oxidative conditions the MIC/MBC values of antimicrobial agents are sensitive to ionic components of culture media and other abiotic factors (Jin et. al. 2010; Ando et. al. 2010; Eva et. al. 1999; Li et. al. 2011).

The results of this antimicrobial study comply with the findings of other researchers that irradiated TiO_2 exhibits bactericidal activity (Galvez et. al. 2007; Vohra et. al. 2005) and the efficacy of this disinfection process is proportionally correlated with the TiO_2 dose and the time of exposure. An approach of this kind, to solar disinfection of water using cost effective and reusable photocatalyst such as TiO_2 is very promising. The potential of this multifaceted compound for disinfection in environmental and medical fields is immense, and further research needs to be done to harness its exceptional properties.

In order to minimize the hazard to environment and health, there is an urgent need to maintain the toxic pollutants at acceptable levels for their safe disposal in the environment. Hence the measurement of such parameters as BOD, TSS and Chemical Oxygen Demand (COD) are very important as they are good indicators of the quality of water. COD is defined as a measure of the oxygen equivalent of the organic matter content of a sample susceptible to oxidation by a strong chemical oxidant. Table 1 shows the measure of COD in mg/liter for sewage water, photocatalytically treated with synthesized TiO_2 as well as the commercial, Hombikat TiO_2. It was observed that after photocatalytic treatment with sunlight for 40 minutes, there was a reduction in COD from 735 mg/l to 112 mg/l in case of synthesized TiO_2 (84.7 % reduction) and 104 mg/l for the commercial Hombikat TiO_2 (85.8 % reduction). The COD of the tap water was found to be 28 mg/l. Photocatalysis has been used for the removal of organic contaminants and to lower the levels of COD in sewage water (Raposo et. al. 2008; Augugliaro et. al. 2006; Shivaraju, 2011; Tiwari et. al. 2011). One study reported a significant reduction in COD of phenol contaminated water after 5 hrs treatment with 0.2 g/l TiO_2 under UV light, while a 45 % reduction in COD was reported for photocatalysis under sunlight after 4 hrs (Priya et. al. 2008; Tiwari et. al.

2011). In another photocatalytic study under sunlight and a photocatalyst concentration of 70 mg/50 ml, a COD percentage reduction of 39 % was reported after 1 hr and a 89 % reduction, after 5 hrs of photocatalytic treatment (Shivaraju, 2011). Moreover, the same study showed a 94 % reduction in COD levels under similar experimental conditions with UV as the light source. Hence, the efficiency of the photocatalytic technologies can be further improved by optimizing the concentration and time of photocatalytic treatment under suitable light source. The conventional adsorption based technologies using low-cost carbonaceous materials, activated carbon, stratified sand filters, etc. are being used to lower the levels of COD in the environment (Devi et. al. 2008; Healy et. al. 2006). However, these technologies need time consuming pretreatment processing, cannot ensure the removal of trace organic contaminants and can be very difficult to implement for small scale operation (Al-Jlil, 2009; Shivaraju, 2011). Hence using photocatalytic treatment of waste water contaminants to lower the COD levels can prove to be a very efficient and convenient technology.

Table 2.1. The COD values obtained for the sewage water (SW) sample treated with TiO_2 nanoparticles in Sunlight.

Sample	COD (mg/L)
SW + sunlight (Positive Control)	735
SW + Hombikat TiO_2 + sunlight	104
SW + prepared TiO_2 + sunlight	112
Tap water (Negative Control)	28

The use of TiO_2 in the photocatalytic oxidation of dyes in organic systems represents a promising remediation strategy for wastewater systems. The removal of synthetic dye contaminants such as methylene blue from aquatic systems is extremely important from the environmental point of view because most of these dyes are toxic, mutagenic and carcinogenic. Methylene blue is a cationic dye and a photosensitizer used to create singlet oxygen when exposed to both oxygen and light. It is used in this regard to make organic peroxides. The methylene blue colored water is a source of aesthetic pollution, that also causes imbalance to aquatic life (Chen et al. 2007; Kyung et al. 2005; Bergwerff and Scherpenisse, 2003). Hence, removal of these synthetic dye pollutants or their degradation is very important. The TiO_2 photodegradation of methylene blue was carried out and monitored by recording the UV-visible spectra at regular time intervals (10, 20, 40, 60 and 80 minutes). After photodegradation for a duration of 80 minutes, the methylene blue solution was observed to turn completely white under sunlight as well as UV light as shown in the plots in figure 2.8.

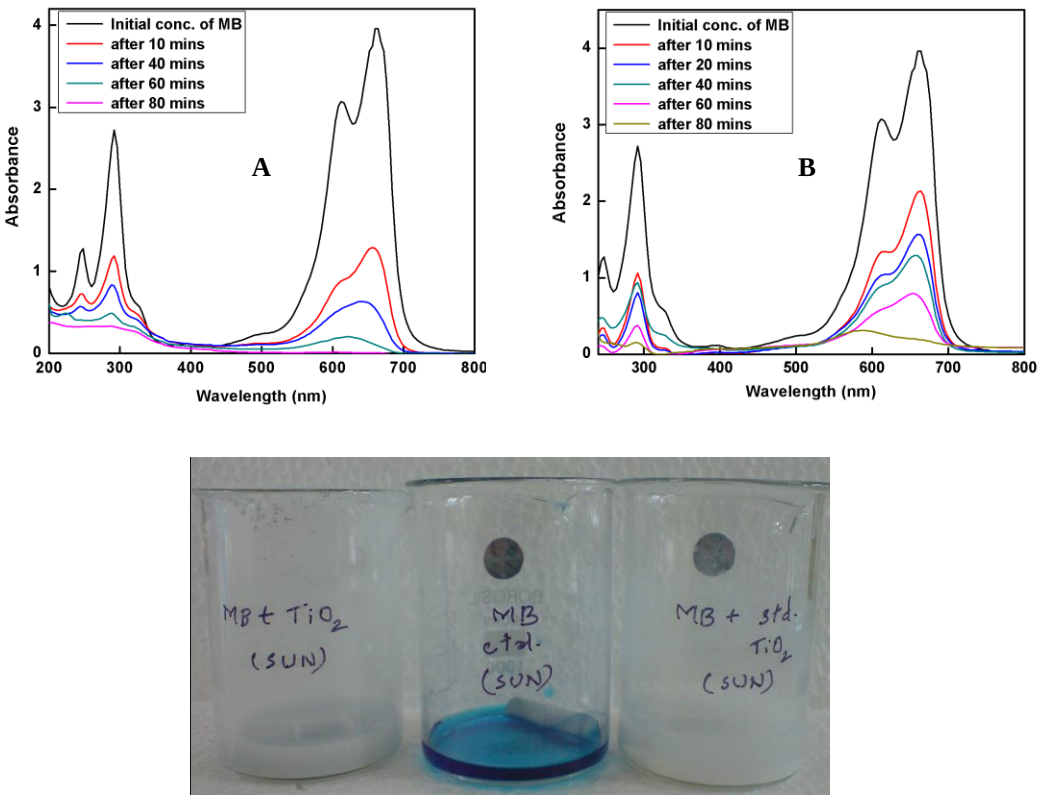

Fig. 2.8. Photocatalytic degradation of methylene blue (0.1 mM) by aqueous TiO_2 nanoparticle dispersion as a function of 80 minutes of irradiation time under: A] Sunlight, B] UV light.

Malachite green is widely used as a biocide in the aquaculture industry and is known to be toxic to fishes as well as fish eggs and fungi. Moreover, it is reported to have harmful effects on the immune and reproductive systems and is known for its genotoxic and carcinogenic properties (Chen et al. 2007). During the photocatalytic reaction between TiO_2 and malachite green, the malachite green adsorbs onto the negatively charged TiO_2 surface through the positive ammonium groups (Li et al. 1999; Chen et al. 2007). The complete photodegradation of malachite green was achieved after 30 minutes of sunlight exposure and 60 minutes for UV light exposure as observed from the UV-visible absorption plots and the change in colour (Fig. 2.10).

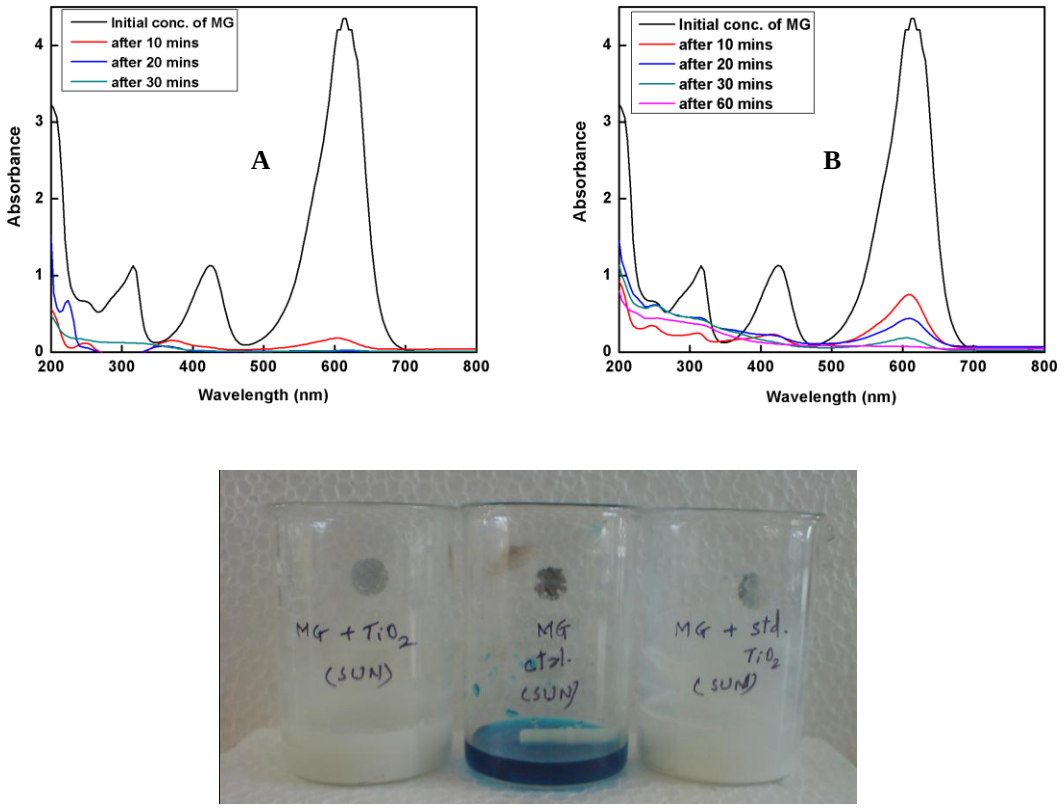

Fig. 2.9. Photocatalytic degradation of malachite green (0.1 mM) by aqueous TiO_2 nanoparticle dispersion as a function of irradiation time under: A] Sunlight, B] UV light.

A closer analysis of the photodegradation of methylene blue, malachite green and methyl red indicates that in case of methylene blue and malachite green the sunlight is equally or more effective than the UV light. This could be because the complete photodegradation of methylene blue and malachite green is achieved within 30 and 80 minutes respectively in sunlight, which is a relatively short time for any variation in the intensity of sunlight and hence the photodegradation is effective.

The semiconductor TiO_2 is an excellent photocatalyst for the degradation of organic pollutants such as dyes and their mineralization under UV irradiation. After activation of the TiO_2 particles with UV light, electrons at the surface of particles are scavenged

by the molecular oxygen to generate the superoxide radical anion, $O_2^{\cdot}$-, which on protonation yields the $^{\cdot}OOH$ radical, whereas the valence band holes are trapped as the surface-bound $^{\cdot}OH$ radicals on oxidation of either the surface OH^- groups and/or the surface H_2O molecules (Wu et al. 1998; Chen et al. 2007; Nogueira and Jardim, 1993). The trapped electron after formation of the $^{\cdot}OOH$ can also form $^{\cdot}OH$ radical. All these active oxygen species $O_2^{\cdot}$-, $^{\cdot}OOH$, or $^{\cdot}OH$ radicals especially $^{\cdot}OH$ are involved in the degradation of various organic dyes.

However, the visible-irradiation mechanism is different from the UV driven mechanism as visible light causes the excitation of the dye and not the semiconductor TiO_2 (Wu et al. 1998; Wu et al. 1999; Chen et al. 2007):

$$Dye_{ads}^{\cdot}{}^{+} + \{^{\cdot}OOH, {}^{\cdot}OH \text{ or } O_2\} \longrightarrow \text{peroxides or hydroxylated intermediates} \longrightarrow$$

$$\longrightarrow \text{degraded or mineralized products} \ldots$$

On excitation the dye injects an electron to the conduction band of TiO_2, from where it is scavenged by pre-adsorbed oxygen, O_2, to form active oxygen radicals such as $O_2^{\cdot}$-, $^{\cdot}OOH$, or $^{\cdot}OH$. These reactive radicals cause the photodegradation or mineralization of organic pollutants such as dyes. Here, TiO_2 acts as an electron carrier causing the separation of injected electrons and the dye radicals. Photodegradation of the dye by sunlight/visible light is much more advantageous than the UV driven process as more of the freely available and abundant sunlight is used. This aspect attributes a major economic advantage to this technology (Wu et al. 1998; Wu et al. 1999; Chen et al. 2007; Nogueira and Jardim, 1993). Since methylene blue and malachite green are known to be good photosensitizers, the photodegradation of these dyes in presence of TiO_2 is very effective in sunlight and UV light.

The above results suggest that the degradation of self-photosensitized dyes such as methylene blue and malachite green in the presence of TiO_2 nanoparticles by visible light might, in some cases, be preferable in its applicability and economic perspective than the UV-driven pathway. The photodegradation of dye pollutants can be driven by sunlight during daylight hours and at other times by relatively inexpensive (as compared to UV) artificial lamps that emit visible radiation.

Conclusion

In the light of the recent changes in the environmental scenario and emergence of newer environmental challenges, simple and environment friendly technologies such as photocatalysis have attracted worldwide attention. Anatase titanium dioxide nanoparticles have been synthesized by a simple sol-gel technique. These nanoparticles have a crystallite size of ~13 nm and exhibit photocatalytic activity in presence of sunlight. Photocatalytic activity of TiO_2 under UV light irradiation is well established. The TiO_2 synthesized by sol-gel method exhibits bactericidal activity when irradiated with sunlight against the common human pathogens tested as well as the microorganisms from treated sewage water sample. The COD analysis of the photodegraded sewage sample shows that the organic content of the sewage water is almost completely degraded. Further, TiO_2 photocatalysis is also effective in the degradation of toxic dyes to their mineral compounds in sunlight as well as UV light. This opens up newer avenues for the development of solar assisted alternative technologies for disinfection of water bodies contaminated with toxic organic pollutants as well as pathogenic microorganisms.

CHAPTER III

Chapter 3

Doping/surface modification of TiO_2 nanoparticles for improved photocatalytic activity under visible light irradiation

Abstract

Titanium dioxide (TiO_2) is considered an ideal photocatalyst because of its photocatalytic properties, chemical stability, non toxicity in the environment and cost efficiency. However, TiO_2 has a wide band gap of 3.2 eV and hence its photocatalytic activity is limited primarily to the ultraviolet (UV) region of the light spectrum which is only 4 % of the total solar energy available. This in turn limits the practical applications of TiO_2. Moreover, the usage of UV light activated TiO_2 is impractical not only because of the ill effects of UV exposure but also because it is highly uneconomical. Doping and surface modification techniques have been proposed to overcome the problems associated with the wide band gap of TiO_2 and to reduce the rate of recombination of charged carriers, thereby increasing the overall efficiency of TiO_2 in solar light. This is important as it can broaden the applications of TiO_2, making it more effective and economical to address the emerging problems of environmental remediation and disinfection. In this chapter we report the modification/doping of TiO_2 with transition metals, non-metal anions, organic acids, amino acids, and phosphate to check its effect on the enhancement of antimicrobial activity.

3.1 Introduction

Photocatalysis using TiO_2 as a photocatalyst has been widely applied for the degradation of organic compounds (Zhao and Yang, 2003; El-Morsi et al. 2000) and function as disinfectants by mineralizing the organic pollutants and microbial contaminants into carbon dioxide, water and inorganics (Liu et al. 2008; Rincon and Pulgarin, 2003; Dunlop et al. 2002; Huang et al. 2000). Several studies have demonstrated the biocidal efficacy of TiO_2 photocatalysis, but the kinetics of the process for complete inactivation and mineralization of microorganisms is comparatively slow and does not match that of the conventional disinfection techniques (Wong et al. 2006; Vohra et al. 2005; Wolfrum et al. 2002). Pristine TiO_2 is known to be active only when irradiated with UV light ($\lambda < 387$ nm) because of its wide band gap (3.2 eV for the anatase TiO_2 crystalline phase) which limits its applications in sunlight (Linsebigler et al. 1995; Diebold U. 2003). The band gap is located between the filled valence band and the higher energy conduction band and the gap between the valence band and conduction band determines both the electrical conductivity and the wavelength sensitivity of the semiconductor (Hamal and Klabunde, 2007; Diebold U. 2003; Asahi et al. 2000). A material with a larger bandgap requires higher energy radiation for electron transfer to occur from valence band to the conduction band, than one with a smaller band gap. Moreover, the high rate of recombination of photogenerated charged carriers also decreases the efficiency of the photocatalytic process (Anpo and Takeuchi, 2003; Diebold U. 2003). Hence, the major challenge is to develop a photocatalyst with a narrow band gap, exhibiting efficient photocatalytic activity in sunlight, thus enhancing the overall rate of photoinactivation/disinfection process (Chen et al. 2009; Zaleska, A. 2008; Wu et al. 2004).

Several methods have been used in an attempt to improve the overall efficiency of the photocatalytic process. These include doping with transition metal ions to increase electrical conductivity (Nishikawa et al. 2001; Liu et al. 2007; Hu et al. 2006; Rincon & Pulgarin, 2007), doping with non-metal ions as it shows a shift in the threshold of photocatalytic activity to lower energies (Chen et al. 2009; Hamal and Klabunde, 2007), coupling two different photocatalysts, doping with noble metals, capping or surface functionalization etc (Gupta and Tripathi, 2011). The main purpose of doping or modification of TiO_2 is to induce a batho-chromic shift (a decrease in the band gap or introduction of intra-band gap states, which shifts the photo-threshold to the visible light region) (Diebold U. 2003; Carp et al. 2004).

One approach that has shown significant enhancement in the photocatalytic activity of TiO_2 is the introduction of transition metal ions in the lattice of TiO_2 (Shah et al. 2002; Hamal and Klabunde, 2007; Diebold U. 2003; Wu et al. 2004) which can either extend the absorption spectrum of TiO_2 into the visible region or reduce the rate of charge carrier recombination thus improving its photocatalytic efficiency (Linsebigler et al. 1995; Diebold U. 2003; Carp et al. 2004). Doping of TiO_2 with transition metal ions provides a means to increase the lifespan of electron or hole or both the charge carriers by trapping them and as a result, dopants enhance the efficiency of the photocatalyst (Shah et al. 2002; Liu et al. 2007). Another common method successfully used to shorten the band gap of TiO_2 is to attach organic dyes such as Ruthenium complexes to its surfaces. However, this method is expensive, the dyes are degraded easily in aerobic environment, and it cannot be used in an aqueous medium as it is readily washed off from the surface. Doping of TiO_2 with transition metals and non metals is known to shorten the band gap of TiO_2, but may suffer thermal instability and low quantum yields in the process due to continuum of inter band

states of transition metals (Wan et al. 2007; Yates et al. 2006). Reduction of TiO_2 by hydrogenation improves visible light activation by narrowing the band gap but it lowers the conduction band thus reducing the photocatalytic reduction power of the system (Barnard and Zapol, 2004). Doping or surface modification can improve the physicochemical properties of TiO_2 such as size, surface area, and improve its thermal behavior, stability and surface properties that can influence its interaction with different adsorbates, and, as a result its overall photocatalytic activity.

The objective of the study was to synthesize doped/modified photocatalyst with photocatalytic activity in the visible range. The doped/modified TiO_2 synthesis was carried out with transition metal dopants (Iron and Silver), non metal dopants (Nitrogen, Carbon, and Sulfur) and surface modification was carried out with organic acids (Folic acid, Fumaric acid, Succinic acid, Malic acid and Salicylic acid), amino acids (L-arginine and Cysteine), and phosphate, and the effect of surface modification on antibacterial activity was tested.

3.2 Materials and methods

Chemicals and solvents used were of analytical grades purchased from Merck, Sd-fine Chemicals, Himedia, India, and used without any further purification. All the glassware and accessories used were washed with distilled water and then autoclaved at 121 ^{o}C for 15 minutes. All the solutions used were prepared with deionized water.

3.2.1 Doping with non metal anions

3.2.1.1 Nitrogen doped TiO_2

The synthesis of N-doped TiO_2 was carried out by a modified sol-gel method which proceeds through solution phase forming ionic intermediate but without forming polymer chains. It has been proposed that this method helps in effective doping with better homogeneity than other synthesis routes. The nitrogen doping is achieved by using EDTA (Sd fine chemicals, India) as the N source (Etacheri et al. 2010). In the synthesis of nitrogen doped TiO_2 sample, 10.94 ml of titanium isopropoxide (Merck, India), the precursor solution, was dissolved in 28.47 ml isopropanol (Sd fine chemicals, India). The solution was then mixed with 4.27 ml of glacial acetic acid (Sd fine chemicals) followed by the addition of 22.10 g of the doping agent, EDTA. The solution was stirred until a precipitate was obtained. The precipitate was then mixed with 66.94 ml of deionized water, and stirred continuously for ~2 h to allow the formation of a sol. The sol was then subjected to dialysis against deionized water for approximately 12 hrs to form a solid gel, heated in an oven at 80 ℃ to form an intermittent solution, which on further heating is transformed into a solid gel. The xerogel thus obtained, after 24 h was calcined at 400 ℃ for 2 h at a heating rate of 10 °C/min. The control sample without EDTA was also prepared using the same synthesis method as described above. The molar ratio between titanium isopropoxide, acetic acid, isopropanol, and water was 1:2:10:100.

3.2.1.2 Synthesis of metal and non metal ions (C, N, S, and Fe)-doped TiO_2

Thiourea was used as the precursor for nonmetal atoms and iron chloride as the precursor for metallic iron. In the synthesis, 3.8 g thiourea was added to a beaker containing 150 ml deionized water kept in an ice bath. While under continuous

stirring, an amount of iron chloride, corresponding to the desired Fe^{3+} doping content, was added to the solution. Titanium precursor was added dropwise to the aqueous solution and the mixture was stirred for 12 h and dialyzed for 24 h before drying in air at 80 ℃. The dried powder was ground and calcined at 500 ℃ in air for 2 h to obtain the doped TiO_2.

The Fe doping was done at 0.1, 0.3, and 0.5 wt %, and controls with no Fe and plain TiO_2 without thiourea and iron chloride (No dopants) were also synthesized by the same procedure.

3.2.1.3 Synthesis of metal ion doped TiO_2 (Ag-TiO_2)

It is well known that noble metals such as Ag and Au possess unique electronic and catalytic properties. Silver is also known for its high antimicrobial activity in both metallic as well as ionic form (Hamal and Klabunde, 2007; Zhang and Chen, 2009; Rai et al. 2009). Moreover, in an Ag doped TiO_2 the well-dispersed Ag^+ ions trap photoinduced electrons, decreasing the charge-carrier recombination rate and hence increasing the photocatalytic efficiency of the doped TiO_2 (Hamal and Klabunde, 2007; Elahifard et al. 2007; Hu et al. 2006). The $AgTiO_2$ nanoparticles (1 atomic % silver) were synthesized by simple sol-gel method. Titanium (IV) chloride (≥ 99 %) was added dropwise to deionized water with dissolved silver nitrate in an ice bath (99.8 %, Hi-media Laboratories, India). The sol obtained was thoroughly dialysed for ~12 hrs in a dialysis membrane (Himedia Laboratories, India) with frequent changes of deionized water (every 2 h) allowing slow growth of particles and resulting in the formation of gel. The gel was dried at 100 ℃ and ground to obtain fine $AgTiO_2$ powder.

3.2.2 Synthesis of Phosphate modified TiO_2 (P-TiO_2):

The TiO_2 nanoparticles used were synthesized as described in chapter 2 section 2.2.1. To load the phosphate anion, the highly crystallized TiO_2 was soaked in 0.3 M phosphoric acid (Sd fine chemicals, India) at 30 °C for 5 h, and then separated by centrifugation. To strengthen the interaction between the phosphate anion and the surface Ti site, it was dried directly at 100 °C and further heated at 300 °C for 1.5 h. After thoroughly washing it with water, it was dried, and designated as P-TiO_2.

3.2.3 Modification of TiO_2 with organic acids (Salicylic acid, Folic acid, Fumaric acid, Succinic acid and Malic acid)

3.2.3.1 Salicylic acid modified TiO_2 (S-TiO_2)

The TiO_2 used for modification was synthesized as described in chapter 2 section 2.2.1. Surface modification was carried out by stirring the TiO_2 nanoparticles for 30 min in a saturated solution of salicylic acid, resulting in a light yellow colouration of the TiO_2 surface. The pH of the solution was adjusted to 1.1 and 3.4 by adding HCl. After filtering with 0.45 μm membrane filter, the modified TiO_2 (S-TiO_2) was washed three times with water and heat-treated for 30 min at 105 °C. Noteworthy was the observation that the colour developed imminently, implying chemisorption of salicylic acid on TiO_2 surface.

3.2.3.2 Folic acid, Fumaric acid, Succinic acid and Malic acid modified TiO_2

The TiO_2 was synthesized as described in chapter 2 section 2.2.1. For surface modification the specific amount of organic acid solution (folic acid: 1.3 mM, fumaric acid: 8.6 mM, Succinic acid: 15.2 mM and Malic acid: 16.7 mM) prepared in DMF (99.8 %, Fisher Scientific, India) was heated at 80 °C for 10 min. The solutions were

cooled to room temperature and filtered (To remove any suspended solids) after addition of an equal volume of deionized water. The TiO_2 powder was added to the filtered solution of modifying agents and stirred for 10 min. The modified TiO_2 was washed five times each with DMF followed by distilled water and dried in air to obtain a fine powder. The modified TiO_2 powders were designated as FA-TiO_2, Fu-TiO_2, SA-TiO_2 and MA-TiO_2 for folic acid, fumaric acid, succinic acid and malic acid modified TiO_2, respectively.

3.2.4 Synthesis and modification of TiO_2 with amino acids

3.2.4.1 Arginine modified TiO_2 (Arg-TiO_2)

Titanium (IV) tetrachloride was hydrolyzed in deionised water at 4 °C and stirred continuously for 4-5 hrs, to obtain a whitish opaque colloidal solution. To this colloidal solution, 25 ml of 0.03 M solution of L-arginine prepared in deionised water was added drop wise and the beaker was allowed to stand still for ~1 hr for complete complexation. After ~18-24 hrs of dialysis against deionised water, gelation was observed in the beaker. The beaker was then kept for drying at 100 °C overnight to obtain whitish crystals. The crystals were ground in a clean mortar and pestle and a fine powder of Arg-TiO_2 was obtained.

3.2.4.2 Cysteine modified TiO_2 (Cys-TiO_2)

The synthesis and modification of cysteine modified TiO_2 (Cys-TiO_2) was carried out by the same procedure as described above, using 0.1 M solution of cysteine prepared in distilled water.

3.3 FTIR analysis

FTIR spectroscopy was carried out using FTIR-IR Affinity – 1 01660, Shimadzu. All samples were milled with spectroscopic grade potassium bromide (KBr, Merck), and a pellet of the mixture was pressed into a disc, placed in the solid cell, and scanned in the range of 400-4000 cm^{-1} against a KBr control.

3.4 Bacterial cultures

The bacterial strain of *Escherichia coli 2345* was used as the representative strain to carry out all the antibacterial experiments. The bacterial culture was grown overnight in NB (nutrient broth, Himedia, India) medium and aliquots of the culture were inoculated into fresh medium, incubated under aerobic conditions at 37 °C on a rotary shaker at 150 rpm until the exponential growth phase was reached. The standard suspensions of the organism (~10^5 cfu/ml) were obtained by serially diluting the cultures in sterile normal saline.

3.5 Preparation of TiO_2 suspension

The stock suspension of doped/modified TiO_2 nanoparticles was prepared in sterile distilled water. The suspension was thoroughly mixed by sonication and added immediately to the reaction mixture. The suspension was always prepared fresh immediately prior to photocatalytic reaction and kept in the dark.

3.6 Photocatalytic reaction and Cell viability assay

The photocatalytic reaction was carried out in a 100 ml glass beaker containing the bacterial cell suspension to which the TiO_2 nanoparticles homogenized by sonication were added. The concentration of TiO_2 was optimized to 50 µg/ml, by carrying out photocatalytic experiments at different concentrations in sterile PBS (pH - 7.2). The TiO_2-cell suspension was placed on a magnetic stir plate for continuous stirring to

ensure proper nanoparticle-cell contact. The suspension was illuminated with UV light (352 nm), visible light (420 nm) and a dark control was also maintained. The loss of viability of bacterial cells was monitored by recording the viable count at regular time intervals of 60 and 120 minutes. Controls without TiO_2 and with undoped/unmodified TiO_2 were maintained simultaneously. Aliquots of the TiO_2-cell suspension were withdrawn, serially diluted with saline and spread plated in duplicates on nutrient agar plates. All the plates were incubated at 37 ℃ for 24 h. At the end of incubation, the cell viability was checked by recording the number of colonies as colony forming units per ml (cfu/ml).

3.7 Results and discussion

As a semiconductor, TiO_2 has a relatively large band gap, and can only be photoexcited in the UV spectrum of light to carry out photocatalytic activity (Linsebigler et al. 1995; Carp et al. 2004; Thompson and Yates, 2006). In semiconductors, doping is the intentional introduction of impurities in the material to modify its electrical conductivity (Carp et al. 2004; Diebold U. 2003; Chen and Mao, 2007). Hence, an ideal dopant in TiO_2 should increase the valence band edge, thereby reducing the band gap without lowering the conduction band, and minimize the rate of electron-hole recombination, thus improving the photocatalytic efficiency of TiO_2.

3.7.1 N doped TiO_2

Anion doping of TiO_2 is a field that has attracted immense interest and several studies with non metal anions such as C, S, I, and N have been reported. Doping of TiO_2 with anions improves the conductivity and optical properties, increases the percentage of the anatase phase in TiO_2, controls the crystallite size and increases the specific

surface area of TiO_2 (Reddy et al. 2005; Asahi et al. 2000; Wan et al. 2007). N doping has been reported to cause a decrease in the band gap or instead create new electronic states above the valence band thus shifting the absorption edge of the photocatalyst in the visible region (Michalow et al. 2009; Livraghi et al. 2006; Asahi et al. 2001). N doping is a substitutional doping where N anions replace the oxygen in the TiO_2 lattices and is effective due to the mixing of the N2p and O2p states thus causing a significant decrease in the width of the band gap (Ihara et al. 2003; Valentin et al. 2007; Etacheri et al. 2010).

The antibacterial activity of the N-TiO_2 was tested against *E. coli* in PBS. The results of the study showed a 90 % reduction in the number of bacterial cells after 120 minutes of visible light irradiation as compared to 15.5 % reduction with the control TiO_2 (Fig. 3.1).

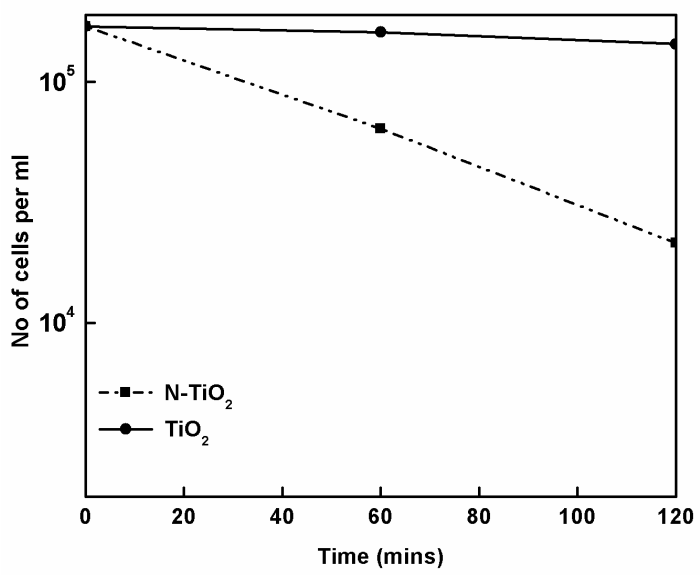

Fig. 3.1. Antibacterial activity of N-TiO_2 at 50 µg/ml under visible light in PBS.

It has been reported that the red shift in the absorption edge of N-TiO_2, facilitates absorption in the visible light spectrum due to the nitrogen atoms substituting the oxygen atoms in TiO_2 (Irie et al. 2003; Yates et al. 2006). Nitrogen doping not only

creates intra band gap states close to the valence band edges which facilitates visible light absorption, but it also shifts the position of flat band potential to a higher level than that of an undoped TiO_2. This increases the driving force of photogenerated electron and accelerates the reductive process of interfacial electron transfer (Torres et al. 2004; Valentin et al. 2007; Chen et al. 2009). Hence, the antibacterial activity of the N doped TiO_2 may be attributed to the combined effects of effective electron-hole separation, a narrow band gap and the improved crystallinity and textural properties.

3.7.2 Fe (C/N/S) doped TiO_2

Codoping of TiO_2 with both metal and non metal ions has been reported to shift the absorption edge of TiO_2 from UV region to the visible light region. Fe doped TiO_2 exhibits a shift of the absorption edge to the visible light region due to the excitation of the 3d electrons of Fe^{3+} to the TiO_2 conduction band (charge-transfer transition) (Wang et al. 1999; Shah et al. 2002; Rincon and Pulgarin, 2007). Non metal anions such as C, N and S are reported to substitute the oxygen atoms in the titania lattices (Chen et al. 2007; Reddy et al. 2005; Chen et al. 2009; Rockafellow et al. 2009). In the dopant anions the mixing of their p states with oxygen 2p states, shifts the valence band edge upwards thereby causing a significant decrease in the width of the overall bandgap (Chen et al. 2007; Reddy et al. 2005; Chen et al. 2009). N is known to be the most effective in substitutional doping as it narrows the band gap significantly, while S is not as effective due to its large ionic radius (Rockafellow et al. 2009; Ihara et al. 2003; Valentin et al. 2007). However, C and S non metal dopants play an important role in stabilizing metal ion dopants in doped TiO_2 systems, thereby increasing the electron-hole separation and decreasing charge carrier recombination (Hamal and Klabunde, 2007; Yu et al. 2005). Generally, when metal ions and non metal anions

are incorporated in metal oxides the impurity levels formed in the band gap of TiO_2 can increase the rate of recombination of charged carriers and improve the physicochemical properties such as crystallite size, surface area of the codoped TiO_2 thereby improving its overall photocatalytic efficiency (Hamal and Klabunde, 2007; Ohno et al. 2006; Xu et al. 2009).

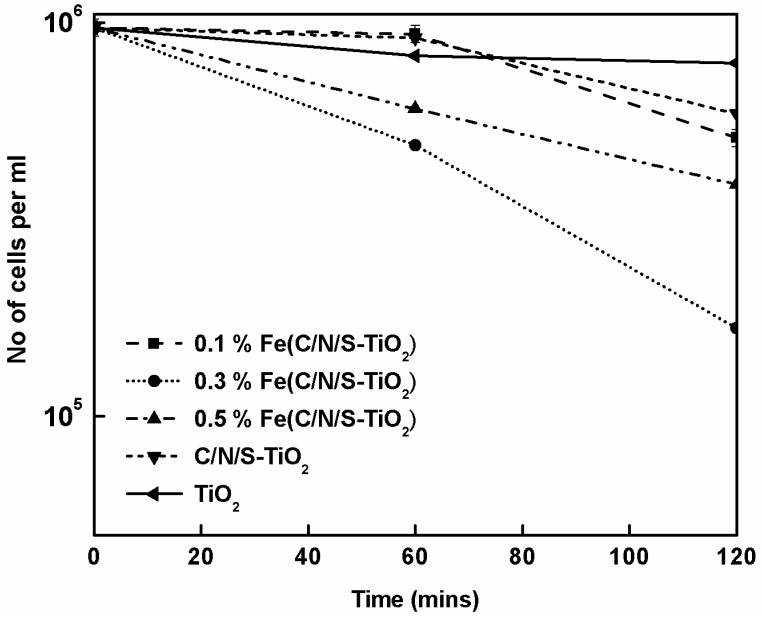

Fig. 3.2. Antibacterial activity of Fe(C/N/S-TiO_2) at 50 µg/ml under visible light in PBS.

Antibacterial studies on TiO_2 codoped with Fe (0.1 %, 0.3 % and 0.5 %) and non metal anions C, N and S showed that the reduction in bacterial count was highest for 0.3 % Fe (C/N/S-TiO_2) at 82.7 % followed by 60 % reduction for 0.5 % Fe, 47.5 % reduction for 0.1 % Fe and 39.5 % reduction for C/N/S-TiO_2 (with no Fe). Fe^{3+} ions adsorbed on the anion doped TiO_2 have been reported to be efficiently trapped by photoexcited electrons, thereby causing an improvement in the charge separation between the charged carriers. The unmodified TiO_2 showed only 15.6 % reduction in the bacterial count (Fig 3.2). The results of the study clearly show that 0.3 % Fe

doped TiO_2 exhibits the highest antibacterial activity followed by 0.5 % Fe doped TiO_2. It has been reported that for metal ion doped TiO_2 there is an optimal level of dopant concentration at which the photoactivity reaches a maximum (Asilturk et al. 2009; Zhou et al. 2005; Ranjit and Viswanathan, 1997). An increase in the dopant concentration above this level causes the metal ions to behave as recombination centers. This is because it narrows the space charge region and the light penetration into TiO_2 exceeds the width of space charge layer, thereby increasing the carrier recombination (Carp et al. 2004; Ranjit and Viswanathan, 1997; Gupta and Tripathi, 2011). Also, increasing the Fe^{3+} concentration decreases the photocatalytic activity because the solubility of iron in TiO_2 is less than 1 wt % and this leads to the formation of a separate phase such as Fe_2TiO_5, which could decrease its activity due to the transfer of charge carriers from TiO_2 to Fe_2TiO_5 (Wang et al. 1999; Zhou et al. 2005). Fe doped C/N/S-TiO_2 shows better antibacterial activity as compared to doped TiO_2 without Fe confirming the role of Fe in the photocatalytic process. Hence, the antibacterial activity could be mainly attributed to the effect of metal and non metal ion dopants that either decrease the band gap of the doped TiO_2 or create a new electronic state above the valence band or below the conduction band (Ohno et al. 2006; Asahi et al. 2000; Wan et al. 2007). A number of studies have reported the enhanced photocatalytic activity of non metal anion doped TiO_2 for the degradation of methylene blue (Wan et al. 2007; Chen et al. 2007) and organic compounds such as acetone and phenol (Ihara et al. 2003; Rockafellow et al. 2009). In the study with C/N/S-TiO_2, a 39.5 % reduction in the bacterial count was observed after 120 minutes of visible light exposure, which is not as significant as compared to 82.7 % reduction obtained with 0.3 % Fe (C/N/S-TiO_2). This could be because the oxygen deficient sites formed during N doping can serve to block reoxidation (Ihara et al. 2003). Also,

while N doping can improve absorption in the visible region, it does not necessarily enhance the quantum yield and the photocatalytic rate (Huang et al. 2006). Moreover, non metal anion such as S is a weak substitutional dopant, due to its ionic radius, and in S doped TiO_2, the substitutional doping sites act as deep hole traps, reducing the oxidizing power of the hole (Rockafellow et al. 2009). All these factors may possibly explain the weak antibacterial activity of C/N/S-TiO_2.

3.7.3 Ag doped TiO_2

Silver nanoparticles are known to show strong visible light absorption because of their size and shape dependent Plasmon resonance and several studies on the synthesis of plasmonic photocatalysts of Ag/AgCl which combines the plasmon resonance of silver with silver halides and exhibit efficient catalysis and stability under visible light (Wang et al. 2012; Ashkarran A, 2011; Hu et al. 2006). The stability of Ag/AgCl is attributed to the photons absorbed on silver nanoparticles as the photogenerated electrons remain in the nanoparticles and are not transferred to ionic form in the halide lattice (Wang et al. 2012; Hamal and Klabunde, 2007). Moreover, silver is known to be an excellent antimicrobial agent in both metallic and ionic form and hence was used for the synthesis of silver doped TiO_2 photocatalyst.

In the antibacterial study of $AgTiO_2$ against *E. coli* at 50 µg/ml, a much better antibacterial activity with a 99.99 % reduction in the bacterial count was observed under visible light irradiation while, only 18.9 % reduction was observed with undoped TiO_2 (Fig. 3.3). The photocatalytic activity of $AgTiO_2$ could be attributed to the strong visible light absorption, stability in dispersion and its high antimicrobial activity. However, similar antimicrobial activity was also observed in the dark controls which were not exposed to light. This indicated that the antibacterial activity

of $AgTiO_2$ was independent of light illumination and was mainly due to the antimicrobial properties of silver. There are several reports on the possible mechanisms by which Ag nanoparticles inhibit microbial growth such as particle attachment to cell membranes causing the changes of membrane permeability and redox cycle in the cytosol, intracellular radical accumulation, and dissipation of the proton motive force for ATP synthesis (Asharani et al. 2009; Rai et al. 2009; Lifen et al. 2009). In general it has been proposed that silver reacts with the disulfide of sulfhydryl groups of cells causing structural damage, disruption of metabolic processes and cell death.

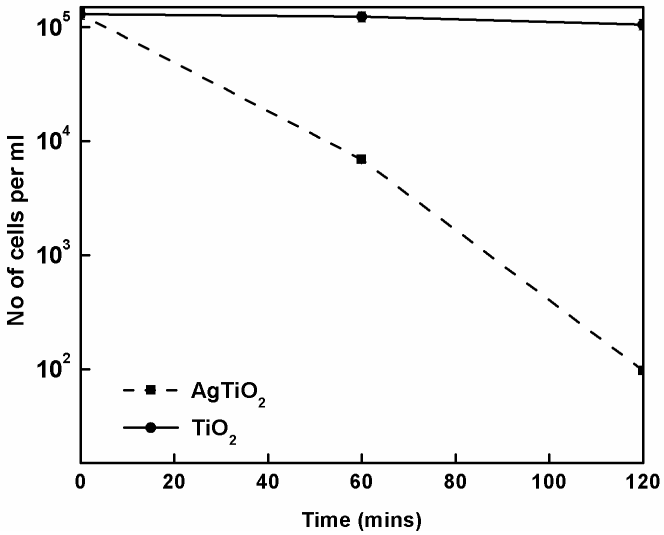

Fig. 3.3. Antibacterial activity of $AgTiO_2$ at 50 µg/ml under visible light in PBS.

3.7.4 Phosphate modified TiO_2

Phosphate anions are reported to have a strong affinity towards the surface of TiO_2 by the formation of inner-sphere surface complex, which can immensely influence the interfacial and surface chemistry of TiO_2 and improve its optical properties by extending the band gap energy (Zhao et al. 2008; Wu et al. 2007). The adsorption of phosphate on TiO_2 takes place mainly through the replacement of the surface

hydroxyl groups by the phosphate anion thereby decreasing the density of the surface hydroxyl group.

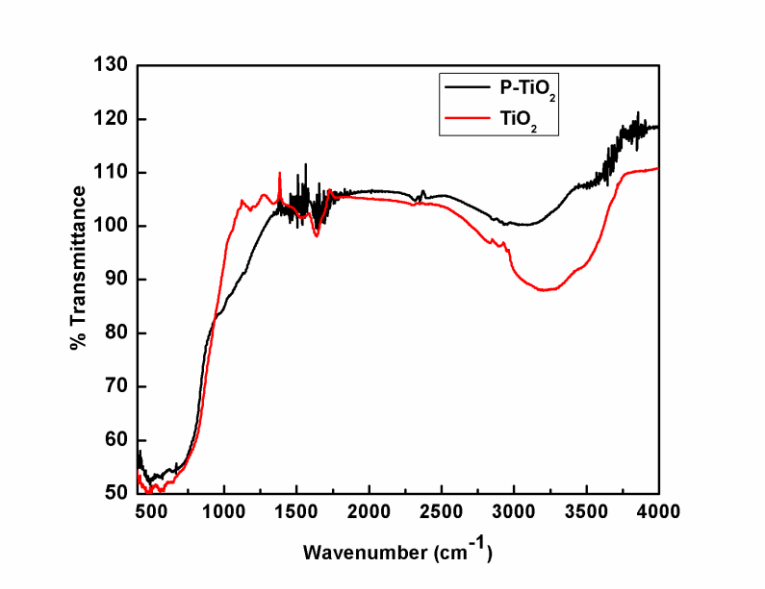

Fig. 3.4. FTIR spectra of P-TiO_2.

FTIR spectroscopy was carried out to establish the adsorption of phosphate onto the TiO_2 surface. The peaks at 747 cm^{-1} and 3200 cm^{-1} assigned for Ti-O-Ti stretching vibration of Ti and for surface adsorbed water molecules, respectively were observed for both the control and the modified TiO_2 (Fig. 3.4). After phosphate modification a new peak at 1086 cm^{-1} appeared on the shoulder of Ti-O-Ti vibration, which is a characteristic frequency of phosphate ions (Fig. 3.4). Similar observations have been reported for the FTIR studies of phosphate modified TiO_2, prepared by sol-gel method and modified with phosphoric acid as the modifying agent (Zhao et al. 2008).

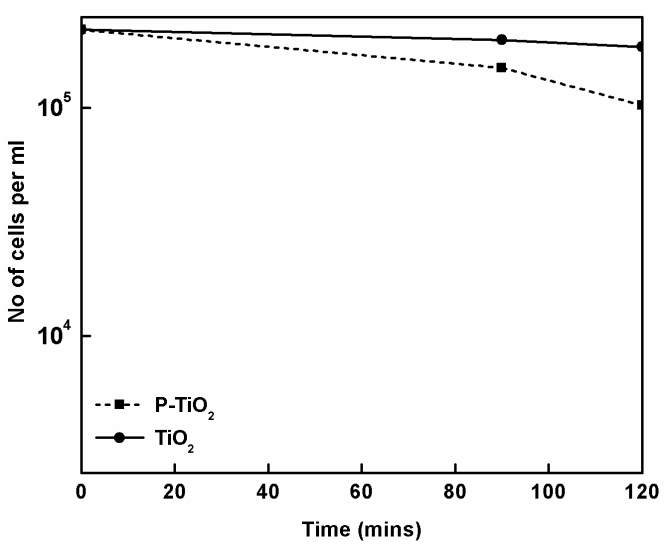

Fig. 3.5. Antibacterial activity of P-TiO_2 at 50 µg/ml under visible light in PBS.

In the antibacterial study, the phosphate modified TiO_2 showed a 31 % reduction in the bacterial count under visible light, as compared to 16.1 % reduction with the unmodified TiO_2 (Fig. 3.5). Several studies have reported high photocatalytic activity of phosphate modified TiO_2 for the degradation of organics such as phenol, n-pentane etc. due to extended band gap energy, large surface area and the presence of Ti ions in a tetrahedral coordination (Zhao et al. 2008). The minimal antibacterial activity observed in this study could be attributed to the phosphate groups adsorbed on TiO_2 surface that facilitate the generation of $^{\cdot}OH$ radicals and accelerate the hydroxyl radical attack by separation of photogenerated holes and electrons due to the negative electrostatic field of the adsorbed surface anion. In addition, phosphate modification can also enhance the surface hole and free hydroxyl radical concentration and aid the hydroxyl radical attack (Zhao et al. 2008). However, as phosphate can inhibit the adsorption of certain substrates, especially those degraded via the direct hole oxidation pathway, and has been shown to suppress the photocatalytic process, the activity of P-TiO_2 depends on the nature of substrate to be degraded (Zhao et al.

2008). This could probably account for the weak antibacterial activity of phosphate modified TiO_2, as the negative surface charge due to phosphate adsorption can hinder the interaction of P-TiO_2 with the negatively charged cell membrane of *E. coli* and decrease its antibacterial efficiency.

3.7.5 Modification of TiO_2 with organic acids (Salicylic acid, Folic acid, Fumaric acid, Malic acid and Succinic acid)

Surface modification of TiO_2 was carried out using salicylic acid, folic acid, fumaric acid, malic acid and succinic acid and tested for its effect on the enhancement of antimicrobial activity. Organic acids are known for their complexation ability and, therefore, the carboxyl groups are widely used as anchors for covalent binding. The interaction between the RCOOH group and TiO_2 surface involves the acid dissociation and exchange of surface hydroxyl groups with carboxylate ions i.e formation of RCOO-Ti bond (Macyk et al. 2010; Regazzoni et al. 1998; Gaweda et al. 2007; Chakraborty et al. 2010). In case of organic acids with adjacent carboxyl groups such as dicarboxylic acids (folic acid, fumaric acid, malic acid and succinic acid), the interaction between the carboxyl groups and TiO_2 surface to form surface complexes is more stable than the monocarboxylic acids.

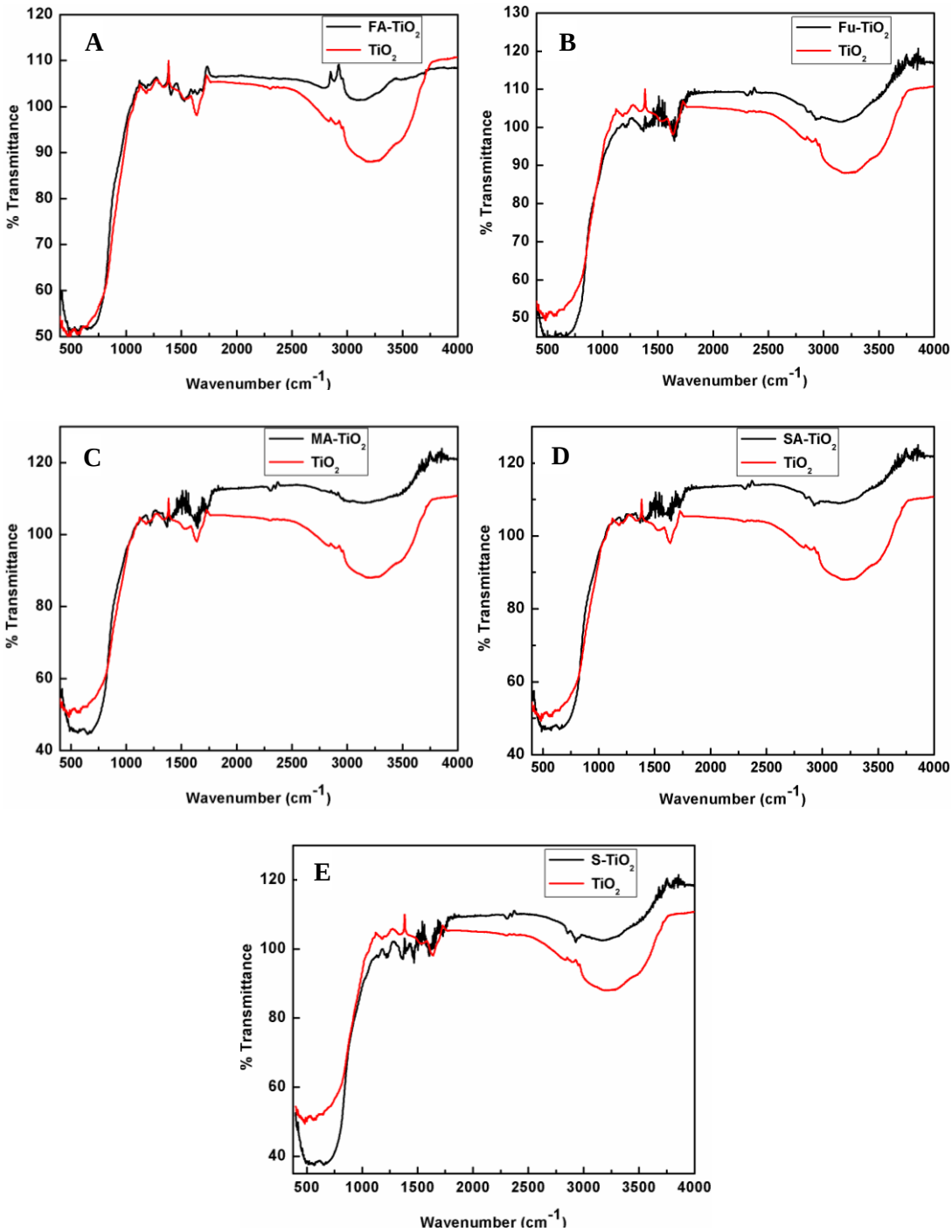

Fig. 3.6. FTIR spectra of A] FA-TiO_2, B] Fu-TiO_2, C] MA-TiO_2, D] SA-TiO_2 and E] S-TiO_2.

The FTIR studies were carried out to confirm the modification of TiO_2 by organic acids. FTIR spectra (Fig. 3.6 A-D) show a broad absorption band in the range of 2500-3600 cm^{-1}, which is a characteristic feature of carboxylic acid (Smith, 1999). A

band at ~1640 cm^{-1} is attributed to the surface adsorbed H_2O and the –OH group of TiO_2 (Baranska et al. 2003, Bullen et al. 2008). The presence of bands due to symmetric stretching vibrations of carboxylate salt (-COOM) at ~1520 cm^{-1} indicates linkage between the carboxylic acid and titanium atom (Fig. 3.6A-E) (Lai and Lee, 2009). Thus, these observations indicate the chemisorption of carboxylic acid on TiO_2 through carboxylate groups.

Hydroxycarboxylic acids such as salicylic acid are photolytes that have a great affinity for aqueous Ti(IV) and a strong tendency to chemisorb (Macyk et al. 2010; Regazzoni et al. 1998). Chemisorption of SA on TiO_2 leads to the formation of inner-sphere titanium (IV) salicylate surface complexes which present a band with optimum absorption at ~420 nm due to the intramolecular ligand to metal charge transfer (LMCT) transition (Macyk et al. 2010; Regazzoni et al. 1998; Jankovic et al. 2009). These complexes are formed as a result of coordinate bonds between adsorbing ligands and the surface metal ions (Macyk et al. 2010; Jancovic et al. 2010).

The FTIR studies of salicylic acid modified TiO_2 shows that, in salicylate bound TiO_2 the carboxyl and hydroxyl group vibrations change but the C-H aryl stretches at 1477 cm^{-1} are not affected (Makarova et al. 2000; Macyk et al. 2010). The carboxylate asymmetric stretch at 1518 cm^{-1} and the symmetric stretch at 1387 cm^{-1} indicates formation of carboxylate salt (Fig. 3.6E). This also implies that both carboxyl and hydroxyl groups of salicylic acid are involved in the binding to the TiO_2 (Makarova et al. 2000).

After the photogeneration of electron-hole pairs, the free holes can react with salicylic acid either due to hole capture by surface hydroxyls and subsequent hydroxyl attack on organic compounds, or direct electron injection by the chemisorbed salicylic acid (Regazzoni et al. 1998; Jancovic et al. 2010). Hence, salicylic acid was used for the

surface modification of TiO_2. The SA modified TiO_2 was observed to be yellowish in color (Regazzoni et al. 1998). In the antibacterial study carried out on *E. coli* in PBS, one log reduction (~90 %) in the bacterial count was observed with the modified S-TiO_2, while only 15.2 % reduction was obtained with unmodified TiO_2 after 120 minutes of visible light irradiation (Fig. 3.7). It has been reported that the affinity of salicylic acid to the titanium surface is dependent on the pH, however, no significant difference in the antimicrobial activity of the S-TiO_2 prepared at pH 1.1 and pH 3.4 was noted (Fig. 3.7). Although S-TiO_2 has been shown to carry out photocatalytic degradation of organic compounds such as monochlorobenzene (Nsib et al. 2013) and 4-nitrophenol (Xing et al. 2006), no significant antimicrobial activity was obtained under visible light irradiation.

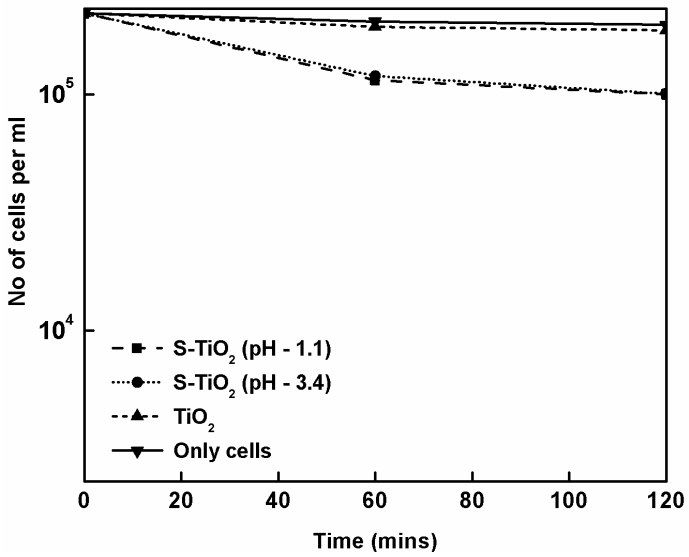

Fig. 3.7. Antibacterial activity of S-TiO_2 at 50 µg/ml under visible light in PBS.

The antibacterial activity of the surface modified TiO_2 (FA-TiO_2, Fu-TiO_2, SA-TiO_2, MA-TiO_2) was tested against *E. coli* under visible light irradiation. FA-TiO_2, Fu-TiO_2 and MA-TiO_2 exhibited 99 % reduction in the bacterial count whereas only 65 % reduction was observed in SA-TiO_2. TiO_2 control showed 13.2 % reduction in the

number of bacterial cells (Fig 3.8). It has been reported that chemisorption of carboxylic acid on TiO_2 causes the substitution of the surface OH groups with anionic species and a shift in valence and conduction bands due to electrostatic repulsion of electrons within TiO_2. In such surface modified TiO_2 structures the localized orbitals of surface-attached ligands are electronically coupled with the delocalized electron levels from the conduction band of TiO_2 photocatalyst (Macyk et al. 2010; Gaweda et al. 2007). Hence, light absorption by charge-transfer complexes leads to excitation of electrons from the ligand to the conduction band of TiO_2 resulting in a red shift of the modified TiO_2 (Gaweda et al. 2007; Carp et al. 2004; Macyk et al. 2010). This could be the reason for the better activity of FA-TiO_2, Fu-TiO_2 and MA-TiO_2 than pure TiO_2. The antibacterial activity of organic acid modified TiO_2 is mainly attributed to the generation of oxidative radicals that cause oxidative stress in the cells and subsequent cell death. The visible light activity of modified TiO_2 may be attributed to the combined effect of carboxylic acid aided absorption in visible light, coupled with properties of the acids such as increased uptake (for folic acid) (Chakraborty et al. 2010; Mohapatra et al. 2007) or antibacterial property (for fumaric acid) (Comes and Beelman, 2002; Alvarez-Ordonez et al. 2009). Antioxidant properties of succinic acid probably interferes with its antibacterial activity (Mokbel and Hashinaga, 2005; Comes and Beelman, 2002). The antioxidative action suppresses the action of ROS involved in photocatalytic inactivation.

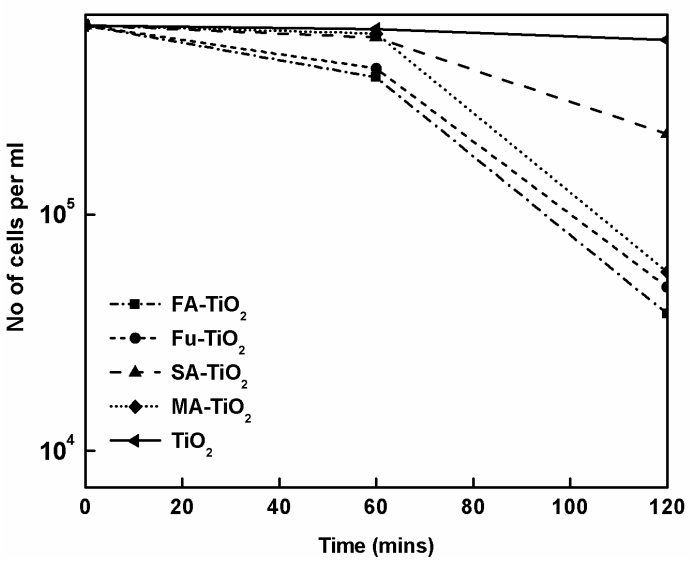

Fig. 3.8. Antibacterial activity of FA/Fu/SA/MA-TiO_2 at 50 µg/ml under visible light in PBS.

3.7.6 Amino acids

Amino acids adsorb on TiO_2 surface due to the exchange of hydroxyl groups with carboxyl ions. During the complexation, ligand to metal charge transfer (LMCT) interaction occurs that enhances the electronic properties of the semiconductor nanoparticles causing a red shift in the absorption spectrum (Rajh et al. 2002; Makarova et al. 2000) The red shift is attributed to the excitation of localized electrons from the modifier molecule into the band continuum states of TiO_2. Apart from altering the optical properties of the modified TiO_2, surface modification also tunes the effective band gap of modified TiO_2 which has been reported to be proportional to the density of delocalized electrons and dipole moment of surface bound titanium enediol ligand complexes (Durupthy et al. 2007; Cropek et al. 2008; Monti S. 2007).

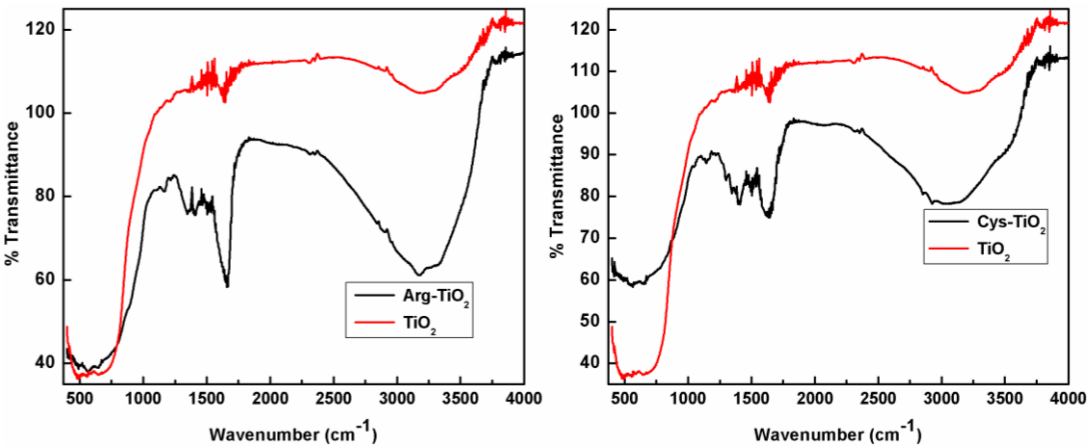

Fig. 3.9. FTIR spectra of Arg-TiO_2 and Cys-TiO_2.

The FTIR analysis was performed to confirm the modification of TiO_2 by amino acids (Fig. 3.9). The FTIR spectra show a broad absorption band between 2600 and 3700 cm^{-1}, centered at ~3200 cm^{-1}, which is the characteristic band for the hydrogen-bonded OH stretching vibration (Smith, 1999). A band at around 1640 cm^{-1} for Arg-TiO_2 and 1625 cm^{-1} for Cys-TiO_2 is attributed to the adsorbed water bending (Makarova et al. 2000; Cropek et al. 2008). NH_2 symmetric stretches at 3298 cm^{-1}, and NH_2 scissoring at 3167 cm^{-1}, are present in the Arg-TiO_2 spectrum. Band at 1403 cm^{-1} is attributed to the -COOM bonds in Cys-TiO_2 ((Makarova et al. 2000).

It has been observed that charged amino acids can strongly adsorb onto titanium materials through direct or indirect interactions of their side chains (Monti S. 2007; Makarova et al. 2000; Durupthy et al. 2007). In this study, TiO_2 was modified with L-arginine and cysteine. The antibacterial study against *E. coli* exhibited a 56 and 54 % reduction in the bacterial count for Arg-TiO_2 and Cys-TiO_2, respectively, under visible light exposure for 120 minutes (Fig. 3.10). These results are not very significant as compared to the antibacterial activity achieved for FA-TiO_2, Fu-TiO_2 and MA-TiO_2 and S-TiO_2 under similar experimental conditions. The lower antibacterial activity of Arg-TiO_2 and Cys-TiO_2 could possibly be due to the

antioxidative action of the amino acids that can suppress the oxidative action of reactive radicals generated during photoirradiation.

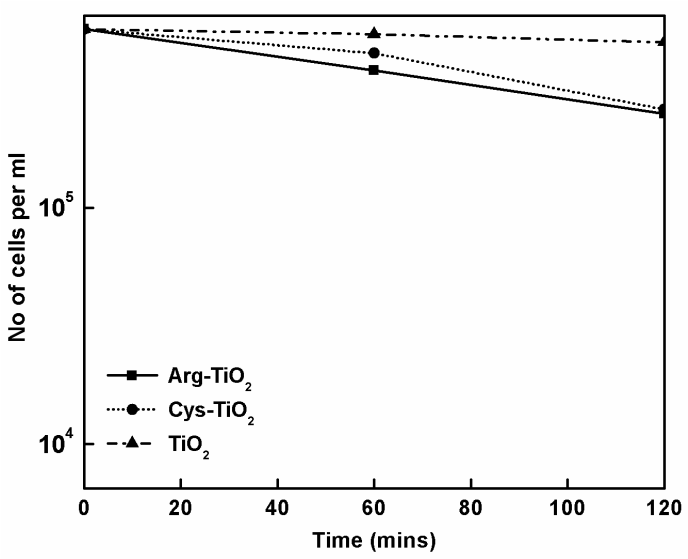

Fig. 3.10. Antibacterial activity of Arg-TiO_2 and Cys-TiO_2 at 50 µg/ml under visible light in PBS.

Among the various modifying/doping agents tested for antimicrobial activity in the visible light, maximal activity was obtained for $AgTiO_2$ with 99.99 % reduction in cell number within 120 min. FA-TiO_2, Fu-TiO_2 and MA-TiO_2 also showed good antibacterial activity with 99 % reduction in cell count. These carboxylic acids can be ideal modifying/functionalizing agents especially since they are generally recognized as safe (GRAS), non immunogenic, low molecular weight and inexpensive molecules (Chakraborty et al. 2010; Mohapatra et al. 2007; Comes and Beelman, 2002; Alvarez-Ordonez et al. 2009). The prospect of using such molecules and silver for development of TiO_2 nanocomposites is a promising strategy for the development of effective and economical antibacterial systems. Hence, further studies have been carried out and reported in this thesis for the synthesis of functionalized silver based TiO_2 nanocomposites which are biocompatible, stable and exhibit good antimicrobial activity against an array of microorganisms.

Conclusion

A number of different doped/modified TiO_2 were synthesized and their antibacterial activity was determined under visible light irradiation against *E. coli*. TiO_2 doping was done with transition metal ions silver and iron; non metals nitrogen, sulphur, carbon and surface modification was done with folic acid, amino acids (L-arginine & Cysteine), organic acids (salicylic acid, fumaric acid, succinic acid and malic acid), and phosphate. Surface modification was confirmed by FTIR analysis. Doping/modification showed both positive and negative results in PBS medium, under different irradiation conditions in comparison to plain TiO_2. Among the transition metal ion doped TiO_2, $AgTiO_2$ was observed to be very effective in visible light conditions, whereas Fe (C/N/S)-TiO_2 little antibacterial activity in visible light. In Fe (C/N/S)-TiO_2 it was observed that the antibacterial activity was dependent on the concentration of Fe^{3+} doped. In the case of N doped TiO_2, the antibacterial activity was observed to be slightly better than undoped TiO_2. Among the modified TiO_2, S-TiO_2 and P-TiO_2 were observed to be more effective than plain TiO_2 under visible light. FA-TiO_2 and Fu-TiO_2 were observed to have weaker antibacterial activity in UV light than unmodified TiO_2, however, under visible light irradiation they showed better antibacterial activity compared to unmodified TiO_2. Overall, while Ag doped TiO_2 exhibited the highest antibacterial activity, P-TiO_2 also showed good antibacterial activity. Among the organic acid modified TiO_2, the antibacterial activity was in the order of FA-TiO_2 > Fu-TiO_2 > MA-TiO_2 > S-TiO_2 > SA-TiO_2 under visible light conditions.

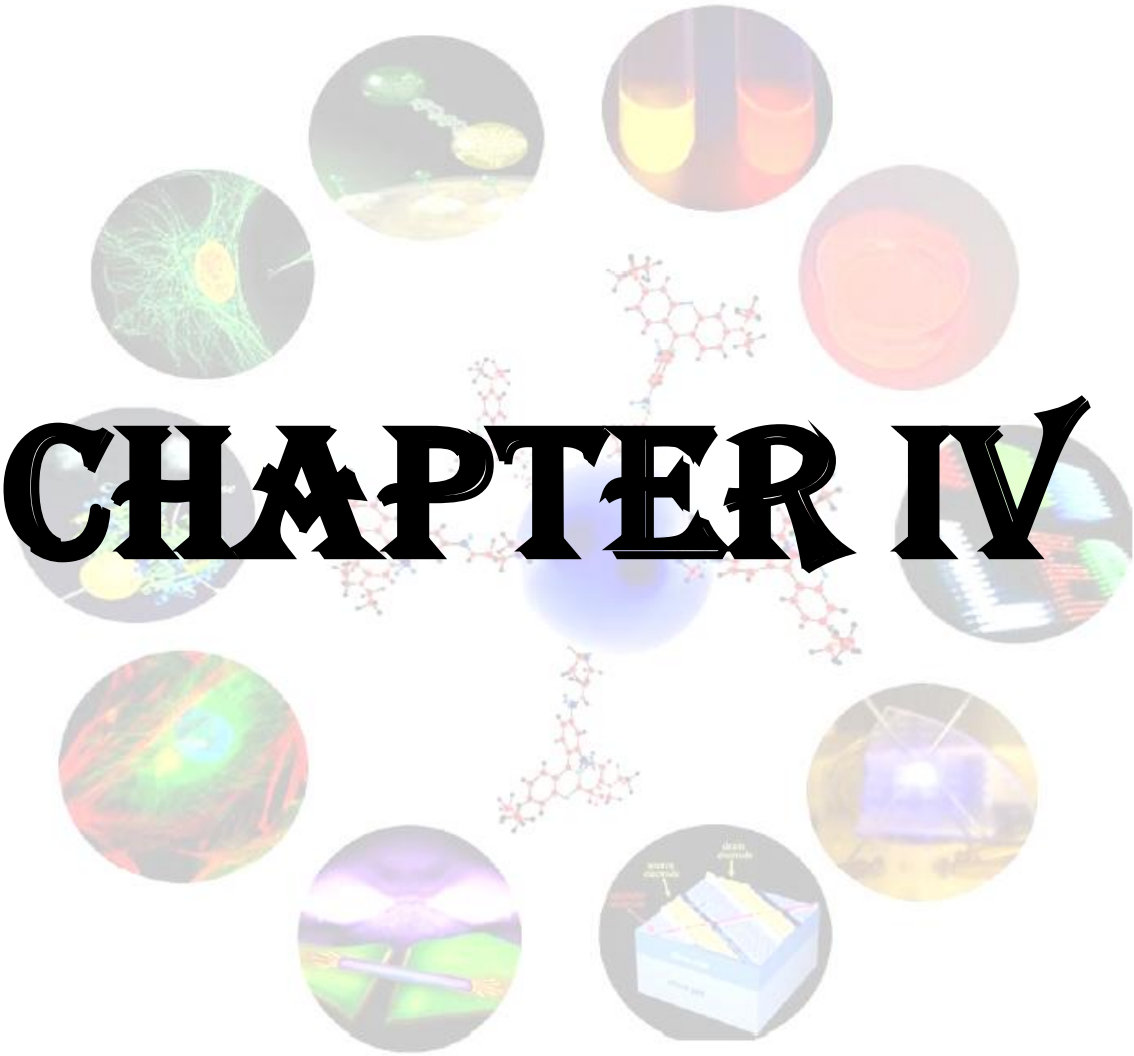

CHAPTER IV

Chapter 4

Functionalization of $AgCl/TiO_2$ nanocomposites and evaluation of its antimicrobial activity against different microorganisms

Abstract

Metal oxide nanoparticles are versatile tools for biological applications and surface functionalization of these metal oxide nanoparticles add to their versatility since hybridization with functional molecules provides biocompatibility, catalytic abilities, and controlled surface properties. Silver based TiO_2 ($AgCl/TiO_2$) composites have attracted considerable attention because of their non toxicity and remarkable catalytic & antibacterial activity. In this chapter we report the synthesis and antimicrobial activity of functionalized $AgCl/TiO_2$ with folic acid (FA-$AgCl/TiO_2$), organic acids (Fumaric acid (Fu-$AgCl/TiO_2$), Malic acid (MA-$AgCl/TiO_2$) and Succinic acid (SA-$AgCl/TiO_2$)) and amino acids L-arginine (Arg-$AgCl/TiO_2$) and L-cysteine (Cys-$AgCl/TiO_2$)). The antimicrobial activity in terms of MIC and MBC of FA-$AgCl/TiO_2$ and Fu-$AgCl/TiO_2$ was found to be better than the unfunctionalized $AgCl/TiO_2$. However, in case of MA-$AgCl/TiO_2$ and SA-$AgCl/TiO_2$ the MIC and MBC was higher than the unfunctionalized $AgCl/TiO_2$. Similarly, Arg-$AgCl/TiO_2$ and Cys-$AgCl/TiO_2$ did not show any enhancement in antimicrobial activity after functionalization. The characterization studies showed no changes in the crystal structure and phase of TiO_2 and a lesser degree of aggregation was observed in case of functionalized $AgCl/TiO_2$ nanocomposites. Further, the physicochemical properties such as size and surface area of FA-$AgCl/TiO_2$ and Fu-$AgCl/TiO_2$ were superior to those of unfunctionalized nanocomposites. The enhanced antimicrobial activity of

FA-$AgCl/TiO_2$ and Fu-$AgCl/TiO_2$ is attributed to the increased uptake of functionalized $AgCl/TiO_2$ that increases the ROS species causing oxidative damage to the microbial cells.

4.1 Introduction

Development of antimicrobial nanocomposites with metal oxide as the host support material is a field of immense research interest. A nanocomposite material that can be successfully used against potential biological threats and can also guarantee the safety of products related to water, food/beverage packaging or containers for biomedical/pharmaceutical materials/devices, is the need of the day. Antimicrobials based on silver nanoparticles, exhibit remarkable activity as they are known to target multiple cellular sites simultaneously (Rai et al. 2009; Kvitek et al. 2008). However, the applications of silver nanoparticles in dispersions are limited by the problem of photooxidation and the formation of spacious aggregates (Ivanova and Zamborini, 2010; Lok et al. 2007). Therefore, an antimicrobial nanocomposite material with highly dispersed, uniform, small Ag particles, with desired level of Ag loading could be a major breakthrough (Zhang and Chen, 2009). Among various nanocomposite structures, TiO_2 based nanocomposites have attracted much attention due to their high chemical stability, non-toxicity, faster electron-transfer ability and low cost (Acosta-Torres et al. 2011; Sun et al. 2009). Further, in such a configuration of $AgTiO_2$ nanocomposite the TiO_2 particles serve as strong anti-aggregation supports, thus increasing the active surface area of the antibacterial agent and thereby, the contact area between the antibacterial agent and the medium (Zhang and Chen, 2009). Hence, silver-TiO_2 nanocomposites are promising candidates for applications in food and beverage industry, water disinfection, therapeutics and biomedical materials (Shah et

al. 2008; Liu et al. 2008; Su et al. 2009). It is important that the support carrier in a supported antibacterial material is chemically durable, biocompatible and antimicrobial in nature (Kawashita et al. 2003; Schierholz et al. 1999). The major strategies to develop such nanomaterials include capping/functionalization with specific molecules, compositing with polymers and bioconjugation.

Surface functionalization: The broad area of conjugate chemistry is based on combining the functionalities of relevant molecules with nonbiologically derived molecular species in conformationally favorable orientations. The stability/biocompatibility of nanocomposites can be improved by functionalization with hydrophilic biomolecules, which modify their surface properties and function as barriers against moisture and oxygen (Vimala et al. 2011; Lu et al. 2008). Moreover, surface charge on the nanoparticles plays an important role in the particle-cell interactions. Therefore, the negative or positive charge of the particle surface coatings may lead to alternative interactions with the cell membrane. Surface functionalization helps in improving particle solubility/dispersibility and stability (Thiel et al. 2007), increases uptake by cells (Win and Feng, 2005), and further enhances the surface chemical reactivity for conjugation of bioactive ligands (Nobs et al. 2003).

Folic acid: Among the various redox-active chromophores, folic acid is a low molecular weight molecule which is stable, inexpensive, and non-immunogenic (Stella et al. 2000). It can easily be immobilized on metal oxide surfaces due to the presence of suitable anchoring groups and its hydrophilic nature enhances its dispersibility and stability in culture medium (Gaweda et al. 2007; Diebold U. 2003). Moreover, the pterin cofactors to which it belongs have various physiological functions involving electron-transfer processes (Gaweda et al. 2007; Kritsky et al.

2001; Moorthy and Hayon, 1977). Folic acid is also essential for nucleotide and cell wall synthesis in bacteria (Chakraborty et al. 2010; Dulaney and Marx, 1971) and therefore, when bacteria interact with folate conjugated nanoparticles, they may be attracted to the folate thereby increasing the prospect of uptake of the nanoparticles by bacteria (Chakraborty et al. 2010; Stella et al. 2000; Henderson and Potuznik, 1982). Folic acid conjugated nanoparticles have been used for specific targeting of cancerous cells (Stella et al. 2000; Lai and Lee, 2009; Asharani et al. 2009). Folic acid tagged chitosan nanoparticles have been used to deliver vancomycin into drug resistant *S. aureus* cells since they can overcome the barrier of the cell membrane (Chakraborty et al. 2010).

Organic acids (Fumaric acid, Malic acid and Succinic acid): Fumaric acid is a low molecular weight, unsaturated organic acid and generally recognized as safe (GRAS) food-grade acidulant (Kondo et al. 2006), which exhibits good dispersibility and stability in aqueous media due to its hydrophilic nature (Kondo et al. 2006; Gaweda et al. 2007). Malic and succinic acids have generally been used because of their bactericidal activity, and are generally recognized as safe (GRAS) (Dickson, 1992; Izat et al. 1989). These are naturally present in a lot of fruits and herbs and are used as food preservatives and food additives due to their antimicrobial properties (Comes and Beelman, 2002; Mokbel and Hashinaga, 2005; Skrivanova et al. 2006). Fumaric acid has been shown to be effective against various microorganisms including pathogenic bacteria such as *Campylobacter jejun*, *Salmonella typhimurium*, *E.coli*, *Listeria monocytogenes* and *S. aureus* (Kondo et al. 2006; Comes and Beelman, 2002; Skrivanova et al. 2006). Malic and succinic acids are also reported to exhibit antibacterial activity against both gram positive as well as gram negative bacteria

(Skrivanova et al. 2006; Mokbel and Hashinaga, 2005). Thus they find applications as preservatives in various food products such as fruit drinks, gelatin desserts, meat and dairy products (Kondo et al. 2006; Comes and Beelman, 2002; Skrivanova et al. 2006). In tissue engineering, fumarate and fumarate based oligomers have been used to synthesize hydrogels and biomedical implants (Shin et al. 2003; Wang et al. 2006).

Amino acid functionalization: Some molecules of direct relevance to the biochemical modification of titanium oxide surfaces are self-complementary amphiphilic oligopeptides that have regular repeating units of charged residues such as amino acids.

L-arginine is a positively charged amino acid with a high affinity for hydrogen-bonding, possesses electron-donating properties and binds to the TiO_2 surface via the carboxyl group (Makarova et al. 2000; Skubal and Meshkov, 2002). The arginine-TiO_2 coupling occurs at different temperatures and most of the electrons are localized as lattice trapped electrons with high negative redox potential and hence are very powerful reducing agents. Several reports suggest that surface modifiers with good affinity to the TiO_2 surface and good electron donating properties, significantly enhance the reduction kinetics (Makarova et al. 2000; Cropek et al. 2008).

In case of L-cysteine modified TiO_2, cysteine molecules bound to the TiO_2 surface trap the holes generated, thereby greatly facilitating the reduction processes (Konovalova et al. 1999). The –COOH functional surface enhances cell uptake in relation to the amount of –COOH functionalized on the nanoparticle surface. This might be due to favorable interactions of the cell with the negatively charged nanoparticle coating (Holzapfel et al. 2006). However studies have also shown that excessive concentration of –COOH on the surface results in a negative charge on the

surface, which may cause unfavorable membrane interactions between particles and cell membranes (Ohya et al. 2004).

The potential use of such molecules to functionalize antimicrobial nanomaterials in order to improve their efficacy is largely unexplored. With the emergence of multi-drug resistance among microbial strains which is now a serious health concern of global dimensions, the prospect of using such molecules for functionalizing antimicrobial agents is a simple but novel and elegant strategy. In this study, we report the synthesis of folic acid, fumaric acid, malic acid, succinic acid as well as L-arginine and cysteine functionalized $AgCl/TiO_2$ by a simple, sol-gel method. Some of the functionalized nanocomposites (FA-$AgCl/TiO_2$ and Fu-$AgCl/TiO_2$) exhibited better antimicrobial activity compared to unfunctionalized $AgCl/TiO_2$ nanocomposites when tested against representative bacterial and fungal cultures.

4.2 Materials and Methods

4.2.1 Synthesis of functionalized nanocomposites

A) Folic acid-$AgCl/TiO_2$ (FA-$AgCl/TiO_2$) nanocomposites

Functionalization of $AgCl/TiO_2$ with folic acid (98 %, Hi-media Laboratories, India) was carried out as per Gaweda et al [27] with modification in folic acid concentration. The $AgCl/TiO_2$ nanoparticles (1 atomic % silver) were synthesized by simple sol-gel method as described in chapter 2, section 2.2.1. For functionalization with folic acid, 1.35 mM solution of folic acid in DMF (99.8 %, Fisher Scientific, India) was heated at 80 °C for 10 min. The solution was cooled and filtered after addition of an equal volume of deionized water. $AgCl/TiO_2$ powder was added to the filtered folic acid solution and stirred for 10 min. The modified $AgCl/TiO_2$ was washed five times each

with DMF followed by distilled water. The folic acid modified $AgCl/TiO_2$ was dried in air to obtain a fine yellow powder and designated as FA-$AgCl/TiO_2$.

B) Fumaric acid-$AgCl/TiO_2$ (Fu-$AgCl/TiO_2$), Malic acid-$AgCl/TiO_2$ (MA-$AgCl/TiO_2$) and Succinic acid-$AgCl/TiO_2$ (SA-$AgCl/TiO_2$) nanocomposites

The synthesis and functionalization of fumaric acid-$AgCl/TiO_2$, malic acid-$AgCl/TiO_2$ and succinic acid-$AgCl/TiO_2$ nanocomposites was carried out using ~8.61 mM fumaric acid and ~16.78 mM of malic & 15.24 mM succinic acid (99 %, Hi-media Laboratories, India), as per the procedure described in section 5.2.1. The fine white powders of fumaric acid, malic acid and succinic acid modified $AgCl/TiO_2$ were designated as Fu-$AgCl/TiO_2$, MA-$AgCl/TiO_2$ and SA-$AgCl/TiO_2$, respectively.

C) Arginine-$AgCl/TiO_2$ (Arg-$AgCl/TiO_2$) and Cysteine-$AgCl/TiO_2$ (Cys-$AgCl/TiO_2$) nanocomposites

The synthesis and functionalization of Arginine-$AgCl/TiO_2$ and Cysteine-$AgCl/TiO_2$ nanocomposites was carried out using L-arginine (~0.015 M in DMF) and L-Cysteine (0.05 M in DMF) (99 %, Sd fine chemicals, India), as per the procedure described in section 5.2.1. The functionalized $AgCl/TiO_2$ was designated as Arg-$AgCl/TiO_2$ and Cys-$AgCl/TiO_2$ for arginine and cysteine, respectively.

4.2.2 Microbial cultures

The microbial cultures were procured from NCIM Pune and MTCC Chandigarh, India. Nutrient broth (NB)/Saborauds Dextrose broth (SDB) medium (Hi-media Laboratories, India) was used for enrichment and growth. Exponential phase cells at a concentration of ~10^5 cfu/ml were used as inoculums for antimicrobial tests. The five microbial cultures used were *Escherichia coli* NCIM 2345, *Micrococcus luteus*,

Pseudomonas aeruginosa MTCC 2581, *Staphylococcus aureus* MTCC 737 and *Candida albicans* MTCC 3958.

4.2.3 Antimicrobial activity evaluation

4.2.3.1 Determination of MIC and MBC

The MICs of the functionalized nanocomposites (FA-AgCl/TiO_2, Fu-AgCl/TiO_2, MA-AgCl/TiO_2, SA-AgCl/TiO_2, Arg-AgCl/TiO_2, and Cys-AgCl/TiO_2) and unfunctionalized AgCl/TiO_2 were determined using a microtitre resazurin assay which is a modification of the Clinical and Laboratory Standards Institute (CLSI)-approved microtitre serial dilution method (LiPuma et al. 2009). All the functionalized nanocomposites along with unfunctionalized AgCl/TiO_2 were tested for antibacterial activity against Gram negative *E. coli* and Gram positive *M. luteus*. Double strength Mueller Hinton broth (MHB) was added to sterile 96 well microtiter plates. This was followed by addition of an appropriate amount of the functionalized nanocomposite and unfunctionalized AgCl/TiO_2 from a stock concentration of 1 mg/ml prepared in sterile deionized water. 10 µl of 0.1 % resazurin sodium salt (Sigma-Aldrich) was subsequently added to each well. Resazurin, a nonfluorescing blue dye, is reduced to resorufin, a fluorescing pink dye, in the presence of actively metabolizing cells. Finally, exponential phase bacterial/fungal cells were added to the wells at a final cell concentration of 10^5 cfu/ml and the volume was made upto 200µl using deionized water. Microtiter plates were incubated in the dark at 37°C on a shaking incubator. The MICs were recorded after 24 h as the lowest concentration of the nanocomposite at which no blue to pink color change was observed. The following controls were run simultaneously during the experiment: i) Only bacteria (Positive control) ii) Only

growth medium iii) Medium + resazurin dye iv) Medium + Resazurin dye + functionalized nanocomposite or unfunctionalized nanocomposite.

To determine MBC, the wells in the microtitre plate with no color change were spot inoculated on nutrient agar (NA) plates and incubated at 37 ℃ for 24 h. The concentration at which no growth was observed was recorded as the MBC value.

Based on the antibacterial results, FA-AgCl/TiO_2 was further tested against Gram positive *S. aureus*, Gram negative *P. aeruginosa* and a fungal strain of *C. albicans* for determination of MIC and MBC using the same procedure described above. Double strength Yeast extract sucrose medium (YES) was used for the MIC studies of *C. albicans* and Sabourauds dextrose agar (SDA) plates were used for the MBC studies. The incubation was carried out at 30 ℃.

4.2.3.2 Study by microbial inactivation kinetics

The time required for the inactivation of test microorganisms in presence of FA-AgCl/TiO_2, Fu-AgCl/TiO_2 and AgCl/TiO_2 was determined by conventional plate count method. Exponential phase microbial cells (10^5 cfu/ml) were added to 50 µg/ml of FA-AgCl/TiO_2 or AgCl/TiO_2 suspension prepared in PBS. The suspension was incubated at 37/30 ℃ and 110 rpm. Similar studies for Fu-AgCl/TiO_2 and AgCl/TiO_2 in PBS were carried out for two bacterial cultures *E. coli* and *M. luteus* at 100 µg/ml. Aliquots were withdrawn after 30, 60, 90 and 120 min and plated out on NA/SDA plates after appropriate dilutions. The plates were incubated at 37/30 ℃ for 24 h and the colony count was calculated and expressed as cfu/ml.

4.2.4 Characterization studies of FA-AgCl/TiO_2 and Fu-AgCl/TiO_2

The synthesized nanocomposites were characterized by XRD analysis, N_2 adsorption-desorption analysis, and TEM imaging as described in section 2.2.2 of chapter 2.

4.2.4.1 Particle size analysis

The particle size of the nanocomposite samples was determined using a particle size analyzer (Delsa Nano S, Backman Coulter, USA) at 25 °C. The average values of the particle size and polydispersity, defined as relative width of the size distribution, were determined from the DLS measurements.

4.2.4.2 FTIR analysis

FTIR spectroscopy was carried out using FTIR-IR Affinity – 1 01660, Shimadzu. All samples were milled with spectroscopic grade potassium bromide (KBr, Merck), and a pellet of the mixture was pressed into a disc, placed in the solid cell, and scanned in the range of 400-4000 cm^{-1} against a KBr control.

4.2.4.3 EDAX analysis

EDAX analysis of the samples was carried out using a SEM-EDAX, JEOL JSM-6360 LV, after coating with platinum by JEOL JFC-1600 Autobine sputter.

4.2.5 Hemolytic assay

For any biomedical applications or *in-vivo* studies, it is essential to assess the hemolytic activity of a new compound or material. Hemolytic activity of FA-AgCl/TiO_2, Fu-AgCl/TiO_2 and AgCl/TiO_2 was evaluated on red blood cells according to the method described by Parnham, Yinghui et al (Landi et al. 2000; Chen et al. 2008). Sterile saline solution (1.25 ml) was added to 1 mg of Ag-HAp. 2 ml blood

was collected from a healthy human and diluted with sterile saline solution to make the final volume to 5 ml. The diluted blood (20µl) was then added to the tubes containing FA-AgCl/TiO_2 at concentrations of 150, 100 and 50 µg/ml; Fu-AgCl/TiO_2 at concentrations of 250, 200 and 150 µg/ml and AgCl/TiO_2 control at 250, 200 and 150 µg/ml, in sterile saline solution and incubated at 37ºC for 30 min. Subsequently, the tubes were incubated for 60 min in water bath shaker at 37ºC and centrifuged at 700X g for 10 min. Sterile saline solution and distilled water were used as the negative and positive controls, respectively. The amount of free hemoglobin was determined by measuring the absorbance of the supernatant at 540 nm (UV Spectrophotometer Shimadzu UV 2450). The hemolysis rate (HR) was calculated using (Zheng et al. 2009):

$$HR = \frac{Dt - Dnc}{Dpc - Dnc} x\ 100\%,$$

Where, *HR* is the hemolysis ratio and *Dt, Dnc* and *Dpc* are the average absorbance values of test samples, negative controls and positive controls, respectively.

The hemolytic assay was carried out in duplicates to ensure repeatability.

4.2.6 Scanning Electron Microscopy (SEM)

Exponential phase *E. coli* cells (~10^5 cfu/ml) were suspended in medium containing FA-AgCl/TiO_2 and Fu-AgCl/TiO_2 (50 µg/ml) and incubated for 2 h at 37 °C. The cells were washed with PBS, and fixed with 2 % glutaraldehyde (Electron microscopy grade, Hi-media Laboratories, India) solution for 1 h (Su et al. 2009; Hartmann et al. 2010). Subsequently, the cells were given three washings with 0.1 M PBS (pH 7.2) and sequentially dehydrated using ethanol/H_2O mixture of 10, 25, 50, 75, 90 (v/v %)

and finally with 100 % ethanol, followed by air drying. The dried cells were then coated with platinum by JEOL JFC-1600 Autobine sputter and the images were taken with a JEOL JSM-6360 LV Scanning Electron Microscope at a voltage of around 6 kV. A control sample wherein the cells were not exposed to FA-AgCl/TiO_2 or Fu-AgCl/TiO_2 was similarly processed.

4.2.7 Detection of intracellular reactive oxygen species (ROS)

Intracellular ROS was estimated using 2',7'- dichlorofluorescein diacetate (DCFH-DA). The oxidation of non-fluorescent DCFH to highly fluorescent 2',7'-dichlorofluorescein (DCF) provides a quantitative estimate of ROS formation (Liu and Hurt, 2010; Su et al. 2009). The bacterial cells (10^5 cfu/ml) were suspended in PBS and exposed to 50 μg/ml FA-AgCl/TiO_2 for 2 h. DCFH-DA (20 μM) was added and the suspension incubated at 30°C for 30 min. Cells were separated by centrifugation at 70 RCF for 4 min and washed with PBS. The pellet was resuspended in PBS and the fluorescence was recorded at 521 nm using JASCO FP-6300 spectrofluorometer (Tokyo, Japan). ROS was also estimated in bacterial cells pre-exposed to 5 mM of N-acetyl cysteine for 2 h in PBS prior to FA-AgCl/TiO_2 exposure. All the experiments for antimicrobial studies were carried out in triplicates to ensure reproducibility.

4.2.8 Study of microbial inactivation kinetics in presence of antioxidants

To further substantiate the role of ROS species in the antimicrobial activity of FA-AgCl/TiO_2, antimicrobial studies against *E. coli* were carried out in presence of two different antioxidants, glutathione (GSH) and N-acetyl cysteine (NAC). FA-AgCl/TiO_2 at a concentration of 400 μg/ml was added to MHB medium followed by

10^5 cfu/ml cells and 10 mM of antioxidants. The suspension was mixed gently and incubated on a shaking incubator at 37 ℃. Aliquots were withdrawn after 30, 60, 90 and 120 min and plated out on nutrient agar plates after appropriate dilution. The plates were incubated at 37 °C for 24 h and the plate count was recorded as cfu/ml.

All glassware and accessories used were washed and rinsed with distilled water and autoclaved at 121 ℃ for 15 min to ensure sterility. Deionized water was used throughout the experiments. PBS used was 0.1 M (pH of 7.2).

4.3 Results and Discussion

4.3.1 Synthesis & characterization of functionalized $AgCl/TiO_2$

The $AgCl/TiO_2$ (1 atomic %) nanocomposites were synthesized by one pot sol-gel method. The sol-gel approach allows narrow crystallite size distribution even at high dopant loading, resulting in high surface area of the active doping agent and is considered to be the most suitable route for the synthesis of supported antimicrobial materials (Zhang and Chen, 2009; Desai and Kowshik, 2009; Thiel et al. 2007). The synthesized nanocrystalline $AgCl/TiO_2$ was functionalized with the following agents: folic acid, fumaric acid, Malic acid, Succinic acid, L-arginine and L-Cysteine by the chemisorption of functionalizing agent onto its surface (Gaweda et al. 2007). This approach, where a functionalizing agent (such as an organic acid) is conjugated on synthesized nanoparticles, is advantageous as the molecules tend to bind only to the surface functional groups of nanoparticles and be available for binding to the target cells instead of getting incorporated into the particles core (Stella et al. 2000). The functionalized $AgCl/TiO_2$ in all the above cases was found to be a more free flowing powder than the unfunctionalized $AgCl/TiO_2$. The antimicrobial studies of the

functionalized nanocomposite samples against *E. coli* and *M. luteus* were carried out to check for the enhancement in antibacterial activity after functionalization. The results of the MIC and MBC obtained for the antimicrobial study are tabulated in table 4.1.

Table 4.1. The MIC and MBC values determined by the resazurin assay.

Nanocomposite sample	***E. coli***		***M. luteus***	
	MIC (µg/ml)	**MBC (µg/ml)**	**MIC (µg/ml)**	**MBC (µg/ml)**
FA-AgCl/TiO_2	100	<125	100	500
Fu-AgCl/TiO_2	150	200	200	300
SA-AgCl/TiO_2	>250	400	300	>500
MA-AgCl/TiO_2	250	350	250	>500
Arg-AgCl/TiO_2	250	300	300	>500
Cys-AgCl/TiO_2	300	>350	300	>500
AgCl/TiO_2	200	250	200	>500

It was observed that FA-AgCl/TiO_2 and Fu-AgCl/TiO_2, both showed improved MIC and MBC values against both *E. coli* and *M. luteus* compared to the unfunctionalized AgCl/TiO_2. However, in case of MA-AgCl/TiO_2, SA-AgCl/TiO_2, Arg-AgCl/TiO_2, and Cys-AgCl/TiO_2, no improvement in antibacterial activity was observed and the unfunctionalized AgCl/TiO_2 appeared to be a more effective antibacterial agent than the functionalized nanocomposites.

Folic acid is an essential nutrient for the nucleotide and cell wall synthesis in bacteria (Chakraborty et al. 2010; Dulaney and Marx, 1971) and bacteria have folate binding proteins on their surfaces (Chakraborty et al. 2010; Stella et al. 2000). Hence, during the interaction of FA-AgCl/TiO_2 nanocomposite with microbial cells, the lure of a nutrient like folic acid combined with the possibility of interaction of folic acid with folate binding proteins, increases the chances of its uptake by the bacterial cells. The antibacterial effect of fumaric acid (in Fu-AgCl/TiO_2) is mainly due to the undissociated form of acids which lack charge, are hydrophobic and hence can diffuse through the cell membrane of bacteria causing cell death (Comes and Beelman, 2002; Alvarez-Ordonez et al. 2009). Fumaric acid alone did not exhibit any antimicrobial activity at the concentration used for functionalization. Fumaric acid, exhibits good antimicrobial activity compared to other organic acids but the concentration at which antimicrobial activity is achieved is quite high, in the range of ~5 mg/ml (Comes and Beelman, 2002; Skrivanova et al. 2006), because of its limited water solubility (Windholz, 1976). However, in combination with other chemical or physical interventions such as UV light, heat, chlorine dioxide, sodium benzoate etc an improved synergistic antimicrobial effect has been achieved (Comes and Beelman, 2002; Skrivanova et al. 2006; Kim et al. 2009). Thus, fumaric acid is a good candidate for functionalization of nanoparticles so as to make them more dispersible, stable and biocompatible for antimicrobial applications.

In case of malic acid and succinic acid functionalized nanocomposites the antibacterial activity is mainly due to the oxidative radicals. However, when such compounds are used in aqueous suspensions they display significant antioxidant properties and low antimicrobial activity (Mokbel and Hashinaga, 2005). Hence,

although the antibacterial activity of the silver based TiO_2 nanocomposites are mainly attributed to the reactive oxygen radicals, the antioxidative action of malic and succinic acid probably neutralized the oxidative reactive radicals thereby decreasing the antibacterial effects of such functionalized nanocomposites.

Arginine and cysteine binds to the TiO_2 surface via the carboxyl group and the binding is most probably bidentate (Makarova et al. 2000; Cropek et al. 2008). Although many surface functional groups have been studied for functionalization, the core groups are the amine (-NH2), hydroxyl (-OH), and carboxyl (-COOH) groups. Interaction of nanoparticles with cells depends on the surface charge and functionality. The antibacterial activity results indicate the higher antibacterial activity of unfunctionalized $AgCl/TiO_2$ than the functionalized $AgCl/TiO_2$, and Arg-$AgCl/TiO_2$ (with positively charged -NH2) shows comparatively better antibacterial activity than the Cys-$AgCl/TiO_2$ (with –SH group). The positively charged -NH2 group facilitates particle aggregation on negatively charged cell membrane thus aiding in particle uptake by cells (Lorenz et al. 2006; Holzapfel et al. 2006). This could explain the mild antibacterial activity of the functionalized $AgCl/TiO_2$. The negative antibacterial effect of functionalized $AgCl/TiO_2$ compared to unfunctionalized $AgCl/TiO_2$ could, on the other hand be attributed to the antioxidative mechanism of action of arginine and cysteine (Cropek et al. 2008; Makarova et al. 2000) which is likely to suppress the oxidative action of the reactive radicals. Also, the thiol group in cysteine can bind to the Ag in the nanocomposite, thereby hindering its interaction with bacterial cells, which could explain the decreased activity of Cys-$AgCl/TiO_2$.

4.3.2 Studies on microbial inactivation kinetics

Mueller Hinton Broth (MHB) is a complex nutrient media containing organic components, minerals, sugars etc and the complexity and ionic strength of a medium are important factors for the antimicrobial activity. Since FA-AgCl/TiO_2 was observed to be the most effective nanocomposite against *E. coli*, and *M. luteus*, it was also tested against three other microbial cultures. Studies on microbial inactivation in PBS showed that inactivation could be achieved at 50-100 μg/ml (0.59 to1.1 μg/ml Ag) in 2 h, as compared to concentrations of 125 to 1000 μg/ml (1.5 to 11.7 μg/ml Ag) required for inactivation in MHB medium. FA-AgCl/TiO_2 exhibited better antimicrobial activity in PBS compared to AgCl/TiO_2, with 10 times higher reduction in microbial count for *E. coli*, *M. luteus* and *C. albicans* and 100 times higher reduction for *P. aeruginosa* after 2 h of exposure (Fig. 4.1). In case of *S. aureus*, complete inhibition was obtained at 100 μg/ml (1.17 μg/ml of Ag) for FA-AgCl/TiO_2 as against a 3 log reduction for AgCl/TiO_2.

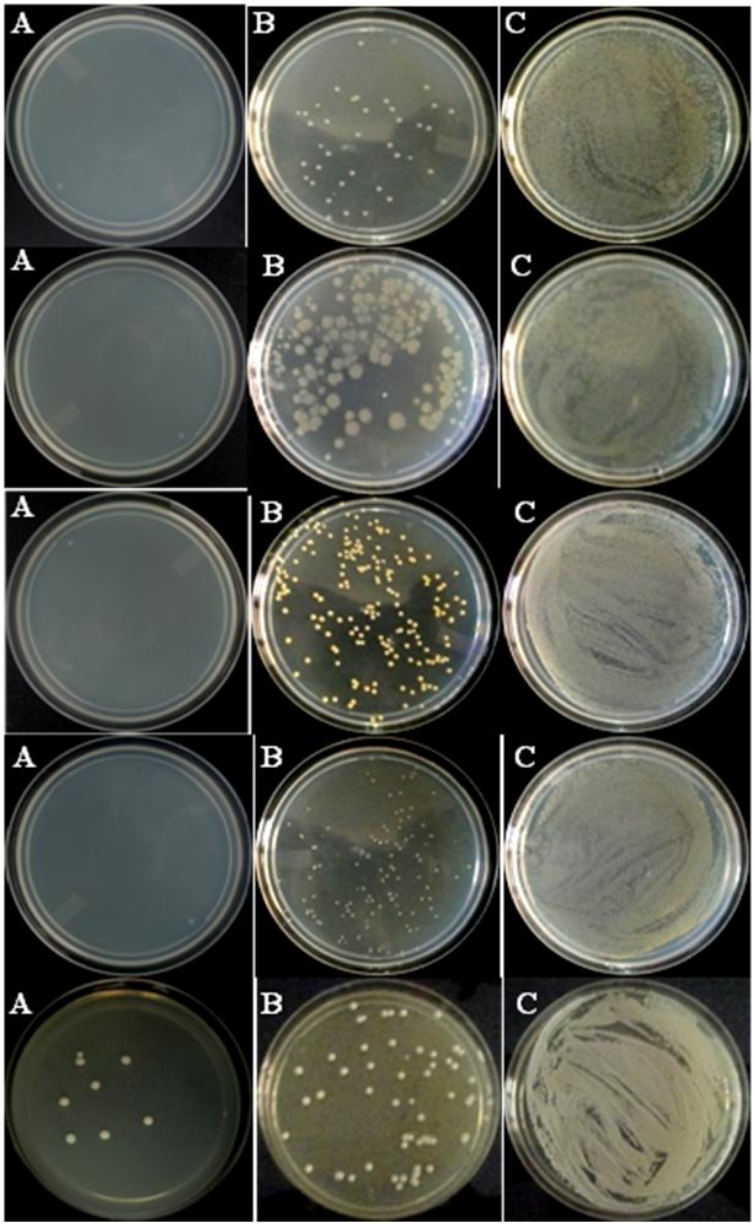

Fig. 4.1. Photographs showing the comparison between antimicrobial activity of (A) FA-AgCl/TiO_2 and (B) AgCl/TiO_2 for the various test organisms (from top to bottom) *E. coli, P. aeruginosa*, *M. luteus, S. aureus** and *C. albicans* at a concentration of 50 µg/ml. For *S. aureus** the concentration used was 100* µg/ml (C) shows the growth of test organisms in the absence of the nanocomposite.

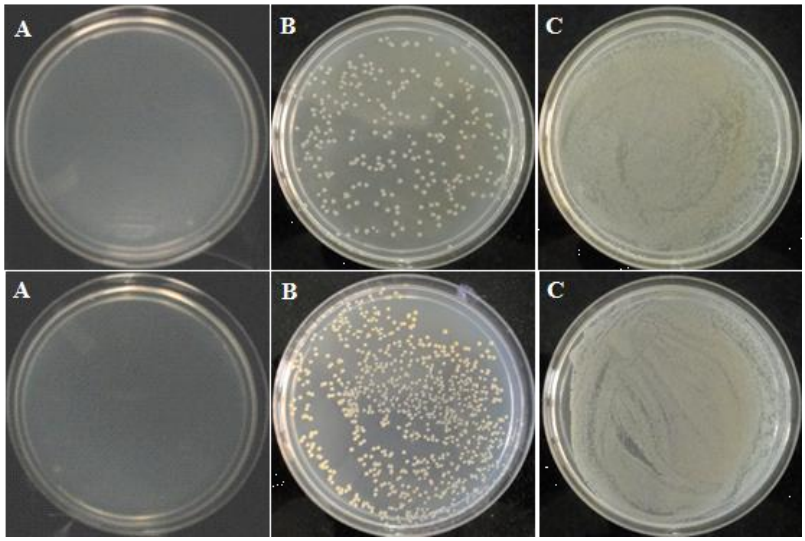

Fig. 4.2. Antimicrobial activity of (A) Fu-AgCl/TiO_2 and (B) AgCl/TiO_2 for the test organisms, *E. coli* (top) and *M .luteus* (bottom) at a concentration of 100 µg/ml. (C) shows matt growth of cells in the absence of nanocomposite.

In case of Fu-AgCl/TiO_2 complete bacterial inactivation was achieved at 100 µg/ml (1.17 µg/ml of Ag) for *E. coli* and *M. luteus*, in PBS as shown in Fig. 4.2. However, in MHB medium the concentration of Fu-AgCl/TiO_2 required for complete bacterial inactivation was 200 µg/ml (2.34 µg/ml of Ag) for *E. coli* and 300 µg/ml (3.51 µg/ml of Ag) for *M. luteus* after 24 h of incubation. This can be attributed to the fact that the complexity and ionic strength of the media, can inhibit the release of antimicrobial components from the composite/material (Noda et al. 2009; Ando et al. 2010). Further, in case of FA-AgCl/TiO_2 and Fu-AgCl/TiO_2 nanocomposites, the reactive oxygen species generated can be scavenged by the components of the complex media thereby lowering its antibacterial activity (Li et al. 2011; Ando et al. 2010). Therefore, the concentration of nanocomposites required for the complete inactivation of microorganisms in PBS is much lower as compared to the concentration required in MHB, which is a complex medium.

Further, the FA-AgCl/TiO_2 showed enhanced antimicrobial activity against Gram negative *P. aeruginosa*, Gram positive *S. aureus* and a fungal strain of *C. albicans*. The MIC and MBC values obtained for FA-AgCl/TiO_2 are shown in Table 4.2.

Table 4.2. The MIC and MBC values obtained for FA-AgCl/TiO_2 and AgCl/TiO_2 against the test microorganisms by resazurin assay.

Microorganisms	**MIC (µg/ml)**		**MBC (µg/ml)**	
	FA-AgCl/TiO_2	**AgCl/TiO_2**	**FA-AgCl/TiO_2**	**AgCl/TiO_2**
Pseudomonas aeruginosa 2581	100	150	100	150
Staphylococcus aureus 737	500	600	1000	>1000
Candida albicans 3958	100	150	350	350

Silver based TiO_2 nanocomposites with support materials such as silica, SBA-15, zeolites have been reported to exhibit antimicrobial activity in growth medium in the concentration range of 15.88 to 358.5 µg/ml (Ag concentration 35.94 µg/ml) for both Gram-negative and Gram-positive cultures (Ferreira et al. 2012; Min et al. 2010; Nino-Martinez et al. 2008; Li et al. 2011). In the present study FA-AgCl/TiO_2 exhibits antimicrobial activity at a much lower concentration of 100 µg/ml (Ag concentration 1.17 µg/ml) for *E. coli*, *P. aeruginosa*, *M. luteus* and *C. albicans*, whereas *S. aureus* was inhibited at 500 µg/ml (Ag concentration 5.85 µg/ml). Thus, the MBC values for the gram-negative cultures are much lower compared to the gram-positive cultures. The antibacterial activity for Fu-AgCl/TiO_2 was obtained at 150 to 200 µg/ml, wherein the effective silver concentration was 1.75-2.34 µg/ml. Similar observations have been reported for various silver based antimicrobial compounds and have been

attributed to the difference in the composition of cell walls of these microorganisms. As compared to Gram negative cells, Gram-positive cells have a thick peptidoglycan layer in the cell walls. Peptidoglycan contains teichoic acids or lipoteichoic acids which bind free Ag^+ ions due to their negative charge. Thus, the thick cell wall of Gram-positive bacteria protects the cell by sequestering free silver ions and preventing their influx into the cytoplasmic membrane (Egger et al. 2009; Li et al. 2011; Feng et al. 2000). In addition, *S. aureus* is known to have the enzyme catalase which could neutralize the H_2O_2 generated during silver toxicity, thereby intercepting the route for formation of $^{\cdot}OH$ by decomposition of H_2O_2 (Chang et al. 2008). The oxidation state of silver plays an important role in its antimicrobial activity and silver ions from AgCl induce more inhibitory effect than the metallic silver when present in nanocomposites (Ferreira et al. 2012; Chang et al. 2008; Sondi and Sondi, 2004).

The MIC and MBC values of FA-AgCl/TiO_2 towards *C. albicans* were 100 μg/ml (1.17 μg/ml of Ag) and 350 μg/ml (4.095 μg/ml of Ag) respectively. The antifungal activity of silver based nanocomposites has not been extensively studied and the MIC values reported for $AgTiO_2$ and Ag-silica are in the range of 15 to 25 μg/ml of Ag (Ferreira et al. 2012; Egger et al. 2009). The IC_{80} values for silver nanoparticles of 3 nm sizes have been reported to be in the range of 2 to 4 μg/ml (Keuk-Jun et al. 2008; Keuk-Jun et al. 2009). In the present study, antimicrobial activity was achieved at a much lower effective silver concentration of 1.17 μg/ml. The antifungal activity of silver nanoparticles against *C. albicans* has been attributed to the disruption of cell membrane structure (Kim et al. 2009).

Since only FA-AgCl/TiO_2 and Fu-AgCl/TiO_2 showed an improvement in antimicrobial activity upon functionalization further characterization studies were

carried out to investigate their physicochemical properties, the efficiency of functionalization and the effects of these factors on antimicrobial activity.

4.3.3 Characterization studies

To investigate the average crystallite size and phase structure of the nanocomposites, X-ray diffraction studies of FA-AgCl/TiO_2 and Fu-AgCl/TiO_2 were carried out. The analysis results showed that the lattice parameters and the crystal structure of TiO_2 in both the nanocomposites corresponded to the anatase phase (ICDD card no. 21-1272) (Fig. 4.3). In addition, the diffraction peaks at 2θ = 27.74°, 32.18°, 46.18° corresponded to the planes for cubic AgCl (chlorargyrite) phase (ICDD card no. 31-1238). The diffraction peaks of AgCl were sharper than the TiO_2 peaks, which suggest that the AgCl nanocrystallites embedded in the nanocomposite matrix were well crystallized. Line broadening of the diffraction peaks was observed indicating that the synthesized material was in nanometer range. The crystallite size calculated for (1 0 1) peak of anatase TiO_2 and (2 0 0) peak of AgCl, using Scherrer's formula was ~6.5 nm and ~42.4 nm for FA-AgCl/TiO_2 and ~6 nm and 43.2 nm for Fu-AgCl/TiO_2, respectively. The XRD analysis results confirm the formation of AgCl/TiO_2 nanocomposite.

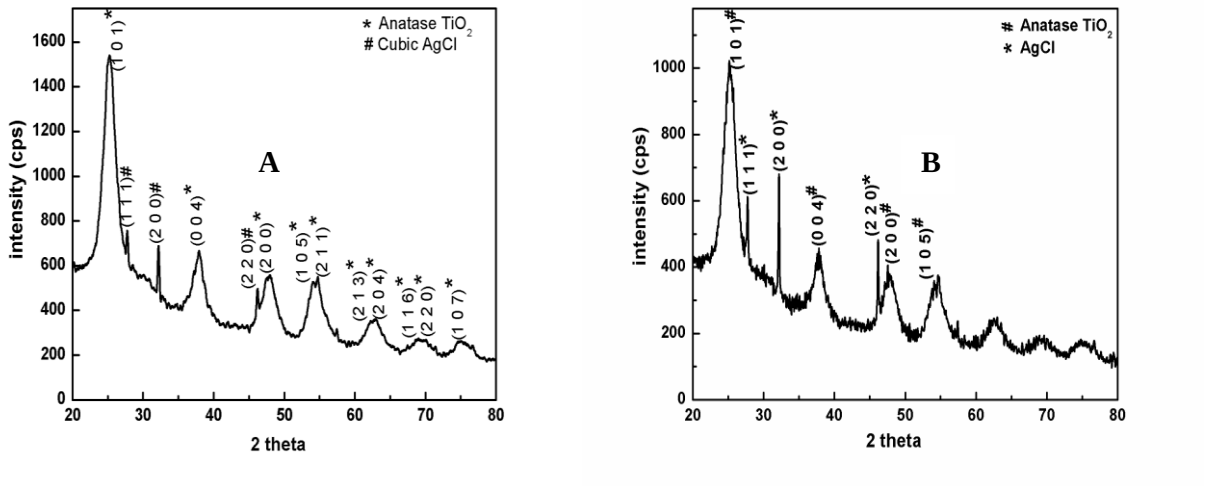

Fig. 4.3. X-ray diffractogram of A] FA-AgCl/TiO_2 and B] Fu-AgCl/TiO_2 nanoparticles showing peaks for the anatase phase of TiO_2 and cubic AgCl.

Several AgCl based composites with different host supports such as silica, titania and alumina have been reported, wherein the highly crystallized AgCl is present as cubic phase of chalcoargyrite and exhibit good antimicrobial activity (Naik et al. 2011; Min et al. 2010; Tan et al. 2009).

The pore size distribution of FA-AgCl/TiO_2 and Fu-AgCl/TiO_2 was determined by nitrogen adsorption-desorption isotherm and showed type IV isotherm with H2 hysteresis loop (Fig. 4.4A and Fig. 4.5), which is a characteristic of mesoporous materials having interconnected pore structure (Sing et al. 1985). The pore volume by BJH (Barrett-Joyner-Halenda) desorption method was found to be 0.28 cm^3/g for FA-AgCl/TiO_2 and 0.34 cm^3/g for Fu-AgCl/TiO_2. The BET (Brunauer-Emmett-Teller) surface area of FA-AgCl/TiO_2 was ~258.5 m^2/g with an average pore size of 3.9 nm (Fig. 4.4B) and ~320.7 m^2/g with an average pore size of 3.8 nm for Fu-AgCl/TiO_2 (Fig. 4.5). The BET surface area of the AgCl/TiO_2 was ~245.25 m^2/g with an average pore size distribution of 4.49 nm. The primary particle size of FA-AgCl/TiO_2 and Fu-

$AgCl/TiO_2$ was also calculated using the BET model and was found to be ~5.5 nm and ~4.42 nm, respectively.

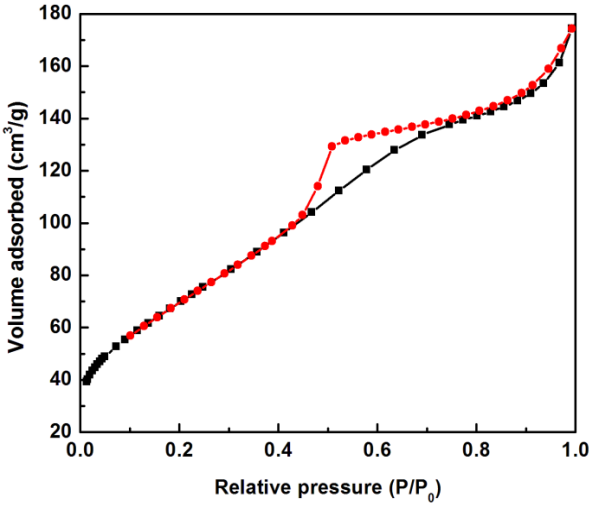

Fig. 4.4A. The N_2 adsorption-desorption isotherm plot for FA-$AgCl/TiO_2$.

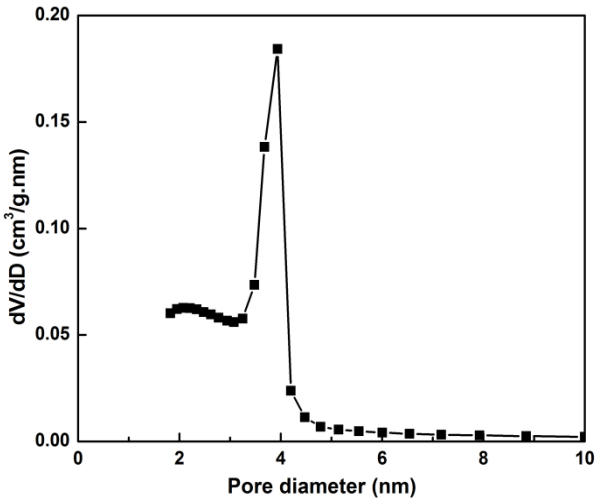

Fig. 4.4B. Plot showing the average pore size distribution in FA-$AgCl/TiO_2$ nanocomposite.

The surface area and pore size analysis of the functionalized nanocomposites exhibits a high surface area and pore volume and is expected to contribute towards the improved antimicrobial activity of the material.

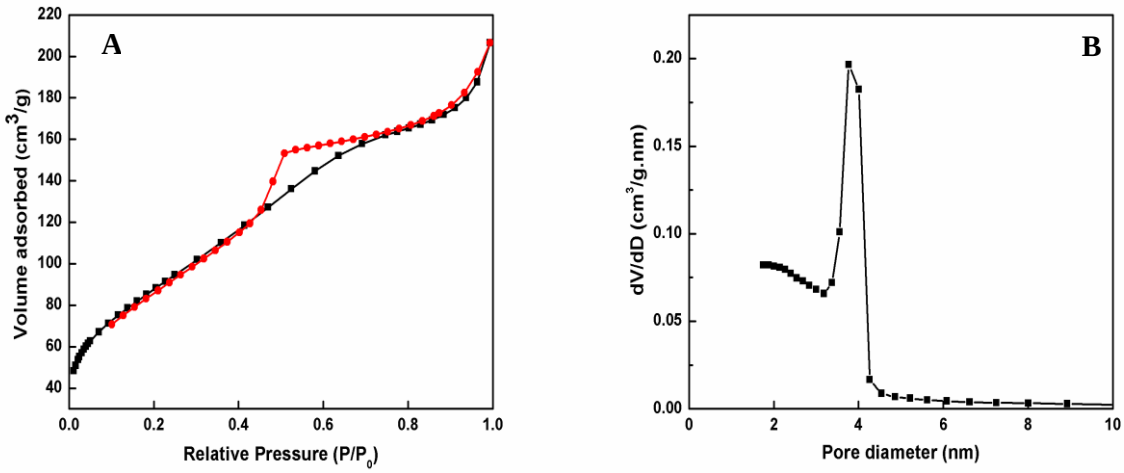

Fig. 4.5. The N_2 adsorption-desorption isotherm of Fu-AgCl/TiO_2: (A) Hysteresis loops and (B) BJH pore size distribution.

It has been suggested that BET surface area of AgCl/TiO_2 nanocomposites depends on the concentration of Ag loading, (Zhang and Chen, 2009; Liu et al. 2008; Tan et al. 2009) temperature and time of calcination, and the precursors used for doping (Hamal and Klabunde, 2007). High BET surface areas as seen in this study have been reported for other silver based nanocomposites such as Ag-silica, Ag-SBA 15 etc (Egger et al. 2009; Min et al. 2010; Naik et al. 2011).

The mesoporous nature of the irregularly ordered TiO_2 matrix was also observed in the TEM micrographs of FA-AgCl/TiO_2 and Fu-AgCl/TiO_2 nanocomposites (Fig. 4.6 and Fig. 4.7). The FA-AgCl/TiO_2 nanocomposite constituted ~5-9 nm nanocrystallites agglomerated together to form a mesoporous structure and appeared slightly foggy possibly due to the presence of folic acid. Similar observations have been reported for folic acid modified TiO_2 (Lai and Lee, 2009). The Fu-AgCl/TiO_2 nanocomposite constituted ~4-5 nm crystallites. Such an agglomerated, mesoporous structure is ideal for higher and improved surface properties, since it helps in the easy adsorption of

reactant molecules on the matrix surface and helps in the controlled release of silver ions (Ferreira et al. 2012; Naik et al. 2011).

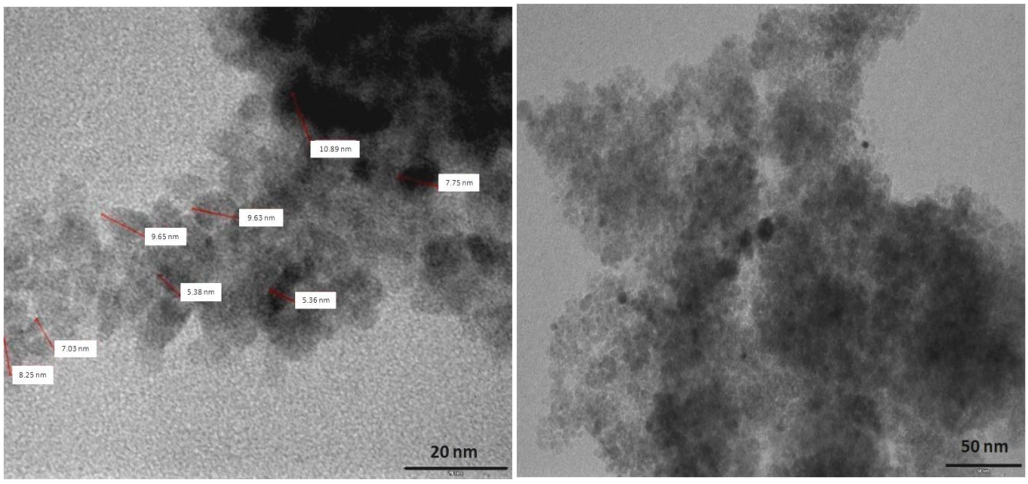

Fig. 4.6. The TEM micrographs showing the nanocrystallite size of FA-AgCl/TiO_2 nanocomposite.

The nanocrystallites were observed to possess a mixed morphology and the TEM observations were in agreement with the N_2 adsorption-desorption data. The results obtained by XRD, TEM and BET studies were found to be in agreement with each other, and the crystallite/particle size of functionalized AgCl/TiO_2 for all these techniques was in the size range of 4-7 nm.

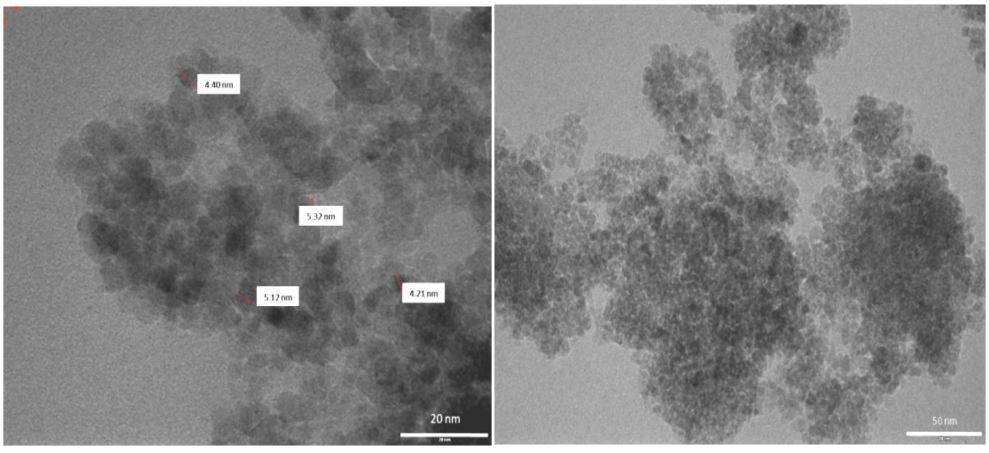

Fig. 4.7. The TEM micrographs showing the nanocrystallite size of Fu-AgCl/TiO_2 nanocomposite.

DLS measurements were carried out to determine the average values of the particle size and the polydispersity of the sample, defined as the relative width of the size distribution. The average particle size obtained for FA-AgCl/TiO_2 was ~241 nm while for Fu-AgCl/TiO_2 it was 290.4 nm (Fig. 4.8A and Fig. 4.9A). The number distribution plots of FA-AgCl/TiO_2 showed that a majority of the particles were in the size range of 4-9 nm which corresponds to the size of nanocrystallites which agglomerate to form a mesoporous matrix (Fig. 4.8B). In Fu-AgCl/TiO_2, the particle size range was observed to be 2-7 nm (Fig. 4.9B). The particle size analysis of unfunctionalized AgCl/TiO_2 showed a cumulant mean diameter of ~206.3 nm as compared to ~241 nm and 290 nm for FA-AgCl/TiO_2 and Fu-AgCl/TiO_2 respectively, suggesting a conjugation between the folic acid/fumaric acid and TiO_2. Similar observations have been reported by Chakraborty et al. and Lai & Lee for folic acid tagged chitosan nanoparticles and folic acid functionalized TiO_2 nanoparticles, respectively. Thus, the nanoparticle aggregation increases size but preserves the surface area within the nanocomposite aggregate (Liu and Hurt, 2010).

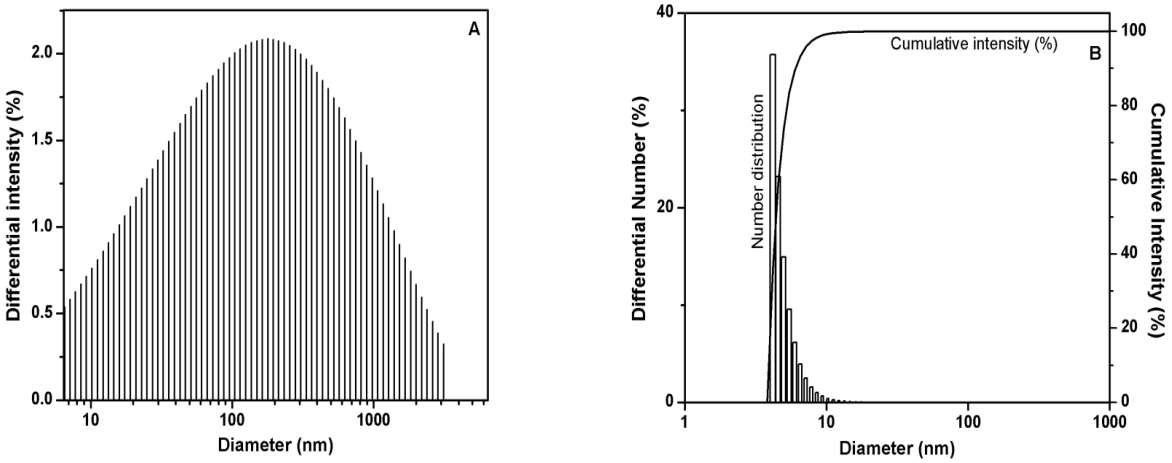

Fig. 4.8. Particle size analysis of FA-AgCl/TiO_2 nanocomposite by A] Intensity size distribution B] Number distribution in DLS.

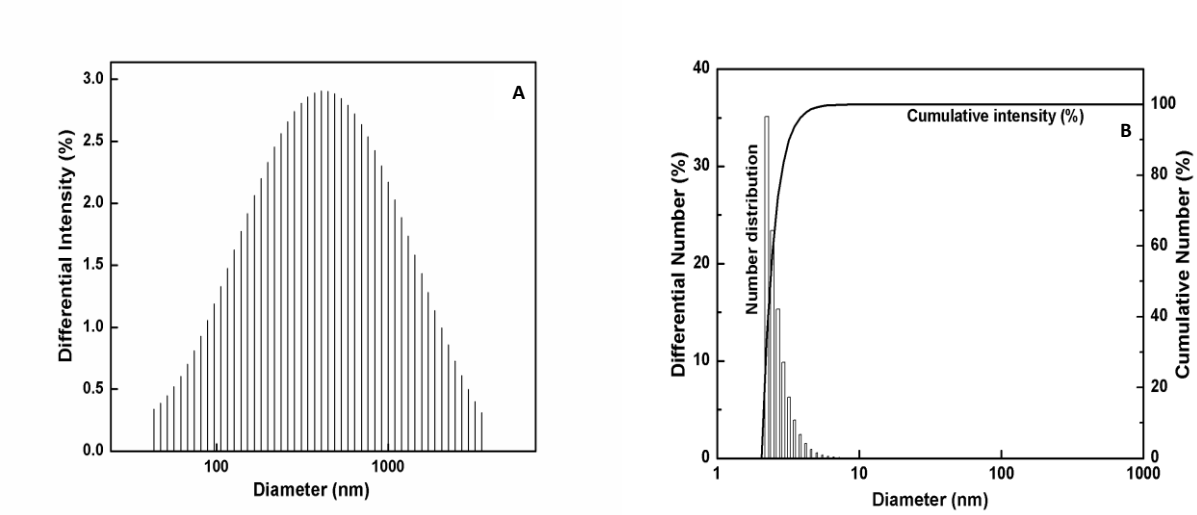

Fig. 4.9. The particle size analysis of Fu-AgCl/TiO_2 nanocomposite by A] Intensity size distribution B] Number distribution in DLS.

FTIR analysis of FA-AgCl/TiO_2 (Fig. 4.10) and Fu-AgCl/TiO_2 (Fig. 4.11) was carried out to study the type of conjugation between the functionalizing agent with AgCl/TiO_2 and the extent of functionalization. Fig 4.10 shows the characteristic IR absorption bands of folic acid at 1610 cm^{-1} for benzene, conjugated double absorption showing that the surface of AgCl/TiO_2 was modified by folic acid (Wan et al. 2011). A broad, intense O-H stretching band observed from 3500 to 2500 cm^{-1} is the characteristic spectral feature of carboxylic acid present in folic acid (Smith, 1999). The broad bands around 3439 cm^{-1} and 1637 cm^{-1} for FA-AgCl/TiO_2 and around 3435 cm^{-1} and 1640 cm^{-1} for Fu-AgCl/TiO_2 are attributed to the surface-adsorbed H_2O and the -OH group of TiO_2 (Tan et al. 2009; Wan et al. 2011). The appearance of bands due to asymmetric and symmetric stretching vibrations of carboxylate salt (–COOM) at 1512 cm^{-1} and 1448 cm^{-1} indicated the formation of linkage between carboxylic acid of FA and the titanium atom (Lai and Lee, 2009). Thus, these observations indicate that chemisorption of folic acid on TiO_2 involves the carboxylate groups of the glutamate side chain, due to the strong affinity of TiO_2 towards COO^- groups (Gaweda et al. 2007; Lai and Lee, 2009).

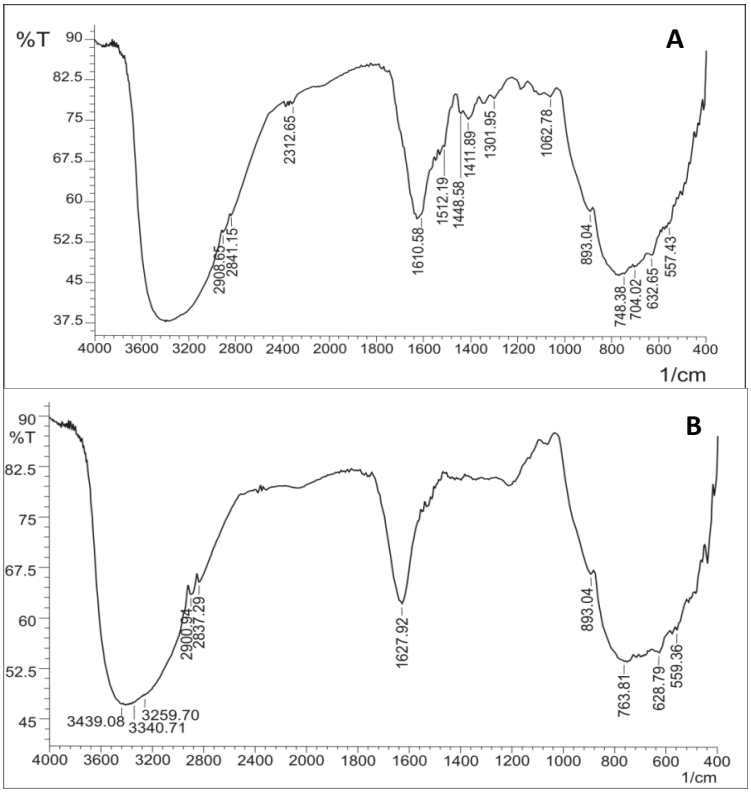

Fig. 4.10. The FTIR spectra of (A) FA-AgCl/TiO_2 and (B) AgCl/TiO_2

An FTIR spectrum for Fu-AgCl/TiO_2 is shown in Figure 4.11. Similar to FA-AgCl/TiO_2 a broad, intense O-H stretching band was observed from 3600 to 2500 cm^{-1}. This is an overriding feature of carboxylic acid present in fumaric acid (Smith, 1999). Characteristic bands at ~1627 cm^{-1} and ~1082 cm^{-1} are attributed to C=C stretching, and asymmetrical C-O-C stretching, respectively. The band at 894 cm^{-1} is ascribed to the esters of fumaric acid. Carboxylate binding site can be identified at ~1620 cm^{-1}, and ~1521 cm^{-1}, carboxylate peaks are detected at 1630 and 1513 cm^{-1}, while C=C aromatic stretch is detected at 1599 cm^{-1} (Cheyne et al. 2011). Hence, the chemisorption of fumaric acid on TiO_2 occurs most probably through the two trans-carboxylic acid groups due to the strong affinity of TiO_2 towards COO^- groups (Gaweda et al. 2007; Cheyne et al. 2011).

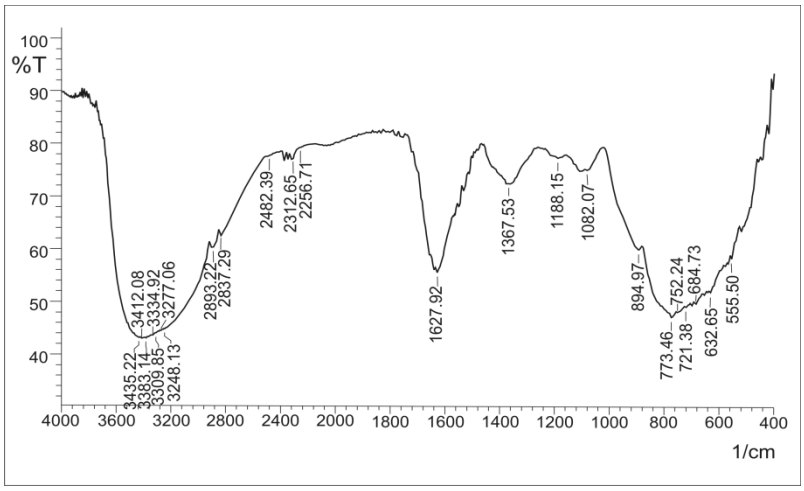

Fig. 4.11. The FTIR spectra of Fu-AgCl/TiO_2 nanocomposite.

The EDAX analysis for AgCl/TiO_2 was carried out to determine the elemental composition of the nanocomposite samples. The Ag and Cl peaks were seen at ~2.7 KeV, followed by stronger Ti peaks at 4.5 KeV and 5 KeV (Fig. 4.12).

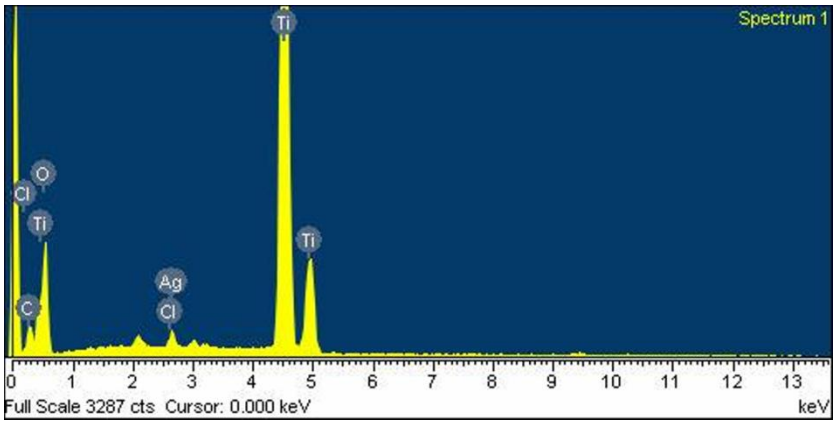

Fig. 4.12. EDAX spectrum of AgCl/TiO_2 nanoparticles.

The improved antimicrobial activity of FA-AgCl/TiO_2 and Fu-AgCl/TiO_2 nanocomposite could be attributed to the surface functionalization, small particle size, and large surface area of the nanocomposites (Zhang and Chen, 2009; Asharani et al. 2009). After uptake, the particle size of the material plays an important role in toxicity towards microorganisms (Pan et al. 2010; Zhang and Chen, 2009; Morones et al. 2005). The smaller particles have more surface active atoms and a large fraction of

atoms on low-coordination and high-energy sites (corners, edges, steps, kinks etc.), that makes them more reactive than larger particles upon contact with bacterial cells (Zhang and Chen, 2009; Raimondi et al. 2005). Since the crystallite size for FA-AgCl/TiO_2 is ~5-9 nm and Fu-AgCl/TiO_2 is ~4-5 nm, the above properties are expected to contribute to their potent antimicrobial activity. The average size of Ag nanoparticles capable of penetrating into an *E. coli* membrane is reported to be 5 ± 2 nm (Raimondi et al. 2005; Choi and Hu, 2008). Colloidal metal nanoparticles at such small sizes present electronic effects, changing the local electronic structure of the surface and enhancing the reactivity of the nanoparticle surfaces (Wan et al. 2011).

Also, the binding strength of the nanoparticles to bacteria depends on the surface area of interaction, with smaller particles having a higher percentage of the surface for direct interaction than bigger particles (Morones et al. 2005; Choi and Hu, 2008). Although, the mechanism of nanoparticle penetration into the bacterial cells is largely unclear, previous reports suggest that in *E. coli* treated with silver nanoparticles, the changes in the membrane morphology may cause a significant increase in its permeability, affecting normal transport through the plasma membrane (Zhang and Chen, 2009; Morones et al. 2005). Further, silver chloride embedded within the TiO_2 matrix release Ag^+ in a slow, controlled manner resulting in long-term antimicrobial activity as compared to silver salts which dissolve completely and make all the silver readily available in its active ionic form. Silver chloride is known to have low solubility in aqueous medium leading to slow release of silver ions. Moreover, in presence of oxygen, it also produces H_2O_2 that has a low rate of decomposition. These factors contribute towards the long lasting residual antimicrobial effect (Min et al. 2010; Chang et al. 2008; Sokmena et al. 2001).

4.3.4 Hemolytic assay results

In the hemolytic study of FA-AgCl/TiO_2, Fu-AgCl/TiO_2 and AgCl/TiO_2, it was observed that AgCl/TiO_2 exhibited higher hemolysis of RBCs as compared to FA-AgCl/TiO_2 and Fu-AgCl/TiO_2. As per the ASTM F 756-00 for the assessment of hemolytic properties of materials, HR < 2, is considered non-hemolytic, HR in the range of 2-5 is considered mildly hemolytic and HR > 5 is considered hemolytic (Chen et al. 2008). In case of FA-AgCl/TiO_2 the HR was 0.29, 0.43 and 1.11 at a concentration of 50, 100, and 150 μg/ml, respectively, while for Fu-AgCl/TiO_2 it was 1.79, 1.84 and 1.89 at a concentration of 150, 200 and 250 μg/ml. Thus, both the functionalized nanoparticles do not exhibit any hemolysis at the MIC concentration as well as at concentrations above the MIC values. However, for AgCl/TiO_2 the HR was observed to be 2.38, 3.16 and 5.20 at a concentration of 150, 200 and 250 μg/ml. This indicates that functionalization of AgCl/TiO_2 increases its antimicrobial potential and decreases the hemolytic activity thereby increasing the biocompatibility for in-vivo applications. Similar observations have been reported for the improved biocompatibility and antibacterial activity of folic acid functionalized chitosan nanoparticles and functionalized TiO_2 nanoparticles for dental implants (Chakraborty et al. 2010; Schliephake and Scharnweber, 2008).

4.3.5 Scanning Electron Microscopy (SEM)

The morphological changes observed in *E. coli* cells exposed to 50 μg/ml FA-AgCl/TiO_2 and Fu-AgCl/TiO_2 for 2 h are shown in Fig. 4.13. It was observed that the cytoplasmic membrane began to shrink and detach from the cell wall forming electron-translucent light regions at both ends of the cells. However, no noticeable damage in the membrane structures of *E. coli* cells was observed. Similar

observations have been reported for silver ions and it has been proposed that the electron light regions protect the DNA from any external harm or mutation (Marambio-Jones and Hoek, 2010; Chang et al. 2008; Feng et al. 2000). The Ag^+ penetrates the cell membranes through ion channels without causing any significant membrane damage. Consequently, the intracellular ROS generated damages cell DNA inducing apoptosis and cell death (Zhang and Chen, 2009; Carlson et al. 2008). As per the theory of hard and soft acids and bases, silver has a high affinity to react with sulfur containing bases due to its reactive electronic structure (Choi and Hu, 2008; Feng et al. 2000; Carlson et al. 2008), leading to the inactivation of proteins, DNA condensation and loss of ability to replicate (Zhang and Chen, 2009; Rai et al. 2009; Feng et al. 2000). Thus, silver ions have multiple targets in the cell such as DNA, cellular/membrane proteins and electron transport chain, making them highly potent against drug resistant microorganisms.

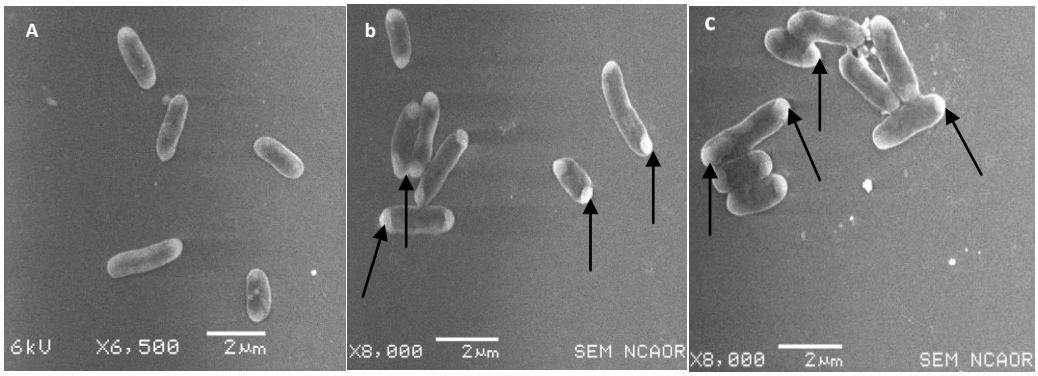

Fig. 4.13. SEM micrographs showing the intact *E. coli* cells unexposed to FA-AgCl/TiO_2 and Fu-AgCl/TiO_2 (a), *E. coli* cells exposed to 50 µg/ml of FA-AgCl/TiO_2 (b) and Fu-AgCl/TiO_2 (c) for 2 h. The micrographs clearly show the electron translucent regions (indicated by arrows) in the cells exposed to FA-AgCl/TiO_2 & Fu-AgCl/TiO_2.

4.3.6 Mechanistic studies of antibacterial activity of FA-AgCl/TiO_2

Further studies were carried out with FA-AgCl/TiO_2 to elucidate the mechanism of its antimicrobial action since it exhibited enhanced antimicrobial activity against different microorganisms. Several studies have been carried out to investigate the mechanism of action of silver containing TiO_2 nanocomposites and study the dynamics that govern the process of inactivation and several different mechanisms have been proposed. Many of the studies have reported that reactive oxygen species may be responsible for oxidation of bacterial cell membranes and hence cell death. Studies were carried out to evaluate the role of reactive oxygen species in the antibacterial activity of FA-AgCl/TiO_2 nanocomposite.

4.3.6.1 Detection of intracellular reactive oxygen species (ROS)

Exposure of FA-AgCl/TiO_2 nanoparticles to microbial cells resulted in an overall increase in intracellular ROS concentrations by 18.1 % as compared to microbial cells that were pre-incubated with antioxidant N-acetyl cysteine (NAC). Silver ions as well as silver nanoparticles are known to pass through the cell wall of bacteria, oxidize the surface proteins on the plasma membrane, generate ROS and consequently disturb the cell homeostasis (Soo-Hwan et al. 2011; Jeon et al. 2003). The high levels of ROS and free radicals generated due to the oxidation of proteins, DNA and impeded electron transport along the respiratory chain can damage cytoplasmic constituents, disrupting the cellular functions and leading to cell death (Su et al. 2009; Kim et al. 2007). These results indicated that AgCl colloids and Ag^+ ions lead to increase in intracellular ROS, and here a correlation between microbial growth inhibition and concentration of intracellular ROS is observed. Recent studies have suggested that the strong bactericidal activity of silver nanoparticles or Ag^+ ions is due to the ROS

generation although the exact mechanism of ROS production remains largely unclear (Zhang and Chen, 2009; Choi and Hu, 2008; Carlson et al. 2008). The present study does not give a direct proof of ROS affecting microbial growth inhibition but a quantitative estimate, because ROS is also formed as a natural byproduct of the normal aerobic metabolism and its levels can increase under environmental stress (Zhang and Chen, 2009; Choi and Hu, 2008).

4.3.6.2 Study of microbial inactivation kinetics in the presence of antioxidants

At MBC concentration, no microbial inactivation was observed in presence of antioxidants glutathione (Fig. 4.14A) and NAC (Fig. 4.14B). The antioxidants used are capable of neutralizing the oxidative action of the reactive radicals generated during the process. GSH, a ubiquitous sulfhydryl-containing tripeptide, is the key antioxidant defense chemical that is responsible for maintaining cellular oxidation-reduction homeostasis (Carlson et al. 2008). Antioxidants alone did not exhibit any antimicrobial activity. Similar results have been reported for silver nanoparticles and AgCl colloids suggesting that the antimicrobial action was related to the formation of free radicals (Morambio-Jones and Hoek, 2010; Choi and Hu, 2008). Surface area also plays a major role in the generation of ROS with smaller sized nanoparticles generating higher levels of ROS than larger nanoparticles at the same concentration (Morambio-Jones and Hoek, 2010; Carlson et al. 2008).

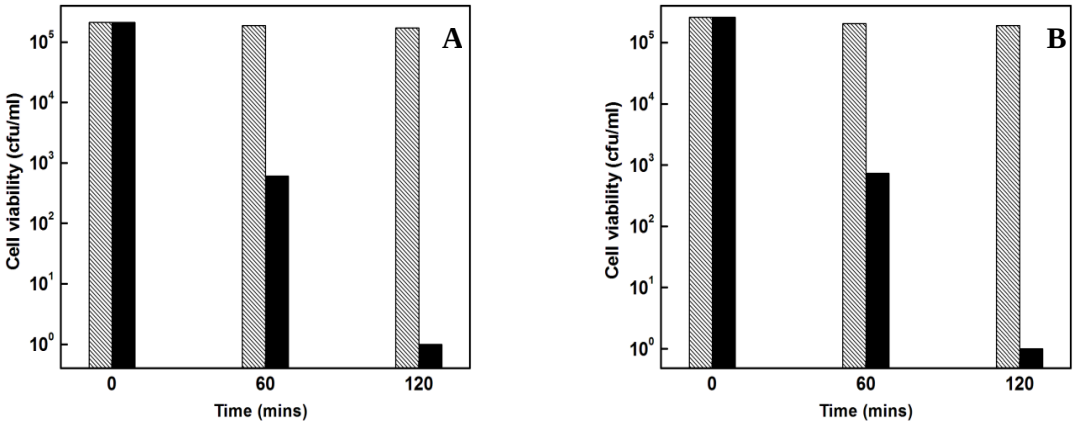

Fig. 4.14. Effect of antioxidants, (A) Glutathione and (B) NAC on the antimicrobial activity of FA-AgCl/TiO_2 against *E. coli* at a concentration of 400 µg/ml in MHB. In presence of antioxidant (▨) and in the absence of antioxidant (■).

Conclusion

The AgCl/TiO_2 nanocomposite powder was synthesized by simple, sol-gel method and functionalized with different functionalizing agents such as folic acid, fumaric acid, malic acid, succinic acid, L-arginine and cysteine by simple chemisorption. Among all the functionalized nanocomposites, only FA-AgCl/TiO_2 and Fu-AgCl/TiO_2 exhibited improved antibacterial activity as compared to the unfunctionalized AgCl/TiO_2. Characterization studies on FA-AgCl/TiO_2 and Fu-AgCl/TiO_2 showed that these compounds exhibited superior physicochemical properties such as size, surface area, stability, dispersibility and higher antimicrobial efficacy compared to the unfunctionalized AgCl/TiO_2. The negative antibacterial activity of MA-AgCl/TiO_2, SA-AgCl/TiO_2 as well as Arg-AgCl/TiO_2 and Cys-AgCl/TiO_2 could be because of the antioxidative properties of the functionalizing agents which are likely to suppress the reactive radicals responsible for cell death. The better antimicrobial activity of FA-AgCl/TiO_2 could be attributed to the increased uptake of nanocomposite particles by

the microorganisms due to the interaction of the folic acid with the folate binding proteins on the cell surface of microorganisms and for Fu-AgCl/TiO_2 to its antibacterial properties. Further, small size with high surface area also plays a vital role in the superior antimicrobial activity of the nanocomposite. The processes of disinfection and the treatment of microbial infections is becoming increasingly difficult with the emergence of the problem of multi-drug resistance and biofilms harboring tolerant bacteria that are responsible for device/implant related chronic and recurrent infections. Silver based nanocomposites are broad spectrum antimicrobial agents and can be a promising alternative for the development of new non-resistance inducing antimicrobial agents due to their multiple mode of action in the target cell.

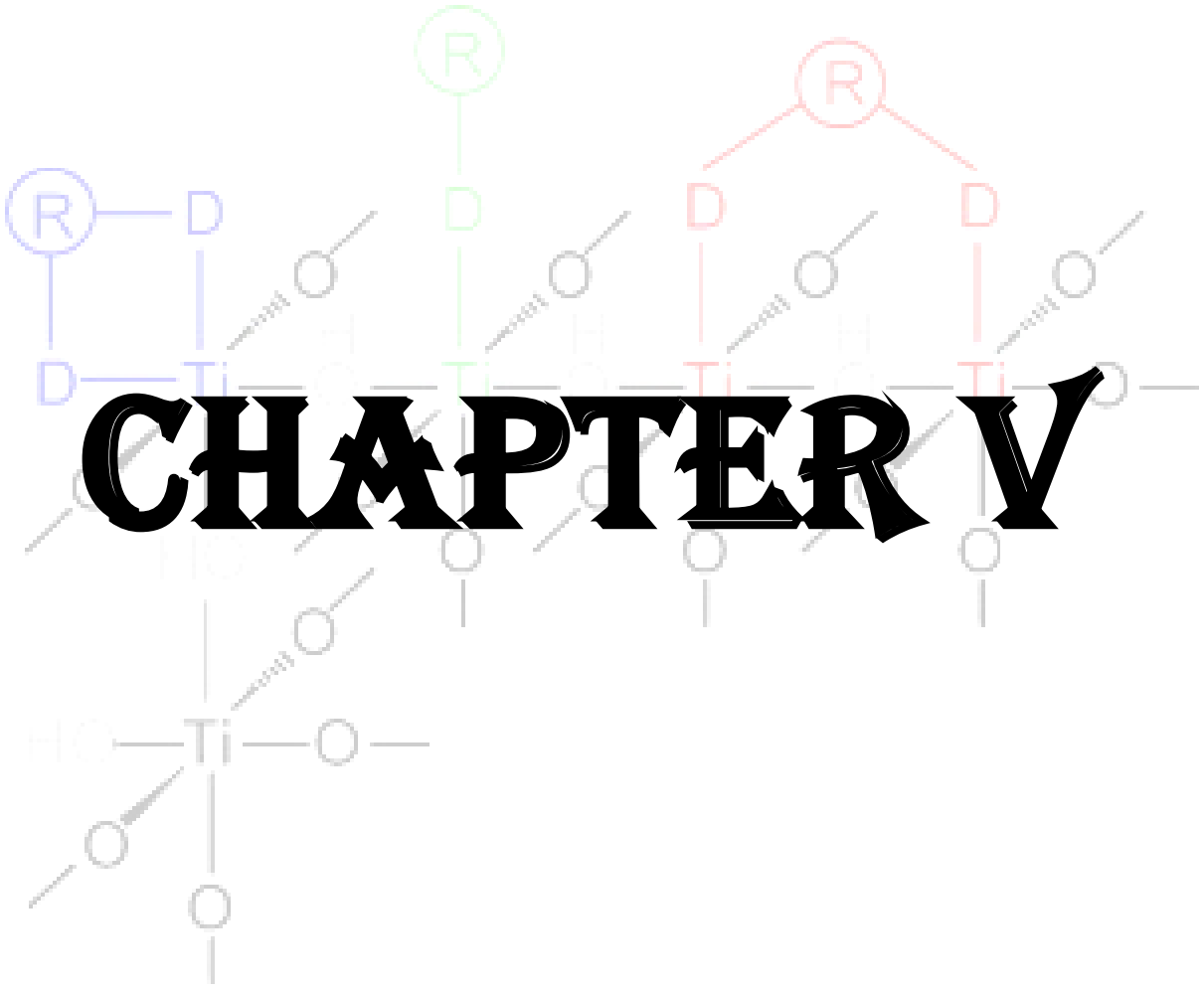

CHAPTER V

Chapter 5

Antimicrobial effects of titanium dioxide nanoparticles and ammonium persulphate in presence of 1, 8-dimethyl-1, 3, 6, 8, 10, 13-hexaazacyclotetradecane) nickel (II) perchlorate

Abstract

Nickel(II) azamacrocyclic complexes are redox active and are known to form relatively reactive Ni(I), and Ni(III) oxidation state species. Ni(I) is known to activate molecular oxygen, and produce reactive oxygen species. Nickel(III) species are highly oxidizing species, capable of causing in-vitro DNA damage. The antimicrobial activity of titanium dioxide nanoparticles in presence of divalent nickel tetraazamacrocyclic complexes is unexplored. The antimicrobial study of TiO_2 in presence of complex 1 show that 20 μM Ni (II) complex + 5 μg/ml TiO_2 is effective for complete inactivation of Gram positive, Gram negative as well as fungal cultures. Nickel(II) azamacrocyclic complexes are also known to be oxidized by persulphate, to produce sulphate radical and Nickel(III) species. However, the effects of the activation of persulphate on microorganisms are not known. In this study, we have studied the reaction between persulphate and Nickel(II) azamacrocyclic complexes and its effect on microbes. Thiobarbituric acid assay (TBA) showed that the complex 1 in presence of oxidant induces significant lipid peroxidation than the complex 1 or the oxidant alone. SEM results also show the loss of membrane integrity for the cells treated with the complex 1 and the oxidant. Effective inhibition of cell growth by complex 1 in presence of oxidant is mainly attributed to its ability to cause damage to the cell membrane than the complex 1 alone in the divalent state.

Keywords: Activation, Titanium dioxide, Nickel (II) azamacrocyclic complexes, cell membrane damage, lipid peroxidation, cell growth inhibition.

5.1 Introduction

Photocatalysis using TiO_2 has been extensively studied, and shown to eliminate toxic organic compounds (Kamat and Meisel, 2003; Liu et al. 2008; Prieto et al. 2005; Hoffman et al, 1995) and also function as disinfectants (Cho et al. 2005; Wong et al. 2006; Huang et al. 1999). Highly reactive ROS are produced during photocatalysis by TiO_2, that possess the ability to mineralize organic compounds (Hoffman et al, 1995; Liu et al. 2008) as well as the bacterial cell mass to carbon dioxide (Jacoby et al. 1998; Wolfrum et al. 2002; Wong et al. 2006). Active research is being pursued to enhance the photocatalytic efficiency of TiO_2 (Choi et al. 1994; Sun and Bolton 1996; Egerton et al. 2005). One approach that has shown a significant enhancement in the photocatalytic activity, has been the introduction of metal ions in the lattice of TiO_2 (Egerton et al. 2005; Zaleska, A. 2008; Choi et al. 1994) which can either extend its absorption spectrum into visible region or reduce the charge carrier recombination limiting the photocatalytic efficiency (Egerton et al. 2005; Zaleska, A. 2008; Kim et al. 2006). There are several reports of using TiO_2 doped with transition metal ions such as iron, nickel, copper, cobalt (Egerton et al. 2005; Chen et al. 2008; Kim et al. 2006; Thompson and Yates, 2006; Zaleska, A. 2008). Several studies have reported the doping of TiO_2 with Ni and its photocatalytic properties (Jiang et al. 2006; Gomathi Devi et al. 2010; Rodriguez et al. 2012; Chen et al. 2008; Yao et al. 2010). However, most of these studies were mainly focused on the photocatalytic properties of TiO_2 and degradation of organic pollutants, while photocatalysis for bacterial disinfection was not studied.

Interestingly, the redox chemistry of nickel (II) azamacrocyclic complexes has been extensively studied and their structural versatility allows the tuning of the redox property of the coordinated metal ions, and these ligands are well known to stabilize the metal ions in their rare oxidation states (Zilbermann et al. 1993; Zeigerson et al. 1982). Oxidation of several nickel (II) complexes has been performed by electrochemical (Jubran et al. 1986; Zeigerson et al. 1982) and photochemical methods (Prakash and Natarajan, 2004; Prakash and Natarajan, 2003; Dhanasekaran et al. 2001; Prakash and Natarajan, 2000; Ferraudi and Muralidharan, 1981). The stability of nickel (III) state is reported to be in the order of a few milliseconds, indicating that trivalent species are readily reactive and act as strong oxidants, showing catalytic activity (Zeigerson et al. 1982; Jaacobi et al. 1979; Lee et al. 2000; Zilbermann et al. 1993). Importantly, some of these reports also show formation of less reactive, stabilised trivalent nickel species (Zeigerson et al. 1982; Zilbermann et al. 1993). Detailed investigations on oxidation of square planar nickel (II) tetraazamacrocyclic complexes reveal that trivalent nickel complexes formed have an octahedral geometry, in which Ni (III) ion is coordinated to four nitrogens of tetraazamacrocyclic ligand and two ligands at axial sites (Zeigerson et al. 1982; Jaacobi et al. 1979; Prakash and Natarajan, 2004; Prakash and Natarajan, 2003; Dhanasekaran et al. 2001; Prakash and Natarajan, 2000; Ferraudi and Muralidharan, 1981; Lee et al. 2000; Zilbermann et al. 1993; Desideri and Raynor 1977; Bencini et al. 1981). Stability of trivalent nickel species was shown to depend on the type of axial ligands (Zeigerson et al. 1982; Jaacobi et al. 1979; Prakash and Natarajan 2004). Several nickel containing enzymes are also known and the Ni (III) oxidation state is found to be important in their catalytic activity (Halcrow and Christou, 1994; Lee et al. 2010) with many reports on DNA damage caused by the oxidation of nickel (II)

complexes to trivalent nickel complexes (Lepentsiotis et al. 1999; Muller et al. 1997). Cynthia Burrows, et al have shown that the trivalent nickel macrocyclic complexes could selectively oxidize the guanine residues present in the DNA, and the oxidation of the nickel (II) azamacrocyclic complexes could be used to probe and manipulate DNA molecules (Burrows and Rokita, 1994; Lepentsiotis et al. 1999; Muller et al. 1997).

In addition, persulphates have received much attention as promising oxidants because of their stability, easy handling, cost effectiveness and non-toxicity to environment (Wu et al. 2012; Smith et al. 2008; Liang and Guo, 2010; Gokulkrishnan et al. 2012). Generally, persulphates are activated by homolysis of its peroxide bond to produce reactive sulphate radicals, which are very reactive towards organic pollutants (Gokulkrishnan et al. 2012; Johnson et al. 2008; Waldemer et al. 2007). Importantly, *in situ* oxidation of phenantherene by persulphate in soil, and consequently, delayed recovery of phenantherene degrading bacteria has been reported, indicating that *in situ* radicals produced due to homolysis of persulphate may have a bacteriostatic effect in soil (Richardson et al. 2011). Persulphate are known to cause oxidation of nickel (II) azamacrocyclic complexes (Gokulkrishnan et al. 2012). Although, the antimicrobial activity of divalent nickel-tetraazamacrocyclic complexes has been reported, the possible mechanisms of cell growth inhibition by these nickel-complexes have not been studied (Chatterjee et al. 2012). Moreover, there are no reports on the effects of oxidation of a nickel (II) azamacrocyclic complex by oxidant on the microbial cells.

As mentioned above, nickel (II) complexes can undergo photochemical oxidation to form stable nickel (III) complexes which are highly reactive and act as strong oxidants. Nickel (II) azamacrocyclic complexes are reactive towards radicals

(Zeigerson et al. 1982; Jaacobi et al. 1979; Lee et al. 2000) and oxides to reactive ligand centered radicals or nickel trivalent species (Zeigerson et al. 1982; Zilbermann et al. 1993). TiO_2 photocatalysis produces highly reactive radicals which could also react with the nickel (II) azamacrocyclic complexes to produce reactive species. It has been reported that Ni(II) can behave as an electron trap and get reduced to Ni^+ forming superoxide radical, or can behave as an hole trap, getting oxidized to Ni^{3+} and produce hydroxyl radicals, both of which radicals along with Ni^{3+} are extremely reactive and can cause degradation of organic compounds (Gomathi Devi, 2010). However, the effect of addition of catalytic amount of nickel (II) azamacrocyclic complex to TiO_2 for the photoinduced inactivation of the microorganisms has not been investigated in these studies.

In view of the above facts, the present study was carried out to investigate the antimicrobial effects of TiO_2 nanoparticles and nickel (II) azamacrocyclic complex during photocatalytic reaction in an aqueous phase on some common pathogenic organisms. The microorganisms tested were *Escherichia coli*, *Klebsiella pneumoniae, Staphylococcus aureus MTCC* 737, *Enterococcus faecalis MTCC* 2080 and *Candida albicans* 3950. Further studies were also carried out to show the oxidation of divalent nickel complex 1 (1, 8-dimethyl-1, 3, 6, 8, 10, 13-hexaazacyclotetradecane) nickel (II) perchlorate) (Chart 1) to stable trivalent nickel species by ammonium persulphate (oxidant). It was observed that, complex 1 along with the TiO_2 nanoparticles and oxidant has higher propensity to induce cell growth inhibition as compared to TiO_2/complex 1 alone. Effective inhibition of cell growth by complex 1 in presence of TiO_2 /oxidant is mainly attributed to its ability to cause damage to the cell membrane.

Chart 5.1: Chemical structure of (a) complex 1, (1, 8-dimethyl-1, 3, 6, 8, 10, 13 hexaazacyclotetradecane) nickel (II) perchlorate) and (b) Ammonium persulphate.

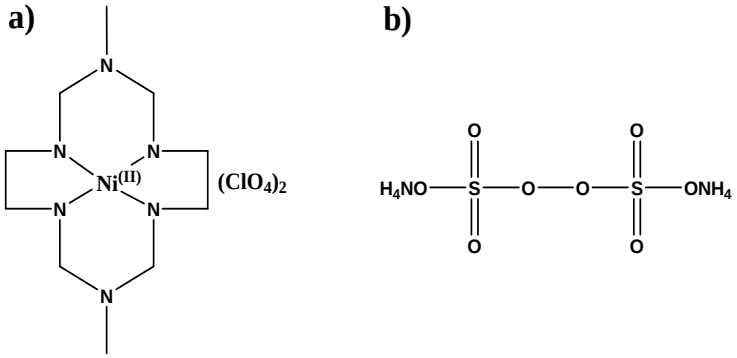

5.2 Materials and methods

Chemicals and solvents used were of guaranteed analytical grades purchased from Merck, Sd-fine Company, India and used without further purification. Hombikat TiO_2 (Fluka, Sigma-Aldrich Chemie GmbH; Anatase) with a surface area of ≥300 m^2/g was used for the experiment. A 1 mg/ml stock suspension of TiO_2 nanoparticles was prepared in sterile distilled water. The suspension was thoroughly mixed by sonication and added immediately to the reaction mixture. The suspension was always prepared fresh immediately prior to photocatalytic reaction and kept in the dark. All the glassware and accessories used were washed with distilled water and then autoclaved at 121 ℃ for 15 minutes. The complex 1 was prepared according to the earlier method (Suh and Kang, 1988). A stock solution of complex 1 (5.7 mM) was prepared in aqueous medium, filter sterilized using a 0.22 μ Millipore membrane filter and appropriate amounts were used for the experiment. Sterile water was used for the experiments.

5.2.1 Bacterial strains and cultures

The following bacterial strains were used: *Escherichia coli, Klebsiella pneumoniae, Staphylococcus aureus MTCC 737, Enterococcus faecalis MTCC 2080* and *Candida albicans 3950* The bacterial strains were grown overnight in NB (nutrient broth) medium/ SDB (Saborauds Dextrose Broth) medium and aliquots of these cultures

were inoculated into fresh medium, incubated under aerobic conditions at 37 ℃/30 ℃ on a rotary shaker at 150 rpm until the exponential growth phase was reached. The standard suspensions of the organisms (~10^5 cfu/ml) were obtained by serially diluting the cultures in sterile normal saline. Simulated sterile ground water (SSGW) was prepared by addition of following components to distilled water: $FeNO_3$ (0.24 µm), $NaHCO_3$ (1.2 mM), Na_2SO_4 (0.34 mM), Na_2HPO_4 (0.28 mM), NaCl (0.86 mM) and resorcinol (9.0 µm) (Dash and Chaudhari, 2005; Marugan et al. 2010).

5.2.2 Photocatalytic reaction and Cell viability assay

The photocatalytic reaction was carried out in sterile 50 ml glass beakers containing the Ni azamacrocyclic complex solution, the TiO_2 suspension and the bacterial cells. The Ni complex solution was used at a concentration of 20 µM, while the concentration of TiO_2 suspension was constant 5 µg/ml throughout. To the beakers ~10^5 cfu/ml of microbial cells were added and the final reaction mixture was made to 5 ml. The beakers were exposed to blacklight blue UV light 352 nm (Sankyo Denki, Japan, 15 W) with continuous stirring on magnetic stirrers so as to prevent the precipitation of TiO_2 nanoparticles and to ensure proper nanoparticle-cell contact. The samples were tested against a set of two relevant controls, (i) Only TiO_2 and cells, (ii) A dark control containing both Ni complex solution and TiO_2 suspension but not exposed to UV light. The dark control beaker was completely covered with aluminium foil to avoid any light interaction.

Aliquots of the exposed reaction mixture were withdrawn at regular time intervals of 15, 30, 45, 60, 90 and 120 minutes, serially diluted with sterile normal saline and plated out on nutrient agar/Saborauds agar plates in duplicates. The plates were

incubated at 37 ℃/30 ℃ for 24 hrs and the loss of cell viability was monitored by taking the viable count at the end of the incubation period.

5.2.3 UV-visible spectral measurements of complex 1 and kinetics studies

UV-visible spectral measurements were performed using a UV-2450 Shimadzu UV-Visible spectrophotometer. The concentration of the complex 1 was determined from absorption coefficient value of 40 $M^{-1}cm^{-1}$ at 444 nm in water as reported earlier (Suh and Kang 1988). A stock solution of complex 1 (5.7 mM) was prepared in water and appropriate concentrations were used for absorption measurements, kinetics of the oxidation of complex 1 by ammonium persulphate, and for experiments to investigate the growth inhibition of the cells, and cell wall damage. Stock solution of ammonium persulphate (2.5 M) was freshly prepared in sterile water.

5.2.4 ESR spectral measurements

ESR spectra of complex 1 were obtained after the addition of appropriate amount of ammonium persulphate to the complex 1 dissolved in either water/nutrient broth (NB). The solutions were frozen using liquid nitrogen, and the spectral measurements were done using Bruker ESR spectrometer facility at TIFR, Mumbai, India. The instrument was calibrated, and g-values were obtained as reported earlier (Desideri and Raynor 1977; Bencini et al. 1981).

5.2.5 Antimicrobial assay of the complex 1 in presence and absence of oxidant

The microbial cells (~10^5 cfu/ml) were suspended in 1ml of (i) sterile ground water, or (ii) NB/SDB media. To these solutions, varying concentrations of APS and appropriate amount of complex 1 were added from the stock solution. Contents of these tubes were mixed and incubated over night in a shaking incubator at 37 ^oC/ (30

^{o}C for fungus) (Jeong et al. 2006; Lorian 2005; Egger et al. 2009). At the end of incubation, 0.1 ml of above suspensions was spread plated on nutrient agar / Saboraud's agar plates and incubated at 37 ^{o}C (30 ^{o}C for fungus) for 24 hrs. Colonies observed on these plates were counted to obtain the number of viable cells as colony forming units per ml (cfu/ml) (Jeong et al. 2006; Lorian 2005; Egger et al. 2009). All microbial assays were performed in replicates, with appropriate controls i.e, (i) cells with APS alone (ii) cells with complex 1 alone. The antimicrobial activity was determined for *Escherichia coli*, *Staphylococcus aureus MTCC 737*, and *Candida albicans.*

5.2.6 Determination of lipid peroxidation

Lipid peroxidation is used as an indicator of oxidative stress in cells and one of the products of lipid peroxidation is malondialdehyde (MDA). Formation of MDA is used as an index to measure the extent of lipid peroxidation (Maness et al. 2009; Esterbauer and Cheeseman, 1990). MDA formation was investigated based on its reaction with Thiobarbituric acid (TBA) to form a pink TBA-MDA adduct, which could be monitored spectrophotometrically. It has been reported that the TBA-MDA adduct shows an absorption band with maximum around 540 nm (Maness et al. 2009; Esterbauer and Cheeseman, 1990). Log phase cells (~10^{8} cfu/ml) were suspended in 1 ml of NB medium containing 2.5 mM complex 1 and 2 mM oxidant. This suspension was incubated overnight at 37°C on a rotary shaker at 120 rpm and at the end of the incubation period, 2 ml of 10 % (wt/vol) trichloroacetic acid was added. Then, the contents were centrifuged at 11,000 g for 50 min, and the supernatant were taken for the analysis of MDA as follows. To ~3 ml of the supernatant, 3 ml of freshly prepared 0.67 % (wt/vol) TBA solution was added. The sample tubes were then incubated in a boiling water bath for 10 min, cooled to room temperature and the absorption band

corresponding to the TBA-MDA adduct was determined. The TBA assay was performed with the following controls i) Cells with complex 1 without oxidant ii) Only cells without complex 1 and oxidant. iii) Cells with only oxidant.

5.2.7 Sample preparation for Scanning Electron Microscopy (SEM)

Log phase *E. coli* cells of about 10^8 cfu/ml were suspended in NB medium containing complex 1 (312 µM) and ammonium persulphate (2 mM) and the mixture was incubated for 30 minutes. After incubation, the mixture was centrifuged, and the cells were fixed with 2% glutaraldehyde solution for 1 h (Su et al. 2009; Kang et al. 2008; Hartmann et al. 2010). The cells were then washed thrice with 0.1 M phosphate buffer saline (pH 7.2), gradually dehydrated using the following ethanol/H_2O mixture of 10, 25, 50, 75, 90 (v/v %) and finally with 100 % ethanol followed by air drying. The dried cells were then coated with platinum by JEOL JFC-1600 Autobine sputter and the images were taken with a JEOL JSM-6360 LV Scanning Electron Microscope at a voltage of around 10 kV. A control sample wherein the cells were not exposed to complex 1 and oxidant was similarly processed.

5.3 Results and discussion (A: (Ni (II) complex + TiO_2)

The reduction in the cell viability of *E. coli* cells on varying the concentration of Hombikat TiO_2 is presented in table 5.1. The result indicates that increasing the concentration of TiO_2 causes a decrease in bacterial count, and the minimum concentration required to kill the bacteria was determined to be 25 µg/ml, on 120 minutes of UV light irradiation. The antimicrobial activity of Ni (II) azamacrocyclic complex alone at different concentrations is shown in table 5.2. These results indicate that Ni (II) complex is not toxic to bacteria on photolysis. Interestingly, it was determined that as low as 5 µg/ml of Hombikat TiO_2 in presence of 20 µM of Ni (II)

complex caused significant decrease in the cell viability of *E. coli* cells within 120 minutes of UV irradiation (Table 5.3). Thus, the results clearly indicate the effective concentration of the TiO_2 required to kill the bacteria is significantly reduced on addition of the Ni (II) complex solution.

Table 5.1. Antibacterial effects of TiO_2 at varying concentrations under UV light (352 nm) exposure.

Conc. Of TiO_2	**0 mins**	**60 mins**	**120 mins**
5 µg/ml + *E.coli*	6.2×10^5	3.81×10^4	1.72×10^4
10 µg/ml + *E.coli*		2.45×10^4	1.17×10^4
25 µg/ml + *E.coli*		3.39×10^2	13
50 µg/ml + *E.coli*		108	0

Table 5.2. Antibacterial effects of Ni (II) azamacrocyclic complex solution at varying concentrations.

Conc. Of Ni (II) complex	**0 mins**	**60 mins**	**120 mins**
100 µM + *E.coli*	5.79×10^5	2.19×10^5	1.09×10^4
50 µM + *E.coli*		4.22×10^5	2.15×10^5
20 µM + *E.coli*		4.81×10^5	3.53×10^5

Table 5.3. Antibacterial effects of TiO_2 (5 µg/ml) at varying concentrations of Ni (II) azamacrocyclic complex solution under UV light irradiation.

Conc. Of Ni (II) complex + TiO_2	**0 mins**	**60 mins**	**120 mins**
100 µM + 5 µg/ml + *E.coli*	3.8×10^5	9.31×10^2	0
50 µM + 5 µg/ml + *E.coli*		1.18×10^3	3
20 µM + 5 µg/ml + *E.coli*		1.43×10^3	8
10 µM + 5 µg/ml + *E.coli*		2.32×10^4	1.13×10^2

Combination of 20 µM Ni (II) complex + 5 µg TiO_2 showed complete inactivation of *K. pneumoniae* after just 90 minutes of irradiation whereas the control (TiO_2) showed no noticeable decrease in bacterial (Fig. 5.1). *E. coli* and *K. pneumoniae* are both Gram negative bacteria, and the present results show that the combination of nickel and TiO_2 has the ability to inactivate the Gram negative species. Similarly, Gram positive bacterial cultures *S. aureus* and *E. faecalis* were also completely inactivated after ~90 minutes and 120 minutes of UV irradiation in presence of nickel(II) complex and TiO_2, indicating that the nickel (II) complex and TiO_2 is also effective for the inactivation of the Gram positive bacterial species (Fig. 5.2). The irradiation of fungal culture *C. albicans* (at 20 µM Ni (II) complex + 5 µg TiO_2) also showed complete reduction after 120 minutes (Fig. 5.3).

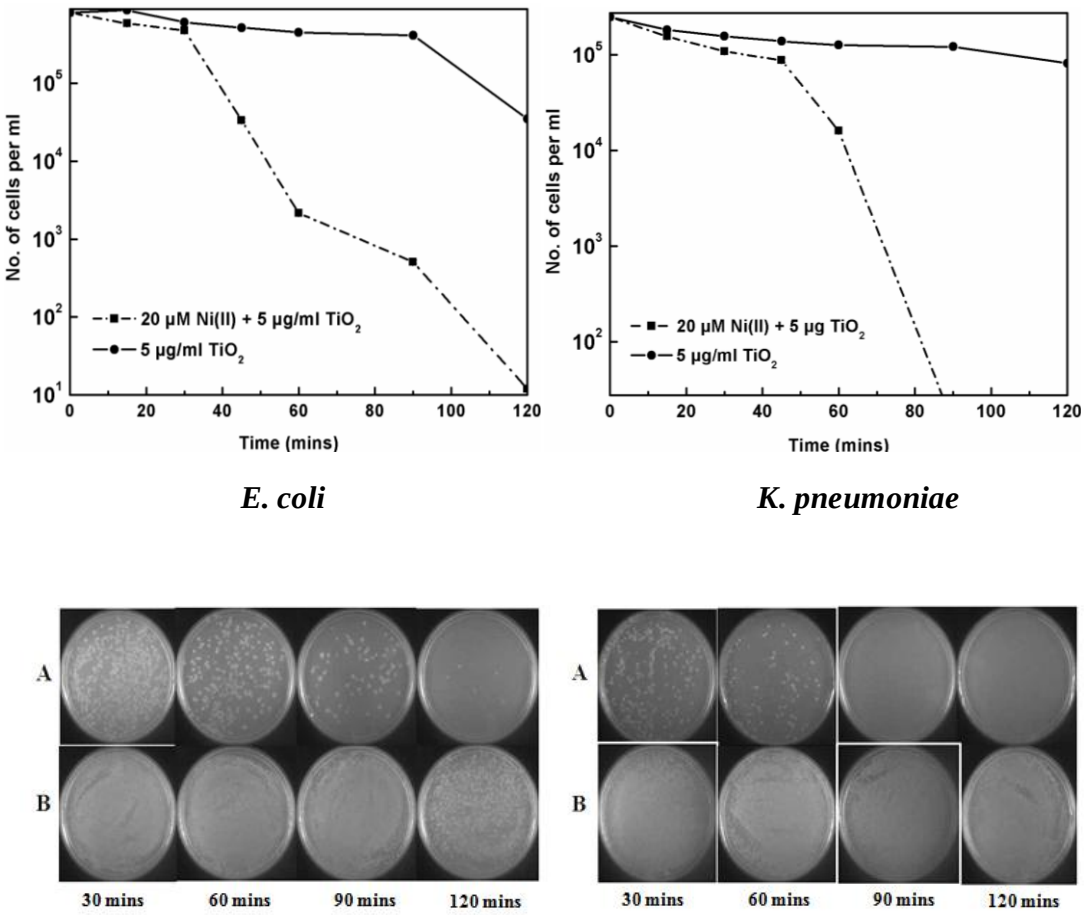

A: 20 μM Ni(II) + 5 μg/ml TiO_2

B: 5 μg/ml TiO_2

Fig. 5.1. Figure showing the antibacterial effects of 20 μM Ni(II) complex solution + 5 μg/ml TiO_2 and 5 μg/ml TiO_2 alone, on Gram negative bacterial cultures *E. coli* (Left) and *K. pneumoniae* (Right).

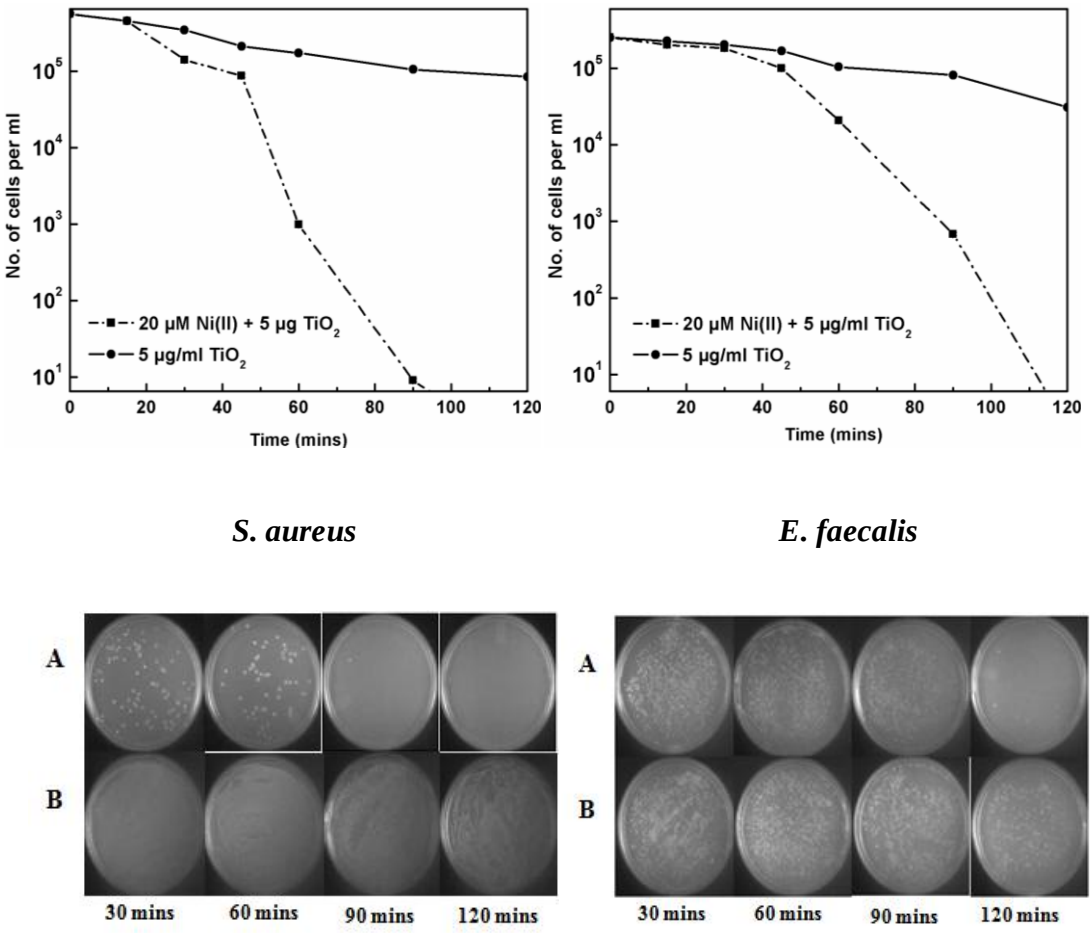

A: 20 µM Ni(II) + 5 µg/ml TiO_2

B: 5 µg/ml TiO_2

Fig. 5.2. Figure showing the antibacterial effects of 20 µM Ni(II) complex solution + 5 µg/ml TiO_2 and 5 µg/ml TiO_2 alone, on Gram positive bacterial cultures *S. aureus* (Left) and *E. faecalis* (Right).

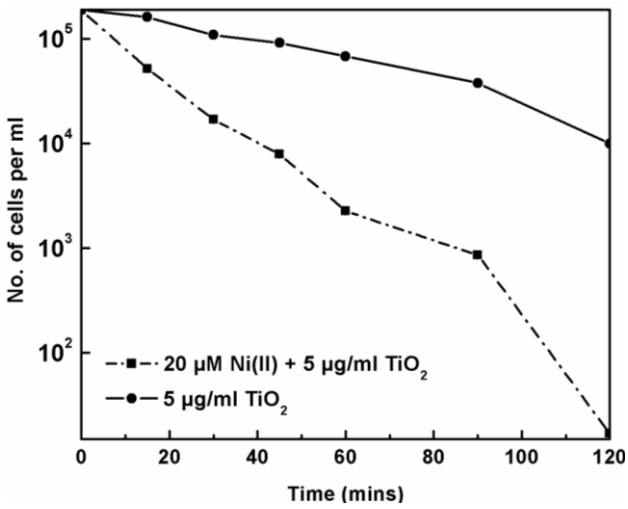

C. albicans

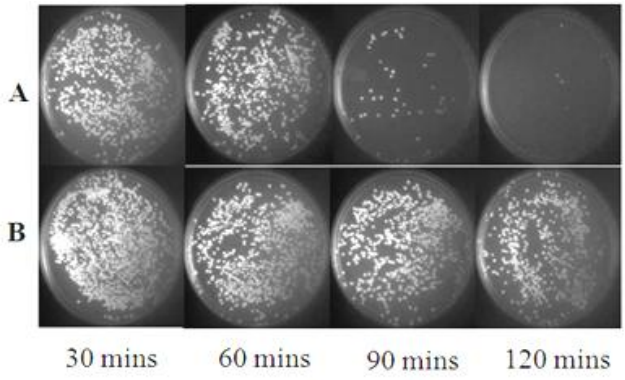

A: 20 μM Ni(II) + 5 μg/ml TiO_2

B: 5 μg/ml TiO_2

Fig. 5.3. Figure showing the antifungal effects of 20 μM Ni(II) complex solution + 5 μg/ml TiO_2 and 5 μg/ml TiO_2 alone, on *C. albicans*.

If Ni (II) is assumed to trap an electron of the conduction band of TiO_2, it gets reduced to Ni^+ and the trapped electron may be transferred to an oxygen molecule forming superoxide radical.

$$Ni^{2+} + e^- \rightarrow Ni^+$$

$$Ni^+ + O_2 \rightarrow Ni^{2+} + O_2^{-\bullet}$$

Also, Ni^{+} can trap valence band holes and get oxidized to Ni^{2+}

$$Ni^{+} + h^{+} \rightarrow Ni^{2+}$$

If Ni^{2+} ions behave as a hole trap, they would get oxidized to Ni^{3+}.

$$Ni^{2+} + h^{+} \rightarrow Ni^{3+}$$

The trapped hole on the surface of TiO_2 can be transferred to the hydroxide ion

$$Ni^{3+} + OH^{-} \rightarrow Ni^{2+} + OH^{\bullet}$$

Based on the above mechanisms, Gomathi Devi et al. 2010, Xu et al. 1992, Yao et al. 2010 have suggested that the Ni (II) complex in presence of TiO_2 increases the interfacial charge transfer and facilitate the generation of highly oxidative free radicals such as hydroxyl and super oxide radicals that can effectively inactivate the adsorbed microorganisms (Chen et al. 2008; Xu et al. 1992; Gomathi Devi et al. 2010; Yao et al. 2010). In many of the antimicrobial studies carried out with TiO_2, the reported concentration of TiO_2 has been in the range of 0.1 – 1 mg/ml (Cho et al. 2005; Maness et al. 1999). However, the present study shows that a low TiO_2 concentration of 5 μg/ml with 20 μM Ni (II) complex is effective in inhibiting the growth of different microorganisms under UV light.

Although, the present results show that the nickel (II) complex is not an effective antimicrobial, and used in very low amounts (micromolar range) for activation of the persulphate or photoassist the TiO_2, it is desirable to remove the complex from the water media. Importantly, ion exchange (Vilensky et al. 2002; Rengaraj et al. 2003), electrochemical processes (Rengaraj et al. 2003; Rana et al. 2004), and adsorption (Zaporozhets et al. 1999; Kasaini et al. 2000) are effective for the removal of metal ions and their complexes and these complexes have a scope in water

purification/treatment. Several studies have reported the usage of such complexes as ruthenium bipyramidal complexes anchored onto the surface of TiO_2 photoactalysts to develop solar remediation technologies for degradation of pollutants and for the development of dye-sensitized solar cells (Bae et al. 2004; Litter M. 1999; Eslava et al. 2010). Heterometallic transition metal titanium complexes have been reported to have potentially broad applications in photocatalysis, photovoltaics, and photosensors (Eslava et al. 2010).

5.3 B: (Ni (II) complex + Ammonium persulphate)

5.3.1 UV-visible spectra and kinetic studies of the complex 1

After the addition of the oxidant ammonium persulphate to the complex 1, the changes in absorbance at ~290 nm were determined with respect to time. These plots showing the change in absorbance at 290 nm vs time were fitted to first order rate equation, and the rate constants (k_{obs}) for the formation of trivalent nickel complex was determined, as reported earlier (Haines and Rowley, 2003; Haines and Northcott, 1992; Zilbermann et al. 1993). The kinetics data analysis for the oxidation of the complex 1 by ammonium persulphate via ion-pair mechanism involving the following reactions (equations 1-3) were performed and the value of the ion-pair dissociation constant (K_1) was determined.

$$[Ni(II)L]^{2+} + S_2O_8^{2-} \underset{}{\overset{K_1}{\rightleftharpoons}} \{Ni(II)L^{2+}, S_2O_8^{2-}\} \quad \text{ion-pair} \qquad ....1$$

$$\{Ni(II)L^{2+}, S_2O_8^{2-}\} \xrightarrow{K_2} [Ni(III)L(SO_4)]^{+} + SO_4^{\cdot} \qquad ....2$$

$$[Ni(II)L]^{2+} + SO_4^{\cdot} \xrightarrow{\text{fast}} [Ni(III)L(SO_4)]^{+} \qquad .....3$$

The rate law derived from this scheme is

$$\text{Rate} = \frac{2K_2K_1[S_2O_8^{2-}]}{1 + K_1[S_2O_8^{2-}]} [Ni(II)L]_{total} \qquad .....4$$

Thus, the overall reaction for the oxidation of nickel (II) tetra- and penta-azamacrocyclic complexes has been proposed as

$$2[Ni(II)L]^{2+} + S_2O_8^{2-} \xrightarrow{H_2O} 2[Ni(III)L(SO_4)(H_2O)]^{+} \qquad ….5$$

L = tetra-, penta-azamacrocyclic ligands.

The variation in the rate constants on increasing the concentration of the oxidant was performed by maintaining the concentration of the complex 1 at 250 µM and increasing the oxidant concentration, such that the concentration ratios of complex 1 to oxidant are 1:1, 1:2, 1:5 and 1:10. Kinetics studies of the oxidation of the complex 1 by ammonium persulphate in SSGW and in nutrient broth medium were performed.

The absorption spectrum of complex 1 in water showed a single d-d absorption band with maxima at 444 nm (ε = 40 $M^{-1}cm^{-1}$) in the visible region revealing that the complex 1 exist predominantly in the square planar-low spin form, as reported earlier (Fig. 5.4). Addition of the oxidant ammonium persulphate to the

complex 1 resulted in the formation of an intense absorption band with maximum around 290 nm (Fig. 5.4).

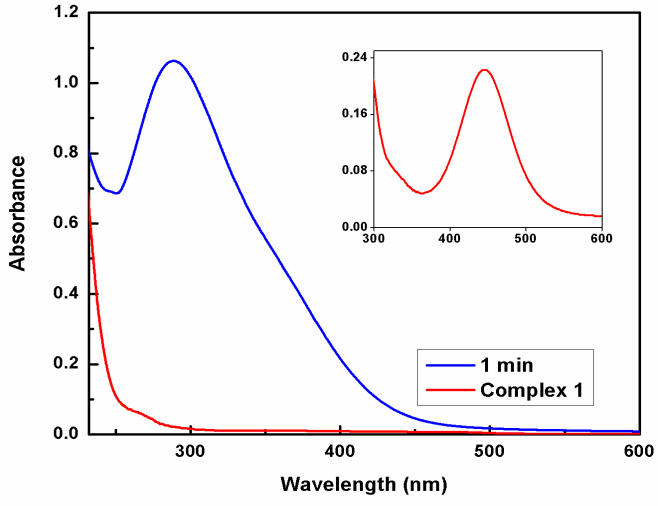

Fig. 5.4. Absorption spectrum of the complex 1 in water and the spectral changes changes on addition of oxidant ammonium persulphate in water. [Complex 1] = 250 µm and [Oxidant] = 1250 µM. The inset shows the d-d absorption band of complex 1 in water. [Complex 1] = 5.7 mM.

The changes in absorbance at 290 nm with time was determined for the solutions with 1:1, 1:2, 1:5 and 1:10 ratios of complex 1 and oxidant, respectively, (Fig. 5.5). These spectral changes indicate that the reaction between the complex 1 and oxidant at 1:5 and 1:10 ratios of was very effective and the absorbance reached the saturation indicate that the reaction was completed within 600 sec, while at 1:1 and 1:2 ratios, the reaction was not effective and the absorpbance changes were not saturated (Fig. 5.5).

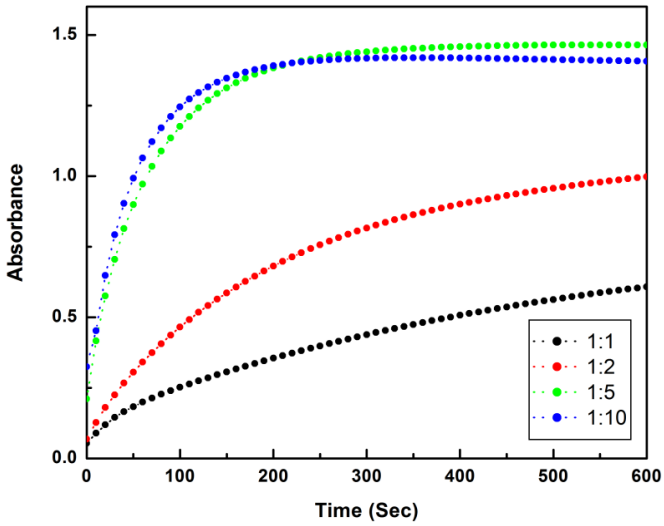

Fig. 5.5. Absorption changes with time at 300 nm for the solutions having 1:1, 1:2, 1:5 and 1:10 ratios of complex 1 and oxidant, respectively in water . [Complex 1] = 250 µm.

The first order rate constant values, (K_{obs}) were determined from the spectral changes over the time and the values are tabulated in Table 5.4.

Table. 5.4. First order rate constants (K_{obs}) for the reaction between complex 1 and oxidant:

Complex 1*: APS	$K_{(obs)}$ SSGW (S^{-1})	$K_{(obs)}$ NB (S^{-1})
1:1	2.26 (±0.10) x 10^{-3}	1.69 (±0.08) x 10^{-3}
1:2	3.90 (±0.19) x 10^{-3}	1.38 (±0.06) x 10^{-3}
1:5	1.48 (±0.07) x 10^{-2}	1.25 (±0.06) x 10^{-3}
1:10	1.87 (±0.09) x 10^{-2}	2.18 (±0.10) x 10^{-3}

*[Complex 1] = 250µM.

The above absorption spectral changes and kinetic results obtained for the reaction between the complex 1 and oxidant are similar to those reported for the oxidation of

nickel(II) tetra- and penta- azamacrocyclic complexes by ammonium persulphate to trivalent nickel complexes with absorption maximum around 290 nm, by an ion-pair mechanism (Haines and Rowley, 2003; Haines and Northcott, 1992). The rate constant (K_{obs}) for the reaction between complex 1 and APS increased with increase in the concentration of APS. $1/k_{(obs)}$ vs 1/[APS] (reciprocal plot) was found to be linear and from the slope and intercept of this reciprocal plot, ion-pair constant (K_1) and rate of electron transfer (K_2) were determined to be 21.46 (± 1.00) and 0.21 (± 0.01) S^{-1}, respectively (Haines and Rowley, 2003, Haines and Northcott, 1992). Importantly, stable trivalent nickel azamacrocyclic complexes are generally known to exist in the octahedral geometry, in which the ligands like sulphate ions, water are axially coordinated to the trivalent nickel ion, at pH ~7 (Zilbermann et al. 1993; Zeigerson et al. 1982). Thus, $[Ni(III)L(SO_4)(H_2O)]^+$ (L= tetra, penta, hexa-azamacrocyclic ligands) is proposed to be the predominant species in the solution with absorption maximum around 290 nm. It is also known that $[Ni(III)L(SO_4)(H_2O)]^+$ could convert to $[Ni(III)L(SO_4)_2]^-$ in presence of excess sulphate ions with spectral features similar to that of the $[Ni(III)L(SO_4)(H_2O)]^+$ species.

The reaction between the complex 1 and the oxidant carried out Nutrient Broth medium were also followed spectrophotometrically (Fig. 5.6). The absorption band with maximum around 290 nm was observed under these conditions, as observed for the reaction being carried out in neat water.

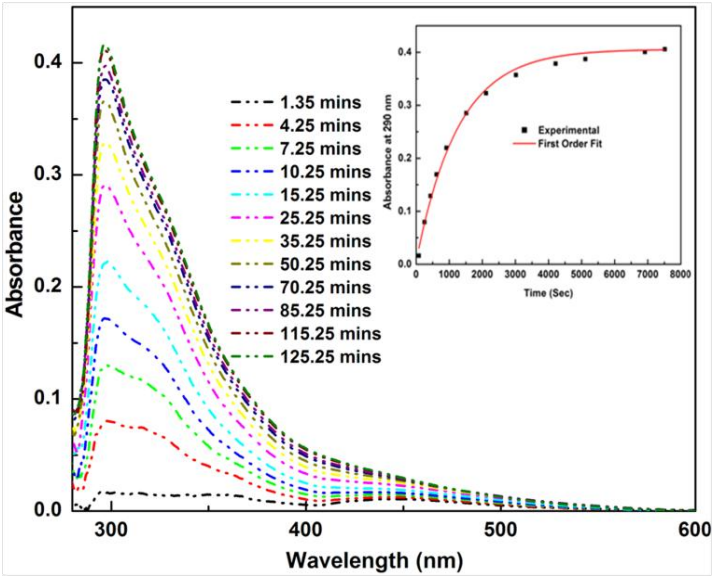

Fig. 5.6. Absorption spectral changes during the oxidation of complex 1 by ammonium persulphate in 1x-NB medium. Formation of the trivalent nickel species with absorption maximum ~290 nm with time on addition of the oxidant to the complex 1. [Complex 1] = 250 µm and [oxidant] = 1250 µM. (inset) Change in the absorption at 300 nm Vs time and the first order fit for the absorption change.

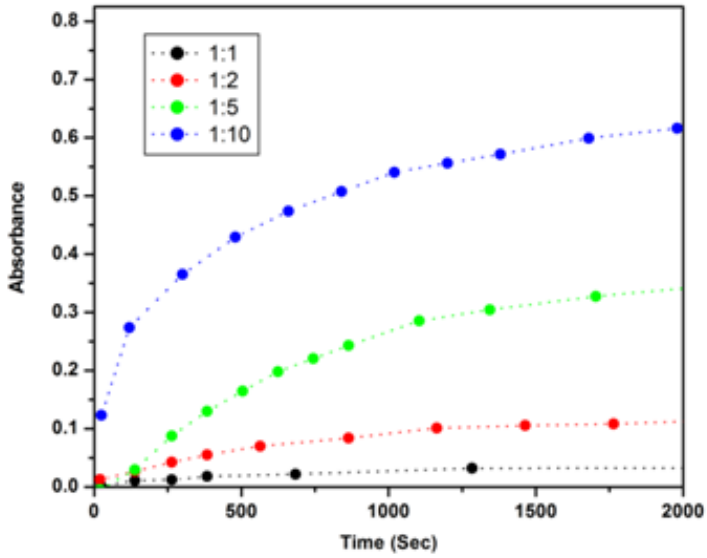

Fig. 5.7. Absorption changes with time at 300 nm for the solutions with 1:1, 1:2, 1:5 and 1:10 ratios of complex 1 and oxidant, in 1X NB . [Complex 1] = 250 µm.

However, (K_{obs}) values observed for the above mentioned conditions i.e. reaction in 1x NB medium was lower than reaction carried out in water (Table 5.4). In an ion pair reaction mechanism, the observed rate constants (K_{obs}) decreases on increasing the ionic strength due to the interference of the added ions in the formation of ion-pair between the divalent nickel complex and ammonium persulphate oxidant (Haines and Rowley, 2003). Thus, the presence of ionic salts like sodium chloride interfere with the ion-pair formation between the complex 1 and the oxidant, and hence the trivalent nickel complex with absorption maximum around 290 nm is not effectively formed compared to the oxidation of complex in water alone (Fig. 5.7).

The formation of stable trivalent nickel ion after the addition of ammonium persulphate to complex 1 in NB medium was also confirmed by ESR spectrum, (Fig. 5.8), which showed an anisotropic axial signal with $g_{\perp}$ = 2.069 and $g_{\parallel}$ = 2.239 values. Similar g values have also been reported for the oxidation of complex 1 by ammonium persulphate in water.

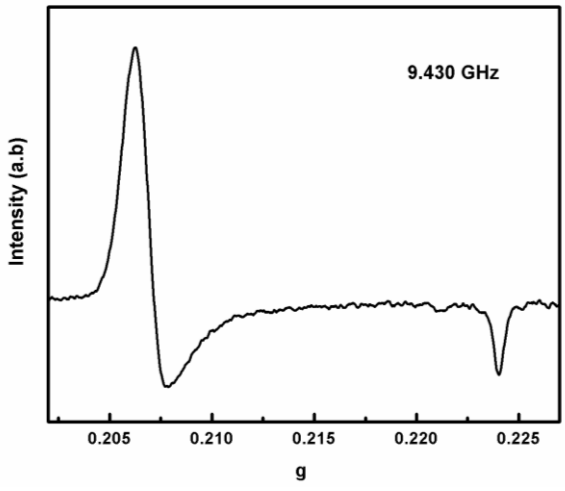

Fig. 5.8. Electron spin resonance spectrum observed after the addition of ammonium persulphate to complex 1 in NB medium. Temperature = 90 K. [Complex 1] = 265 µm [oxidant] = 2 mM.

Moreover, the axial signal indicates that the stable trivalent nickel complex formed due to the oxidation reaction has an octahedral geometry (Desideri and Raynor, 1977; Bencini et al. 1981). Importantly, the observed ESR spectrum is similar to the earlier reported octahedral nickel (III) tetraazamacrocyclic complexes with a N_4O_2 type coordination environment around the trivalent nickel ion, in which the nickel (III) ion is coordinated to four N-dendates of the azamacrocyclic ligand and two O-dendates of axially coordinated ligands (Zeigerson et al. 1982; Zilbermann et al. 1993; Desideri and Raynor, 1977; Bencini et al. 1981). The two O-dendates of the axially coordinated ligands are attributed to the coordination of sulphate ions formed during the oxidation reaction, water molecules and the carboxylic groups of acidic amino acid present in 1x NB, at pH ~7 (Haines and Rowley, 2003; Haines and Northcott, 1992; Zeigerson et al. 1982; Zilbermann et al. 1993). Thus, above results indicate that complex 1 is effectively oxidised by APS, consequently resulting in effective activation of APS and formation of reactive species (reactions 2), which could be deleterious for microorganisms.

5.3.2 Antimicrobial assay of the complex 1 in presence and absence of oxidant

5.3.2.1 Effect of APS alone, and in presence of complex 1 on Microorganisms

It was determined that 15 mM APS was required for complete inactivation of *E. coli* and *C. albicans*, and 10 mM APS was required for the inactivation of *S. aureus* in complex nutrient rich media (Table 5.5). These results indicated that APS alone could inactivate the microorganisms. Interestingly, in presence of 1 mM of complex 1, it was determined that 8 mM of APS caused complete inactivation of *E. coli,* and *S. aureus* and *C. albicans* (Table 5.5), showing that the effective concentration of APS to inactivate microorganisms was reduced in presence of complex 1 (Table 5.5). As

mentioned above, reaction between APS and complex 1 result in the generation of highly reactive oxidising species such as sulphate radicals, which could cause oxidative stress leading to cell membrane damage and cell death. In the absence of complex 1, APS is decomposed very slowly to produce sulphate radicals (Haines and Rowley 2003, Haines and Northcott 1992, Kolthoff and Miller 1951). The reduction in the effective concentration of APS in presence of complex 1 to inactivate bacteria and fungus compared to APS alone is attributed to the activation of persulphate by complex 1 (reaction 1-5). Importantly, suspension of bacteria into preincubated mixture of persulphate (375 μM) and complex 1 (75 μM) showed no significant reduction in cell viability. In addition, stable dichloro (1, 8-dimethyl-1, 3, 6, 8, 10, 13-hexaazacyclotetradecane) nickel (III) perchlorate hydrate complex (75 μM) was also found to be ineffective to inactivate the bacteria. However, addition of complex 1 to the suspension of bacteria containing APS or addition of APS to the bacterial suspension containing complex 1 caused complete inactivation of bacteria (Table 5.6). Thus, these results reveal that bacterial inactivation is mainly due to activation of persulphate by complex 1, with generation of reactive species such as sulphate radicals.

It was also observed that, in simulated ground water, 5 mM of APS alone completely inactivated *E. coli* and *S. aureus* while 8 mM of APS completely inactivated *C. albicans*. These results show that the effective concentration of the APS was significantly reduced in ground water than in complex nutrient rich media. As mentioned earlier, it is important to note that the reactive radical species produced in the reaction between complex 1 and APS, in complex medium (NB/SDB) could be easily scavenged by the constituents of the media, which is not favourable for inactivation of microbes. Thus, higher concentration of APS is required for

inactivation of microbes in NB/SDB media compared to that observed in the ground water. Additionally, in presence of 75 µM of complex 1 and 2 mM of APS *E. coli*, *S. aureus* and *C. albicans* were completely inactivated (Table 5.6). This significant reduction in the concentration of APS to inactivate the microorganisms is attributed to the effective activation of APS by complex 1 in simulated ground water.

Table 5.5. Effective concentrations of APS alone and APS in presence of complex 1 for inactivation of microorganisms in NB/SDB media and SGW (all experiments were carried out in replicates)

Medium	Conc. Of APS (mM)	Cell viability (log reduction)		
		E. coli	*S. aureus*	*C. albicans*
NB/SDB	5	No reduction	No reduction	No reduction
NB/SDB	8	1 log reduction	2 log reduction	1 log reduction
NB/SDB	10	3 log reduction	Complete reduction	2 log reduction
NB/SDB	15	Complete reduction	ND*	Complete reduction
SGW	3	No reduction	1 log reduction	No reduction
SGW	5	Complete reduction	Complete reduction	2 log reduction
SGW	8	ND	ND	Complete reduction

ND*: Not done

Table 5.6. Effective concentrations of APS in presence of complex 1 for inactivation of microorganisms in NB/SDB media and SGW (all experiments were carried out in replicates).

Medium	Complex1:APS (mM)	Cell viability (log reduction)		
		E. coli	*S. aureus*	*C. albicans*
NB/SDB	1 : 5	1 log reduction	1 log reduction	1 log reduction
NB/SDB	1 : 8	Complete reduction	Complete reduction	Complete reduction
SGW	0.075 : 1	1 log reduction	2 log reduction	No reduction
SGW	0.075 : 2	Complete reduction	Complete reduction	Complete reduction

NB and SDB media are complex nutrient media containing minerals and are rich in organic compounds such as sugars, vitamins and peptides. During the reaction between complex 1 and APS in such complex media, reactive oxidising species such as sulphate radicals and trivalent nickel species produced could be easily scavenged by these organic compounds. Moreover, rate of reaction was found to be ten time greater in ground water than rate of the reaction in NB medium, indicating that the activation of persulphate by complex 1 in ground water was better than in case of complex NB. Thus, these results reveal that activation of persulphate by complex 1 depends on the media, and in complex medium such as NB, the activation is not effective compared to that observed in water. Therefore, we envisaged that, in a medium with less organic and inorganic content such as ground water, it should be possible to achieve complete inactivation of microorganisms at lower concentrations of APS and complex 1. Interestingly, complete inactivation of microorganisms (*E.*

coli, S. aureus and *C. albicans*) in ground water was achieved at lower concentrations (micromolar range, Table 5.6).

Further, relatively lower concentration of APS alone was required to kill the microorganisms compared to the concentration determined in nutrient rich NB/SDB medium (Table 5.5), which further emphasise that MBC depends on complexity of the medium, and constituents of the complex NB/SDB media could scavenge the reactive species.

5.3.2.2 Effect of stable trivalent nickel species on *E. coli* cell viability

In order to understand the effect of stable trivalent nickel species produced during activation of persulphate, bacteria were suspended into preincubated mixture of persulphate (375 μM) and complex 1 (75 μM) that formed stable trivalent species (Fig. 5.4), and it was observed that there was no significant reduction in cell viability. In addition, stable dichloro (1, 8-dimethyl-1, 3, 6, 8, 10, 13-hexaazacyclotetradecane) nickel (III) perchlorate hydrate complex (75 μM) was also found to be ineffective to inactivate the bacteria. However, addition of complex 1 to the suspension of bacteria containing APS or addition of APS to the bacterial suspension containing complex 1 caused complete inactivation of bacteria. Thus, these results reveal that bacterial inactivation is mainly due to activation of persulphate by complex 1, with generation of reactive species (reaction 2) than stable trivalent nickel species finally produced in the reaction.

Microbial growth inhibition under oxidative conditions is commonly due to the cell membrane damage (Maness et al. 2009; Esterbauer and Cheeseman, 1990). Hence we presumed that the combination of complex 1 and oxidant may effectively induce cell wall damage while the divalent nickel ion is not effective. Thus, we

performed lipid peroxidation assay. Lipid peroxidation of the cell membrane results in the formation of malondialdehyde. Thiobarbituric acid forms an adduct with malondialdehyde to produce a deep pink color solution with absorption maximum around 540 nm (Maness et al. 2009, Esterbauer and Cheeseman, 1990). In the present investigation a deep pink color solution with absorption maximum around 540 nm was observed only in the case of cells treated with complex 1 (2.5 mM) and ammonium persulphate (2 mM) (Fig. 5.9), while the absorption band of the adducts from the controls (i.e cells without both complex 1 and ammonium persulphate, cells with complex 1 (2.5 mM) and without oxidant, and cells without complex 1 and with oxidant) were significantly lower (Fig. 5.10).

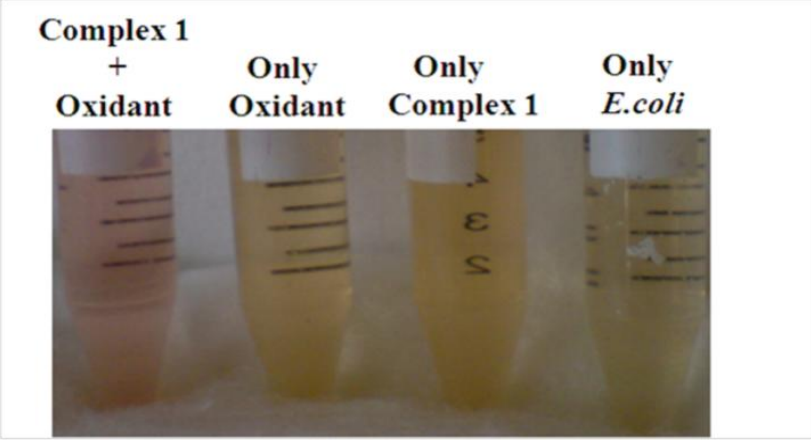

Fig. 5.9. Picture showing the formation of pink coloured adduct (TBA-MDA) as a result of MDA reacting with thiobarbituric acid (TBA) in case of cells exposed to complex 1 and oxidant. [Complex 1] = 2.5 mM [oxidant] = 2 mM cell concentration of 10^8 cfu/ml were used in the assay. The pink coloured adduct is observed only in case of complex 1 + oxidant, whereas no pink color formation was seen in the other three controls.

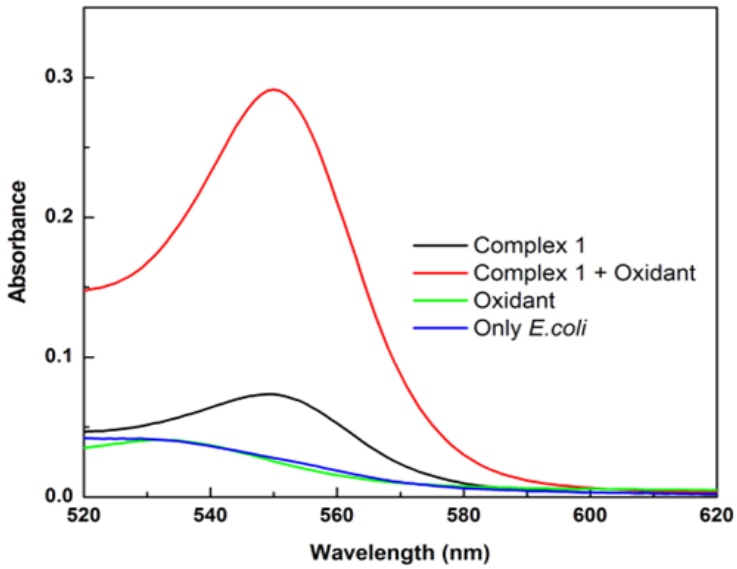

Fig. 5.10. Absorption spectra of the MDA-TBA adduct. The absorption band of adduct was clearly observed for the cells treated with complex 1 (2.5 mM) + oxidant (2 mM). The absorption of the adduct was not significant for the controls, i.e cells treated with 2.5 mM (complex 1); cells treated with 2 mM (oxidant); cells without complex 1 and oxidant (only *E.coli*). [Cell]= 10^8 cfu/ml.

Thus, thiobarbituric acid based assay for the detection of lipid peroxidation of the cell membrane clearly shows that the nickel trivalent complex has very high propensity to induce the cell membrane damage while divalent nickel complex 1 does not induce significant membrane damage even at very high concentrations.

Further, the changes in morphology of *E. coli* cells exposed to complex 1 and ammonium persulphate were determined using scanning electron microscopy (SEM). It was observed that cells in the control (without complex 1 & oxidant) were intact and maintained their cellular intergrity and outer membrane structure Fig. 5.11B. However, cells exposed to 312 μM complex 1 with 2 mM ammonium persulphate for 30 minutes showed severe membrane damage with loss of cellular integrity Fig

5.11A, indicating irreversible cell damage (Su et al. 2009, Kang et al. 2008, Hartmann et al. 2010). Hence, the SEM results clearly emphasize the cell membrane damage, which is in accordance with the TBA assay.

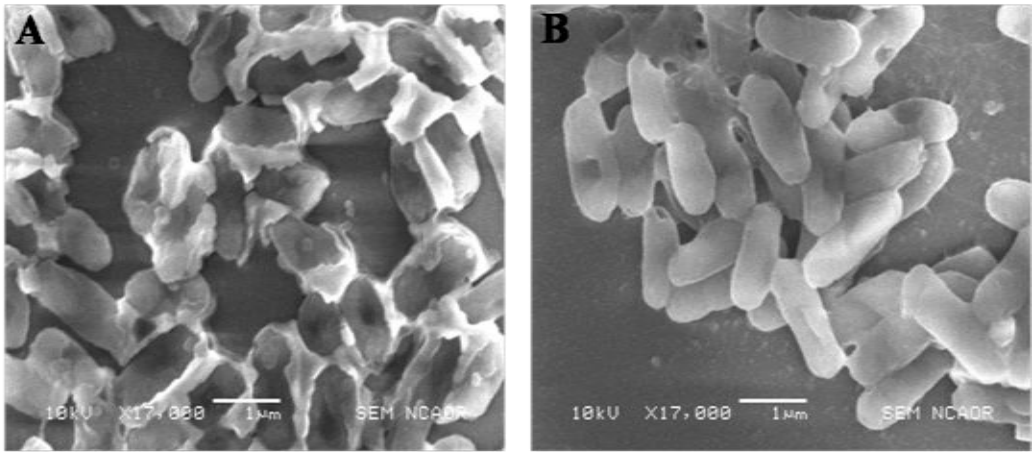

Fig. 5.11. Scanning electron micrograph showing the effect of complex 1 + ammonium persulphate on *E.coli* cells after 30 minutes of incubation. A) *E.coli* cells after treatment with 312 µM complex 1 and 2 mM ammonium persulphate B) *E.coli* cells alone not treated with complex 1 or ammonium persulphate.

Conclusion

The results of this investigation reveal that a combination of 20 µM Ni (II) complex and 5 µg TiO_2 is effective in complete inactivation of various microorganisms (irrespective of their Gram nature) under UV light irradiation. Similarly, the nickel (II) azamacrocyclic complex in presence of ammonium persulphate was found to be effective against different microorganisms at lower concentrations compared to either nickel (II) azamacrocyclic complex or ammonium persulphate alone. Ni^{2+} doped TiO_2 has been used for the degradation of methyl orange as it can form reactive Ni^{+} or Ni^{3+} species on reduction or oxidation, however, this is the first study that describes the

antimicrobial activity of nickel (II) azamacrocyclic complexes by TiO_2 or ammonium persulphate.

Many bacterial functions, such as semipermeability, respiration, and oxidative phosphorylation reactions, rely on an intact membrane structure. The combination of ammonium persulphate in presence of complex 1 caused a significant lipid peroxidation of cell membrane than in the absence of complex 1, and complete cell death was mainly attributed to cell membrane damage shown by Thiobarbituric acid assay (TBA) and SEM. Another key finding in this study is that the combination of complex 1 and oxidant is highly lethal to both Gram positive and Gram negative bacteria, as well as against fungus, indicating that the reactive radicals are very potent oxidants and are nonselective in their reactivity. Hence, nickel (II) azamacrocyclic complexes with TiO_2 or ammonium persulphate can be applied for the disinfection of pathogens, as antifouling agents, for treatment of microbial biofilms, and other environmental and medical related problems. The structural versatility of the azamacrocyclic ligands, its rich coordination chemistry with nickel (II) ion, in combination with various oxidants, provides immense scope to further investigate and develop a variety of microbicidal agents.


SUMMARY
AND
CONCLUSIONS

Summary of results and conclusions

The results obtained during the course of the present research work can be briefly summarized as follows:

1) An extensive and thorough literature survey revealed that (a) a major driving force for pursuing research on the nanocrystalline TiO_2 is its extremely broad range of applications and the expectations that further studies on the surface properties at fundamental level will improve the performance of TiO_2 nanomaterials and related devices in different areas. (b) The applications of the novel properties of these nanomaterials are possible only when the materials are available with desired size, morphology, surface properties and chemical composition. This makes the "synthesis and processing" aspect of nanomaterials all the more important in nanotechnology.

2) The work was initiated by the synthesis of TiO_2 nanoparticles at an optimal concentration of $TiCl_4$: water (1:100), by a simple sol-gel method. The sol-gel synthesis route used in the present work is an attractive method for obtaining nanoparticles with high surface area, porosity and monodispersity. Moreover, the sol-gel synthesis method used in this study had short processing time, needed fewer chemical reagents, lab controlled annealing temperature and relatively short curing time. The characterization results showed the formation of pure, anatase phase TiO_2, mesoporous in nature possessing good physicochemical properties with a crystallite size of ~13 nm and surface area of 72.80 m^2/g. The photocatalytic activity of the TiO_2 was evaluated for the degradation of toxic dyes methylene blue and malachite green as well as its antibacterial activity against pure bacterial cultures and microorganisms from treated sewage water from a local sewage treatment plant. A TiO_2 concentration of 0.1 M was found to be optimal for the complete photodegradation of methylene blue in 80 minutes under both UV light (352 nm) as well as sunlight, whereas,

malachite green was completely degraded within 30 minutes under sunlight and 60 minutes under UV light. Moreover, the levels of organic pollutants in the sewage water were determined by COD analysis. It was observed that after photocatalytic treatment of sewage water for 40 minutes at 0.1 M TiO_2 concentration, a ~85 % reduction in the COD was achieved under sunlight irradiation. The antibacterial studies showed a complete reduction in bacterial count after 40 minutes of sunlight exposure and a 99.9 % reduction in case of *E. coli*, for pure cultures. The order of susceptibility of the microorganisms to inactivation by TiO_2 was *Staphylococcus aureus* > *Klebsiella pneumoniae* > *Pseudomonas aeruginosa* > *Escherichia coli*. Similar studies for the inactivation of microorganisms by TiO_2 photocatalysis in sewage water sample showed a 99 % (2 log reduction) reduction in the microbial load after 40 minutes of exposure in both UV as well as sunlight.

3) Further, to lower the band gap of TiO_2 to enable the effective utilization of the cheaper visible light sources or the greater quantity of the inexhaustible sunlight to carry out the process of photocatalysis, TiO_2 was doped with transition metal dopants (Iron/carbon/sulfur and Silver), non metal dopants (Nitrogen) and surface modification was carried out with organic acids (Folic acid, Fumaric acid, Succinic acid, Malic acid and Salicylic acid), amino acids (L-arginine and L-cysteine), and phosphate, and the effect of surface modification on antibacterial activity was tested against *E. coli*. In the metal ion doped TiO_2, $AgTiO_2$ exhibited highest antibacterial activity with 99.99 % reduction in bacterial count after 120 minutes of visible light (420 nm) irradiation at 50 µg/ml. For nitrogen doped TiO_2, a 90 % reduction in the number of bacterial cells was observed after 120 minutes of visible light irradiation as compared to 15.5 % reduction with the control TiO_2. In case of surface modified TiO_2, FA-TiO_2, Fu-TiO_2 and MA-TiO_2 exhibited 99 % reduction followed by S-TiO_2 with a

90 % reduction in the bacterial count after 120 minutes of visible light (420 nm) exposure at 50 µg/ml. The efficiency of antibacterial activity was in the order of FA-TiO_2 > Fu-TiO_2 > MA-TiO_2 > S-TiO_2 > SA-TiO_2 under visible light conditions.

4) Since $AgTiO_2$ showed good antibacterial activity along with the organic acid modified TiO_2, further studies were performed, where silver containing nanocomposites were synthesized and functionalized with organic acids (Folic acid, Fumaric acid, Succinic acid, and Malic acid) and amino acids (L-arginine and Cysteine), in order to enhance the antibacterial activity of these functionalized nanocomposites. The antimicrobial activity in terms of MIC and MBC of FA-$AgCl/TiO_2$ and Fu-$AgCl/TiO_2$ was found to be better than the unfunctionalized $AgCl/TiO_2$. However, in case of MA-$AgCl/TiO_2$ and SA-$AgCl/TiO_2$ the MIC and MBC was lower than the unfunctionalized $AgCl/TiO_2$. Similarly, no enhancement in antimicrobial activity was observed for Arg-$AgCl/TiO_2$ and Cys-$AgCl/TiO_2$ after functionalization. The characterization studies of FA-$AgCl/TiO_2$ and Fu-$AgCl/TiO_2$ showed superior physicochemical properties with a particle size of 6.5 nm and 6 nm respectively and a surface area of 258.5 m^2/g and 320.7 m^2/g respectively. Studies on microbial inactivation in PBS showed that inactivation could be achieved at 50 µg/ml (0.59 µg/ml Ag) for *E. coli, M. luteus, C. albicans, P. aeruginosa* and 100 µg/ml (1.1 µg/ml Ag) for *S. aureus* in 2 h without photoactivation. In case of Fu-$AgCl/TiO_2$ complete bacterial inactivation was achieved at 100 µg/ml (1.17 µg/ml of Ag) for *E. coli* and *M. luteus*, in PBS after 2 h.

5) Further studies were carried out to investigate the effects of addition of catalytic amount of nickel (II) azamacrocyclic complex to TiO_2 in a photocatalytic reaction and its effects on microorganisms. Among different concentrations of Ni (II): TiO_2, the highest antimicrobial activity was achieved at an optimal combination of 20 µM Ni

(II) + 5 μg/ml TiO_2 for complete inactivation of Gram positive, Gram negative as well as fungal cultures. The control studies with TiO_2 alone or Ni (II) alone did not show any significant antibacterial activity.

Thus some of the prominent points and important contributions emerging from the present thesis are:

1. The synthesized TiO_2 exhibits good photocatalytic activity against toxic dyes, organic pollutants, and microorganisms under both UV light as well as sunlight. Given, the drawbacks of TiO_2 due to its wide band gap, this photocatalytic study has potential applications in the photocatalytic treatment of dye/toxic compounds polluted waters of the textile industry, paint industry etc. or water with high microbial load, and its efficacy of photodegradation makes it a good, economical alternative to other conventional technologies.

2. The usage of organic acids (Folic acid, Fumaric acid, Succinic acid, Malic acid and Salicylic acid), and amino acids (L-arginine and Cysteine) modified TiO_2, to enhance its antibacterial activity in the visible light has been highly unexplored. Hence, the results of this study are novel and promising.

3. This is the first time the synthesis of functionalized silver containing TiO_2 nanocomposites and its enhanced antimicrobial activity (FA-AgCl/TiO_2 and Fu-AgCl/TiO_2) without photoacttivation has been reported. This study is especially important, because silver based nanocomposites are broad spectrum antimicrobial agents and can be a promising alternative for the development of new non-resistance inducing antimicrobial agents due to their multiple mode of action in the target cell.

4. This is also the first study that describes the efficient antimicrobial activity of nickel (II) azamacrocyclic complexes with TiO_2 against various microorganisms (irrespective of their Gram nature).

5. In view of the above information, it is evident that the present research work reports several novel findings and emphasize the fact that TiO_2 in doped/modified/functionalized form can be a very promising photocatalyst with a broad range of applications in different fields.

Future scope of work

1. A major challenge with using TiO_2 in aqueous suspensions (Slurry systems) is the separation of TiO_2 powder from the treated water. Hence, there is a great scope for designing efficient photoreactors, where TiO_2 powder is uniformly coated on substrates such as glass, ceramic or a metal surface to obtain durable thin films.

2. In this study a limited number of molecules such as organic acids, amino acids and vitamins were tested for functionalization of antimicrobial TiO_2 nanocomposites. However, in order to further harness the tremendous potential of such nanocomposites a variety of other molecules with different functionalities may be tested to functionalize TiO_2 nanocomposites, to improve their stability, biocompatibility and overall antimicrobial efficacy against various microorganisms including drug resistant microbial strains.

3. In chapter 5 the study is based on the usage of homogeneous nickel (II) complex in combination with TiO_2. However, it is important to anchor the metal complex to the TiO_2 photocatalyst and future work will have to focus on this aspect of TiO_2 photocatalysts so that the water bodies are free from free metal complexes.

References

Acosta-Torres LS, Lopez-Marın LM, Nunez-Anita RE, Hernandez-Padron G, and Castano VM (2011). Biocompatible Metal-Oxide Nanoparticles: Nanotechnology Improvement of Conventional Prosthetic Acrylic Resins. *J Nanomater*, 2011, 1-8.

Agarwala S, Kevin M, Wong ASW, Peh CKN, Thavasi V, and Ho GW (2010). Mesophase Ordering of TiO_2 Film with High Surface Area and Strong Light Harvesting for Dye-Sensitized Solar Cell. *App. Mater. Interf.,* 2, 1844-1850.

Al-Jlil SA (2009). COD and BOD Reduction of Domestic Wastewater using Activated Sludge, Sand Filters and Activated Carbon in Saudi Arabia. *Biotechnology*, 8, 473-477.

Alvarez-Ordonez A, Fernandez A, Bernardo A, and Lopez M (2009). Comparison of acids on the induction of an acid tolerance response in *Salmonella Typhimurium*, consequences for food safety. *Meat Sci*. 81, 65-70.

Ando Y, Miyamoto H, Noda I, Miyaji F, Shimazaki T, Yonekura Y, Miyazaki M, Mawatari M, and Hotokebuchi T (2010). Effect of Bacterial Media on the Evaluation of the Antibacterial Activity of a Biomaterial Containing Inorganic Antibacterial Reagents or Antibiotics. *Biocontrol Sci*, 15, 15-19.

Anipsitakis GP, and Dionysiou DD (2004). Radical generation by the interaction of transition metals with common oxidants. *Environ..Sci. Technol.* 38, 3705-3712.

Anpo M (2000). Utilization of TiO_2 photocatalysts in green chemistry. *Pure Appl. Chem*, 72: 1265-1270.

Anpo M, and Takeuchi M (2003). "The design and development of highly reactive titanium oxide photocatalysts operating under visible light irradiation." *J. of Catal.*. 216, 505-516.

Asahi R, Morikawa T, Ohwaki T, Aoki K, and Taga Y (2001). Visible-light photocatalysis in nitrogen-doped titanium oxides. *Science*, 293, (5528), 269-271.

Asahi R, Taga Y, Mannstadt W, and Freeman AJ, (2000). Electronic and optical properties of anatase TiO2. *Phys. Rev. B*, 61 (11), 7459.

Asharani PV, Low Kah MG, Hande MP, and Valiyaveettil S (2009). Cytotoxicity and genotoxicity of silver nanoparticles in human cells. *ACS Nano*, 3, 279-290.

Ashkarran AA (2011) Antibacterial properties of silver-doped TiO_2 nanoparticles under solar simulated light. *J. Theoret. and Appl. Phys.*, 4, 1-8.

Asilturk M, Sayilkan F, and Arpac E, (2009). Effect of Fe^{3+} ion doping to TiO_2 on the photocatalytic degradation of Malachite Green dye under UV and vis-irradiation. *J. Photochem. Photobiol. A: Chemistry*, 203, 64-71.

Augugliaro V, Litter M, Palmisano L, and Soria J (2006). The combination of heterogeneous photocatalysis with chemical and physical operations: A tool for improving the photoprocess performance. *J. Photochem. Photobiol. C: Photochemistry Reviews*. 7, 127-144.

Azizi R, Rasouli S, Ahmadi NP, kolaei AJJ, and Azizi M (2012). A systematic investigation of experimental conditions on the particle size and structure of TiO_2 nanoparticles synthesized by a sol-gel method. *J. Cer. Process. Res.*, 13, 164-169.

Bae E, Choi W, Park J, Shin HS, Kim SB, and Lee JS (2004). Effects of Surface Anchoring Groups (Carboxylate vs Phosphonate) in Ruthenium-Complex-Sensitized TiO_2 on Visible Light Reactivity in Aqueous Suspensions. *J. Phys. Chem. B*, 108, 14093-14101.

Bahnemann D, Bockelmann D, and Goslich R (1991). Mechanistic studies of water detoxification in illuminated TiO_2 suspensions. *Sol. Energy Mater.* 24, 564-583.

Baranska H, Kuduk-Jaworska J, Szostak R and Romaniewska A (2003). Vibrational spectra of racemic and enantiomeric malic acids. *J. Raman Spectrosc.* 34, 68-76.

Barnard AS, and Zapol P (2004). Effects of particle morphology and surface hydrogenation on the phase stability of TiO_2. *Phys. Rev., B*, 70, 235403-235415.

Begum NS, Farveez Ahmed HM, and Gunashekar KR (2008). Effects of Ni doping on photocatalytic activity of TiO_2 thin films prepared by liquid phase deposition technique. *Bull. Mater. Sci.* 31, 747-751.

Bencini A, Fabbrizzi L, and Poggi A (1981). Formation of Nickel (III) Complexes with n-Dentate Amine Macrocycles (n = 4, 5, 6). ESR and Electrochemical Studies. *Inorg. Chem.* 20, 2544-2549.

Benedix R, Dehn F, Quaas J, Orgass M (2000). Application of Titanium Dioxide Photocatalysis to Create Self-Cleaning Building Materials. *LACER*, 5, 157-168.

Bergwerff AA, and Scherpenisse P (2003). Determination of residues of malachite green in aqueous animals. *J Chromatogr. B*, 788, 351-359.

Bessekhouad Y, Robert D, Weber JV (2004). Bi_2S_3/TiO_2 and CdS/TiO_2 heterojunctions as an available configuration for photocatalytic degradation of organic pollutant. *J. Photochem. Photobiol. A Chem*, 163: 569–580.

Beydoun D, Amal R, Low G, and McEvoy S (1999). Role of nanoparticles in photocatalysis. *J. Nanopart. Res.*, 1, 439-458.

Bullen HA, Oehrle SA, Bennett AF, Taylor NM, and Barton HA (2008). Use of Attenuated Total Reflectance Fourier Transform Infrared Spectroscopy To Identify Microbial Metabolic Products on Carbonate Mineral Surfaces. *Appl. Environ. Microbiol.* 74, 4553-4559.

Burrows CJ, and Rokita SE (1994). Recognition of Guanine Structure in Nucleic Acids by Nickel Complexes. *Acc. Of Chem. Res.* 27, 295-301.

Cao G (2004). Nanostructures And Nanomaterials: Synthesis, Properties, and Applications. Imperial college press, London.

Carlson C, Hussain SM, Schrand AM, Braydich-Stolle LK, Hess KL, Jones RL, and Schlager JJ (2008). Unique Cellular Interaction of Silver Nanoparticles: Size-Dependent Generation of Reactive Oxygen Species. *J Phys Chem B*, 112, 13608-13619.

Carp O, Huisman CL, and Reller A (2004). Photoinduced reactivity of titanium dioxide. *Progress in Solid State Chemistry*. 32, 33-177.

Chakraborty SP, Sahu SK, Mahapatra SK, Santra S, Bal M, Roy S, and Pramanik P (2010). Nanoconjugated vancomycin: new opportunities for the development of anti-VRSA agents, *Nanotechnology*, 21, 1-9.

Chang Q, He H, and Ma Z (2008). Efficient disinfection of Escherichia coli in water by silver loaded alumina. *J Inorg Biochem*, 102, 1736-1742.

Chatterjee D, Banerjee P, Bose KJC, Mukhopadhyay S (2012). Peroxydisulfate activation by $[Ru^{II}(tpy)(pic)(H_2O)]^+$. Kinetic, mechanistic and anti-microbial activity studies. *Dalton Trans*. 41, 2694-2698.

Chen C, Lu C, and Chung Y (2006). Photocatalytic degradation of ethyl violet in aqueous solution mediated by TiO_2 suspensions. *J. Photochem. Photobiol. A Chem*. 181, 120-125.

Chen CC, Lu CS, Chung YC, and Jan JL (2007). UV light induced photodegradation of malachite green on TiO_2 nanoparticles. *J. Hazard. Mater.*, 141, 520-528.

Chen D, Jiang Z, Geng J, Wang Q, and Yang D (2009). Carbon and Nitrogen Co-doped TiO_2 with Enhanced Visible-Light Photocatalytic Activity. *Ind. Eng. Chem. Res.*, 46 (9), 2741-2746.

Chen J, Yao M, and Wang X (2008). Investigation of transition metal ion doping behaviors on TiO_2 nanoparticles. *J Nanopart Res.* 10, 163-171.

Chen X, and Mao SS (2007). Titanium dioxide nanomaterials: Synthesis, properties, modifications, and applications. *Chem Rev*, 107, 2891-2959.

Chen Y, Wang K, and Lou L (2004). Photodegradation of dye pollutants on silica gel supported TiO2 particles under visible light irradiation. *J. Photochem. Photobiol. A: Chemistry*, 163, 281-287.

Chen Y, Zheng X, Xie Y, Ding C, Ruan H, and Fan C (2008). Anti-bacterial and cytotoxic properties of plasma sprayed silver – containing HA coating, *J Mater Sci : Mater Med.* 19, 3603–3609.

Cheyne RW, Smith Tim AD, Trembleau L, and Mclaughlin AC (2011). Synthesis and characterisation of biologically compatible TiO_2 nanoparticles. *Nanoscale Res Lett,* 6, 423-428.

Cho M, Chung H, Choi W, and Yoon J (2005). Different inactivation behaviors of MS-2 phage and *Escherichia coli* in TiO_2 photocatalytic disinfection. *Appl. Environ. Microbiol*, 71: 270-275.

Cho M, Hyenmi C, Wonyong C, Yoon J (2004). Linear correlation between inactivation of *E.coli* and OH radical concentration in TiO_2 photocatalytic disinfection. *Wat. Res.*, 38, 1069-1077.

Choi O, and Hu Z (2008). Size Dependent and Reactive Oxygen Species Related Nanosilver Toxicity to Nitrifying Bacteria. *Environ. Sci. Technol,* 42, 4583-4588.

Choi W, Termin A, and Hoffmann MR (1994). The Role of Metal Ion Dopants in Quantum-Sized TiO_2: Correlation between Photoreactivity and Charge Carrier Recombination Dynamics. *J. Phys. Chem.* 98, 13669-13679.

Comes JE, and Beelman RB (2002). Addition of fumaric acid and sodium benzoate as an alternative method to achieve a 5-log reduction of *Escherichia coli* O157:H7 populations in apple cider. *J. Food Prot*. 65, 476-483.

Cropek D, Kemme PA, Makarova OV, Chen LX, and Rajh T (2008). Selective Photocatalytic Decomposition of Nitrobenzene Using Surface Modified TiO_2 Nanoparticles. *J. Phys. Chem. C*, 112, 8311-8318.

Daoud WA, Xin JH, and Zhang Y-H (2005). Surface functionalization of cellulose fibers with titanium dioxide nanoparticles and their combined bactericidal activities. *Surf. Sci.* 599, 69-75.

Dash BP, and Chaudhari S (2005). Electrochemical denitrificaton of simulated ground water. *Water Res*. 39, 4065-4072.

Desai VS, Kowshik M, (2009). Antimicrobial activity of titanium dioxide nanoparticles synthesized by sol-gel technique. *Res. Journ. Microbiol.*, 3, 97-103.

Desideri A, Raynor JB (1977). Electron spin resonance spectroscopy of some dianiono(1,4,8,11-tetra-azacyclotetradecane)-iron(III) and -nickel(III) salts. *J. Chem. Soc. Dalton Trans.* 20, 2051-2054.

Devi R, and Dahiya RP (2008). COD and BOD removal from domestic wastewater generated in decentralized sectors. *Bioresour. Technol*, 99, 344-349.

Dhanasekaran T, Prakash H, and Natarajan P (2001). Photooxidation of nickel (II) macrocyclic complexes on excitation in the charge-transfer-to-solvent band in aqueous solution and in the presence of oxygen. *J. Photochem.Photobiol. A: Chemistry*, 141, 17-24.

Dickson JS, and Anderson ME (1992). Microbiological decontamination of food animal carcasses by washing and sanitizing systems: a review. *J. Food Protect.* 55, 133-140.

Diebold U (2003). The surface science of titanium dioxide. *Surf. Sci. Rep*, 48, 53-229.

Dovranova D, Brevoza V, Mazur M, and Malati M (2002). "Investigations of metal-doped titanium dioxide photocatalysts." *Appl. Catal. B Environ*, 37, 91-105.

Dulaney EL, and Marx LM (1971). A folic acid linked system in bacterial cell wall synthesis? *The Journal Of Antibiotics*, 10, 713-714.

Dunlop PSM, Byrne JA, Manga N, and Eggins BR (2002). "The Photocatalytic removal of bacterial pollutants from drinking water," *J. Photochem. Photobiol. A. Chem.*, 148, 355-363.

Dunlop PSM, Byrne JA, Manga N, and Eggins BR, (2002). The photocatalytic removal of bacterial pollutants from drinking water. *J. Photochem. Photobiol. A*, 148, 355-363.

Durupthy O, Bill J, and Aldinger F (2007). Bioinspired Synthesis of Crystalline TiO_2: Effect of Amino Acids on Nanoparticles Structure and Shape. *Crystal Growth & Design*, 7, 2696-2704.

Dvoranova D, Brezova V, Mazur M, and Malati MA (2002). Investigation of metal-doped titanium dioxide photocatalysis. *Appl Catal B Environ*, 37, 91-105.

Egerton TA, Kosa SAM, and Christensen PA (2005). Photoelectrocatalytic disinfection of *E.coli* suspensions by iron doped TiO_2. *Phys. Chem. Chem. Phys*, 8, 398-406.

Egger S, Lehmann RP, Height MJ, Loessner MJ, and Schuppler M (2009). Antimicrobial Properties of a Novel Silver-Silica Nanocomposite Material. *Appl Environ Microbiol*, 9, 2973-2976.

Elahifard MR, Rahimnejad S, Haghighi S, and Gholami MR (2007). Apatite-Coated Ag/AgBr/TiO_2 Visible-Light Photocatalyst for Destruction of Bacteria. *J. Am. Chem. Soc*. 129, 9552-9553.

El-Morsi TM, Budakowski WR, Abd-El-Aziz AS, and Friesen KJ (2000). Photocatalytic degradation of 1,10-dichlorodecane in aqueous suspensions of TiO_2: a reaction of adsorbed chlorinated alkane with surface hydroxyl radicals. *Environ. Sci. Technol.* 34, 1018-1022.

Enterkin JA, Poeppelmeier KR, and Marks LD (2011). Oriented Catalytic Platinum Nanoparticles on High Surface Area Strontium Titanate Nanocuboids. *Nano Lett.* 11, 993-997.

Esterbauer H, and Cheeseman KH (1990). Determination of aldehydiclipid peroxidation products: malonaldehyde and 4-hydroxynonenal peroxidation. *Methods Enzymol.* 186B, 407-421.

Etacheri V, Seery MK, Hinder SJ, and Pillai SC (2010). Highly Visible Light Active $TiO_{2-x}N_x$ Heterojunction Photocatalysts. *Chem. Mater.* 22, 3843-3853.

Eva J, Helmerhorst EJ, Reijnders IM, Hof W, Veerman ECI, and Amerongen AVN (1999). A critical comparison of the hemolytic and fungicidal activities of cationic antimicrobial peptides. *FEBS Lett*. 449, 105-110.

Feng QL, Wu J, Chen GQ, Cui FZ, Kim TN, and Kim JO (2000). A mechanistic study of the antibacterial effect of silver ions on *Escherichia coli* and *Staphylococcus aureus. J Biomed Mater Res Part A*, 4, 662-668.

Ferraudi G, and Muralidharan S (1981). Photoinduced Dimerization of Macrocyclic Complexes Mediated by a Metal- Assisted Oxidation of the Macrocycle. *Inorg. Chem*, 20, 4262-4267.

Ferreira L, Fonseca AM, Botelho G, Almeida-Aguiar C, and Neves IC (2012). Antimicrobial activity of faujasite zeolites doped with silver. *Micropor. Mesopor. Mater*, 160, 126–132.

Fox MA, and Dulay MT (1993). "Heterogeneous photocatalysis," *Chem. Rev.*, 93, 341-357.

Fujishima A, and Honda K (1972). Electrochemical photolysis of water at a semiconductor electrode. *Nature*, 238, 37-38.

Fujishima A, Rao TN, and Tryk DA (2000). Titanium dioxide photocatalysis. *J. Photochem. Photobiol. C: Photochemistry Reviews*, 1, 1-21.

Fujishima A, Zhang X, and Tryk DA (2008). TiO_2 photocatalysis and related surface phenomena. *Surf. Sci. Reports*, 63, 515-582.

Furman OS, Teel AL, Watts RJ (2010). Mechanism of Base Activation of Persulfate. *Environ. Sci. Technol*. 44, 6423-6428.

Galvez JB, Ibanez PF, and Sixto MR (2007). Solar photocatalytic detoxification and disinfection of water: Recent overview. *J. solar Energy Engg*. 129.

Garcez AS, Nunez SC, Baptista MS, Daghastanli NA, Itri R, Hamblin MR, and Ribeiro MS (2011). Antimicrobial mechanisms behind photodynamic effect in the presence of hydrogen peroxide. *Photochem. Photobiol. Sci.* 10, 483-490.

Gaweda S, Stochel G, and Szaciłowski K (2007). Bioinspired Nanodevice Based on the Folic Acid/Titanium Dioxide System. *Chem. Asian J*, 2, 580-590.

Gerrity D, Ryu H, Crittenden J, and Abbaszadegan M (2008). Photocatalytic inactivation of viruses using titanium dioxide nanoparticles and low-pressure UV light. *J. Environ. Sci. and Health Part A*, 43: 1264-1270.

Gokulakrishnan S, Parakh P, Prakash H (2012). Degradation of Malachite green by Potassium persulphate, its enhancement by 1,8-dimethyl-1,3,6,8,10,13 hexaazacyclotetradecane nickel (II) perchlorate complex, and removal of antibacterial activity. *J. Hazard. Mater*. 213, 19-27.

Gomathi Devi L, Kottam N, Girish Kumar S, and Rajashekhar KE (2010). Preparation, characterization and enhanced photocatalytic activity of Ni^{2+} doped titania under solar light. *Cent. Eur. J. Chem.* 8, 142-148.

Guin D, Manorama SV, Latha JNL, and Singh S (2007). Photoreduction of silver on bare and colloidal TiO_2 Nanoparticles/Nanotubes: Synthesis, characterization, and tested for antibacterial outcome. *J. Phys. Chem.C*, 111, 13393-13397.

Gupta SM, and Tripathi M (2011). A review of TiO_2 nanoparticles. *Chinese Sci Bull.* 56, 1639-1657.

Hagfeldtt A, and Grätzel M (1995). Light-induced redox reactions in nanocrystalline systems. *Chem Rev*, 95, 49-68.

Haines RI, and Rowley JE (2003). Structure and Kinetics of Oxidation of Amphiphilic Nickel (II) Pentaazamacrocycles by Peroxodisulfate and by a Nickel (III) Pendant-Arm Macrocycle. *J. Incl. Phen. Macro. Chem.* 47, 25-32.

Haines RI, Northcott SJ (1992). Kinetics and mechanism of oxidation of nickel (II) tetraazamacrocycles by the peroxydisulphate anion in aqueous and binary aqueous mixtures. *Can. J. Chem.* 70, 2785-2791.

Halcrow MA, and Christou G (1994). Biomimetic Chemistry of Nickel. *Chem. Rev.* 94, 2421-2481.

Hamal DB, and Klabunde KJ (2007). Synthesis, characterization, and visible light activity of new nanoparticle photocatalysts based on silver, carbon, and sulfur-doped TiO_2. *J. Colloid and Interf. Sci.*, 311, 514-522.

Han Y, Kim HS, and Kim H (2012). Relationship between Synthesis Conditions and Photocatalytic Activity of Nanocrystalline TiO_2. *J. Nanomater.*, Volume 2012, Article ID 427453, 1-10.

Hartmann M, Berditsch M, Hawecker J, Ardakani MF, Gerthsen D, and Ulrich AS (2010). Damage of the Bacterial Cell Envelope by Antimicrobial Peptides Gramicidin S and PGLa as Revealed by Transmission and Scanning Electron Microscopy. *Antimicrob Agents Chemother,* 54, 3132-3142.

Hashimoto K, Irie H, and Fujishima A (2005). TiO_2 Photocatalysis: A Historical Overview and Future Prospects. *Jap. Journ. Appl. Phys.,* 44, 8269-8285.

Healy MG, Rodgers M, and Mulqueen J (2006). Performance of a stratified sand filter in removal of chemical oxygen demand, total suspended solids and ammonia nitrogen from high strength waste water. *J. Environ. Manage*, 83, 409-415.

Henderson GB, and Potuznik S (1982). Cation-Dependent Binding of Substrate to the Folate Transport Protein of Lactobacillus casei. *J. Bacteriol.,* 3, 1098-1102.

Henderson MA (2011). A Surface Science Perspective on TiO_2 Photocatalysis. *Surf. Sci. Reports*, 66, 185-297.

Herrmann JM (2005). Heterogeneous photocatalysis: state of the art and present applications. *Topics in Catalysis*. 34, 49-65.

Hirakawa KM, Mori M, Yoshida S, Oikawa, and Kawanishi S (2004). Photo-irradiated titanium dioxide catalyzes site specific DNA damage via generation of hydrogen peroxide. *Free Radic. Res*, 38: 439–447.

Hoffmann MR, Martin ST, Choi W, and Bahnemann DW (1995). "Environmental applications of semiconductor photocatalysis." *Chem. Rev*, 95, 69-96.

Holzapfel V, Lorenz M, Weiss CK, Schrezenmeier H, Landfester K, and Mailander V (2006). Synthesis and Biomedical Application of Functionalized Fluorescent and Magnetic Dual Reporter Nanoparticles as Obtained in a Miniemulsion Process. *Journal of Physics: Condensed Matter*, 18, S2581-S2594.

Hosokawa M, Nogi K, Naito M, and Yokoyama T (2007). Nanoparticle Technology Handbook, First edition. Elsevier, Linacre House, Jordan Hill, Oxford OX2 8DP, UK.

House DA (1962). Kinetics and mechanism of oxidations by peroxydisulfate. *Chem. Rev*. 62, 185–203.

Hu C, Hu X, Wang L, Qu J, and Wang A (2006). Visible-light-induced photocatalytic degradation of azodyes in aqueous AgI/TiO_2 dispersion. *Environ. Sci. Technol.* 40, 7903-7907.

Huang DG, Liao SJ, Liu JM, Dang Z, and Petrik L (2006). "Preparation of visible-light responsive N-F-codoped TiO_2 photocatalyst by a sol-gel solvothermal method," *J. Photochem. Photobiol. A: Chemistry*. 184, 282-288.

Huang IW, Hong CS, and Bush B (1996). "Photocatalytic degradation of PCBs in TiO_2 aqueous suspensions. *Chemosphere*, 32, 1869-1881.

Huang Z, Maness PC, Blake DM, Wolfrum EJ, Smolinksi SL, and Jacoby WA (2000). Bactericidal mode of titanium dioxide photocatalysis. *J. Photochem. Photobiol.* A, 130, 163-170.

Hur JS, and Koh Y (2002). Bactericidal activity and water purification of immobilized TiO_2 photocatalyst in beam sprout cultivation. *Biotechnology letters*, 24, 23-25.

Ihara T, Miyoshi M, Iriyama Y, Matsumoto O, and Sugihara S (2003). Visible-light-active titanium oxide photocatalyst realized by an oxygen-deficient structure and by nitrogen doping. *Applied Catalysis B: Environmental*, 42, 403-409.

Irie H, Watanabe Y, and Hashimoto K (2003). "Nitrogen-Concentration Dependence on Photocatalytic Activity of TiO_2-xNx Powders." *J. Phys. Chem. B,* 107, 5483-5486.

Ivanova OS, and Zamborini FP (2010). Size-Dependent Electrochemical Oxidation of Silver Nanoparticles. *J Am Chem Soc*, 132, 70-72.

Izat AL, Colberg M, Adams MH, Reiber A, and Waldroup PW (1989). Production and processing studies to reduce the incidence of *salmonellae* on commercial broilers. *J. Food Protect.* 52, 670-673.

Jaacobi M, Meyerstein D, and Lilie J (1979). Oxidation of a Nickel (II) Complex with an Unsaturated Macrocyclic Ligand in Aqueous Solutions. A Pulse Radiolytic Study. *Inorg. Chem*, 18, 429-433.

Jacoby WA, Maness PC, Wolfrum EJ, Blake DM, and Fennell JA (1998). Mineralization of Bacterial Cell Mass on a Photocatalytic Surface in Air. *Environ. Sci. Technol.* 32, 2650-2653.

Jankovic IA, Saponjic ZV, Comor MI, and Nedeljkovic JM (2009). Surface Modification of Colloidal TiO_2 Nanoparticles with Bidentate Benzene Derivatives. *J. Phys. Chem. C*, 113, 12645-12652.

Jankovic IA, Saponjic ZV, Dzunuzovic ES, and Nedeljkovic JM, (2010). New Hybrid Properties of TiO_2 Nanoparticles Surface Modified With Catecholate Type Ligands. *Nanoscale Res Lett*. 5, 81-88.

Jeon HJ, Yi SC, and Oh SG (2003). "Preparation and Antibacterial Effects of Ag–SiO_2 Thin Films by Sol-Gel Method". *Biomaterials*, 27, 4921-4928.

Jeong J, Kim JY, and Yoon J (2006). The Role of Reactive Oxygen Species in the Electrochemical Inactivation of Microorganisms. *Environ. Sci. Technol.* 40, 6117-6122.

Jiang J, Gao Q, Chen Z, Hu J, and Wu C (2006). Syntheses, characterization and properties of novel nanostructures consisting of Ni/titanate and Ni/titania. *Materials Letters*, 60, 3803-3808.

Jin X, Ali M, Wang J, Marambio-Jones C, Peng F, Huang X, Damoiseaux R, and Hoek EMV (2010). High-Throughput Screening of Silver nanoparticle Stability and Bacterial Inactivation in Aquatic Media: Influence of Specific Ions. *Environ. Sci. Technol.* 44, 7321-7328.

Johnson RL, Tratnyek PG, and Johnson RO (2008). Persulfate Persistence under Thermal Activation Conditions. *Environ. Sci. Technol*. 42, 9350-9356.

Jubran N, Meyerstein D, Koresh J, and Cohen H (1986). Ring size effects on the chemical properties of tervalent nickel complexes with tetra-azamacrocyclic ligands in aqueous solutions. An electrochemical and pulse radiolytic study. *J. Chem. Soc. Dalton Trans.* 2509-2513.

Kamat PV, and Meisel D (2003). Nanoscience opportunities in environmental remediation. *C. R. Chimie*, 6, 999-1007.

Kang S, Herzberg M, Rodrigues DF, Elimelech M (2008). Antibacterial Effects of Carbon Nanotubes: Size Does Matter! *Langmuir*, 24, 6409-6413.

Kasaini H, Goto M, and Furusaki S (2000). Selective Separation of Pd(II), Rh(III), and Ru(III) Ions from a Mixed Chloride Solution Using Activated Carbon Pellets. *Separation Science And Technology*, 35, 1307-1327.

Kau JH, Sun DS, Huang HH, Wong MS, Lin HC, and Chang HH (2009). Role of visible-light activated photocatalyst on the reduction of Anthrax spore-induced mortality in mice. *PLOS One*, 4, 1-8.

Kawashita M, Toda S, Kim H, Kokubo MT, and Masuda N (2003). Preparation of Antibacterial Silver-Doped Silica Glass Microspheres. *J Biomed Mater Res A*, 2, 266-274.

Keuk-Jun K, Sung WS, Moon SK, Choi JS, Kim JG, and Lee DG (2008). Antifungal Effect of Silver Nanoparticles on Dermatophytes. *J. Microbiol. Biotechnol.* 8, 1482-1484.

Keuk-Jun K, Sung WS, Suh BK, Moon SK, Choi JS, Kim JG, and Lee DG (2009). Antifungal activity and mode of action of silver nano-particles on *Candida albicans*. *Biometals.* 22, 235-242.

Kikuchi YK, Sunada T, Iyada K, Hashimoto and Fujishima A (1997). Photocatalytic bactericidal effect of TiO_2 thin films: dynamic view of the active oxygen species responsible for the effect. *J. Photochem. Photobiol. A* 160, 51-56.

Kim JS, Kuk E, Yu KN, Kim JH, Park SJ, Lee HJ, Kim SH, Park YK, Park YH, Hwang CY, Kim YK, Lee YS, Jeong DH, and Cho MH (2007). Antimicrobial effects of silver nanoparticles. *Nanomed Nanotech Biol Med.* 3, 95-101.

Kim YJ, Kim MH, and Song KB (2009). Efficacy of aqueous chlorine dioxide and fumaric acid for inactivating pre-existing microorganisms and *Escherichia coli* O157:H7, *Salmonella typhimurium*, and *Listeria monocytogenes* on broccoli sprouts. *Food Control*, 20, 1002-1005.

Kim YS, Chung YC, and Lee KS (2006). The electronic structure of Ni doped rutile TiO_2. *J. Electroceram*, 17, 951–953.

Kohler M, and Fritzsche W (2004). Nanotechnology: An Introduction to Nanostructuring Techniques. WILEY-VCH Verlag GmbH & Co. KGaA, Weinheim.

Kolthoff IM, Miller IK (1951). The Chemistry of Persulfate. I. The Kinetics and Mechanism of the Decomposition of the Persulfate Ion in Aqueous Medium. *J. Am. Chem. Soc.* 73, 3055-3059.

Kondo N, Murata M, and Isshiki K (2006). Efficiency of sodium hypochlorite, fumaric acid, and mild heat in killing native microflora and *Escherichia coli* O157:H7,

Salmonella Typhimurium DT104, and *Staphylococcus aureus* attached to fresh-cut lettuce. *J Food Prot*, 69, 323-329.

Konovalova TA, Kispert LD, and Konovalov VV (1999). Surface Modification of TiO_2 Nanoparticles with Carotenoids. EPR Study. *J. Phys. Chem. B*, 103, 4672-4677.

Kritsky MS, Telegina TA, Lyudnikova TA, Umrikhina AV, and Zemskova YL (2001). Participation of Free Radicals in Photoreduction of Pterins and Folic Acid. *Dokl. Biochem. Biophys*. 380, 336-338.

Kumar A, and Jain AK (2001). Photophysics and photochemistry of colloidal CdS-TiO_2 coupled semiconductors-photocatalytic oxidation of indole. *J. Mol. Catal. A Chemical*, 165: 265-273.

Kvıtek L, Panacek A, Soukupova J, Kolar M, Vecerova R, Prucek R, Holecova M, and Zboril R (2008). Effect of Surfactants and Polymers on Stability and Antibacterial Activity of Silver Nanoparticles (NPs). *J Phys Chem C*, 112, 5825-5834.

Kyung H, Lee J, and Choi W (2005). Simultaneous and synergistic conversion of dyes and heavy metal ions in aqueous TiO_2 suspensions under visible-light illumination. *Environ. Sci. Technol*, 39, 2376-2382.

Lai TY, and Lee WC, (2009). Killing of cancer cell line by photoexcitation of folic acid-modified titanium dioxide nanoparticles. *J. Photochem. Photobiol. A: Chem.* 204, 148-153.

Landi E, Tampieri A, Celotti G, and Spiro S (2000). Densification behavior and mechanisms of synthetic hydroxyapatite. *J. Eur. Ceram. Soc.* 20, 2377-2387.

Lau TK, Chu W, Graham NJD (2007). The Aqueous Degradation of Butylated Hydroxyanisole by UV/$S_2O_8^{2-}$: Study of Reaction Mechanisms via Dimerization and Mineralization. *Environ. Sci. Technol.* 41, 613-619.

Lee CM, Chen CH, Liao FX, Hu CH, Lee GH (2010). Mononuclear Ni^{III}-Alkyl Complexes (Alkyl=Me and Et): Relevance to the Acetyl-CoA Synthase and Methyl-CoM Reductase. *J. Am. Chem. Soc.* 132, 9256-9258.

Lee D, Bang H, Suh MP (2000). Epoxidation of an alkene promoted by various nickel(II) multiazamacrocyclic complexes. *J. Mol. Catal. A: Chemical.* 151, 71-78.

Lee MS, Hong SS, and Mohseni M (2005). Synthesis of photocatalytic nanosized TiO_2–Ag particles with sol–gel method using reduction agent. *J. Mol.Catal. A: Chem*., 242, 135-140.

Lee MS, Hong SS, Mohseni M (2005). Synthesis of photocatalytic nanosized TiO_2–Ag particles with sol–gel method using reduction agent. *J. Mol. Catal. A: Chemical*, 242, 135-140.

Lee S, Otaki NM, and Ohgaki S (1997). Photocatalytic inactivation of phage QB by immobilized titanium dioxide mediated photocatalyst. *Water Sci. Technol*, 35: 101-106.

Lepentsiotis V, Domagala J, Grgic I, Eldik R, Muller JG, and Burrows CJ (1999). Mechanistic Information on the Redox Cycling of Nickel(II/III) Complexes in the Presence of Sulfur Oxides and Oxygen. Correlation with DNA Damage Experiments. *Inorg. Chem.* 38, 3500-3505.

Lewis A, Taha H, Strinkovski A, Manevitch A, Khatchatouriants A, Dekhter R, and Ammann E, (2003). Near Field optics: from subwavelength illumination to nanometric shadowing. *Nat. Biotechnol.* 21, 1378-86.

Li M, Zhu L, and Lin D (2011). Toxicity of ZnO Nanoparticles to *Escherichia coli*: Mechanism and the Influence of Medium Components. *Environ. Sci. Technol.* 45, 1977-1983.

Li R, Chen W, and Wang W (2009). Magnetoswitchable controlled photocatalytic system using ferromagnetic Fe-doped titania nanorods photocatalysts with enhanced photoactivity. *Sep. Purif. Technol*, 66: 171-176.

Li WR, Xie XB, Shi QS, Duan SS, Ouyang YS, and Chen YB (2011). Antibacterial effect of silver nanoparticles on *Staphylococcus aureus. Biometals*, 24, 135–141.

Li X, Liu G, and Zhao J (1999). Two competitive primary processes in the photodegradation of cationic triarylmethane dyes under visible irradiation in TiO_2 dispersions. *New J. Chem.* 23, 1193-1196.

Liang C, and Guo YY (2010). Mass Transfer and Chemical Oxidation of Naphthalene Particles with Zerovalent Iron Activated Persulfate. *Environ. Sci. Technol.* 44, 8203-8208.

Liang C, and Su HW (2009). Identification of Sulfate and Hydroxyl Radicals in Thermally Activated Persulfate. *Ind. Eng. Chem. Res.* 48, 5558-5562.

Lifen L, Barford J, and Lun YK (2009). Non-UV germicidal activity of fresh TiO_2 and Ag/TiO_2. *Journal of Environmental Sciences*. 21, 700-706.

Linsebigler AL, Lu G, and Yates JT (1995). "Photocatalysis on TiO_2 Surfaces: Principles, Mechanisms, and Selected Results." *Chem. Rev.*, 95, 735-758.

LiPuma JJ, Rathinavelu S, Foster BK, Keoleian JC, Makidon PE, Kalikin LM, and Baker JR Jr. (2009). In Vitro Activities of a Novel Nanoemulsion against *Burkholderia* and Other Multidrug-Resistant Cystic Fibrosis-Associated Bacterial Species. *Antimicrob Agents Chemother*, 1, 249-255.

Litter MI (1999). Heterogeneous photocatalysis Transition metal ions in photocatalytic systems. *Applied Catalysis B: Environmental*, 23, 89-114.

Liu C, Fu L, and Economy J (2004). A simple, template-free route for the synthesis of mesoporous titanium dioxide materials. *J. Mater. Chem*, 14, 1187-1189.

Liu JY and Hurt R (2010). Ion Release Kinetics and Particle Persistence in Aqueous Nano-Silver Colloids. *Environ. Sci. Technol*, 44, 2169-2175.

Liu LF, Barford J, and Yeung KL (2007). Non-UV based germicidal activity of metal-doped TiO_2 coating on solid surfaces. *Journal of Environmental Sciences*. 19, 745-750.

Liu S, Lim M, Fabris R, Chow C, Drikas M, and Amal R (2008). TiO_2 Photocatalysis of Natural Organic Matter in Surface Water: Impact on Trihalomethane and Haloacetic Acid Formation Potential. *Environ. Sci. Technol.* 42, 6218-6223.

Liu Y, Wang X, Yang F, and Yang X (2008). Excellent antimicrobial properties of mesoporous anatase TiO_2 and Ag/TiO_2 composite films. *Micropor. Mesopor. Mater.*, 114, 431-439.

Livraghi S, Paganini MC, Giamello E, Selloni A, Valentin CD, and Pacchioni G (2006). Origin of Photoactivity of Nitrogen-Doped Titanium Dioxide under Visible Light. *J. Am. Chem. Soc.*, 128, 15666-15671.

Lok CN, Ho CM, Chen R, He QY, Yu WY, Sun H, Tam PKH, Chiu JF, and Che CM (2007). Silver nanoparticles: partial oxidation and antibacterial activities. *J Biol Inorg Chem*, 12, 527-534.

Lorenz MR, Holzapfel V, Musyanovych A, Nothelfer K, Walther P, Frank H, Landfester K, Schrezenmeier H, and Mailander V (2006). Uptake of Functionalized, Fluorescently-Labeled Polymeric Particles in Different Cell Lines and Stem Cells. *Biomaterials*, 27, 2820-2828.

Lorian V (2005). Antibiotics in Laboratory Medicine, fifth ed. Lippincott Williams & Wilkins, Philadelphia.

Lu S, Gao W, and Gu HY (2008). "Construction, Application and Biosafety of Silver Nanocrystalline Chitosan Wound Dressing." *Burns*, 5, 623-628.

Macyk W, Szacilowski K, Stochel G, Buchalska M, Kuncewicz J, and Labuz P (2010). Titanium(IV) complexes as direct TiO_2 photosensitizers. *Coord. Chem. Rev.* 254, 2687-2701.

Makarova OV, Rajh T, and Thurnauer MC (2000). Surface Modification of TiO_2 Nanoparticles For Photochemical Reduction of Nitrobenzene. *Environ. Sci. Technol.* 34, 4797-4803.

Maness PC, Smolinski S, Blake DM, Huang Z, Wolfrum EJ, and Jacoby WA (1999). Bactericidal activity of photocatalytic TiO_2 reaction: toward an understanding of its killing mechanism. *Appl. Environ. Microbiol.* 65, 4094-4098.

Marambio-Jones C, and Hoek EMV (2010). A review of the antibacterial effects of silver nanomaterials and potential implications for human health and the environment. *J Nanopart Res*, 12, 1531–1551.

Marugan J, Grieken RV, Pablos C, and Sordo C (2010). Analogies and differences between photocatalytic oxidation of chemicals and photocatalytic inactivation of microorganisms, *Water Res*. 44, 789-796.

Matsunaga T, Tomoda R, Nakajima T, Nakamura N, and Komine T (1988). Continuous-sterilization system that uses photosemiconductor powders. *Appl. Environ. Microbiol*, 54: 1330-1333.

Matsunaga T, Tomodam R, Nakajima T, and Wake H (1985). Photochemical sterilization of microbial cells by semiconductor powders. *FEMS Microbiol. Lett.* 29, 211-214.

Michalow KA, Logvinovich D, Weidenkaff A, Amberg M, Fortunato G, Heel A, Graule T, and Rekas M (2009). Synthesis, characterization and electronic structure of nitrogen-doped TiO_2 nanopowder, *Catalysis Today*, 144, 7-12.

Mills A, Hodgen S, and Lee SK (2005). Self-cleaning titania films: An overview of direct, lateral and remote photo-oxidation processes. *Res Chem Intermed,* 31: 295-308.

Min SH, Yang JH, Kim JY, and Kwon YU (2010). Development of white antibacterial pigment based on silver chloride nanoparticles and mesoporous silica and its polymer composite. *Microporous and Mesoporous Mater,* 128, 19–25.

Mitoraj D, Janczyk A, Strus M, Kisch H, Stochel G, Heczko PB, and Macyk W (2007). Visible light inactivation of bacteria and fungi by modified titanium dioxide. *Photochem. Photobiol. Sci.*, 6, 642-648.

Mo S, and Ching W (1995). Electronic and optical properties of three phases of titanium dioxide: Rutile, anatase and brookite. *Phys Rev B,* 51: 13023-13032.

Mohapatra S, Mallick SK, Maiti TK, Ghosh SK and Pramanik (2007). Synthesis of highly stable folic acid conjugated magnetite nanoparticles for targeting cancer cells. *Nanotechnology*, 18, 385102.

Mokbel MS, and Hashinaga F (2005). Antibacterial and Antioxidant Activities of Banana (*Musa*, AAA cv. Cavendish) Fruits Peel. *Amer. Journ. Biochem. Biotech.,* 1, 125-131.

Monti S (2007). RAD16II β-Sheet Filaments onto Titanium Dioxide: Dynamics and Adsorption Properties. *J. Phys. Chem. C,* 111, 16962-16973.

Moorthy PN and Hayon E (1977). One-electron redox reactions of water-soluble vitamins. 4. Thiamin (vitamin B1), biotin and pantothenic acid. *J. Org. Chem*, 42, 879-885.

Morones JR, Elechiguerra JL, Camacho A, Holt K, Kouri JB, Ramirez JT, and Yacaman MJ (2005). The bactericidal effect of silver nanoparticles. *Nanotechnology,* 16, 2346-2353.

Muller JG, Hickerson RP, Perez RJ, Burrows CJ (1997). DNA Damage from Sulfite Autoxidation Catalyzed by a Nickel(II) Peptide. *J. Am. Chem. Soc*. 119, 1501-1506.

Naik B, Desai V, Kowshik M, Prasad VS, Fernando GF, and Ghosh NN (2011). Synthesis of Ag/AgCl–mesoporous silica nanocomposites using a simple aqueous solution-based chemical method and a study of their antibacterial activity on *E. coli*. *Particuology,* 9, 243-247.

Nel A, Xia T, Madler L, and Li N (2006). Toxic potential of materials at nanolevel. *Science,* 311, 622-627.

Nino-Martınez N, Martınez-Castanon GA, Aragon-Pina A, Martınez-Gutierrez F, Martınez-Mendoza JR, and Ruiz F (2008). Characterization of silver nanoparticles synthesized on titanium dioxide fine particles. *Nanotechnology*, 19, 1-8.

Nishikawa T, Nakajima T, and Shinohara Y (2001). "An exploratory study on the effect of the isomorphic replacement of Ti^{4+} ions by various metal ions in the light absorption character of TiO_2." *Journal of Molecular Structure*. 545, 67-74.

Nobs L, Buchegger F, Gurny R, and Allemann E (2003). Surface Modification of Poly(Lactic Acid) Nanoparticles by Covalent Attachment of Thiol Groups by Means of Three Methods. *International Journal of Pharmaceutics*, 250, 327-337.

Noda I, Miyaji F, Ando Y, Miyamoto H, Shimazaki T, Yonekura Y, Miyazaki M, Mawatari M, and Hotokebuchi T (2009). Development of novel thermal sprayed antibacterial coating and evaluation of release properties of silver ions. *J. Biomed. Mater. Res. Part B: Appl. Biomater*, 89, 456-465.

Nogueira RFP and Jardim WF (1993). Photodegradation of Methylene Blue Using Solar Light and Semiconductor (TiO_2). *Journal of Chemical Education*, 70, 861-862.

Nsib MF, Maayoufi A, Moussa N, Tarhouni N, Massouri A, Houas A, and Chevalier Y (2013). TiO_2 modified by salicylic acid as a photocatalyst for the degradation of monochlorobenzene via Pickering emulsion way. *J. Photochem. Photobiol. A: Chemistry*, 251, 10-17.

Oh SY, Kim HW, Park JM, Park HS, and Yoon C (2009). Oxidation of polyvinyl alcohol by persulfate activated with heat, Fe^{2+}, and zero-valent iron. *J. Hazard. Mater.* 168, 346-351.

Ohno T, Miyamoto Z, Nishijima K, Kanemitsu H, and Xueyuan F (2006). Sensitization of photocatalytic activity of S- or N-doped TiO_2 particles by adsorbing Fe^{3+} cations. *Applied Catalysis A: General*, 302, 62-68.

Ohno T, Sarukawa K, Tokieda K, and Matsumura M (2001). "Morphology of a TiO_2 photocatalyst (Degussa, P-25) consisting of anatase and rutile crystalline phases." *J. Catal.*, 203, 82-86.

Ohya Y, Matsunami H, and Ouchi T (2004). Cell Growth on Porous Sponges Prepared From Poly(Depsipeptide-co-Lactide) Having Various Functional Groups. *Journal of Biomaterials Science: Polymer Edition*, 15, 111-123.

Oskam G, Nellore A, Penn RL, and Searson PC (2003). The Growth Kinetics of TiO_2 Nanoparticles from Titanium (IV) Alkoxide at High Water/Titanium Ratio. *J. Phys. Chem. B*, 107, 1734-1738.

Pan X, Medina-Ramirez I, Mernaugh R, and Liu J (2010). Nanocharacterization and bactericidal performance of silver modified titania photocatalyst. *Colloids Surf B,* 77, 82-89.

Parkin IP, and Palgrave RG (2005). Self-cleaning coatings. *J Mater Chem,* 15: 1689-1695.

Peng T, Zhao D, Dai K, Shi W, and Hirao K, (2005). Synthesis of Titanium dioxide nanparticles with mesoporous anatase wall and high photocatalytic activity. *J. Phys. Chem. B,* 109: 4947-4952.

Peral J, Domenech X, and Ollis DF (1997). Hetrogeneous photocatalysis for purification, decontamination and deodorization of air. *J. Chem. Tech. Biotech.* 70, 117-140.

Prakash H, and Natarajan P (2000). Photooxidation of nickel(II) macrocyclic complexes by mono- and biphotonic processes from the charge-transfer to solvent excited states in aqueous solutions. *Chem. Phys. Lett*. 329, 357-362.

Prakash H, and Natarajan P (2003). Novel facile photochemical method for the synthesis of trivalent nickel azamacrocyclic complexes. *Inorg. Chem. Comm.* 6, 1071-1073.

Prakash H, and Natarajan P (2004). Photooxidation of nickel (II) azamacrocyclic complexes to trivalent nickel complexes on excitation in the charge-transfer-to-solvent band. *J. Photochem Photobiol A: Chemistry.* 168, 81-90.

Prieto O, Fermoso J, Nunez Y, del Valle JL, and Irusta R (2005). Decolouration of textile dyes in wastewaters by photocatalysis with TiO_2. *Solar Energy*, 79, 376-383.

Priya SS, Premalatha M, and Anantharaman N (2008). Solar Photocatalytic Treatment Of Phenolic Wastewater- Potential, Challenges And Opportunities. *ARPN Journal of Engineering and Applied Sciences*. 3, 36-41.

Rai M, Yadav A, and Gade A (2009). Silver nanoparticles as a new generation of antimicrobials. *Biotechnol Adv,* 27, 76-83.

Raimondi F, Scherer GG, Kotz R, and Wokaun A (2005). Nanoparticles in Energy Technology: Examples from Electrochemistry and Catalysis. *Angew. Chem. Int. Ed,* 44, 2190-2209.

Rajeshwar K, de Tacconi NR, Chenthamarakshan CR (2001). Semiconductor-based composite materials: Preparation, properties, and performance. *Chem. Mater*, 13: 2765-2782.

Rajh T, Chen LX, Lukas K, Liu T, Thurnauer MC, and Tiede DM (2002). Surface Restructuring of Nanoparticles: An Efficient Route for Ligand-Metal Oxide Crosstalk. *J. Phys. Chem. B.* 106, 10543-10552.

Rana P, Mohan N, and Rajagopal C (2004). Electrochemical removal of chromium from wastewater by using carbon aerogel electrodes. *Water Res.* 38, 2811-2820.

Ranjit KT, and Viswanathan B (1997). Photocatalytic properties of iron-doped titania semiconductors (1997). *J. Photochem. Photobiol. A: Chem.* 108, 79-84.

Raposo F, de la Rubia MA, Borja R, and Alaiz M (2008). Assessment of a modified and optimised method for determining chemical oxygen demand of solid substrates and solutions with high suspended solid content. *Talanta,* 76, 448-453.

Reddy KM, Baruwati B, Jayalakshmi M, Rao MM, and Manorama SV (2005). "S-, N- and C-doped titanium dioxide nanoparticles: Synthesis, characterization and redox charge transfer study." *Journal of Solid State Chemistry*. 178, 3352-3358.

Regazzoni AE, Mandelbaum P, Matsuyoshi M, Schiller S, Bilmes SA, and Blesa MA (1998). Adsorption and Photooxidation of Salicylic Acid on Titanium Dioxide: A Surface Complexation Description. *Langmuir*, 14, 868-874.

Rengaraj S, Joo CK, Kim Y, and Yi J (2003). Kinetics of removal of chromium from water and electronic process wastewater by ion exchange resins: 1200H, 1500H and IRN97H. *Journal of Hazardous Materials.* B102, 257-275.

Richardson SD, Lebron BL, Miller CT, and Aitken MD (2011). Recovery of Phenanthrene-Degrading Bacteria after Simulated in Situ Persulfate Oxidation in Contaminated Soil. *Environ. Sci. Technol.* 45, 719-725.

Riegel G, and Bolton JR (1995). "Photocatalytic efficiency variability in TiO_2 particles," *J. Phys. Chem*, 99, 4215-4224.

Rincon AG, and Pulgarin C (2004)."Bacterial action of illuminated TiO_2 on pure *Escherichia coli* and natural consortia: post-irradiation events in the dark and

assessment of the effective disinfection time". *Applied Catalysis B-Environmental*, 49, 99-112.

Rincon AG, and Pulgarin C, (2003). Photocatalytical inactivation of *E. coli*: effect of (continuous–intermittent) light intensity and of (suspended–fixed) TiO_2 concentration. *Appl, Catal. B*, 44, 263-284.

Rincon AG, and Pulgarin C, (2007). Absence of *E. coli* regrowth after Fe^{3+} and TiO_2 solar photoassisted disinfection of water in CPC solar photoreactor. *Catal. Today*, 124, 204-214.

Rincon AG, Pulgarin C (2005). Use of coaxial photocatalytic reactor (CAPHORE) in the TiO_2 photo-assisted treatment of mixed *E. coli* and *Bacillus* sp. and bacterial community present in wastewater. *Catal Today*, 101: 331-344.

Rincon AG, Pulgarin C, Adler N, Peringer P., (2001). Interaction between *E. coli* inactivation and DBP-precursors dihydroxybenzene isomers in the photocatalytic process of drinking-water disinfection with TiO_2. *J. Photochem. Photobiol. A*, 139, 233-241.

Rockafellow EM, Stewart LK, and Jenks WS (2009). Is sulfur-doped TiO_2 an effective visible light photocatalyst for remediation? *Applied Catalysis B: Environmental*, 91, 554-562.

Rodriguez JA, and Fernancez-Garcia M. (2007). Wiley-Interscience, JohnWiley & Sons, Inc., Hoboken, New Jersey.

Rodríguez JL, Valenzuela MA, Pola F, Tiznado H, and Poznyak T (2012). Photodeposition of Ni nanoparticles on TiO2 and their application in the catalytic ozonation of 2,4-dichlorophenoxyacetic acid. *Journal of Molecular Catalysis A: Chemical*, 353-354, 29-36.

Saggioro EM, Oliveira AS, Pavesi T, Maia CG, Ferreira LFV, and Moreira JC (2011). Use of Titanium Dioxide Photocatalysis on the Remediation of Model Textile Wastewaters Containing Azo Dyes. *Molecules*, 16, 10370-10386.

Saito T, Iwase T, and Morioka T (1992). Mode of photocatalytic bactericidal action of powdered semiconductor TiO_2 on mutants streptococci. *J. Photochem. Photobiol.-B Biol.*, 14: 369-79.

Sakai H, Ito E, Cai RX, Yoshioka T, Hashimoto K, and Fujishima A (1994). Intracellular Ca^{+2} concentration change of T24 cell under irradiation in the presence of TiO_2 ultrafine particles. *Biochim Biophys Acta*. 1201, 259-265.

Schierholz JM, Beuth J, Pulverer G, and Konig DP (1999). Silver-Containing Polymers. *Antimicrob Agents Chemother*, 11, 2819-2821.

Schliephake H, and Scharnweber D, (2008). Chemical and biological functionalization of titanium for dental implants. *J. Mater. Chem*, 18, 2404-2414.

Schwitzgebel J, Ekerdt JG, Gerischer H, and Heller A (1995). Role of the oxygen molecule and of the photogenerated electron in TiO_2-photocatalyzed air oxidation reactions. *J. Phys. Chem.* 99, 5633-5638.

Serpone N, and Emeline AV (2005). Modeling Heterogeneous Photocatalysis by Metal-Oxide Nanostructured Semiconductor and Insulator Materials. Factors that Affects the Activity and Selectivity of Photocatalysts. *Res. Chem. Intermed*, 31, 391-432.

Shah SAS, Md., Nag M, Kalagara T, Singh S, and Manorama SV (2008). Silver on PEG-PU-TiO2 Polymer Nanocomposite Films: An Excellent System for Antibacterial Applications. *Chem Mater*, 20, 2455-60.

Shah SI, Li W, Huang CP, Jung O, and Ni C (2002). Study of Nd^{3+}, Pd^{2+}, Pt^{4+}, and Fe^{3+} dopant effect on photoreactivity of TiO_2 nanoparticles. *Proc. Natl. Acad. Sci.U.S.A*, 99, 6482-6486.

Shin H, Ruhe PQ, Mikos AG, and Jansen JA (2003). In vivo bone and soft tissue response to injectable, biodegradable oligo poly (ethylene glycol) fumarate) hydrogels. *Biomaterials*, 24, 3201-3211.

Shivaraju HP (2011). Removal of Organic Pollutants in the Municipal Sewage Water by TiO_2 based Heterogeneous Photocatalysis. *Inter. Journ. Environmen. Sci.*, 1, 911-923.

Sing KSW, Everett DH, Haul RAW, Moscou L, Pierotti RA, Rouquerol J (1985). Reporting physisorption data for gas/solid systems with special reference to the determination of surface area and porosity. *Pure and Applied Chemistry*, 57, 603-619.

Skrivanova E, Marounek M, Benda V, and Brezina P (2006). Susceptibility of Escherichia coli, Salmonella sp. and Clostridium perfringens to organic acids and monolaurin. *Veterinarni Medicina*, 51, 81–88.

Skubal LR, and Meshkov NK (2002). "Reduction and removal of mercury from water using arginine-modified TiO_2." *J. Photochem. Photobiol. A Chem.*, 148, 211-214.

Smith B (1999). Infrared Spectral Interpretation: a systematic approach. CRC Press, USA.

Smith MM, Silva JAK, Munakata-Marr J, and Mccray JE (2008). Compatibility of Polymers and Chemical Oxidants for Enhanced Groundwater Remediation. *Environ. Sci. Technol*. 42, 9296-9301.

Soekmen M, Candan F, Suemer Z, (2001). Disinfection of *E. coli* by the Ag-TiO_2/UV system: lipidperoxidation. *Journal of Photochemistry and photobiology: A chemistry*, 143, 240-244.

Sondi I, and Sondi BS (2004). Silver Nanoparticles as Antimicrobial Agent: A Case Study on *E. coli* as Gram-negative bacteria. *J Colloid Interface Sci*, 275, 177-182.

Soo-Hwan K, Lee HS, Ryu DS, Choi SJ, and Lee DS (2011). Antibacterial Activity of Silver-nanoparticles Against *Staphylococcus aureus* and *Escherichia coli. Korean J. Microbiol. Biotechnol*, 1, 77-85.

Sopyan I, Marasawa S, Hashimoto K, and Fujishima A (1999). Highly efficient TiO_2 film photocatalyst, degradation of gaseous acetaldehyde. *Chem. Lett.* 723-726.

Sreethawong T, Suzuki Y, and Yoshikawa S (2005). Synthesis, characterization, and photocatalytic activity for hydrogen evolution of nanocrystalline mesoporous titania prepared by surfactant-assisted templating sol-gel process. *J Solid State Chem*, 178, 329-338.

Srinivasan C, and Somasundaram N (2003). Bactericidal and detoxification effects of irradiated semiconductor catalyst, TiO_2. *Current Science*, 85, 1431-1438.

Stella B, Arpicco S, Peracchia MT, Desmaele D, Hoebeke J, Renoir M, D'angelo J, Cattel L, and Couvreur P (2000). Design of Folic Acid-Conjugated Nanoparticles for Drug Targeting. *Journal Of Pharmaceutical Sciences*, 11, 1452-1464.

Su C, Hong BY, and Tseng CM, (2004). "Sol-gel preparation and photocatalysis of titanium dioxide." *Catal. Today*, 96, 119-126.

Su HL, Chou CC, Hung DJ, Lin SH, Pao IC, Lin JH, Huang FL, Dong RX, and Lin JJ (2009). The disruption of bacterial membrane integrity through ROS generation induced by nanohybrids of silver and clay. *Biomaterials,* 30, 5979-5987.

Suh MP, and Kang SG (1988). Synthesis and Properties of Nickel(II) and Copper (II) Complexes of 14-Membered HexaazaMacrocycles, 1,8-Dimethyl- and 1,8-Diethyl-1,3,6,8,10,13 hexaazacyclotetradecane. *Inorg.Chem.* 27, 2544-2546.

Suh MP, Lee EY, and Shim BY (1998). Synthesis and properties of nickel (III) complexes of hexaazamacrocyclic ligands. *Inorg. Chimica. Acta*, 269, 337-341.

Sun L, and Bolton JR (1996). Determination of the Quantum Yield for the Photochemical Generation of Hydroxyl Radicals in TiO_2 Suspensions. *J. Phys. Chem.* 100, 4127-4134.

Sun W, Li X, Liu S, and Jiao K (2009). Electrochemistry of Hemoglobin in the Chitosan and TiO_2 Nanoparticles Composite Film Modified Carbon Ionic Liquid Electrode and Its Electrocatalysis. *Bull. Korean Chem. Soc*, 3, 582-588.

Sunanda K, Kikuchi Y, Hashimoto K, and Fujishima A (1998). Bactericidal and detoxification effects of TiO_2 thin film photocatalysts. *Environ. Sci. Technol.* 32, 726-728.

Tahiri H, Serpone N, and Le van Mao R (1996). "Application of concept of relative photonic efficiencies and surface characterization of a new titania photocatalyst designed for environmental remediation." *J. Photochem. Photobiol. A. Chem*, 93, 199-203.

Tan SX, Tan SZ, Chen JX, Liu YL, and Yuan DS (2009). Preparation and properties of antibacterial TiO2@C/Ag core–shell composite. *Sci Technol Adv Mater,* 10, 1-6.

Tanaka K, Capule MFV, and Hisanaga T (1991). "Effect of crystallinity of TiO_2 on its photocatalytic action." *Chem. Phy. Let.*, 187, 73-76.

Teoh WY, Scott JA, and Amal R (2012). Progress in Heterogeneous Photocatalysis: From Classical Radical Chemistry to Engineering Nanomaterials and Solar Reactors. *J. Phys. Chem. Lett*. 3, 629-639.

Thiel J, Pakstis L, Buzby S, Raffi M, Ni C, Pochan DJ, and Shah SI (2007). Antibacterial Properties of Silver-Doped Titania. *Small*, 5, 799-803.

Thompson TL, and Yates Jr JT (2006). Surface science studies of the photoactivation of TiO_2-New photochemical processes. *Chem Rev*, 106, 4428-4453.

Tian G, Fu H, Jing L, and Tian C (2009). "Synthesis and photocatalytic activity of stable nanocrystalline TiO_2 with high crystallinity and large surface area." *Journal of Hazardous Materials*, 161, 1122-1130.

Tiwari R, Sharma MK, and Ameta SC (2011). Photocatalytic Treatment Of Polluted Water Containing Cresol Red. *Int. J. Chem. Sci*, 9, 421-428.

Torres GR, Lindgren T, Lu J, Granqvist CG, and Lindquist SE (2004). Photoelectrochemical Study of Nitrogen-Doped Titanium Dioxide for Water Oxidation," *Journal of Physical Chemistry B.* 108, 5995-6003.

Valentin CD, Finazzi E, Pacchioni G, Selloni A, Livraghi S, Paganini MC, and Giamello E (2007). N-doped TiO_2: Theory and experiment. *Chemical Physics*, 339, 44-56.

Vilensky M, Berkowitz B, and Warshawsky A (2002). In Situ Remediation of Groundwater Contaminated by Heavy- and Transition-Metal Ions by Selective Ion-Exchange Methods. *Environ. Sci. Technol*. 36, 1851-1855.

Vimala K, Mohan YM, Varaprasad K, Redd NN, Ravindra S, Naidu NS, and Raju KM (2011). Fabrication of Curcumin Encapsulated Chitosan-PVA Silver Nanocomposite Films for Improved Antimicrobial Activity. *Journal of Biomaterials and Nanobiotechnology*, 2, 55-64.

Vinodgopal K, and Wynkoop DE (1996). Environmental Photochemistry on Semiconductor Surfaces: Photosensitized Degradation of a Textile Azo Dye, Acid Orange 7, on TiO_2 Particles Using Visible Light. *Environ. Sci. Technol*, 30, 1660-1666.

Vinodgopal K, Bedja I, Kamat PV (1996). Nanostructured semiconductor films for photocatalysis. Photoelectrochemical behavior of SnO_2/TiO_2 composite systems and its role in photocatalytic degradation of a textile azo dye. *Chem. Mater.*, 8: 2180-2187.

Vohra A, Goswami DY, Deshpande DA, and Block SS (2005). Enhanced photocatalytic inactivation of bacterial spores on surfaces in air. *J. Ind. Microbiol. Biotechnol*, 32, 364-370.

Wahi RK, Liu Y, Falkner JC, and Colvin VL (2006). Solvothermal synthesis and characterization of anatase TiO_2 nanocrystals with ultrahigh surface area. *Journal of Colloid and Interface Science*, 302, 530-536.

Waldemer RH, Tratnyek PG, Johnson RL, Nurmi JT (2007). Oxidation of Chlorinated Ethenes by Heat-Activated Persulfate: Kinetics and Products. *Environ. Sci. Technol*. 41, 1010-1015.

Wan L, Li JF, Feng JY, Sun W, and Mao ZQ (2007) Improved optical response and photocatalysis for N-doped titanium oxide (TiO_2) films prepared by oxidation of TiN. *Applied Surface Science*, 253, 4764-4767.

Wan Y, Zhang D, Wang Y, Qi P, Wu J, and Hou B (2011). Vancomycin-functionalized Ag@TiO_2 phototoxicity for bacteria. *J Hazard Mater,* 186, 306-312.

Wang D, Duan Y, Luo Q, Li X, An J, Baoa L, and Shi L (2012). Novel preparation method for a new visible light photocatalyst: mesoporous TiO_2 supported Ag/AgBr. *J. Mater. Chem.* 22, 4847-4854.

Wang R, Hashimoto K, Fujishima A, Chikuni M, Kojima E, Kitamura A, Shimohigoshi M, and Watanabe T (1997). Light-induced amphiphilic surfaces. *Nature,* 388: 431-432.

Wang Y, Cheng H, Hao Y, Ma J, and Li W, and Cai S (1999). Preparation, characterization and photoelectrochemical behaviors of Fe (III)-doped TiO_2 nanoparticles. *Journal of Materials Science*. 34, 3721-3729.

Wang, SH, Lu L, Gruetzmacher J, Currier B, and Yaszemski M (2006). Synthesis and characterizations of biodegradable and crosslinkable poly(e-caprolactone fumarate), poly(ethylene glycol fumarate), and their amphiphilic copolymer. *Biomaterials,* 27, 832-841.

Williams D, Ehrman NSH, and Tracey RPH (2006). Evaluation of the microbial growth response to inorganic nanoparticles. *J. nanobiotech*, 4, 1-8.

Win KY, and Feng SS (2005). Effects of Particle Size and Surface Coating on Cellular Uptake of Polymeric Nanoparticles for Oral Delivery of Anticancer Drugs. *Biomaterials,* 26, 2713-2722.

Windholz M (1976). The Merck Index. In: M. Windholz, et al. (ed.), An encyclopedia of chemicals and drugs. Merck & Co., Inc., Rahway, NJ.

Wolfrum EJ, Huang J, Blake DM, Maness PC, Huang Z, and Fiest J (2002). Photocatalytic Oxidation of Bacteria, Bacterial and Fungal Spores, and Model Biofilm Components to Carbon Dioxide on Titanium Dioxide-Coated Surfaces. *Environ. Sci. Technol.* 36, 3412-3419.

Wong MC, Chu WC, Sun DS, Huang HS, Chen JH, Tsai PJ, Lin NT, Yu MS, Hsu SF, Wang SL, and Chang HH (2006). Visible-Light-Induced Bactericidal Activity of a Nitrogen-Doped Titanium Photocatalyst against Human Pathogens. *Appl. Environ. Microbiol.* 72, 6111-6116.

Wu C, Chao C, and Kuo F (2004). "Enhancement of the photocatalytic performance of TiO_2 catalysts via transition metal modification." *Catalysis Today*. 97, 103-112.

Wu HP, Cheng TL, and Tseng WL (2007) Phosphate-Modified TiO_2 Nanoparticles for Selective Detection of Dopamine, Levodopa, Adrenaline, and Catechol Based on Fluorescence Quenching *Langmuir*, 23, 7880-7885

Wu J, Zhang H, and Qiu J (2012). Degradation of Acid Orange 7 in aqueous solution by novel electro/Fe^{2+}/peroxydisulfate process. *J. Hazard. Mater*. 215–216, 138–145.

Wu T, Lin T, Zhao J, Hidaka H, and Serpone N (1999). TiO_2-Assisted Photodegradation of Dyes. 9. Photooxidation of a Squarylium Cyanine Dye in Aqueous Dispersions under Visible Light Irradiation. *Environ. Sci. Technol.*, 33, 1379-1387.

Wu, T., Lin, T., Zhao, J., Hidaka, H., and Serpone, N., (1998). Photoassisted degradation of dye pollutants. V. Self-photosensitized oxidative transformation of rhodamine B under visible light irradiation in aqueous TiO2 dispersions. *J. Phys. Chem. B*, 102, 5845-5851.

Xing LS, Ying ZF, Lian CW, Qin HA, and Kun XY (2006). Surface modification of nanometer size TiO_2 with salicylic acid for photocatalytic degradation of 4-nitrophenol. *Journal of Hazardous Materials B*, 135, 431-436.

Xu AW, Gao Y, and Liu HQ (2002). The Preparation, Characterization, and their Photocatalytic Activities of Rare-Earth-Doped TiO_2 Nanoparticles. *J. Catal.* 207, 151-157.

Xu J, Ao Y, and Fu D (2009). A novel Ce, C-codoped TiO_2 nanoparticles and its photocatalytic activity under visible light. *Appl Surf Sci.* 256, 884-888.

Yang L, Zhu L, Liu C, Fang M, Liu G, and Yu X (2008). Synthesis and photocatalytic property of porous TiO_2 microspheres. *Materials Research Bulletin*, 43, 806-810.

Yao HT, Kuo CS, Huang CH, Li YY, Chou PW, Cheng CL, and Wong MS (2006). Visible-light–responsive nano-TiO_2 with mixed crystal lattice and its photocatalytic activity. *Nanotechnology*, 17, 2490-2497.

Yao Z, Jia F, Tian S, Li C, Jiang Z, and Bai X (2010). Microporous Ni-Doped TiO_2 film Photocatalyst by Plasma Electrolytic Oxidation. *Appl. Mat. Interfaces*. 2, 2617-2622.

Yates HM, Nolan MG, Sheel DW, and Pemble ME (2006). "The role of nitrogen doping on the development of visible light-induced photocatalytic activity in thin TiO_2 films grown on glass by chemical vapour deposition." *Journal of Photochemistry and Photobiology A: Chemistry*, 179, 213-223.

You X, Chen F, and Zhang J (2005). Effects of calcination on the physical and photocatalytic properties of TiO_2 powders prepared by sol-gel template method. *J Sol-Gel Sci Tech*, 34, 181-187.

Yu JC, Ho W, Yu J, Yip H, Wong PK, and Zhao J (2005), Efficient visible-light-induced photocatalytic disinfection on sulfur-doped nanocrystalline titania. *Environ. Sci. Technol.* 39, 1175-1179.

Zaleska A (2008). Doped-TiO_2: A Review. *Recent Patents on Engineering*, 2, 157-164.

Zaporozhets O, Gawer O, and Sukhan V (1999). The interaction of Fe (II), Cu (II) and Ag (I) ions and their complexes with 1,10-phenanthroline adsorbed on silica gel. *Colloids and Surfaces A: Physicochemical and Engineering Aspects*, 147, 273-281

Zeigerson E, Bar I, Bernstein J, Kirschenbaum LJ, and Meyerstein D (1982). Stabilization of the Tervalent Nickel Complex with meso-5,7,7,12,14,14-Hexamethyl-1,4,8,1l-tetraazacyclotetradecanbey Axial Coordination of Anions in Aqueous Solution. *Inorg. Chem.* 21, 73-80.

Zhang AP, and Sun YP (2004). Photocatalytic killing effect of TiO_2 nanoparticles on Ls-174-t human carcinamo cells. *World J Gastroenterol*, 10, 3191-3193.

Zhang HJ, and Chen G (2009). Potent Antibacterial Activities of Ag/TiO_2 Nanocomposite Powders Synthesized by a One-Pot Sol-Gel Method. *Environ. Sci. Technol,* 43, 2905-2910.

Zhang S, Chen Z, Li Y, Wang Q, Wan L, and You Y (2008). Preparation of TiO_2 fibers by two-step synthesis method and their photocatalytic activity. *Materials Chemistry and Physics*, 107, 1-5.

Zhang Z, Wang CC, Zakaria R, and Ying JY (1998). Role of Particle Size in Nanocrystalline TiO_2-Based Photocatalysts. *J. Phys. Chem. B*, 102, 10871-10878.

Zhao D, Chen C, Wang Y, Ji H, Ma W, Zang L, and Zhao J (2008). Surface Modification of TiO_2 by Phosphate: Effect on Photocatalytic Activity and Mechanism Implication. *J. Phys. Chem. C*, 112, 5993-6001.

Zhao J, and Yang XD (2003). Photocatalytic oxidation for indoor air purification: A literature review. *Building and Environment*, 38, 645-654.

Zhou M, Yu J, Cheng B, and Yu H (2005). Preparation and photocatalytic activity of Fe-doped mesoporous titanium dioxide nanocrystalline photocatalysts. *Chem. Phys.* 93, 159-163.

Zilbermann I, Meshulam A, Cohen H, Meyerstein D (1993). Stabilization of nickel (III)-1,8-dimethyl-1,3,6,8,10,13-hexaazacyclotetradecane by axial binding of anions in neutral aqueous solutions. *Inorg. Chimica. Acta.* 206, 127-130.

Conferences and workshops

1. Bactericidal activity of TiO_2 photocatalysts synthesized by sol-gel process **(Poster presentation)**, 48th Annual conference of Association of Microbiologists of India **(AMI)** at Indian Institute of Technology Madras, Chennai-600036, 18-21 December, 2007.
2. Antibacterial activity of photocatalytic Titanium nanoparticles **(Poster presentation)**, 49th Annual conference of Association of Microbiologists of India **(AMI)** at University of Delhi, Delhi, 18-20 November, 2008.
3. Bactericidal activity of Titanium dioxide nanoparticles synthesized by sol-gel process. **(Oral presentation)**, International Congress of Environmental Research **(ICER-2008)**, at BITS, Pilani Goa Campus, 18-20 December, 2008.
4. Photocatalytic activity of titanium dioxide nanoparticles synthesized by sol-gel process. **(Poster presentation)**, National conference on Emerging Trends in Life Sciences Research **(ETLSR)**, BITS, Pilani, Rajasthan, India, 6-7 March, 2009.
5. Participated in the "**Cancer and Nanotechnology: Therapeutics and Diagnostics"** workshop held on 17 February 2010, as a part of **International Conference on Nano Science and Technology (ICONSAT 2010)** held from 17-20 February, 2010 at Indian Institute of Technology, Bombay, Mumbai.
6. Synthesis and characterization of $AgTiO_2$ nanocomposites functionalized with folic acid and studies on its antibacterial activity **(Poster presentation), International Conference on Nano Science and Technology (ICONSAT 2012) organized by** International Advanced Research Center for Powder Metallurgy and New Materials (ARCI), from January 20-24, 2012 at Hyderabad, India.

7. Study of the cytotoxic activity of $AgTiO_2$ nanocomposites synthesized by simple sol-gel method **(Oral presentation)**, National Seminar on "Nanomaterials: Synthesis, characterization and applications, at Smt. Parvatibai Chowgule College of Arts & Science, Goa University, India, 2-3 February, 2012.

List of Publications

1. **Vilas Desai**, Bhanudas Naik, Narendra Nath Ghosh and Meenal Kowshik. Functionalization of nano silver-titania with folic acid - a promising strategy for enhancement of antimicrobial activity. *Sci. Adv. Mater*, 5 (5): 1-9, 2013.

2. **Vilas Desai** and Meenal Kowshik. Synthesis and characterization of fumaric acid functionalized AgCl/titania nanocomposite with enhanced antibacterial activity. *J. Nanosci. Nanotechnol.* 13, 2826-2834, 2013.

3. Meenal Kowshik, **Vilas Desai**, Kshipra Naik. Functionalization of Silver-Titanium dioxide nanoparticles, a novel strategy for enhancement of antimicrobial activity. *Proceedings of Green Nanotechnology*, Centre for Nanotechnology, Visvesvaraya Technological University, Belgaum 590018, Karnataka, India. 26-27 Nov. 2012, 53-61.

4. **Desai, V.**, Kowshik, M., Antimicrobial activity of titanium dioxide nanoparticles synthesized by sol-gel technique, *Res. J. Microbiol*, 4 (3): 97-103, 2009.

Brief Biography of the Candidate

Personal details

Name Mr. Vilas Desai

Education M.Sc. (Microbiology): Goa University (2005).

B.Sc. (Chemistry, Microbiology), P.E.S. college, Goa, (2003)

E-mail desvila@gmail.com

Work experience:

Worked as a JRF and SRF on a DST sponsored project entitled "Preparation and characterization of nanosized TiO_2 and studies on its photodegradation capability of model organic pollutants" from 08/08/2007 to 30/06/2010.

Research experience abroad

Worked at the Department of Chemical and Materials Engineering, Lunghwa University of Science and Technology, Taiwan, from June to October 2009. The highlights of my research in Taiwan were peptide synthesis, synthesis and characterization of Solid lipid nanoparticles (SLNs), Nanostructured Lipid Carriers (NLCs) and TiO_2 based nanomaterials.

No. of conferences/workshops attended 07

No. of publications 05

A Brief Biography of the Supervisor

Meenal Kowshik received her M.Sc in Microbiology from Goa University in 1997. She worked on the biological synthesis of metallic and metal sulfide nanoparticles using yeasts at Agarkar Research Institute, and obtained her Ph.D. degree from Pune University (1999–2003). Subsequently, she joined Birla Institute of Technology and Science, Pilani-K. K. Birla Goa Campus, and is currently working as Associate Professor in the Department of Biological Sciences. Her research interests include studies on biofunctionalization of silver based nanocomposites for antimicrobial applications; synthesis of biocompatible nanomaterials for tissue engineering; application of nanomaterials in molecular biology research; interactions of nanomaterials and microorganisms with respect to nanomaterial synthesis as well as toxicity, with special emphasis on halophilic archaebacteria. She has received research grants from Department of Science and technology for two projects which have been completed and has an ongoing project from the Ministry of Earth Sciences. She has been a co-investigator on four other projects sanctioned by the agencies; Department of Biotechnology, DRDO and UGC. She has published 22 research papers in International and National journals of repute; has 3 patents to her credit and has delivered several invited talks at International and National conferences.